Catalysis in Membrane Mimetic Reaction Media

Jaap Klijn

Het onderzoek beschreven in dit proefschrift is gefinancierd door de National Research School Combination Catalysis.

RIJKSUNIVERSITEIT GRONINGEN

Catalysis in Membrane Mimetic Reaction Media

Proefschrift

ter verkrijging van het doctoraat in de
Wiskunde en Natuurwetenschappen
aan de Rijksuniversiteit Groningen
op gezag van de
Rector Magnificus, dr. F. Zwarts,
in het openbaar te verdedigen op
vrijdag 3 september 2004
om 14.45 uur

door

Jaap Eduard Klijn
geboren op 25 april 1976
te Haarlem

Promotor:
prof. dr. J. B. F. N. Engberts

Beoordelingscommissie:
prof. dr. B. L. Feringa
prof. dr. A. J. Kirby
prof. dr. R. J. M. Nolte

ISBN 90-367-2088-5

Dankwoord

Tien jaar geleden, in 1994, arriveerde ik in Groningen om er scheikunde te gaan studeren. Voor die tijd was ik er slechts enkele malen geweest en kende ik de stad enkel van open dagen van de universiteit. De onbekendheid strekte zich vanzelfsprekend ook uit tot zijn inwoners. Inmiddels is die situatie wel veranderd. Niet alleen ben ik inmiddels wel in alle wijken van de stad geweest, maar ook het aantal mensen dat ik heb leren kennen is danig toegenomen. Daarnaast is mijn chemische kennis ook wel wat bijgeschaafd, hetgeen uiteindelijk heeft geresulteerd in dit boekwerkje. Dit dankwoord wil ik dan ook aan hen richten die in de afgelopen vier jaar, waarin ik een aanstelling had als AIO, hebben bijgedragen aan de totstandkoming hiervan.

Allereerst wil ik Jan Engberts bedanken. Immers, zonder hem zou ik nooit aan dit onderzoek zijn begonnen. Jan, bedankt voor alle steun, de vrijheid in het onderzoek en de stimulatie om mijn culturele en chemische horizon te verbreden in Bressanone, Venetië, Basel en binnenkort zelfs in Shanghai. Tevens ben ik je erg dankbaar voor het verwerven van een talentvolle onderzoeksgroep. Een capabele en gemêleerde groep met een bepaalde minimale hoeveelheid AIO's, postdocs, studenten en ondersteunend personeel is cruciaal voor het goed functioneren van een onderzoeker. In de jaren die ik in je groep heb mogen doorbrengen waren deze mensen in juiste mate aanwezig. De constante factor in de groep collega's is Anno Wagenaar. Er zijn maar weinig mensen die altijd tijd voor je hebben (en zelfs koffie voor je zetten 's ochtends!). Anno, bedankt en geniet van je verdiende pensioen volgend jaar! De laatste vier jaar heb ik labzaal en bureauruimte mogen delen met Niek Buurma, Theo Rispens en Reinskje Talhout. Dank voor de overdaad aan mentale, wetenschappelijke en technische steun zowel binnen als buiten het lab in de afgelopen jaren. Met Marco Scarzello, Markus Johnsson en Marc Stuart heb ik de laatste jaren meer koffie gedronken dan goed voor me is. De (wetenschappelijke) conversatie was natuurlijk nooit genoeg!

Mahthild Jongejan en Arjan Linthorst heb ik tijdens hun hoofdvakonderzoek mogen begeleiden. Mahthild, ik waardeer je doorzettingsvermogen. Zelfs nadat ik je een jaar lang een hopeloze synthese heb laten uitvoeren (tja, suikers...), liet je het hoofd niet hangen. Je hebt een mooi stukje werk neergezet. Arjan, jouw kritische houding en enthousiasme zijn ongeëvenaard. Dit ondanks je drukke leven. Ik ben blij dat beide hoofdvakonderzoeken hebben geleid tot wetenschappelijke publicaties; een ware prestatie! I have supervised Fausto Carraro in the three months he stayed here as a Socrates student. Fausto, unfortunately your work has not led to a publication, but it definitely increased my knowledge about the (in)stability of vesicles and the life of foreign students in Groningen.

Ich habe meinen zweimonatlichen Aufenthalt in der schönen Stadt Basel als eine fantastische Zeit erlebt. Besonders möchte ich Prof Seelig und seiner Arbeitsgruppe danken für ihre Gastfreundlichkeit und große Hilfsbereitschaft. Ich habe mich stets sehr wohl gefühlt am Institut. Die Diskussionen und Gespräche mit Heiko, Halina, Alekos und allen anderen Gruppenmitglieder haben sehr zu meinem Erfolg beigetragen. Neben der Arbeit habe ich auch immer viel Spaß gehabt in der Gruppe. Dies alles hätte ich nicht verpassen wollen!

De leescommissie, bestaande uit Prof. A.J. Kirby, Prof. R.M.J. Nolte en Prof. B.L. Feringa dank ik voor het vlot lezen van het manuscript. Het moet niet meegevallen zijn dit proefschrift in zo'n korte tijd door te lezen.
Verder mag ik natuurlijk niet vergeten om, in alfabetische volgorde, de (voormalige) groepsgenoten Nabil Asaad, Paul Bell, Rixt Buwalda, Jan van Esch, Dorien Jonker, Marjon Kuiper, Egid Mubofu, Dirk Pijper, Patrick van Rijn, Rasha Sami-al-Abd, Paola Serena, Jan Spoelstra, Inge Visscher, Wilke Weringa, Michel Wijnhold en Marco Willemsma te bedanken voor de fantastische sfeer in de groep door de jaren heen.
Daarnaast hebben diverse personen van het ondersteunend personeel en uit andere onderzoeksgroepen mijn werk en tijd op het werk veraangenaamd. Van de (voormalige) vakgroep biochemie heb ik ruim gebruik kunnen maken van hun stopped-flow apparaat, DSC en ITC. De gastvrijheid en hulp die ik altijd belangeloos heb gekregen van Gea Schuurman-Wolters, Piet Wietzes en Marco Fraaije is me goed bevallen. Bedankt!
Daarnaast wil ik van OMAC met name Hilda Biemold, de mensen van de bibliotheek en de electronische dienst noemen. Zonder hen was ik zonder twijfel vastgelopen in bureaucratie, onvindbare literatuur en niet-functionerende apparaten.
Een veelvoud aan mensen hebben mijn vrije tijd glans bezorgd en mij daarmee in staat gesteld om ontspannen mijn werk te verrichten. Deze mensen vallen vooral (maar niet allemaal) onder de categoriën "1-Noordvrienden", (ex)-voetbalteamleden van Lycurgus en actieve PvdA-leden.
De onderzoeksschool NRSC-Catalysis wil ik bedanken voor de financiële en wetenschappelijke ondersteuning. Zij hebben het mogelijk gemaakt dat ik nu goed op de hoogte ben van wat er, chemisch gezien, in Nederland gebeurd, maar ook dat ik naar Basel kon en zelfs naar Shanghai ga!
Tot slot wil ik vier personen noemen die chemisch gezien niets hebben bijgedragen, maar wel de factoren er omheen in bijzondere mate hebben veraangenaamd. Dit zijn mijn ouders, Gert Klijn en Willie Nuijens, mijn broer Jan en mijn vriendin Eveline van Raaij. Alle vier hartelijk bedankt, ik ben jullie veel verschuldigd!

Jaap

Contents

3. Effects of Catanionic Double-Tailed Vesicles on the Kemp Elimination Reaction

4. Effects of Various Long-Tailed Alcohols on the Vesicle-Catalysed Kemp Elimination Reaction

CHAPTER 1

INTRODUCTION

This chapter introduces the experimental work described in the following chapters. This work includes the study of the influence of four classes of additives on a number of properties of cationic vesicles. Particular attention is placed on the *catalytic* properties of these vesicles on a model deprotonation reaction. The results possess relevance for understanding non-enzymatic reactions proceeding at the polar-apolar interface of biological membranes, since biological membranes are complex mixtures of a wide variety of compounds.

In this chapter driving forces for surfactant aggregate formation in water will be discussed first with a particular focus on vesicles, since they can serve as mimics for biological membranes. Then the composition and some properties of biological membranes will be briefly discussed. A comparison between the properties of biological membranes and vesicles formed from synthetic amphiphiles will be made. Then an introduction into vesicular catalysis will be presented including important differences between catalysis in micellar and vesicular solutions. Finally, the aims of this thesis are outlined.

1.1 Water and Aggregation Processes in Water

1.1.1 Hydrophobic Hydration

Water is a special liquid due to its low molecular weight (and hence small molar volume) it has a high melting temperature and a high boiling temperature.[1,2] These properties are a result of a, for such a small molecule unique, three-dimensional hydrogen bond network, based on two hydrogen-bond donating and two hydrogen-bond accepting sites. The high heat capacity of water is related to this hydrogen-bonding ability. Another feature of the 3-D hydrogen bond network is that apolar molecules, such as hydrocarbons, have a limited solubility in water. Unlike, for example, glucose, hydrocarbons fit only poorly into the "structure" of water ("hydrophobic hydration"). As a result, the Gibbs energy of transfer of hydrocarbons from the gas phase to water is large and positive. For example, at 25°C the Gibbs energy of solvation ($\Delta_{solv}G$) of gaseous methane into a series of organic solvents (*n*-hexadecane to methanol) varies between 12.7 and 17.5 kJ mol^{-1}, whereas $\Delta_{solv}G$ in water is 25.5 kJ mol^{-1}.[3] Contrary to what might be anticipated on the basis of the large Gibbs energy, interactions between water and organic substrates are not unfavourable. In fact, London dispersion interactions between water and apolar solutes are quite favourable.[4]

At room temperature $\Delta_{solv}H$ of apolar gasses in water is favourable. However, the entropic contribution is much more unfavourable than that the enthalpy is favourable, and hence, the Gibbs energy is positive. Interestingly, as the surface area of the apolar molecule increases, the enthalpy decreases, but at the same time the entropy ($T\Delta_{solv}S$) decreases to almost the same extent, leading to $\Delta_{solv}G$ that is only weakly dependent on the size of the

apolar solute. In contrast, $\Delta_{solv}G$ of the same molecules in *n*-hexane decreases upon an increase in surface area, due to a decrease in enthalpy that is larger than the loss in entropy.

In addition, the heat capacity of transfer of apolar molecules to water is large and positive, leading to unfavourable enthalpic contributions at higher temperatures. However, since hydrogen bonds are progressively broken upon increasing the temperature, the entropic contribution decreases, and hence the Gibbs energy is almost constant with temperature.[5] As a consequence, at room temperature the large positive Gibbs energy originates from a large unfavourable entropic contribution, whereas at higher temperatures it results from a large unfavourable enthalpic contribution. Polar groups generally have a heat capacity that is slightly negative. Interestingly, the ability of arenes to form "weak" hydrogen bonds leads to a negative Gibbs energy.[6,7]

In conclusion, the large and positive heat capacity, the large entropic contribution at room temperature, the large enthalpic contribution at higher temperatures, and the poor solubility of organic substrates in water is what distinguishes hydrophobic hydration from other solvation effects.[8-12]

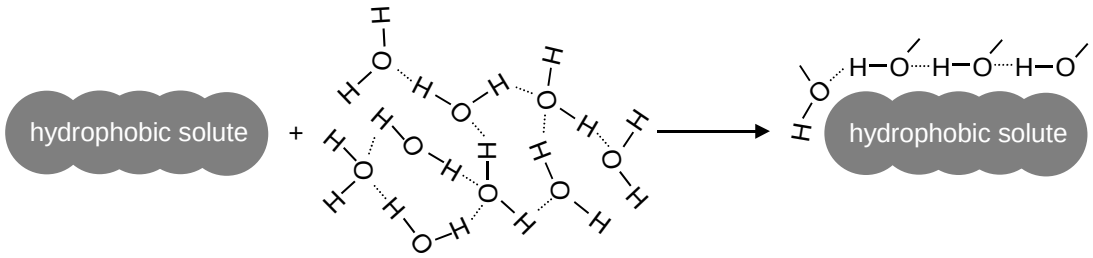

Scheme 1.1. *Schematic representation of the change in the three-dimensional hydrogen-bond network as a result of the hydration of an apolar solute.*

In 1945 Frank and Evans proposed the existence of iceberg-like water structures around apolar solutes.[13] In this model, water molecules are highly ordered in an ice-like structure. The unfavourable entropy term was connected to the formation of highly structured water, involving stronger or more hydrogen bonds in the hydrophobic hydration shell as compared to bulk water. This idea was widely accepted for some time until experiments started to cast doubt on this theory. Since then there have been many debates in the literature about the physical origin of hydrophobic hydration.[14-21] In the past few years, it has been accepted that in the hydrophobic hydration shell water molecules are oriented in such a way that a maximum number of hydrogen bonds is preserved.[17-21] This is the case when the water molecules have preferentially one of their hydrogen-oxygen bonds oriented tangential to the hydrophobic surface (Scheme 1.1).

1.1.2 Hydrophobic Interactions and Colloidal Aggregates

1.1.2.1 Important Parameters

When the hydrophobic hydration shells of two apolar solutes in water overlap, water molecules are released into the bulk solution. As a result, at room temperature this process is driven by a favourable change in entropy. Since this process is essentially a reversal of

hydrophobic hydration, similar thermodynamic trends are observed. Above a certain concentration of solute, the apolar solutes start to interact extensively, accompanied by a release of water molecules. Depending on the nature of the solute(s) this can lead to several type of processes. These can be divided into pairwise (1:1) interactions, interactions involved in small aggregates ("moving units"; aggregation number between 3 and 10) and bulk interactions. Examples of pairwise interactions are enzyme-inhibitor interactions[22] and hydrotrope complexes.[23] Examples of interactions playing a role in the formation of "moving units" occur when short (C_2-C_7) alcohols are dissolved into water.[24] Bulk interactions are involved in phase separation and colloidal aggregation.[25] Examples of the former are observed in mixtures of water and hydrocarbons. Above a threshold concentration the mixture becomes oversaturated in hydrocarbons and as a result forms a two-phase system. Molecules bearing both a polar and an apolar group may separate on a microscopic scale when dissolved in water. The mechanism and driving forces are similar as for hydrocarbons. However, transfer of a polar group from water to an organic solvent(-like) phase is highly unfavourable.[26,27] Therefore, macroscopic phase separation is unfavourable and hence the molecules reorganise in such a way that the favourable interactions of the polar groups with water are largely retained. As a result different types of colloidal aggregates are formed (Scheme 1.2).

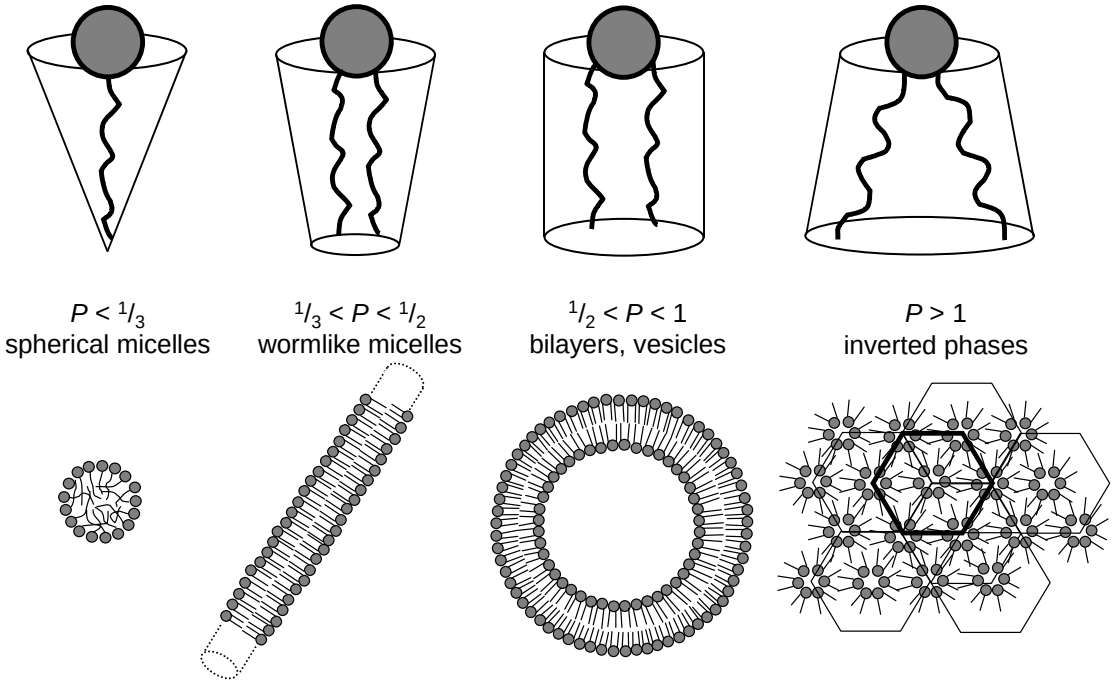

Scheme 1.2. *Schematic representation of structures that can be formed as a function of the packing parameter.*

Molecules that form these aggregates are known as surfactants (surface active agents) or amphiphiles ("αμφι φιλος" means "loved on both sides" in ancient Greek). The exact morphology of the aggregate is determined by a subtle interplay between the nature of the polar group and the size of the apolar group.[28,29] The packing parameter *P*, developed by Israelachvili and Ninham, gives a prediction of the structure of the aggregate that is formed:[30]

$$P = \frac{V}{a_0 l_c} \tag{1.1}$$

In this equation V is the volume of the hydrophobic part of the molecule, a_0 the mean cross-sectional head group surface area and l_c the length of the extended all-trans alkyl tail. As can be seen in Scheme 1.2, when the packing parameter is small (< $^1/_3$) the shape of the surfactant favours a large positive curvature, leading to small aggregates (micelles), whereas when the packing parameter is large (>1) there is a negative curvature leading to inverted structures (*e.g.* hexagonal, cubic, etc.). In between these extremes various structures may form, such as worm-like micelles, (flat) bilayer fragments and vesicles. Under certain circumstances also two different types of aggregates can coexist.
In the following two subparagraphs micelles and vesicles will be discussed in more detail, since they are relevant for understanding the observations described in the other chapters of this thesis. Description of other structures and their properties can be found in an excellent book by Evans and Wennerström.[25]

1.1.2.2 Micelles

Spherical micelles are usually formed from surfactants with a single alkyl tail that contains between 8 and 18 carbon atoms. The head group may be cationic, anionic, zwitterionic, or nonionic. Molecules with shorter alkyl tails, such as hydrotropes, form short-lived non-micellar aggregates. Longer alkyl tails cause the crystal packing to be more favourable than the solubilisation process into water. The concentration, above which surfactants aggregate into micelles, is called critical micelle concentration (cmc). The cmc is typically in the order of 10^{-6} to 10^{-2} M. Above the cmc the solution consists of micelles and monomers. The monomer concentration roughly equals the cmc. Due to the lack of ionic repulsion, the cmc of nonionic surfactants is typically 1-2 orders of magnitude lower than that for typical ionic surfactants. Increasing the size of the tail decreases the cmc. Due to the binding of counterions to the surface, the head group repulsion will be reduced and the high charge density in the polar-apolar interface of micelles (the Stern region) will be lowered. The counterion binding is typically in the order of 70-90 %.

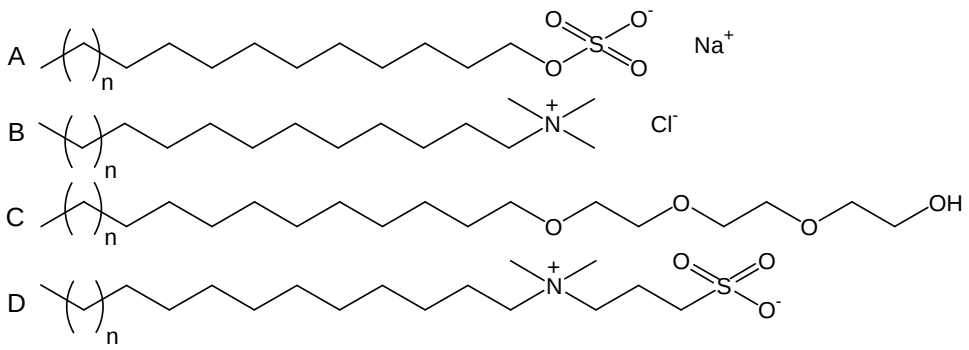

Scheme 1.3. *Examples of an anionic, a cationic, a nonionic and a zwitterionic micelle-forming surfactant (top to bottom). Sodium n-alkylsulfate (A); n-alkyltrimethyl-ammonium chloride (B); tri-ethylene glycol mono-n-alkyl ether (C); n-alkyldimethyl-propanesultaine (D). Typically n ranges from 1 (n-dodecyl) to 7 (n-octadecyl).*

Micelles are dynamic and relatively small aggregates (diameters around 5-6 nm).[31] Their average lifetime is in the order of milliseconds, but monomers enter and leave the aggregate on the microsecond timescale.[32] The polar head groups are on the outside, and the inside of the micelle consists of hydrocarbon chains that are largely in the liquid phase.[28] Typically, the number of molecules in a micelle is about 50-100, although there are many exceptions to this rough estimate. Some examples of micelle-forming surfactants are shown in Scheme 1.3.

At surfactant concentrations above 50-100 mM, interactions between individual spherical micelles start to become important. As a result, long worm-like micelles are formed. The packing parameter no longer predicts the correct aggregate morphology. Due to these elongated structures the viscosity of the solution increases.

1.1.2.3 Vesicles

Vesicles are usually formed from amphiphiles containing two alkyl tails (Scheme 1.4). Similar to micelles, vesicles are also formed above a critical concentration (critical vesicular concentration; cvc). Due to the doubling of the number of carbon atoms, the cvc is generally lower than the cmc of corresponding single-tailed micelle-forming surfactants (*e.g. n*-hexadecyltrimethylammonium bromide versus di-*n*-hexadecyldimethylammonium bromide). The morphology of vesicles is significantly different from the micellar structure. Vesicles consist of a double layer of surfactants that entraps an aqueous compartment (Scheme 1.2). This means that the outer leaflet has a positive curvature, and the inner leaflet a negative curvature.

Due to a decrease in curvature, vesicles have a diameter that that can range from 30 nm up to 10 µm. The average size and size distribution will depend on the method of vesicle preparation.[33] In the past a popular procedure was the so-called ethanol or chloroform injection method.[34-37] In this procedure the amphiphile is dissolved in a small amount of ethanol or chloroform in order to obtain a homogeneous solution. Then, a small volume is injected into water, usually followed by heating of the aqueous solution in order to evaporate the organic solvent. However, this latter process does not necessarily remove all the organic solvent from the mixture. Although the volume percentage of the organic solvent is usually small,[38] the effect on the resulting vesicles can be large.[39,40] Particularly the addition of ethanol can lead to undesired behaviour or properties.[40-44] These procedures are often used in order to obtain vesicles with a well-defined size (distribution). Nowadays other procedures are known to make vesicles with a well-defined size without the disadvantage of potentially having residual organic solvent in the vesicular solution. Small vesicles (*ca.* 30 nm in diameter) can be obtained by dissolving the amphiphiles in water, followed by extensive tip-sonication above the main phase transition temperature. Larger vesicles, up to several micrometers, can be obtained by dissolving the amphiphile in a small amount of an organic solvent, and subsequently evaporating the solvent by slowly rotating the tube containing the solution under a stream of nitrogen. In this way a slowly formed thin film of amphiphile is formed. After leaving this film under reduced pressure for several hours, all the organic solvent is evaporated. Then the film can be hydrated by addition of the appropriate amount of water. Repeatedly freezing the solution in liquid nitrogen and thawing it in warm water yields large multilamellar vesicles. If these vesicles are then

pushed several times through a membrane with a well-defined pore size, vesicles with that particular size are obtained.[31,45]

Due to the morphological differences compared with micelles, vesicles have different dynamics and stability. In addition, vesicles have a number of properties that are unknown for micelles, such as the phase of the tails, the permeability of the membrane towards ionic and nonionic molecules and the vesicle size and shape. In the following section these properties will be addressed in more detail.

Vesicles formed from a non-equimolar mixture of cationic and anionic (single-tailed) surfactants are thermodynamically stable, but vesicles formed from other surfactants or surfactant mixtures are metastable.[46,47] Hence, these latter vesicles precipitate with time, although the rate of this process varies between seconds and months. This approximately 10^7-fold time difference is the result of a very complex interplay of several processes that are involved in the precipitation process. Usually, with time vesicles aggregate, fuse and precipitate, or the tails crystallise, after which the bilayer fragments precipitate. Both processes can occur simultaneously as well. Fusion can be minimised using charged vesicles, or vesicles that are sterically stabilised. However, these processes depend on many more parameters, such as temperature, vesicle size and vesicle preparation method.[32,48,49]

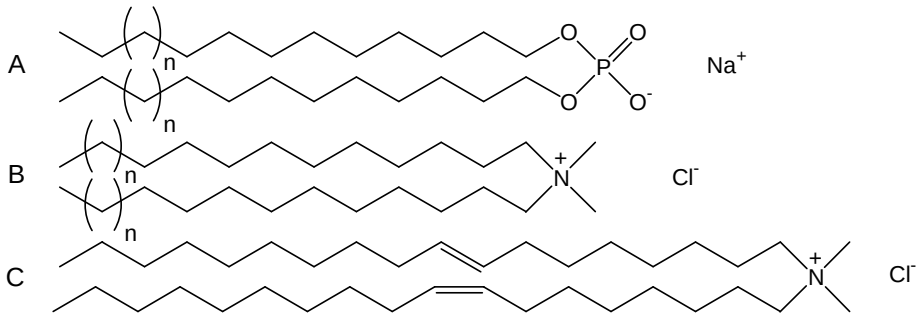

Scheme 1.4. *Examples of an anionic and two cationic vesicle -forming surfactant (top to bottom). Sodium di-n-alkylphosphate (A); di-n-alkyldimethylammonium chloride (B); dimethyldioleylammonium chloride (C). Typically n ranges from 1 (n-dodecyl) to 7 (n-octadecyl).*

Within the bilayer the alkyl tails can exist in phases that differ in their fluidity. At low temperatures the tails are in a highly ordered, rigid (gel-like) state (Scheme 1.5). Above a critical temperature (T_m) the tails are transformed into a more fluid (liquid-crystalline) state. In this state the tails have the freedom to adopt a large variety of conformations. Many of the vesicular properties depend on the phase of the tails, such as permeability, microviscosity, the ability to bind small molecules, susceptibility to pore formation, the extent of water penetration, amphiphile diffusion and vesicle fusion.[50] For example, below the T_m the microviscosity decreases with temperature. At the T_m the microviscosity makes a jump downwards, and then, above the T_m, the microviscosity decreases to a smaller extent.[51-53] Another example is given by the lateral diffusion of amphiphiles (movement of amphiphiles with respect to the bilayer plane). Lateral movement is diffusion-controlled when the tails are in the liquid-crystalline phase (10^{-11}-10^{-13} m^2 s^{-1}), but it becomes 100-1000 times slower when the tails are in the gel-like state.[50]

The main phase transition temperature is raised upon an increase in length of the alkyl tail. For example, di-*n*-dodecyldimethylammonium bromide has a T_m of 15°C,[54] and dimethyldi-

n-octadecylammonium bromide has a T_m of about 45°C. However, introduction of a double bond in both tails leads to a lowering of the T_m to temperatures below 0°C. The increase in T_m upon an increase in tail size is related to the increasing melting temperature of linear paraffins,[25] which is caused by a stronger crystal packing. Introduction of a double bond leads to a disturbance of the packing (especially in the case of a *cis* double bond). Hence the main phase transition temperature is lowered.

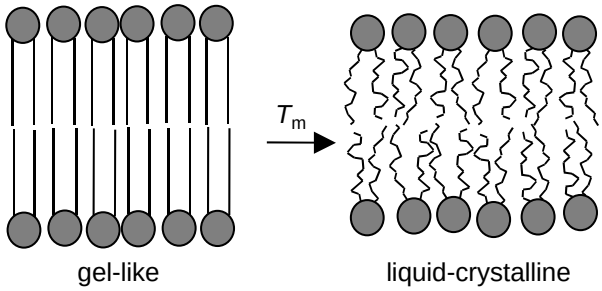

Scheme 1.5. *Schematic representation of a phase transition from a gel-like to a liquid-crystalline state.*

The permeability of the bilayer membranes towards small nonionic organic molecules is high,[55,56] but it is small (10^{-12}-10^{-16} m/s) towards ions, such as chloride ions,[57-59] since it requires the passage of polar groups through an apolar environment.[60] However, hydroxide ions and protons cross the bilayer relatively fast (10^{-6} m/s), despite their ionic character.[59,61-63] Diffusion of water is in the same order of magnitude, and the permeation of H^+ and OH^- ions has been linked to this observation.[64] Whereas water can just diffuse through membranes, random pore formation is required for other ions to cross the membrane. However, it has been suggested that the hydrated ions cross over the membrane rather than dehydrated ions, whereas the smaller hydrated ions pass more easily than larger ones.[65] On the contrary, it has also been shown that anionic vesicles are impermeable towards hydroxide ions,[66] and cationic vesicles only poorly permeable.[67] It has been suggested that permeation of a hydroxide ion requires (slow) permeation of an inert anion in the opposite direction in order to maintain charge neutrality.[68] As a result, the fast permeation of hydroxide ions might be slower depending on the inert ion. The permeation rate constant is estimated to be 10^{-5}-10^{-3} s^{-1}.[69]

Around the main phase transition temperature (and also around other transitions[70]) the membrane is usually more permeable than below or above this temperature.[65,70-76] Addition of single-tailed micelle-forming surfactant enhances pore formation and hence ions diffuse through the membrane more easily.[77]

In accordance with the crossing of small ions, flip-flop (transfer) of amphiphiles from the inner to the outer leaflet and vice versa is also a slow process (k=5· 10^{-5} s^{-1}),[60] but flip-flop is fastest around the T_m.[78,79] Apparently, around the T_m the bilayer packing is not very efficient leading to extensive pore formation or packing defects. This is further exemplified by the observation that around the T_m vesicles are most susceptible to fusion.[80]

1.2 Biological Membranes

1.2.1 General Properties

Vesicles are often used as mimics for biological membranes.[32,48,81] However, besides compartmentalising the cell, biological membranes are much more complex and fulfil a number of vital functions for living cells. The type of function and the conditions under which these functions have to be fulfilled, determine the composition of the membranes. Each cell has a number of membranes with each their own composition. For example, the nucleus requires a different type of membrane than the membrane which compartmentalises the cell. A major function of membranes is to carefully control which and how many molecules can enter and leave the cell. These functions rely on strongly specific recognition of those molecules. Failure of this mechanism will lead to malfunctioning of the cell, and in the worst case to cell death.
Through evolution nature has developed membranes that are capable of being adjusted for their task by just using a different composition or by modification of the compounds that make up membranes. For example, whereas most cells only need to survive around neutral pH and ambient temperatures, other cells such as those of the Sulfolobus Acidocaldarius survive at temperatures of around 85°C and pH 2 to 3 by just slightly modifying some of its components.[82-84] Despite this large variety of requirements, all membranes are composed of similar classes of compounds. These classes are (glyco)lipids, steroids and proteins.[85-88]

1.2.2 Components of Biological Membranes

1.2.2.1 Lipids

Despite the wide variety of lipid structures,[85-88] their general structure is similar. They consist of three building blocks. In these building blocks there is a large variety of possible structures, leading to thousands of potential final structures (Scheme 1.6). Interestingly, this is quite similar to the way that most factories construct their products. The use of (simple) standard building blocks makes it easy to design products that meet specific requirements without the need to completely redesign a new product. In this way many different products can be designed from just a few building blocks. It is not only cheap, but also very efficient. A nice example is given by IKEA, where costumers can design their own cupboards from three main building blocks (shelves, vertical framework, sideways framework).[89]
The polar building block of the lipid (head group) is nonionic, zwitterionic or anionic, the apolar building block (tails) typically contains 16 to 24 carbon atoms. In between the tail and the head group is the third building block (linker) that can be glycerol- or serine (sphingomyelin)–based. The name of a phospholipid is usually (but not necessarily) based on the structure of the head group in combination with the linker. For glycerol-based lipids the name is usually derived from the type of head group. Important lipids include phosphatidylcholine (PC) and phosphatidylethanolamine (PE; Scheme 1.6). Zwitterionic and

anionic lipids with a serine-based linker are usually referred to as sphingomyelins (SM). The structure of the tails is not included in the name.

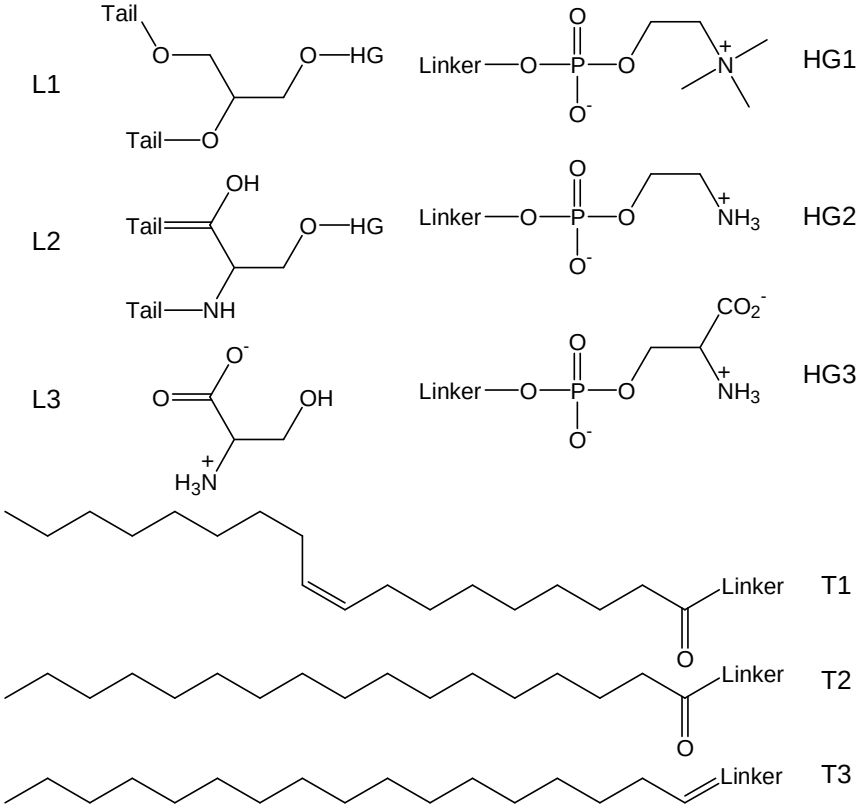

Scheme 1.6. *Some examples of the building blocks of natural occurring phospholipids. Head groups (HG): phosphatidylcholine (PC; HG1), phosphatidylethanolamine (PE; HG2) and phosphatidylserine (PS; HG3). Linkers (L): Glycerol (L1) and Serine-based linker (L2). L3 is the α-amino acid serine. Tails (T): Oleyl (mainly cis; T1) and palmitoyl (T2 and T3). T3 can only be linked to the 1-position in L2. T1 and T2 can be connected to both linkers, but not to the 1-position in L2.*

Nevertheless, the tails are the most important part of the lipid, since they control most of the properties. The tails of phospholipids often contain one or more double bonds. Typically, the number of tails that contains one or more double bonds varies between 50 and 75% (Table 1.1).[90] The tails of SMs (Scheme 1.7) contain considerably fewer double bonds. The origin and function of this observation will be discussed in Section 1.2.3.2. The composition of the tails depends not only on the type of membrane, but also on the head group to which the tails are attached. For example, tails connected to a phosphatidylcholine head group contain 20-30 mol% *n*-hexadecyl tails, whereas the tails connected to a phosphatidyl-ethanolamine contain almost no *n*-hexadecyl tails.

The reason for the presence of double bonds in the tails is that the double bonds maintain the fluid structure of the bilayer, and thereby prevent crystallisation of the tails. For example, vesicles formed from synthetic amphiphiles can break up into fragments below the main phase transition temperature.[91,92] Most of the double bonds have a *cis*-configuration since this has the most pronounced effect on the fluidity. The main phase transition temperature of a phospholipid containing a *trans* double bond is in between the main phase

transition temperature of a saturated tail and one containing a *cis* double bond. In animal cells phospholipids containing both a saturated and an unsaturated tail have the latter tail usually attached to the *sn*-2 position.[86]

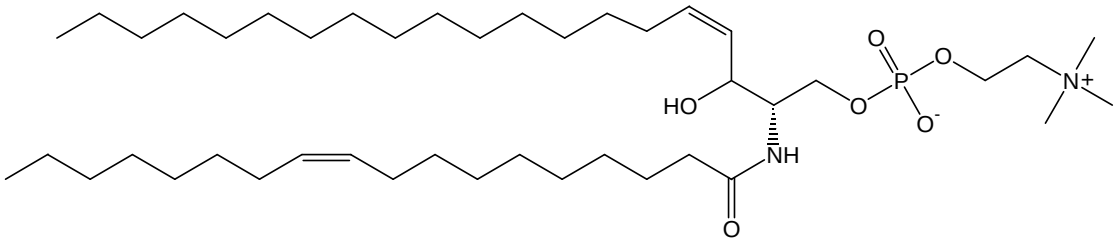

Scheme 1.7. *Example of a sphingomyelin (SM).*

Certain bacteria can adapt the amounts of *cis* and *trans* double bonds in their membranes as a response to fluctuations in the external temperature.[93] In extreme cases (high temperatures) bacteria are known to produce membrane-spanning amphiphiles (bola-amphiphiles), that essentially are two phospholipid molecules connected via the tail ends.[84] Other special biological lipid tails include ladderanes.[94]

As discussed, the variety in linkers is limited to only two types of linker. One type is the glycerol-based linker and the other type a serine-based linker. They find their use in their combined action, *i.e.* the fact that both types of linkers are present within the same membrane. Their function will be discussed in more detail in Section 1.2.3.2.

The head groups of phospholipids are nonionic, anionic or zwitterionic. However, they are present in a large variety of structures, which are often closely structurally related (*e.g.* compare PC vs. PE). For each of the individual lipids their function in biological membranes is not clear. Hence, their importance probably comes, just like the linkers, from a combined action in a complex mixture in the membrane.

Table 1.1. *Composition of the tails of a few selected cellular membranes (in mol%).*

Tail[a)]	Brain PC	Heart PC	Brain PE	Heart PE	Milk SM
16:0	31	23	5	1	19
18:0	16	6	19	30	3
18:1	39	13	31	4	
18:2	1	43	1	21	
20:4	5	6	19	30	2
22:6	2		9		
other	6	9	16	14	76[c)]
%U[b)]	51	69	71	65	5

[a)] 16:1 means a tail with sixteen carbon atoms and one double bond.

[b)] Mole percentage of unsaturated tails. [c)] Other tails are 20:0 (1%), 22:0 (19%), 23:0 (33%), 24:0 (20%) and 24:1 (3%).

Glycolipids (GL), *i.e.* lipids with a nonionic or anionic oligosaccharide head group, deserve special attention, since they are important for the interactions of a cell with the environment. Their function is broad, ranging from cell adhesion to signal transduction.[96,97] They play a major role in recognition processes by viruses, toxins and bacteria.[98,99] However, many of the details remain not very well understood until now.[100,101] Their behaviour as single component in aqueous solutions has been excellently summarised.[102] In order to allow specificity in their interactions, there is a wide variety of GLs with structural variations in tail, linker, and, most importantly, in the head group. The head group can be as simple as a single sugar, and as complex as a branched oligosaccharide chain (Scheme 1.8). Up to 25 mol% of biological membranes can consist of GLs.[28,88]

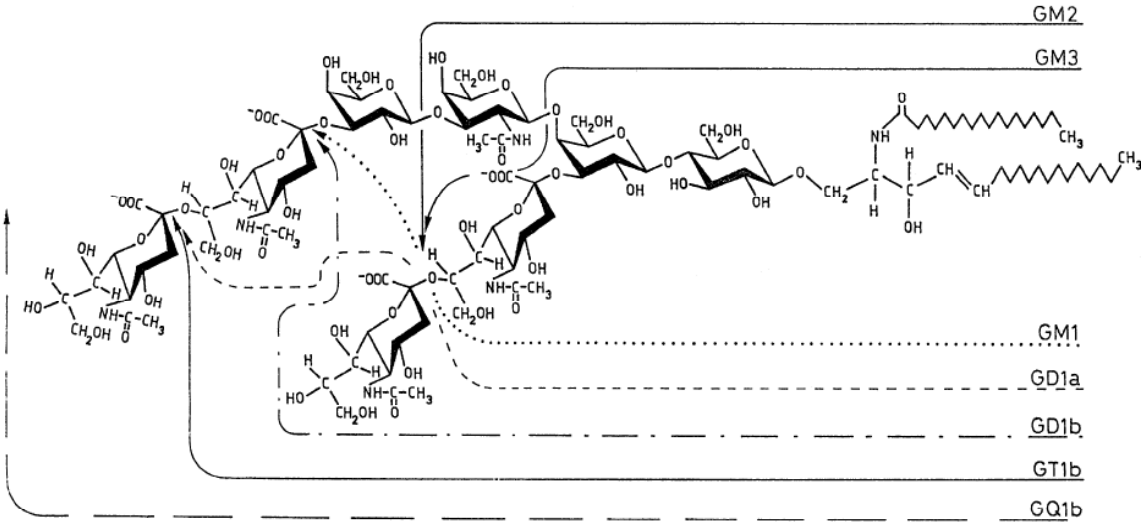

Scheme 1.8. *Example illustrating the complex structure of glycolipids. This picture, for example, represents seven different glycolipids. Taken from Tettamanti et. al.*[95]

The biosynthesis of lipid molecules is a complex and multistep and -path process regulated by a series of enzymes. Most of the lipids are synthesised in the endoplasmic reticulum,[103] but also in other places lipids are synthesised, degraded or repaired.[104,105] Briefly, the general procedure of the biosynthesis[85] of glycerol-based phospholipids starts with L-glycerol-3-phosphate (**1**; Scheme 1.9) to which two fatty acid chains are esterified at the hydroxyl groups on the glycerol. The resulting phosphatidic acid (**2**) is then esterified on the phosphoryl group to yield the required phospholipid (**3**). In nerve and muscle cell membranes considerable amounts of plasmalogens (**4**) are present. In these lipids an ether linkage replaces the ester linker on the *sn*-1 of the glycerol.[106]

Biosynthesis of sphingomyelin-based phospholipids starts with serine (**5**) to which a fatty acid is connected via a double bond. The resulting molecule is known as sphingosine (**6**), which is the only naturally occurring cationic surfactant at physiological pH.[107] Additional attachment of another fatty acid via an amide bond leads to ceramides (**7**). Then it is phosphorylated and the appropriate head group is attached, which leads to sphingomyelin (**9**).

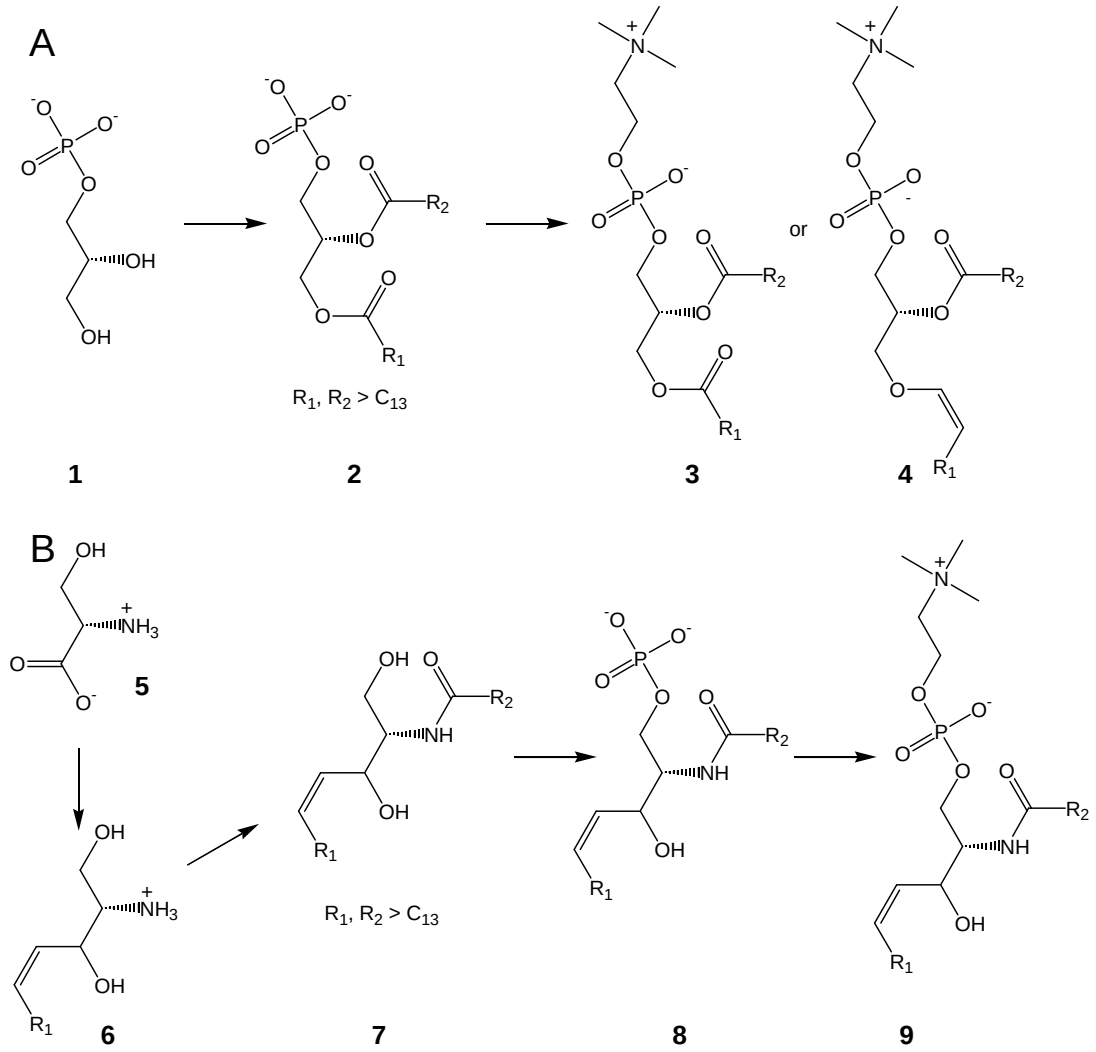

Scheme 1.9. *Simplified representation of the biosynthetic pathway of glycerol-based phospholipids (A) and sphingomyelin-based phospholipids (B).*

The role of ceramides and sphingosine in biological membranes is strongly controversial (over 4000 papers). It has been linked to being messenger for apoptosis (programmed cell death) as a result of sphingomyelin hydrolysis,[108-112] or alternatively to play a role in membrane permeability (channel formation), fusion and other membrane properties.[113] It is also possible that the latter properties are involved in apoptosis.[114]

1.2.2.2 Steroids

Steroids are the second major component in biological membranes. Cholesterol and its derivatives, such as cholate (Scheme 1.10) are the most important contributors. Many studies on cholesterol incorporated into model membranes have been performed, much less attention has been paid to derivatives of cholesterol. However, usually the effect of other steroids is much less pronounced compared to cholesterol.[115] Biological membranes usually contain up to 30 mol% of cholesterol,[87,88] although mole fractions up to 67% have been

isolated from certain membranes.[116,117] Other derivatives of cholesterol that are commonly found in biological membranes include desmosterol, stigmasterol and ergosterol.[118]

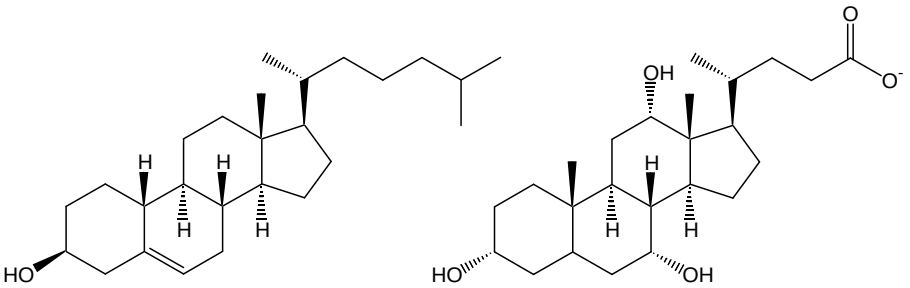

Scheme 1.10. *Cholesterol (left) and cholate (right).*

Incorporation of cholesterol improves the chain packing (condensing effect; decrease in the mean molecular area),[119-121] leading to segregation into cholesterol-rich and cholesterol-poor domains above a critical mole fraction.[120,122] In addition, the lateral diffusion of phospholipids decreases upon increasing amounts of cholesterol,[120] as does the permeability towards water[58,123], small ions,[124,125] fluorescent dyes[121,126] and nonionic hydrophilic molecules.[118,127-129] Also non-enzyme mediated flip-flop between inner and outer leaflet is strongly reduced.[79] Interestingly, despite the improved packing, the main phase transition temperatures are hardly affected upon addition of cholesterol.[130-132] However, the transition severely broadens and the enthalpy of the transition decreases at higher mole fractions of cholesterol. This indicates that the corresponding peaks in DSC scans are due to domains poor in cholesterol, since vesicles with a high mole fraction of cholesterol have no transition.[71] In membranes containing several types of lipids, cholesterol prefers to be near those with the lowest phase transition temperature.[131,133,134] Most of the above-mentioned properties of cholesterol do not depend much on the structure of the tails of the lipid.[58,115,131,133,134]

The mechanism through which cholesterol acts is not well understood. Van der Waals interactions alone are not sufficient to explain the above-mentioned observed effects. Therefore, several authors have pointed to the presence of a hydroxyl group in the 3β position of cholesterol-based steroids as being a key factor in their activity.[130] It has been claimed that it forms hydrogen bonds with the carbonyl of the phospholipids, but this appears to be unlikely.[135] The unsaturation in the B-ring has also been taken as the origin of the relatively large condensing effect.[115]

1.2.2.3 Proteins

Proteins control a wide variety of processes and therefore many different proteins are present in membranes. Processes being controlled by proteins include the transport processes between the inner and outer part of the cell and reactions at the surface of the cell that maintain the structural integrity of the membrane. In this thesis, the behaviour of membrane-bound proteins and their interactions with lipids and the cellular environment will not be further discussed.

1.2.3 Features of Biological Membranes

1.2.3.1 Composition

In order to get an idea of the relative abundance of several phospholipids and steroids, the composition of three biological membranes is shown in Table 1.2. The composition of the tails of some phospholipids was already shown in Table 1.1. Being together about 75 mol% of the total lipid/steroid content, it is clear that phosphatidylcholine (PC), phosphatidylethanolamine (PE) and cholesterol are the main components of biological membranes. However, their relative amounts can vary, even if one compares membranes from the same type of cell, but originating from different animals.

Table 1.2. *Composition of a few selected cellular membranes (in mol%).*

Lipid/Steroid	Erythrocyte (human)[86]	Erythrocyte (rat)[85]	Mitochondrion (rat)[85]
PC	25	31	48
PE	22	15	24
PS	10	7	2
SM	18	8.5	4
Cholesterol	25	24	4
GL[a)]	n.d.[b)]	3	-
PI[c)]	n.d.[b)]	2	10
PA[d)]	n.d.[b)]	0.1	1
others[e)]	-	-	13

[a)] Glycolipid. [b)] Not determined. [c)] Phosphatidylinositol. [d)] Phosphatidic acid .
[e)] Others include phosphatidylglycerol and cardiolipin.

1.2.3.2 Lateral and Transverse Asymmetry

Knowledge of the composition of biological membranes is important. However, understanding their local organisation is crucial if one wants to understand the details of how biological membranes operate. For example, cholesterol and sphingomyelins (SM) are known to form liquid-ordered domains ("rafts") in membranes, to which certain proteins prefer to bind.[135,136] These rafts, that are insoluble towards detergents, such as Triton X-100, are domains in which the lipids are ordered, similar to the gel phase, but they undergo fast diffusion as in the liquid phase. The driving force for this domain formation has been related to the relatively high abundance of saturated tails and the hydrophobic nature of the sphingosine linker in SMs, and the possibility to form hydrogen bonds via the amide functionality in the linker. Hydrogen bonds with cholesterol seem to play an important role as well,[137-140] whereas this type of interaction does not occur with glycerol-based phospholipids.[135] This additional interaction with SMs is required to explain the high concentration of cholesterol in these rafts, since cholesterol prefers to be in the presence of

phospholipids with the lowest T_m (Section 1.2.2.2). Lipids with the lowest T_m can be found in the liquid-disordered matrix formed by unsaturated phospholipids, rather than in the rafts formed by saturated SMs. Using a variety of techniques, the size of these domains has been estimated to be between 10 and 1000 nm in diameter. However, this large distribution of reported sizes indicates a lack of detailed knowledge of these domains rather than an understanding of the origin of and driving forces for raft formation.[141]

Several authors have attempted to unravel potential driving forces of segregation other than raft formation in model membranes.[142-150] The results are often in disagreement with each other, which makes understanding difficult. However, little debate exists over the observation that when a phospholipid with two identical tails is mixed with a phospholipid with tails which are at least four carbon atoms longer or shorter segregation into domains occurs.[151,152] The effect is not only related to the mismatch in size of the tail, but it can also be a result of the two lipids having different phases (liquid-crystalline versus gel-like).[153] The presence of cholesterol in such mixtures has led to controversy with respect to whether it strengthens segregation,[154-157] or diminishes it.[158-160]

In conclusion, segregation can occur as a result of several parameters. However, in model membranes segregation strongly depends on the structure of the lipids and the presence of additives in the bilayer. Its mechanism is unclear. In biological membranes raft formation plays a crucial role. However, the mechanism of raft formation remains only poorly understood.[136] The biological need for raft formation is related to protein sorting and cell signalling. A excellent review including more detailed information on raft formations and its function has been written by Brown.[135]

Another key factor in the functioning of biological membranes is the asymmetric distribution of lipids over the inner and outer leaflet. In order to perform their role in the interaction of cells with their environment glycolipids reside preferably in the outer leaflet of membranes.[161] In addition, also SM and PC are mainly found in the outer leaflet, whereas the amine-containing glycerophospholipids, such as PS and PE, are mainly found in the inner leaflet.[162]

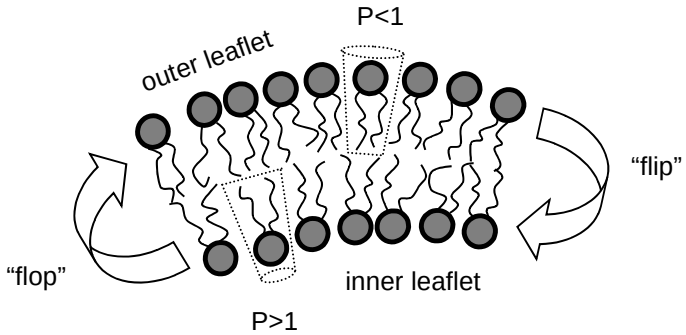

Scheme 1.11. *Schematic representation of flip-flop and the spatial requirements for phospholipids in the inner and outer leaflet of a cell membrane.*

Since spontaneous flip-flop is slow (several hours to days depending on the composition of the membrane),[60,79,163] especially in cholesterol-containing membranes,[79] nature makes use of three classes of proteins to promote and control flip-flop.[164,165] At this point it should be noted that, as depicted in Scheme 1.11, the transport of a lipid from the outer leaflet to the inner leaflet is called "flip", and that the reverse process is called "flop". Two of the protein classes involved, flippase and floppase, selectively transport lipids from one leaflet to the

other in an ATP-driven process. Flippase very selectively transports PS from the outer to the inner leaflet, but floppase seems to be less selective in its transport of lipids to the outer leaflet. A non-ATP-driven class of proteins, scramblase, randomly and non-selectively transports lipids between either leaflets. Scramblase is required in biological membranes since lipid biosynthesis typically occurs in only one of the leaflets. For example, PS, PC and PE are mainly synthesised in the inner leaflet of the endoplasmic reticulum.
Besides protein-mediated asymmetry, the asymmetric distribution is also reasonable from a physical point of view. Lipids, such as PE, have a packing parameter that is larger than 1 (Section 1.1.2.1; Scheme 1.11), which is required for having an efficiently packed inner leaflet.[166] In the outer leaflet lipids require on average a packing parameter smaller than 1, which is the case in PC and SM rich leaflets. Due to their large head group, glycolipids have a relatively small packing parameter. GM1 (Scheme 1.8), for example, forms micelles when dissolved in water.[167] These observations indicate that the asymmetry in biological membranes is, at least partially, maintained by a difference in the packing parameter.[168]

1.3 Catalysis of Organic Reactions in Aggregates

1.3.1 General Considerations

Catalysis of organic reactions by micelles has been studied for a long time.[169-171] In several of these early studies it was pointed out that these systems were model systems for biological membranes or even enzymes. Unfortunately, a model to fit the experimental data was absent until 1967 when Menger and Portnoy developed such a model (Scheme 1.12B) to account for the hydroxide-ion catalysed hydrolysis of several esters in both the aqueous and micellar phase of anionic and cationic micelles.[172] They adopted a model (Scheme 1.12A) used to calculate the catalysed and uncatalysed rate constant for the acetolysis of 2,4,7-trinitro-9-fluorenyl-*p*-toluenesulfonate in the presence of phenanthrene with which it forms a 1:1 complex.[173] Unfortunately, the model made it only possible to fit the data of solutions for which inhibition of the reaction was observed, since binding of hydroxide ions to the micellar surface was not taken into account. However, despite this limitation it was possible to prove that the hydroxide-ion catalysed reaction did not take place in anionic micelles.[174] Later several authors refined the theory to include binding of more than one organic substrate or hydrophilic ions.[175-186]

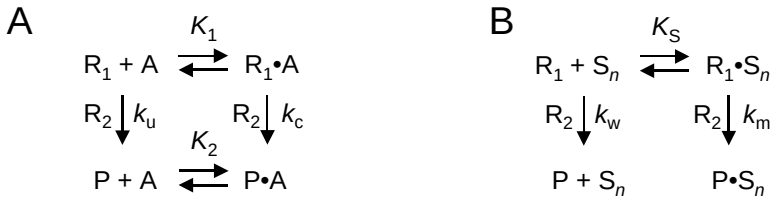

Scheme 1.12. *Schematic representation of the models used to describe catalysis by a 1:1 complex (A) and by micelle-formation. R_1 and R_2 are the reactants and P the products. K_1, K_2 and K_S are binding constants to A (non reactive additive), and S_n (micelle), respectively. k_u, k_c, k_w and k_m are the uncatalysed, catalysed, aqueous and micellar rate constant, respectively.*

In general, two major effects lead to catalysis of bimolecular reactions in micellar and vesicular aggregates.[184] The first effect is entropic in nature and results from substrate-aggregate binding. Charged micelles and vesicles provide a good environment for hydrophobic and oppositely charged molecules to bind, thereby increasing the chances of two substrates to meet and react because the effective reaction volume is reduced.[187] Particularly when one of the two reactants can bind as a counterion to the aggregate, efficient catalysis is found, since the concentration of head groups in the Stern layer of micelles is in the order of 1 to 5 M.[188,189] By contrast, when only one of the two reactants binds to the aggregate, inhibition is observed.

The second effect results from the decreased local polarity at the micellar and vesicular binding sites compared to water. Of course the latter effect is only beneficial when the organic reaction is accelerated in less polar environments. The decrease in polarity is due to a decrease in water concentration and the presence of the (apolar) tails of the amphiphile in the polar-apolar interface. This decrease in polarity is partially counteracted by the presence of polar (charged) head groups. The dielectric constant (at 25°C) of the micellar or vesicular surface is *ca.* 32, which is much lower that the dielectric constant of water (78).[190] Upon binding to aggregates, the reactants are (partially) dehydrated. As a result, the difference between the Gibbs energy of the initial state and the activated complex can change and hence the rate constant in the aggregate is affected. An increase in vesicular or micellar rate constant is particularly observed when one of the reactants is a hydrophilic counterion. The importance of dehydration for these types of reactions has been exemplified by gas phase experiments. It has been revealed that in S_N2 reactions dehydration of the ion is the major factor in the reactivity which may lead to rate accelerations up to 10^{17}.[191-196] Upon binding of one water molecule to the anion the rate constant drops 35%, whereas the heat of the reaction goes from -232 kJ $mole^{-1}$ when water is absent to +3 kJ $mole^{-1}$ when 3 water molecules hydrate the anion.[192]

In reactions where the hydroxide ion is one of the reactants, attention should be drawn to the abnormal behaviour of hydroxide ions with respect to their bulk aqueous behaviour. For example, their mobility is high compared to other anions (similar relationship as between protons and other cations). Although the (complex) mechanisms for this high mobility are different for protons than for hydroxide ions, this special behaviour is a result of the structural similarity of these ions with water.[197-200] Little is known about the implications of this behaviour for micellar and vesicular catalysis where the hydroxide ion is one of the reactants.

The exact binding location of organic molecules in aggregates has long been under debate. However, it is now well established that fully apolar molecules, such as hydrocarbons, bind deeply into the bilayer or micelle. Introduction of any polar group leads to preferential binding at the polar-apolar interface.[201-204] In addition, the orientation of the reactive centre of the reactants with respect to the second reactant in the aggregate has been studied as well.[205-208] For example, if the reactive centre of a substrate is orientated towards the inner core of a bilayer or micelle the reaction with hydrophilic ions is slowed down or inhibited, rather than catalysed. However, in cases where the substrate is small, there is no restriction or preference in orientation or movement within aggregates.

For clarity and completeness, we will briefly address the most important features of the kinetic (mathematical) model as shown in Scheme 1.12B. Slightly different models exist, such as the one derived by Berezin[175-179] and the one derived by Romsted,[181] but they are

based on the same principles and lead to similar results. The model takes into account two pseudophases, an aqueous one and an aggregate pseudophase, in which the reaction proceeds with an aqueous rate constant (k_w) and the aggregate rate constant (k_{agg}), respectively. Therefore, the model is called the pseudophase model. Distribution of the reactants among the pseudophases can be calculated in two different ways, either using partition coefficients P (distribution is a function of the aggregate volume), or the binding constants K (distribution is a function of the aggregate concentration).[209]

When one of the reactants is a hydrophilic counterion in competition with inert ions to bind to the apolar (but charged) pseudophase, the pseudophase model with ion exchange (PPIE) can be used. This model considers the total fraction of bound reactive and inert ions to be independent of the concentration of surfactant. However, there is competition between the counterions to bind to charged surfaces. In systems with only one highly hydrophilic ion, such as hydroxide, cyanide and fluoride ions, these assumptions fail, and alternative models to account for ion binding have to be used.[183,210-213] In addition, charged surfactants with these types of counterions behave differently compared to "normal" counterions. For example, micelles with relatively low aggregation numbers, high cmc and/or a (variable) low counterion binding are formed,[214-220] or micelles are formed from surfactants that usually aggregate into vesicles.[221-223]

After considering the above-mentioned remarks, the observed rate constant can be calculated as a location- and rate-average of the reaction proceeding in the aqueous pseudophase and the aggregate pseudophase.

The reaction in the aggregate pseudophase should be corrected for the volume of the aggregate, since the reaction in the aggregate pseudophase only takes place in the volume of the aggregates, whereas the surfactant concentration is expressed as a function of the total volume. This correction is always somewhat troublesome, since the reaction does not necessarily have to take place in the whole volume of the aggregate.[224]

Finally, special care has to be taken with respect to parameter compensation, since this can play a major role in the analysis of the kinetic data.[183,225-229] A more detailed analysis of parameter compensation and the mathematical description of the pseudophase model can be found in Chapter 3.

1.3.2 Vesicular Catalysis

Ever since the design and synthesis of the first synthetic bilayer-forming amphiphiles by Kunitake[230,231] and Fendler[61] many reactions have been performed in the presence of vesicles derived from synthetic amphiphiles. One of the first examples of vesicular catalysis involves the unimolecular decarboxylation reaction of 6-nitrobenzisoxazole-3-carboxylate (6-NBIC; **10**) under basic conditions (Scheme 1.13). This reaction has been studied in detail both in a variety of solvents and in micellar solutions.[232-236] The rate constant strongly depends on the polarity of the medium (an increase in polarity increases the rate constant) and the ability to form hydrogen bonds to the carboxylate group (hydrogen bonds decrease the rate constant). For example, in the series water, methanol, ethanol, 1,4-dioxane, DMSO and HMPA[237] the rate constant relative to the rate constant in water is 1, 34, 135, 5400, 1.3×10^6 and 10^8, respectively. In vesicles formed from di-*n*-alkyldimethylammonium bromide

(n=1-7; Scheme 1.4B) the rate constant of the decarboxylation reaction is higher with respect to the aqueous rate constant, but also with respect to the rate constant in CTAB micelles (n-hexadecyltrimethylammonium bromide; Scheme 1.3A).[235] In micelles formed from CTAB the catalytic rate acceleration relative to water (k_{agg}/k_w) amounts to *ca.* 54 at 30°C. Rough estimates indicate that in cationic vesicles the catalytic rate acceleration is about 10^2 below the main phase transition temperature and 10^3 above the main phase transition temperature.[238,239] The origin of the difference in the catalytic rate acceleration below and above the main phase transition temperature is difficult to pinpoint, but probably arises not so much from a change in polarity,[240] but rather comes from a change in the mobility of water molecules near the amphiphile head groups.[241,242] Phospholipid liposomes catalyse the decarboxylation reaction of **10** about 4-15 times less efficient than synthetic cationic vesicles.[239]

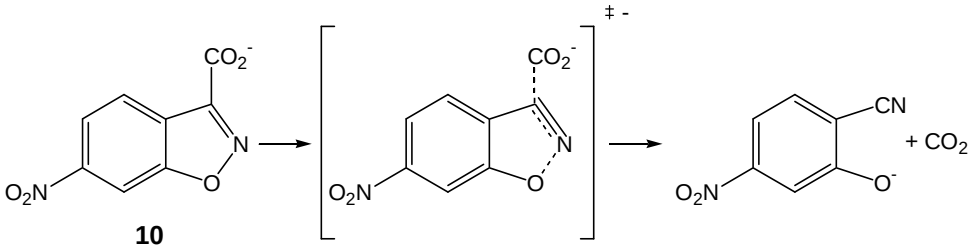

10

Scheme 1.13. *Unimolecular decarboxylation of 6-nitrobenzisoxazole-3-carboxylate (6-NBIC;* ***10****).*

For bimolecular reactions in the presence of vesicles several parameters have to be taken into account that are not important for bimolecular reactions in micelles. These parameters include the phase of the tails, the permeability of the membrane towards both reactants, the rate constant of the inner leaflet (endovesicular rate constant; Scheme 1.14) compared to the rate constant of the outer leaflet (exovesicular rate constant) and the rate constant as a function of the size of the vesicles.

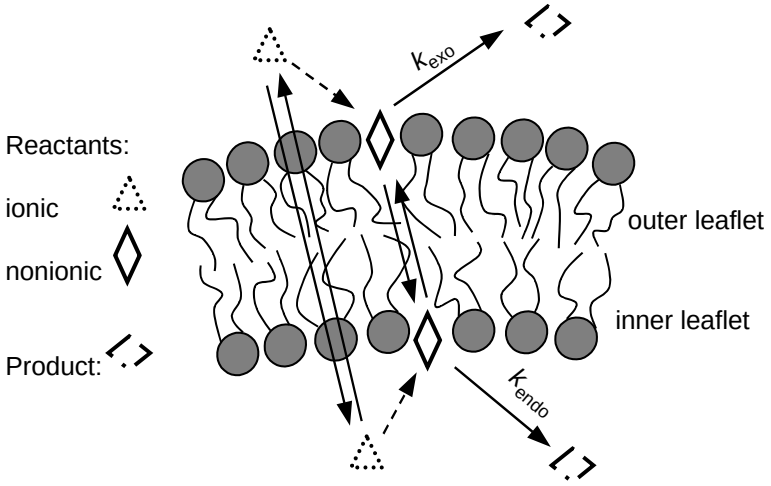

Scheme 1.14. *Schematic representation of the distribution of a nonionic and an ionic reactant in a vesicular solution over the inner and outer leaflet. The reaction proceeds with the rate constant k_{exo} in the interface of the outer leaflet and with k_{endo} in the interface of the inner leaflet.*

It is especially important to address the influence of the phase of the tails, since, besides its influence on the vesicular rate constant, some of the bilayer properties depend on the phase of the tails (Section 1.1.2.3) For example, the permeability is a function of the phase of the tails. Especially around the T_m an increase in the permeability occurs.
Permeability-dependent rate constants have been addressed in detail by Moss *et al.*.[243-245] They studied the reaction of **11** with a series of anions in vesicles formed from dimethyldi-*n*-octadecylammonium chloride at 25°C. At this temperature the tails are in the gel-like state. Using various thiolate anions it was possible to follow the permeation-rate dependent observed endovesicular rate constant relative to the non-permeation-dependent observed exovesicular rate constant. Similar permeation-rate dependent observed rate constants have been measured for another series of reactions.[246-248] Discrimination between the endovesicular rate constant and the exovesicular rate constant was lost by decreasing the size of the tails with two CH_2 units, since then the rate constants were measured around the T_m of di-*n*-hexadecyldimethylammonium bromide.[69,78,244,245,249] Around the T_m, the rate of permeation of the thiolate ions through the bilayer is faster than the rate constant, and hence permeation is no longer the rate-determining step for the endovesicular reaction. The permeation-dependence was also lost when single-tailed surfactants were added.[67] This dependence was also lost after addition of 0.2 wt% of 1-hexanol which lowers the T_m to 25°C.[245]

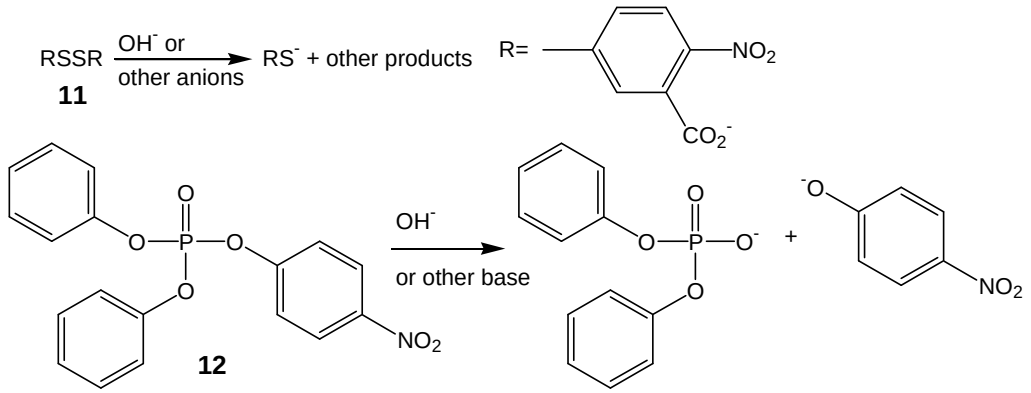

Scheme 1.15. *The reaction of 5,5'-dithiobis(2-nitrobenzoic acid) (DTNB; **11**) and p-nitrophenyl diphenyl phosphate (**12**) under alkaline conditions.*

Care has to be taken in assigning changes in absorbance to endo- or exovesicular rate constants, as is exemplified by the following example. In the vesicle-catalysed[250] alkaline hydrolysis of **12** a slow and a fast process were observed (Scheme 1.15).[251-253] The rate of deprotonation of a fluorescent dye indicated that permeation of the bilayer by hydroxide ions was fast on the time scale of the reaction and therefore the two processes were assigned to the observed endo- and exovesicular rate constant. It was found that the observed exovesicular rate constant is about 15-30 times faster than the observed endovesicular rate constant. However, they also observed that at most 20% of the reaction took place in the endovesicular phase. Later, the slow process was assigned to a slow reorganisation of vesicles after placing them under osmotic stress (a result of the kinetic experiment), which led to a small and slow change in turbidity.[254]
The phase of the tails alone on the rate constant were studied in the following examples where permeation of reactants did not play a role. As discussed above, the unimolecular

decarboxylation of **10** is about ten times faster above the T_m, as was measured by reducing the size of the hydrophobic tails.[235] The hydroxide-ion catalysed reaction of **13** (Scheme 1.16; Kemp elimination) and the imidazole-catalysed hydrolysis of an ester are also faster when the amphiphile is above the T_m.[255,256] When the amphiphiles are structurally varied in order to perform the kinetic experiments above the T_m at a constant temperature, usually the tails are decreased in length, since a decrease in tail length leads to a lowering of the T_m. In general, a decrease in tail length leads to a slightly higher local polarity, which usually leads to a lower vesicular rate constant. Instead a higher vesicular rate constant is mostly observed. Hence, this indicates that the small change in local polarity is not so important, but that an increase in fluidity of the tails is usually more important.
Alternatively to structural variation of the amphiphile, the influence of the phase of the tails can be studied by construction of an Arrhenius plot (log(*k*) versus 1/*T*). Upon increasing the temperature the Arrhenius plot of the imidazole-catalysed hydrolysis of an ester, described above, deviates from linearity around the T_m of the amphiphile, whereas above and below the T_m the experimental data points are on a straight line. Both the intercept and the slope of the straight lines change at the T_m. This illustrates that both $\Delta^{\ddagger}H^{\circ}$ and $\Delta^{\ddagger}S^{\circ}$ are affected by changing the phase of the tails.[257] However, the hydroxide-ion catalysed hydrolysis of the same ester shows no break in the Arrhenius plot. The alkaline hydrolysis of a different ester is relatively slowed down above the T_m.[258] These results show that not in all cases a change in fluidity of the membranes leads to a beneficial increase in the rate constant. In addition, the effect of a change in fluidity of the tails leads to a complex change of interactions as is indicated by changes in both $\Delta^{\ddagger}H^{\circ}$ and $\Delta^{\ddagger}S^{\circ}$.

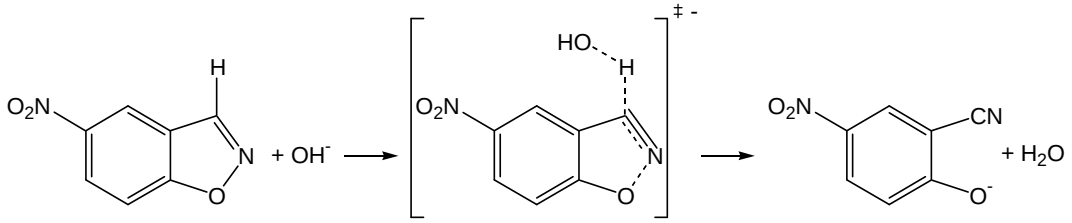

13

Scheme 1.16. *General base-catalysed deprotonation reaction of 5-nitrobenzisoxazole (5-NB;* ***13****)*

Different rate constant for the inner and outer leaflet were subject of study by Chaimovich *et al.*[259] By selectively binding of **11** to the inner leaflet of dimethyldi-*n*-octadecylammonium chloride vesicles, they were able to follow the reaction with hydroxide ions to both leaflets independently. It was found that **11** did not leak out of the vesicles in a period of 24 h, which is reasonable considering the phase of the tails and the fact that **11** is a dianion. They did not find a marked difference between the endo- and exovesicular rate constant, indicating that the inner and outer leaflet are not significantly different in structure.
Few studies concern vesicular catalysis as a function of the size of the vesicle. However, in two of these studies differently-sized vesicles were prepared by comparing sonicated vesicles and ethanol-injected vesicles.[39,253] As discussed in section 1.1.2.3, the addition of ethanol can induce changes in the properties, and hence comparison these two types of vesicles is dangerous. If the influence of ethanol in the vesicular solution is neglected, it can be concluded that the trend in the alkaline hydrolysis and thiolysis of *p*-nitrophenyl octanoate

as a function of vesicle size (between 22 and 285 nm) depends on the counterion (bromide or chloride) of the cationic amphiphile.[39] With increasing vesicle size the rate constants increased for vesicles with a chloride counterion, but decreased for vesicles with a bromide counterion. The hydrolysis of **12** is slowed down by increasing the vesicle size (between 50 and 160 nm).[253] In a third study, the rate of Diels-Alder reactions was measured as a function of the vesicle size (30 and 300 nm).[261] The vesicles were prepared by sonication (30 nm) or hydration of an amphiphile film and subsequent extrusion (300 nm). No significant change in the rate constant was observed.

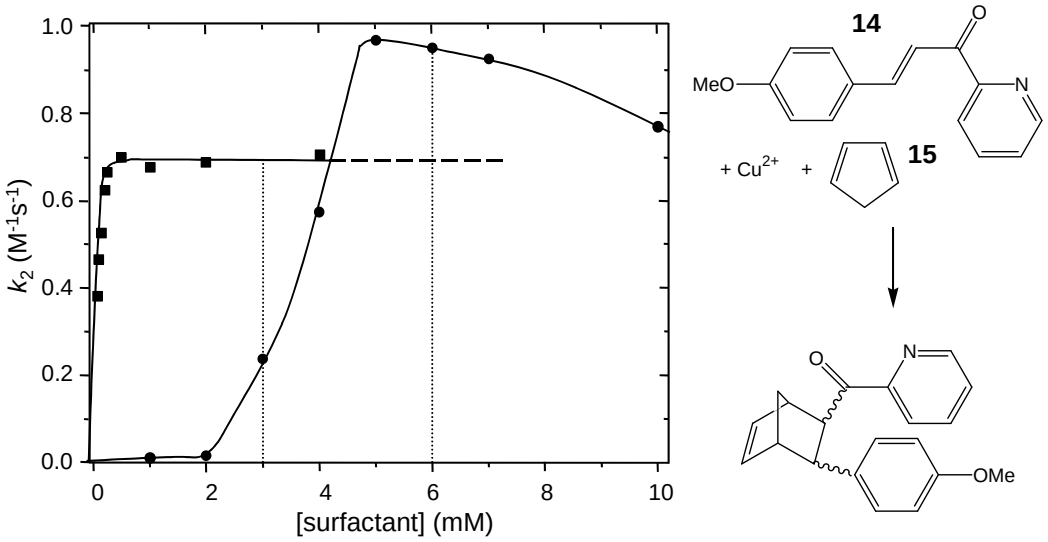

Figure 1.1. *Example of complications arising from comparing observed rate constants for the Diels-Alder reaction of* ***14*** *and* ***15*** *in the presence of* Cu^{2+}*, catalysed by micelles (●) and vesicles (■). The rate constants presented are the observed (pseudo)-first-order rate constants divided by the concentration of* ***15****. Taken from Rispens et al.*[260]

In many of the studies observed rate constants at a certain amphiphile concentration are compared with each other. In these cases care has to be taken, since the observed rate constant depends both on the distribution of the reactants between the aqueous and vesicular phase and the vesicular and aqueous rate constants as discussed in 1.3.1. In summary, the distribution of the reactants over the two pseudophases is a function of both the binding constant of the reactants and the amphiphile concentration. The binding constant and the vesicular rate constant depend on the structure of the amphiphile and temperature. Hence, due to these complex dependences, it can be ambitious to compare observed rate constants. For example, several authors have compared observed rate constants in micellar and vesicular solutions, leading to the conclusions that vesicles are better catalysts,[235,245,253,256,262,263] or that micelles are better catalysts.[246,247,264,265] An example is given in Figure 1.1, where the observed rate constants of the micelle- and vesicle-catalysed Diels-Alder reaction of **14** and **15** at two different surfactant concentrations are compared.[260] It can be concluded that both vesicles and micelles are better catalysts depending on the concentration of surfactant at which this comparison is made. At 3 mM surfactant the ratio of the observed micellar rate constant and observed vesicular rate constant ($k_{obs,mic}/k_{obs,ves}$) is 0.4, whereas at 6 mM this ratio is 1.4.

Finally, examples of the wide variety of reactions that can be catalysed in the presence of vesicles are given. These include peptide bond cleavage,[264] bromination,[265] ester hydrolysis,[266] ester thiolysis,[267] DNA hydrolysis,[268] oxidation,[269] electron transfer reactions,[270-274] diazo coupling reactions,[262,275] arenediazonium ion decomposition,[276] styrene polymerisation[277] and nitroso group transfer.[278] It has been proven that in these cases the observed rate constants were higher than those in water, but no new insights into the mechanism of vesicular catalysis were obtained.

1.4 Aim and Outline of this Thesis

Due to its relative simplicity, both in handling and interpretation (discussed above), micellar catalysis is more widely discussed in the literature than vesicular catalysis.[185] However, vesicles are much more akin to biological membranes than micelles. This does not necessarily mean that studying vesicular catalysis leads to further insight into processes in biological membranes. So far, most studies involving vesicular catalysis have been mainly carried out in single-component systems, *i.e.* amphiphiles are the only hydrophobic component in the system. By contrast, biological membranes have a complex composition with many different components. Studies of properties of model membranes involving phospholipids, sphingomyelins and steroids are important and have a high biological relevance, but understanding of the observations is often troubled by multiple possible interactions between the components. This is exemplified by the extensive discussion about the origin of raft formation, and which interactions are driving forces for this phenomenon. Therefore, limiting the number of possible interactions between the components, but introducing small structural variation within a series of additives, might reveal some of the factors that are important in catalysis occurring in biological membranes.

Based on the considerations above, we decided to examine the influence of the composition of the vesicle bilayer on vesicular catalysis. A suitable probe reaction for these vesicles is the hydroxide-ion-catalysed deprotonation reaction of **13** (Kemp elimination). The mechanism of the E2 Kemp elimination reaction has been well studied,[279-281] and efficient catalysis has been found in micelles, vesicles, (synthetic) anti-bodies and modified cyclodextrines.[256,282-291] Important factors for significant rate enhancements were found to be desolvation of the base, a hydrophobic binding site and a decrease of the reaction volume as a result from binding of the two reactants to a hydrophobic binding site in an aggregate.

Dimethyldi-*n*-octadecylammonium chloride was selected as vesicle forming amphiphile, since its properties have been well studied (including vesicular catalysis; Section 1.3.2). In addition, it is structurally simple, which is beneficial for understanding interactions with its environment. Similar considerations were made in selecting a wide variety of additives. This choice of additives allows relatively easy correlation between the obtained results and the structural variation of the additives.

In vesicles, both reactants permeate fast through the bilayer and the two reactants are dependent on different parameters to bind to bilayers. Whereas **13** binds to vesicles due to hydrophobic interactions, the hydroxide ion only binds as a result of the electrostatic attraction. This introduces more independent parameters for different types of interactions.

Chapter 1 includes a brief introduction of hydrophobic interactions with the focus on aggregate formation. Specific attention is paid to vesicles and their general properties. Then the components and behaviour of biological membranes are discussed. In the last part vesicular catalysis as a mimetic medium for biological membranes is discussed, including parameters that are important in vesicular catalysis.
Chapter 2 describes the influence of the additives that are used throughout Chapter 3 to 6 on vesicle properties, such as vesicle shape and size, the main phase transition temperature and membrane polarity.
Chapter 3 describes the kinetic model that is derived in order to study the influence of the additives on vesicular catalysis. Parameters obtained from the analysis include the vesicular rate constant, the binding constant of the kinetic probe to the vesicle, the counterion binding to the charged head groups of the cationic amphiphile and the competition between the anions in solution to bind to the vesicles. The limitations of the kinetic model are discussed as well. The influence of the addition of anionic double-tailed amphiphiles on the probe reaction is delineated. The anionic amphiphiles introduced into the vesicles have either two decyl tails, or a decyl and an octadecyl tail.
Chapter 4 deals with the influence of long linear mono- and dihydric alcohols in the vesicles on the probe reaction. The monohydric alcohols include *n*-decanol, *n*-octadecanol and oleyl alcohol. The dihydric alcohol is 3-*n*-octadecyloxy-propane-1,2-diol (batyl alcohol). Despite their structural similarity each alcohol has its own specific effect.
Chapter 5 discusses the effects on the catalysis of the presence of ethylene glycol units in the Stern region. The ethylene glycol units are attached via two different hydrophobic anchors. One anchor is a hexadecyl tail, the other is based on a (cationic) SAINT-2 amphiphile (*N*-methyl-4-(dioleylmethyl)pyridinium chloride).
Chapter 6 reports the influence of glucose and maltose, anchored into the bilayer, on the catalytic decomposition of **13**. These additives were chosen as mimics for glycolipids. Glycolipids play an important role in the structural integrity of biological membranes and the communication of cells and their environment.
Chapter 7 reviews the most important conclusions from this thesis and, based on that, suggests new research projects in the field of vesicular catalysis and its relevance for understanding biological membranes.

1.5 Acknowledgements

Theo Rispens is acknowledged for fruitful discussions on hydrophobic interactions and catalysis in aggregates.

1.6 References

(1) *Water: A Comprehensive Treatise* Volume 1-7; Franks, F., ed.; Plenum Press: New York, **1982**
(2) Ball, P. *H_2O: A Biography of Water*; Weidenfeld and Nicholson: London, **1999**.
(3) Abraham, M. H. *J.Am.Chem.Soc.* **1982**, *104*, 2085-2094.
(4) Hildebrand, J. H. *Proc.Natl.Acad.Sci.USA* **1979**, *76*, 194.
(5) Lee, B. *Biopolymers* **1991**, *31*, 993-1008.
(6) Makhatadze, G. I.; Privalov, P. L. *Biophys.Chem.* **1994**, *50*, 285-291.
(7) Costas, M.; Kronberg, B. *Biophys.Chem.* **1998**, *74*, 83-87.
(8) Gill, S. J.; Dec, S. F.; Olofsson, G.; Wadso, I. *J.Phys.Chem.* **1985**, *89*, 3758-3761.
(9) Naghibi, H.; Dec, S. F.; Gill, S. J. *J.Phys.Chem.* **1987**, *91*, 245-248.
(10) Madan, B.; Sharp, K. A. *J.Phys.Chem.* **1996**, *100*, 7713-7721.
(11) Sharp, K. A.; Madan, B. *J.Phys.Chem.B* **1997**, *101*, 4343-4348.
(12) Madan, B.; Sharp, K. A. *J.Phys.Chem.B* **1997**, *101*, 11237-11242.
(13) Frank, H. S.; Evans, M. W. *J.Chem.Phys.* **1945**, *13*, 507-532.
(14) Bowron, D. T.; Filipponi, A.; Lobban, C.; Finney, J. L. *Chem.Phys.Lett.* **1998**, *293*, 33-37.
(15) Graziano, G. *J.Chem.Soc., Faraday Trans.* **1998**, *94*, 3345-3352.
(16) Otto, S.; Engberts, J. B. F. N. *Org.Biomol.Chem.* **2003**, *1*, 2809-2820.
(17) Finney, J. L.; Soper, A. K. *Chem.Soc.Rev.* **1994**, *23*, 1-10.
(18) Soper, A. K.; Luzar, A. *J.Phys.Chem.* **1996**, *100*, 1357-1367.
(19) Blokzijl, W.; Engberts, J. B. F. N. *Angew.Chem.,Int.Ed.Engl.* **1993**, *32*, 1545-1579.
(20) Pratt, L. R.; Pohorille, A. *Chem.Rev.* **2002**, *102*, 2671-2691.
(21) Southall, N. T.; Dill, K. A.; Haymet, A. D. J. *J.Phys.Chem.B* **2002**, *106*, 521-533.
(22) Talhout, R.; Villa, A.; Mark, A. E.; Engberts, J. B. F. N. *J.Am.Chem.Soc.* **2003**, *125*, 10570-10579.
(23) Buurma, N. J.; Blandamer, M. J.; Engberts, J. B. F. N. *Adv.Synth.Catal.* **2002**, *344*, 413-420.
(24) Zana, R. *Adv.Colloid Interface Sci.* **1995**, *57*, 1-64.
(25) Evans, D. F.; Wennerström, H. *The Colloidal Domain: Where Physics, Chemistry, Biology and Technology Meet*; Wiley-VCH: New York, **1999**.
(26) Marcus, Y. *Pure Appl.Chem.* **1990**, *62*, 899-940.
(27) Hefter, G. T. *Pure Appl.Chem.* **1991**, *63*, 1749-1758.
(28) Tanford, C. *The Hydrophobic Effect: Formation of Micelles and Biological Membranes*; Wiley: New York, **1980**.
(29) Sein, A.; Engberts, J. B. F. N. *Langmuir* **1995**, *11*, 455-465.
(30) Israelachvili, J. N.; Mitchell, D. J.; Ninham, B. W. *J.Chem.Soc., Faraday Trans.2* **1976**, *72*, 1525-1568.
(31) Johnsson, M.; Wagenaar, A.; Engberts, J. B. F. N. *J.Am.Chem.Soc.* **2003**, *125*, 757-760.
(32) Fendler, J. H. *Membrane Mimetic Chemistry*; Wiley: New York, **1982**.
(33) Abuin, E. B.; Lissi, E. A.; Aravena, D.; Zanocco, A.; Macuer, M. *J.Colloid Interface Sci.* **1988**, *122*, 201-208.
(34) Carmona-Ribeiro, A. M.; Chaimovich, H. *Biochim.Biophys.Acta* **1983**, *733*, 172-179.
(35) Cuccovia, I. M.; Feitosa, E.; Chaimovich, H.; Sepúlveda, L.; Reed, W. *J.Phys.Chem.* **1990**, *94*, 3722-3725.
(36) Cuccovia, I. M.; Sesso, A.; Abuin, E. B.; Okino, P. F.; Tavares, P. G.; Campos, J. F. S.; Florenzano, F. H.; Chaimovich, H. *J.Mol.Liq.* **1997**, *72*, 323-336.
(37) Feitosa, E.; Barreleiro, P. C. A.; Olofsson, G. *Chem.Phys.Lipids* **2000**, *105*, 201-213.
(38) Usually around 5 v/v%. In the case of ethanol, this leads to a concentration of ethanol of around 850 mM.
(39) Kawamuro, M. K.; Chaimovich, H.; Abuin, E. B.; Lissi, E. A.; Cuccovia, I. M. *J.Phys.Chem.* **1991**, *95*, 1458-1463.
(40) Blandamer, M. J.; Briggs, B.; Cullis, P. M.; Green, J. A.; Waters, M.; Soldi, G.; Engberts, J. B. F. N.; Hoekstra, D. *J.Chem.Soc., Faraday Trans.* **1992**, *88*, 3431-3434.
(41) Hui, F. K.; Barton, P. G. *Biochim.Biophys.Acta* **1973**, *296*, 510-517.
(42) Li, S. S.; Lin, H. N.; Wang, G. Q.; Huang, C. *Biophys.J.* **1996**, *70*, 2784-2794.
(43) Huang, C.; McIntosh, T. J. *Biophys.J.* **1997**, *72*, 2702-2709.
(44) Durvasula, R. V.; Huang, C. H. *Biochim.Biophys.Acta* **1999**, *1417*, 101-110.
(45) Johnsson, M.; Wagenaar, A.; Stuart, M. C. A.; Engberts, J. B. F. N. *Langmuir* **2003**, *19*, 4609-4618.
(46) Kaler, E. W.; Herrington, K. L.; Murthy, A. K.; Zasadzinski, J. A. N. *J.Phys.Chem.* **1992**, *96*, 6698-6707.
(47) Jung, H. T.; Coldren, B.; Zasadzinski, J. A.; Iampietro, D. J.; Kaler, E. W. *Proc.Natl.Acad.Sci.USA* **2001**, *98*, 1353-1357.
(48) Fendler, J. H. *Acc.Chem.Res.* **1980**, *13*, 7-13.

(49) Carmona-Ribeiro, A. M.; Yoshida, L. S.; Chaimovich, H. *J.Phys.Chem.* **1985**, *89*, 2928-2933.
(50) Raudino, A. *Adv.Colloid Interface Sci.* **1995**, *57*, 229-285.
(51) Lentz, B. R.; Barenholz, Y.; Thompson, T. E. *Biochemistry* **1976**, *15*, 4521-4528.
(52) Lentz, B. R.; Barenholz, Y.; Thompson, T. E. *Biochemistry* **1976**, *15*, 4529-4537.
(53) Shinitzky, M.; Barenholz, Y. *Biochim.Biophys.Acta* **1978**, *515*, 367-394.
(54) Marques, E. F.; Khan, A.; Lindman, B. J. *Thermochim.Acta* **2002**, *394*, 31-37.
(55) Hervés, P.; Leis, J. R.; Mejuto, J. C.; Pérez-Juste, J. *Langmuir* **1997**, *13*, 6633-6637.
(56) Heerklotz, H.; Seelig, J. *Biochim.Biophys.Acta* **2000**, *1508*, 69-85.
(57) Carmona-Ribeiro, A. M.; Yoshida, L. S.; Sesso, A.; Chaimovich, H. *J.Colloid Interface Sci.* **1984**, *100*, 433-443.
(58) Deamer, D. W.; Bramhall, J. *Chem.Phys.Lipids* **1986**, *40*, 167-188.
(59) Kaiser, S.; Hoffmann, H. *J.Colloid Interface Sci.* **1996**, *184*, 1-10.
(60) Kornberg, R. D.; Mcconnel, H. M. *Biochemistry* **1971**, *10*, 1111-1120.
(61) Tran, C. D.; Klahn, P. L.; Romero, A.; Fendler, J. H. *J.Am.Chem.Soc.* **1978**, *100*, 1622-1624.
(62) Nichols, J. W.; Deamer, D. W. *Proc.Natl.Acad.Sci.USA* **1980**, *77*, 2038-2042.
(63) Kachel, K.; Asuncion-Punzalan, E.; London, E. *Biochim.Biophys.Acta* **1998**, *1374*, 63-76.
(64) Bramhall, J. *Biochemistry* **1987**, *26*, 2848-2855.
(65) Georgallas, A.; MacArthur, J. D.; Ma, X. P.; Nguyen, C. V.; Palmer, G. R.; Singer, M. A.; Tse, M. Y. *J.Chem.Phys.* **1987**, *86*, 7218-7226.
(66) Moss, R. A.; Swarup, S. *J.Am.Chem.Soc.* **1986**, *108*, 5341-5342.
(67) Moss, R. A.; Bhattacharya, S.; Scrimin, P.; Swarup, S. *J.Am.Chem.Soc.* **1987**, *109*, 5740-5744.
(68) Or permeation of an oppositely charged ion in the same direction.
(69) Moss, R. A.; Bhattacharya, S.; Chatterjee, S. *J.Am.Chem.Soc.* **1989**, *111*, 3680-3687.
(70) Singer, M. A.; Finegold, L. *Biochim.Biophys.Acta* **1985**, *816*, 303-312.
(71) Papahadjopoulos, D.; Jacobson, K.; Nir, S.; Isac, T. *Biochim.Biophys.Acta* **1973**, *311*, 330-348.
(72) Antonov, V. F.; Petrov, V. V.; Molnar, A. A.; Predvoditelev, D. A.; Ivanov, A. S. *Nature* **1980**, *283*, 585-586.
(73) Carruthers, A.; Melchior, D. L. *Biochemistry* **1983**, *22*, 5797-5807.
(74) Bramhall, J. *Biochim.Biophys.Acta* **1984**, *778*, 393-399.
(75) El-Mashak, E. M.; Tsong, T. Y. *Biochemistry* **1985**, *24*, 2884-2888.
(76) Bramhall, J.; Hofmann, J.; Deguzman, R.; Montestruque, S.; Schell, R. *Biochemistry* **1987**, *26*, 6330-6340.
(77) Nagawa, Y.; Regen, S. L. *J.Am.Chem.Soc.* **1992**, *114*, 1668-1672.
(78) Moss, R. A.; Fujita, T.; Ganguli, S. *Langmuir* **1990**, *6*, 1197-1199.
(79) John, K.; Schreiber, S.; Kubelt, J.; Herrmann, A.; Muller, P. *Biophys.J.* **2002**, *83*, 3315-3323.
(80) Herrmann, U.; Fendler, J. H. *Chem.Phys.Lett.* **1979**, *64*, 270-274.
(81) Fendler, J. H. *Pure Appl.Chem.* **1982**, *54*, 1809-1817.
(82) Elferink, M. G. L.; De Wit, J. G.; Demel, R.; Driessen, A. J. M.; Konings, W. N. *J.Biol.Chem.* **1992**, *267*, 1375-1381.
(83) Elferink, M. G. L.; De Wit, J. G.; Driessen, A. J. M.; Konings, W. N. *Biochim.Biophys.Acta* **1994**, *1193*, 247-254.
(84) Elferink, M. G. L.; Van Breemen, J.; Konings, W. N.; Driessen, A. J. M.; Wilschut, J. *Chem.Phys.Lipids* **1997**, *88*, 37-43.
(85) Zubay, G. *Biochemistry*; Addison-Wesley Publishing Company: Reading (USA), **1983**.
(86) Gennis, R. B. In *Biomembranes: Molecular Structure and Function*; Springer-Verlag: New York, **1989**; pp 20-35.
(87) Darnell, J.; Lodish, H.; Baltimore, D. In *Molecular Cell Biology*; Scientific American Books: New York, **1990**; pp 491-499.
(88) Alberts, B.; Bray, D.; Lewis, J.; Raff, M.; Roberts, K.; Watson, J. D. In *Molecular Biology of the Cell*; Garland Publishing: New York, **1994**; pp 477-485.
(89) www.ikea.com.
(90) http://www.avantilipids.com/NaturalProducts.html.
(91) Hammerström, L.; Velikian, I.; Karlsson, G.; Edwards, K. *Langmuir* **1995**, *11*, 408-410.
(92) Andersson, M.; Hammerström, L.; Edwards, K. *J.Phys.Chem.* **1995**, *99*, 14531-14538.
(93) Okuyama, H.; Okajima, N.; Sasaki, S.; Higashi, S.; Murata, N. *Biochim.Biophys.Acta* **1991**, *1084*, 13-20.
(94) Sinninghe Damsté, J. S.; Strous, M.; Rijpstra, W. I. C.; Hopmans, E. C.; Geenevasen, J. A. J.; Van Duin, A. C. T.; Van Niftrik, L. A.; Jetten, M. S. M. *Nature* **2002**, *419*, 708-712.
(95) Tettamanti, G.; Bassi, R.; Viani, P.; Riboni, L. *Biochimie* **2003**, *85*, 423-437.
(96) Kasahara, K.; Watanabe, Y.; Yamamoto, T.; Sanai, Y. *J.Biol.Chem.* **1997**, *272*, 29947-29953.
(97) Huwiler, A.; Kolter, T.; Pfeilschifter, J.; Sandhoff, K. *Biochim.Biophys.Acta* **2000**, *1485*, 63-99.

(98) Markwell, M. A. K.; Svennerholm, L.; Paulson, J. C. *Proc.Natl.Acad.Sci.USA* **1981**, *78*, 5406-5410.
(99) Karlsson, K. A. *Curr.Opin.Struct.Biol.* **1995**, *5*, 622-635.
(100) Saxena, K.; Zimmermann, P.; Schmidt, R. R.; Shipley, G. G. *Biophys.J.* **2000**, *78*, 306-312.
(101) Popova, A. V.; Hincha, D. K. *Biophys.J.* **2003**, *85*, 1682-1690.
(102) Koynova, R.; Caffrey, M. *Chem.Phys.Lipids* **1994**, *69*, 181-207.
(103) Hjelmstad, R. H.; Bell, R. M. *Biochemistry* **1991**, *30*, 1731-1740.
(104) Dawidowicz, E. A. *Ann.Rev.Biochem.* **1987**, *56*, 43-57.
(105) Vanmeer, G. *Annu.Rev.Cell Biol.* **1989**, *5*, 247-275.
(106) Paltauf, F. *Chem.Phys.Lipids* **1994**, *74*, 101-139.
(107) Merrill, A. H.; Stevens, V. L. *Biochim.Biophys.Acta* **1989**, *1010*, 131-139.
(108) Pettus, B. J.; Chalfant, C. E.; Hannun, Y. A. *Biochim.Biophys.Acta* **2002**, *1585*, 114-125.
(109) Andrieu-Abadie, N.; Levade, T. *Biochim.Biophys.Acta* **2002**, *1585*, 126-134.
(110) Cuvillier, O. *Biochim.Biophys.Acta* **2002**, *1585*, 153-162.
(111) Maceyka, M.; Payne, S. G.; Milstien, S.; Spiegel, S. *Biochim.Biophys.Acta* **2002**, *1585*, 193-201.
(112) Hoekstra, D.; Maier, O.; Van der Wouden, J. M.; Slimane, T. A.; Van IJzendoorn, S. C. D. *J.Lipid Res.* **2003**, *44*, 869-877.
(113) Van Blitterswijk, W. J.; Van der Luit, A. H.; Veldman, R. J.; Verheij, M.; Borst, J. *Biochem.J.* **2003**, *369*, 199-211.
(114) Siskind, L. J.; Davoody, A.; Lewin, N.; Marshall, S.; Colombini, M. *Biophys.J.* **2003**, *85*, 1560-1575.
(115) Ghosh, D.; Tinoco, J. *Biochim.Biophys.Acta* **1972**, *266*, 41-49.
(116) Ashworth, L. A.; Green, C. *Science* **1966**, *151*, 210-211.
(117) Lee, T. C.; Stephens, N.; Moehl, A.; Snyder, F. *Biochim.Biophys.Acta* **1973**, *291*, 86-92.
(118) Demel, R. A.; De Kruijff, B. *Biochim.Biophys.Acta* **1976**, *457*, 109-132.
(119) Hjort Ipsen, J.; Karlström, G.; Mouritsen, O. G.; Wennerström, H.; Zuckermann, M. J. *Biochim.Biophys.Acta* **1987**, *905*, 162-172.
(120) Almeida, P. F. F.; Vaz, W. L. C.; Thompson, T. E. *Biochemistry* **1992**, *31*, 6739-6747.
(121) Luk, A. S.; Kaler, E. W.; Lee, S. P. *Biochemistry* **1997**, *36*, 5633-5644.
(122) Sankaram, M. B.; Thompson, T. E. *Proc.Natl.Acad.Sci.USA* **1991**, *88*, 8686-8690.
(123) Bittman, R.; Blau, L. *Biochemistry* **1972**, *11*, 4831-4839.
(124) Papahadjopoulos, D.; Watkins, J. C. *Biochim.Biophys.Acta* **1967**, *135*, 639-652.
(125) Demel, R. A.; Bruckdor, K. R.; Van Deenen, L. L. M. *Biochim.Biophys.Acta* **1972**, *255*, 321-330.
(126) Cócera, M.; López, O.; Coderch, L.; Parra, J. L.; De la Maza, A. *Colloids Surf.A* **2003**, *221*, 9-17.
(127) De Kruyff, B.; Van Deenen, L. L. M.; Demel, R. A. *Biochim.Biophys.Acta* **1972**, *255*, 331-347.
(128) Demel, R. A.; Van Deenen, L. L. M.; Geurts van Kessel, W. S. *Biochim.Biophys.Acta* **1972**, *266*, 26-40.
(129) Clejan, S.; Bittman, R.; Deroo, P. W.; Isaacson, Y. A.; Rosenthal, A. F. *Biochemistry* **1979**, *18*, 2118-2125.
(130) De Kruyff, B.; Demel, R. A.; Slotboom, A. J.; Van Deenen, L. L. M.; Rosentha, A. F. *Biochim.Biophys.Acta* **1973**, *307*, 1-19.
(131) De Kruyff, B.; Van Dijck, P. W. M.; Demel, R. A.; Schuijff, A.; Brants, F.; Van Deenen, L. L. M. *Biochim.Biophys.Acta* **1974**, *356*, 1-7.
(132) Demel, R. A.; Jansen, J. W. C. M.; Van Dijck, P. W. M.; Van Deenen, L. L. M. *Biochim.Biophys.Acta* **1977**, *465*, 1-10.
(133) Urbina, J. A.; Pekerar, S.; Le, H. B.; Patterson, J.; Montez, B.; Oldfield, E. *Biochim.Biophys.Acta* **1995**, *1238*, 163-176.
(134) Silvius, J. R. *Biochim.Biophys.Acta* **2003**, *1610*, 174-183.
(135) Brown, R. E. *J.Cell Sci.* **1998**, *111*, 1-9.
(136) Edidin, M. *Annu.Rev.Biophys.Biomol.Struct.* **2003**, *32*, 257-283.
(137) Sankaram, M. B.; Thompson, T. E. *Biochemistry* **1990**, *29*, 10670-10675.
(138) Sot, J.; Collado, M. I.; Arrondo, J. L. R.; Alonso, A.; Goñi, F. M. *Langmuir* **2002**, *18*, 2828-2835.
(139) Tokutake, N.; Uragami, M.; Regen, S. L. *Langmuir* **2003**, *19*, 6363-6366.
(140) Bittman, R.; Kasireddy, C. R.; Mattjus, P.; Slotte, J. P. *Biochemistry* **1994**, *33*, 11776-11781.
(141) Binder, W. H.; Barragan, V.; Menger, F. M. *Angew.Chem.,Int.Ed.Engl.* **2003**, *42*, 5802-5827.
(142) Wang, T. Y.; Silvius, J. R. *Biophys.J.* **2000**, *79*, 1478-1489.
(143) Dorfler, H. D. *Colloid Polym.Sci.* **2000**, *278*, 130-136.
(144) Lohner, K.; Latal, A.; Degovics, G.; Garidel, P. *Chem.Phys.Lipids* **2001**, *111*, 177-192.
(145) Percot, A.; Lafleur, M. *Biophys.J.* **2001**, *81*, 2144-2153.

(146) Dietrich, C.; Bagatolli, L. A.; Volovyk, Z. N.; Thompson, N. L.; Levi, M.; Jacobson, K.; Gratton, E. *Biophys.J.* **2001**, *80*, 1417-1428.
(147) Edidin, M. *Trends Cell Biol.* **2001**, *11*, 492-496.
(148) Gandhavadi, M.; Allende, D.; Vidal, A.; Simon, S. A.; McIntosh, T. J. *Biophys.J.* **2002**, *82*, 1469-1482.
(149) Traikia, M.; Warschawski, D. E.; Lambert, O.; Rigaud, J. L.; Devaux, P. F. *Biophys.J.* **2002**, *83*, 1443-1454.
(150) Bagatolli, L. A. *Chem.Phys.Lipids* **2003**, *122*, 137-145.
(151) Wu, S. H. W.; McConell, H. M. *Biochemistry* **1975**, *14*, 847-854.
(152) Davidson, S. M. K.; Regen, S. L. *Chem.Rev.* **1997**, *97*, 1269-1279.
(153) Inoue, T.; Kitahashi, T.; Nibu, Y. *Chem.Phys.Lipids* **1999**, *99*, 103-109.
(154) Krisovitch, S. M.; Regen, S. L. *J.Am.Chem.Soc.* **1993**, *115*, 1199-1200.
(155) Davidson, S. M. K.; Liu, Y.; Regen, S. L. *J.Am.Chem.Soc.* **1993**, *115*, 10104-10110.
(156) Huster, D.; Arnold, K.; Gawrisch, K. *Biochemistry* **1998**, *37*, 17299-17308.
(157) Cao, H.; Tokutake, N.; Regen, S. L. *J.Am.Chem.Soc.* **2003**, *125*, 16182-16183.
(158) Silvius, J. R. *Biochemistry* **1992**, *31*, 3398-3408.
(159) Uragami, M.; Dewa, T.; Inagaki, M.; Hendel, R. A.; Regen, S. L. *J.Am.Chem.Soc.* **1997**, *119*, 3797-3801.
(160) Kishihara, K.; Jing, B. W.; Regen, S. L. *Langmuir* **2002**, *18*, 9635-9637.
(161) Hirai, M.; Iwase, H.; Hayakawa, T.; Koizumi, M.; Takahashi, H. *Biophys.J.* **2003**, *85*, 1600-1610.
(162) Gennis, R. B. In *Biomembranes: Molecular Structure and Function*; Springer-Verlag: New York, **1989**; pp 154-161.
(163) Middelkoop, E.; Lubin, B. H.; Op den Kamp, J. A. F.; Roelofsen, B. *Biochim.Biophys.Acta* **1986**, *855*, 421-424.
(164) Daleke, D. L.; Lyles, J. V. *Biochim.Biophys.Acta* **2000**, *1486*, 108-127.
(165) Daleke, D. L. *J.Lipid Res.* **2003**, *44*, 233-242.
(166) McIntosh, T. J. *Chem.Phys.Lipids* **1996**, *81*, 117-131.
(167) Bagatolli, L. A.; Gratton, E.; Fidelio, G. D. *Biophys.J.* **1998**, *75*, 331-341.
(168) Michaelson, D. M.; Horwitz, A. F.; Klein, M. P. *Biochemistry* **1973**, *12*, 2673-2645.
(169) Duynstee, E. F. J.; Grunwald, E. *J.Am.Chem.Soc.* **1959**, *81*, 4540-4542.
(170) Duynstee, E. F. J.; Grunwald, E. *J.Am.Chem.Soc.* **1959**, *81*, 4542-4548.
(171) Kurz, J. L.; Gutsche, C. D. *J.Am.Chem.Soc.* **1960**, *82*, 2175-2181.
(172) Menger, F. M.; Portnoy, C. E. *J.Am.Chem.Soc.* **1967**, *89*, 4698-4703.
(173) Colter, A. K.; Megerle, G. H.; Ossip, P. S.; Wang, S. S. *J.Am.Chem.Soc.* **1964**, *86*, 3106-3113.
(174) It had been suggested that the presence of micelles changed the properties of the bulk aqueous phase and that, as a result, the aqueous rate constant was affected by the presence of micelles.
(175) Yatsimirskii, A. K.; Martinek, K.; Berezin, I. V. *Tetrahedron* **1971**, *27*, 2855-2868.
(176) Berezin, I. V.; Martinek, K.; Yatsimirskii, A. K. *Russ.Chem.Rev.(Engl.Transl.)* **1973**, *42*, 787-802.
(177) Martinek, K.; Yatsimir, A. K.; Osipov, A. P.; Berezin, I. V. *Tetrahedron* **1973**, *29*, 963-969.
(178) Martinek, K.; Osipov, A. P.; Yatsimirski, A. K.; Dadali, V. A.; Berezin, I. V. *Tetrahedron Lett.* **1975**, 1279-1282.
(179) Martinek, K.; Yatsimirskii, A. K.; Levashov, A. V.; Berezin, I. V. In *Micellization, Solubilization and Microemulsions*; Mittal, K. L., ed., Plenum Press: New York, **1977**; pp 489-508.
(180) Shirahama, K. *Bull.Chem.Soc.Jpn.* **1975**, *48*, 2673-2676.
(181) Romsted, L. S. In *Micellization, Solubilization and Microemulsions*; Mittal, K. L., ed., Plenum Press: New York, **1977**; pp 509-530.
(182) Quina, F. H.; Chaimovich, H. *J.Phys.Chem.* **1979**, *83*, 1844-1850.
(183) Rodenas, E.; Vera, S. *J.Phys.Chem.* **1985**, *89*, 513-516.
(184) Bunton, C. A.; Nome, F.; Quina, F. H.; Romsted, L. S. *Acc.Chem.Res.* **1991**, *24*, 357-364.
(185) Tascioglu, S. *Tetrahedron* **1996**, *52*, 11113-11152.
(186) Romsted, L. S.; Bunton, C. A.; Yao, J. H. *Curr.Opin.Colloid Interface Sci.* **1997**, *2*, 622-628.
(187) Aggregates formed from nonionic or zwitterionic surfactants can well accommodate hydrophobic molecules, but only poorly hydrophilic ions.
(188) Buurma, N. J.; Herranz, A. M.; Engberts, J. B. F. N. *J.Chem.Soc., Perkin Trans.2* **1999**, 113-119.
(189) Soldi, V.; Keiper, J.; Romsted, L. S.; Cuccovia, I. M.; Chaimovich, H. *Langmuir* **2000**, *16*, 59-71.
(190) Lessard, J. G.; Fragata, M. *J.Phys.Chem.* **1986**, *90*, 811-817.
(191) Tanaka, K.; Mackay, G. I.; Payzant, J. D.; Bohme, D. K. *Can.J.Chem.* **1976**, *54*, 1643-1659.
(192) Henchman, M.; Paulson, J. F.; Hierl, P. M. *J.Am.Chem.Soc.* **1983**, *105*, 5509-5510.
(193) Chandrasekhar, J.; Smith, S. F.; Jorgensen, W. L. *J.Am.Chem.Soc.* **1984**, *106*, 3049-3050.

(194) Dewar, M. J. S.; Storch, D. M. *Chem.Commun.* **1985**, 94-96.
(195) Chandrasekhar, J.; Smith, S. F.; Jorgensen, W. L. *J.Am.Chem.Soc.* **1985**, *107*, 154-163.
(196) Madura, J. D.; Jorgensen, W. L. *J.Am.Chem.Soc.* **1986**, *108*, 2517-2527.
(197) Tuckerman, M.; Laasonen, K.; Sprik, M.; Parrinello, M. *J.Chem.Phys.* **1995**, *103*, 150-161.
(198) Tuckerman, M.; Laasonen, K.; Sprik, M.; Parrinello, M. *J.Phys.Chem.* **1995**, *99*, 5749-5752.
(199) Tuckerman, M. E.; Marx, D.; Parrinello, M. *Nature* **2002**, *417*, 925-929.
(200) Botti, A.; Bruni, F.; Imberti, S.; Ricci, M. A.; Soper, A. K. *J.Chem.Phys.* **2003**, *119*, 5001-5004.
(201) Eriksson, J. C.; Gillberg, G. *Acta Chem.Scand.* **1966**, *20*, 2019-2027.
(202) Fendler, J. H.; Fendler, E. J.; Infante, G. A.; Shi, P.-S.; Patterson, L. K. *J.Am.Chem.Soc.* **1974**, *97*, 89-95.
(203) Almgren, M.; Grieser, F.; Thomas, J. K. *J.Am.Chem.Soc.* **1979**, *101*, 279-291.
(204) Gallivan, J. P.; Dougherty, D. A. *Proc.Natl.Acad.Sci.USA* **1999**, *96*, 9459-9464.
(205) Van de Langkruis, G. B.; Engberts, J. B. F. N. *J.Org.Chem.* **1984**, *49*, 4152-4157.
(206) Witte, F. M.; Engberts, J. B. F. N. *J.Org.Chem.* **1985**, *50*, 4130-4134.
(207) Broxton, T. J.; Christie, J. R.; Sango, X. *J.Org.Chem.* **1989**, *54*, 1919-1922.
(208) Rispens, T.; Engberts, J. B. F. N. *J.Org.Chem.* **2002**, *67*, 7369-7377.
(209) Sepúlveda, L.; Lissi, E. A.; Quina, F. H. *Adv.Colloid Interface Sci.* **1986**, *25*, 1-57.
(210) Bunton, C. A.; Romsted, L. S.; Savelli, G. *J.Am.Chem.Soc.* **1979**, *101*, 1253-1259.
(211) Bunton, C. A.; Gan, L. H.; Moffatt, J. R.; Romsted, L. S.; Savelli, G. *J.Phys.Chem.* **1981**, *85*, 4118-4125.
(212) de Fatima Santana Neves, M.; Zanette, D.; Quina, F. H.; Moretti, M. T.; Nome, F. *J.Phys.Chem.* **1989**, *93*, 1502-1505.
(213) Blaskó, A.; Bunton, C. A.; Cerichelli, G.; McKenzie, D. C. *J.Phys.Chem.* **1993**, *97*, 11324-11331.
(214) Bunton, C. A.; Frankson, J.; Romsted, L. S. *J.Phys.Chem.* **1980**, *84*, 2607-2611.
(215) Lianos, P.; Zana, R. *J.Phys.Chem.* **1983**, *87*, 1289-1291.
(216) Brady, J. E.; Evans, D. F.; Warr, G. G.; Grieser, F.; Ninham, B. W. *J.Phys.Chem.* **1986**, *90*, 1853-1859.
(217) de Fatima Santana Neves, M.; Zanette, D.; Quina, F. H.; Moretti, M. T.; Nome, F. *J.Phys.Chem.* **1989**, *93*, 1502-1505.
(218) Schulz, P. C.; Morini, M. A.; Minardi, R. M.; Puig, J. E. *Colloid Polym.Sci.* **1995**, *273*, 959-966.
(219) Morini, M. A.; Schulz, P. C. *Colloid Polym.Sci.* **1997**, *275*, 802-805.
(220) Morini, M. A.; Minardi, R. M.; Schulz, P. C.; Puig, J. E.; Rodriguez, J. L. *Colloid Polym.Sci.* **1998**, *276*, 738-742.
(221) Ninham, B. W.; Evans, D. F.; Wel, G. J. *J.Phys.Chem.* **1983**, *87*, 5020-5025.
(222) Talmon, Y.; Evans, D. F.; Ninham, B. W. *Science* **1983**, *221*, 1047-1048.
(223) Brady, J. E.; Evans, D. F.; Kachar, B.; Ninham, B. W. *J.Am.Chem.Soc.* **1984**, *106*, 4279-4280.
(224) Rispens, T.; Engberts, J. B. F. N. *J.Org.Chem.* **2003**, *68*, 8520-8528.
(225) Al-Lohedan, H.; Bunton, C. A.; Romsted, L. S. *J.Phys.Chem.* **1981**, *85*, 2123-2129.
(226) Al-Lohedan, H.; Bunton, C. A. *J.Org.Chem.* **1982**, *47*, 1160-1166.
(227) Bunton, C. A.; Cuenca, A. *Can.J.Chem.* **1986**, *64*, 1179-1183.
(228) Broxton, T. J.; Christie, J. R.; Sango, X. *J.Org.Chem.* **1987**, *52*, 4814-4817.
(229) Khan, M. N.; Ismail, E. *J.Chem.Soc., Perkin Trans.2* **2001**, *8*, 1346-1350.
(230) Kunitake, T.; Okahata, Y. *J.Am.Chem.Soc.* **1977**, *99*, 3860-3861.
(231) Kunitake, T.; Okahata, Y.; Tamaki, K. *Chem.Lett.* **1977**, 387-390.
(232) Kemp, D. S.; Paul, K. G. *J.Am.Chem.Soc.* **1970**, *92*, 2553-2554.
(233) Kemp, D. S.; Paul, K. G. *J.Am.Chem.Soc.* **1975**, *97*, 7305-7312.
(234) Suh, J.; Scarpa, I. S.; Klotz, I. M. *J.Am.Chem.Soc.* **1976**, *98*, 7060-7064.
(235) Kunitake, T.; Okahata, Y.; Ando, R.; Shinkai, S.; Hirakawa, S. *J.Am.Chem.Soc.* **1980**, *102*, 7877-7881.
(236) Grate, J. W.; McGill, R. A.; Hilvert, D. *J.Am.Chem.Soc.* **1993**, *115*, 8577-8584.
(237) HMPA: hexamethylphosphortriamide.
(238) Germani, R.; Ponti, P. P.; Savelli, G.; Spreti, N.; Cipiciani, A.; Cerichelli, G.; Bunton, C. A. *J.Chem.Soc., Perkin Trans.2* **1989**, 1767-1771.
(239) Scarpa, M. V.; Araujo, P. S.; Schreier, S.; Sesso, A.; Oliveira, A. G.; Chaimovich, H.; Cuccovia, I. M. *Langmuir* **2000**, *16*, 993-999.
(240) Nusselder, J. J. H.; Engberts, J. B. F. N. *Langmuir* **1991**, *7*, 2089-2096.
(241) Parasassi, T.; Destasio, G.; Ravagnan, G.; Rusch, R. M.; Gratton, E. *Biophys.J.* **1991**, *60*, 179-189.
(242) Patel, M. S.; Bijma, K.; Engberts, J. B. F. N. *Langmuir* **1994**, *10*, 2491-2492.
(243) Moss, R. A.; Schreck, R. P. *J.Am.Chem.Soc.* **1985**, *107*, 6634-6639.
(244) Moss, R. A.; Swarup, S.; Schreck, R. P. *Tetrahedron Lett.* **1985**, *26*, 603-606.
(245) Moss, R. A.; Swarup, S. *J.Org.Chem.* **1988**, *53*, 5860-5866.

(246) Moss, R. A.; Bizzigotti, G. O. *Tetrahedron Lett.* **1982**, *23*, 5235-5238.
(247) Moss, R. A.; Swarup, S.; Zhang, H. M. *J.Am.Chem.Soc.* **1988**, *110*, 2914-2919.
(248) Huffman, R. W.; Brown, D. M. *J.Org.Chem.* **1991**, *56*, 6477-6479.
(249) Moss, R. A.; Schreck, R. P. *Tetrahedron Lett.* **1985**, *26*, 6305-6308.
(250) Vesicles used include di-*n*-hexadecyldimethylammonium bromide and derivatives in the absence and presence of cholesterol.
(251) Moss, R. A.; Ihara, Y.; Bizzigotti, G. O. *J.Am.Chem.Soc.* **1982**, *104*, 7476-7478.
(252) Moss, R. A.; Ihara, Y. *J.Org.Chem.* **1983**, *48*, 588-592.
(253) Moss, R. A.; Hui, Y. *Tetrahedron Lett.* **1983**, *24*, 3961-3964.
(254) Moss, R. A.; Swarup, S.; Hendrickson, T. F.; Hui, Y. Z. *Tetrahedron Lett.* **1984**, *25*, 4079-4082.
(255) Kunitake, T.; Sakamoto, T. *Chem.Lett.* **1979**, 1059-1062.
(256) Pérez-Juste, J.; Hollfelder, F.; Kirby, A. J.; Engberts, J. B. F. N. *Org.Lett.* **2000**, *2*, 127-130.
(257) Maskill, H. *The Physical Basis of Organic Chemistry*; Oxford University Press: Oxford, **1990**.
(258) Kunitake, T.; Ihara, H.; Okahata, Y. *J.Am.Chem.Soc.* **1983**, *105*, 6070-6078.
(259) Cuccovia, I. M.; Kawamuro, M. K.; Krutman, M. A. K.; Chaimovich, H. *J.Am.Chem.Soc.* **1989**, *111*, 365-366.
(260) Rispens, T.; Engberts, J. B. F. N. *Org.Lett.* **2001**, *3*, 941-943.
(261) Rispens, T. *Ph.D. Thesis*, University of Groningen, Groningen, **2004.** The thesis can be downloaded from http://www.ub.rug.nl/eldoc/dis/science/t.rispens/
(262) Moss, R. A.; Shin, J. S. *J.Chem.Soc., Chem.Commun.* **1983**, 1027-1028.
(263) Fendler, J. H.; Hinze, W. L. *J.Am.Chem.Soc.* **1981**, *103*, 5439-5447.
(264) Moss, R. A.; Taguchi, T.; Bizzigotti, G. O. *Tetrahedron Lett.* **1982**, *23*, 1985-1988.
(265) Mizutani, T.; Whitten, D. G. *J.Am.Chem.Soc.* **1985**, *107*, 3621-3625.
(266) Kunitake, T.; Sakamoto, T. *J.Am.Chem.Soc.* **1978**, *100*, 4615-4617.
(267) Cuccovia, I. M.; Aleixo, R. M. V.; Mortara, R. A.; Filho, P. B.; Bonilha, J. B. S.; Quina, F. H.; Chaimovich, H. *Tetrahedron Lett.* **1979**, 3065-3068.
(268) Kimizuka, N.; Watanabe, E.; Kunitake, T. *Chem.Lett.* **1999**, 29-30.
(269) Czarniecki, M. F.; Breslow, R. *J.Am.Chem.Soc.* **1979**, *101*, 3675-3676.
(270) Escabi-Perez, J. R.; Romero, A.; Lukac, S.; Fendler, J. H. *J.Am.Chem.Soc.* **1979**, *101*, 2231-2233.
(271) Almgren, M.; Thomas, J. K. *Photochem.Photobiol.* **1980**, *31*, 329-335.
(272) Fendler, J. H. *J.Phys.Chem.* **1980**, *84*, 1485-1491.
(273) Infelta, P. P.; Grätzel, M.; Fendler, J. H. *J.Am.Chem.Soc.* **1980**, *102*, 1479-1483.
(274) Tunuli, M. S.; Fendler, J. H. *J.Am.Chem.Soc.* **1981**, *103*, 2507-2513.
(275) Fuhrhop, J. H.; Bartsch, H.; Fritsch, D. *Angew.Chem.,Int.Ed.Engl.* **1981**, *20*, 804-805.
(276) Scarpa, M. V.; Maximiano, F. A.; Chaimovich, H.; Cuccovia, I. A. *Langmuir* **2002**, *18*, 8817-8823.
(277) Jung, M.; Robinson, B. H.; Steytler, D. C.; German, A. L.; Heenan, R. K. *Langmuir* **2002**, *18*, 2873-2879.
(278) Garcia-Rio, L.; Hervés, P.; Mejuto, J. C.; Pérez-Juste, J.; Rodriguez-Dafonte, P. *New J.Chem.* **2003**, *27*, 372-380.
(279) Casey, M. L.; Kemp, D. S.; Paul, K. G.; Cox, D. D. *J.Org.Chem.* **1973**, *38*, 2294-2301.
(280) Kemp, D. S.; Casey, M. L. *J.Am.Chem.Soc.* **1973**, *95*, 6670-6680.
(281) Kemp, D. S.; Cox, D. D.; Paul, K. G. *J.Am.Chem.Soc.* **1975**, *97*, 7312-7318.
(282) Thorn, S. N.; Daniels, R. G.; Auditor, M.-T. M.; Hilvert, D. *Nature* **1995**, *373*, 228-230.
(283) Hollfelder, F.; Kirby, A. J.; Tawfik, D. S. *Nature* **1996**, *383*, 60-63.
(284) Kennan, A. J.; Whitlock, H. W. *J.Am.Chem.Soc.* **1996**, *118*, 3027-3028.
(285) Genre-Grandpierre, A.; Tellier, C.; Loirat, M. J.; Blanchard, D.; Hodgson, D. R. W.; Hollfelder, F.; Kirby, A. J. *Bioorg.Med.Chem.Lett.* **1997**, *7*, 2497-2502.
(286) Hollfelder, F.; Kirby, A. J.; Tawfik, D. S. *J.Am.Chem.Soc.* **1997**, *119*, 9578-9579.
(287) Hannak, R. B.; Rojas, C. M. *Tetrahedron Lett.* **1998**, *39*, 3465-3468.
(288) McCracken, P. G.; Ferguson, C. G.; Vizitiu, D.; Walkinshaw, C. S.; Wang, Y.; Thatcher, G. R. J. *J.Chem.Soc., Perkin Trans.2* **1999**, 911-912.
(289) Hollfelder, F.; Kirby, A. J.; Tawfik, D. S.; Kikuchi, K.; Hilvert, D. *J.Am.Chem.Soc.* **2000**, *122*, 1022-1029.
(290) Kikuchi, K.; Thorn, S. N.; Hilvert, D. *J.Am.Chem.Soc.* **2000**, *118*, 8184-8185.
(291) Hollfelder, F.; Kirby, A. J.; Tawfik, D. S. *J.Org.Chem.* **2001**, *66*, 5866-5874.

CHAPTER 2

CHARACTERISATION OF CATIONIC VESICLES FORMED IN THE PRESENCE OF DOUBLE-TAILED ANIONIC AMPHIPHILES, LONG LINEAR ALCOHOLS, ALKYL PYRANOSIDES AND A SINGLE-TAILED NONIONIC SURFACTANT

*Incorporation of various additives, such as long linear alcohols, nonionic surfactants and anionic amphiphiles, into vesicles formed from dimethyldi-n-octadecylammonium chloride (**$C_{18}C_{18}$+**) leads to changes in the main phase transition temperature (T_m). The change strongly depends on the mole fraction and structure of the additives. Above 20 mol% of saturated (18 carbons) alcohols the T_m, increases whereas short (ca. 10 carbons) alcohols and single-tailed surfactants lead to a decrease, or even a disappearance of the T_m. Addition of anionic, double-tailed amphiphiles leads in the case of asymmetry in the tails to an increase in T_m at the equimolar ratio, whereas in the case of symmetry this is not observed. Fluorescence and absorbance spectroscopy were used to study changes in the polarity of the vesicular surfaces, but despite the use of five different dyes no significant changes were found as a function of the concentration of the additives. Addition of single-tailed surfactants leads to vesicle solubilisation to form mixed micellar aggregates. This process was followed by turbidity measurements and light scattering experiments.*

2.1 Introduction

As discussed in Chapter 1, the composition of biological membranes is important for performing their task.[1-4] Additives, such as cholesterol, are a key factor in the structural integrity towards, for example, permeability of ions and hydrophilic molecules, such as glucose.[5-8] Also other properties are affected by the exact composition of biological membranes. In fact, the lipids can be regarded as matrix to which other molecules can be added to give the bilayer additional functionalities. Unfortunately, due to this complexity in composition, and also the structural complexity of the phospholipids, and steroid themselves, it is difficult to identify the molecular interaction that is responsible for the properties.

The use of structurally simple molecules limits the number of possible interactions. Then, if these structures are systematically varied, information can be obtained on the importance of certain types of interactions. Upon a gradual increase in structural complexity (*e.g.* introduction of more functional groups) valuable information can be obtained on the molecular interactions in biological membranes.

In this chapter vesicles formed from dimethyldi-*n*-octadecylammonium chloride (**$C_{18}C_{18}$+**; Scheme 2.1) were studied in the absence and presence of various additives. The additives and the double-tailed amphiphile were chosen on the basis of their structural simplicity in

order to be able to relate a change in property to a change in the structure of the additive. The properties of $\mathbf{C_{18}C_{18}+}$ have been studied in the literature.[9-11] In addition, despite the structural simplicity, the additives can be regarded as simple mimics of compounds, other than lipids, that can be found in biological membranes.

The additives can be divided into four classes. The first class consists of anionic double-tailed amphiphiles (sodium di-*n*-decylphosphate and sodium *n*-decyl-*n*-octadecylphosphate), the second class contains long linear alcohols (*n*-decanol, *n*-octadecanol, oleyl alcohol and batyl alcohol), the third class includes ethylene glycol surfactants (Brij 58P and a SAINT-2 derivative) and the fourth class are sugar-based surfactants (*n*-dodecyl-*β*-glucoside, *n*-dodecyl-*β*-maltoside). Finally, also a cationic phospholipid analogue has been studied. A more detailed reasoning for studying vesicles containing these specific additives can be found in the following chapters, where all classes of additives are described with respect to their influence towards a bimolecular reaction that is catalysed in the presence of cationic vesicles. This chapter will describe how properties, such as the main phase transition temperature, local polarity and vesicular size (distributions), are affected by the addition of these types of additives. Their exact structure can be found in those paragraphs where they are first used.

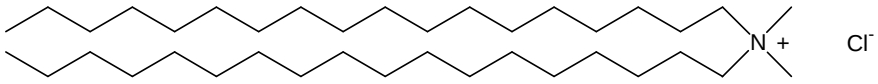

Scheme 2.1. *Di-n-octadecyldimethylammonium chloride (**$\mathbf{C_{18}C_{18}+}$**).*

2.2 Experimental

2.2.1 Materials

Dimethyldi-*n*-octadecylammonium chloride (> 97%; Fluka), dimethylphosphate (98%; Acros), eicosaethylene glycol mono *n*-hexadecyl ether (Brij 58P; Fluka), *n*-decanol (99%; Aldrich), *n*-octadecanol (95%; Acros), oleyl alcohol (Aldrich), batyl alcohol (99%; Aldrich), *n*-dodecyl-*β*-glucoside (>99%; Fluka), *n*-dodecyl-*β*-maltoside (>99.5%; Glycon), sodium hydroxide (titrisol; Merck), pyrene (>99%; Aldrich), 8-anilino-1-naphthalenesulfonic acid ammonium salt (ANS; Sigma), 6-dodecanol-2-dimethylaminonaphthalene (laurdan; >99%; Molecular Probes), 9-diethylamino-5H-benzo[α]phenoxazine-5-one (Nile Red; 99%; Acros) and sodium hydroxide (titrisol) were used as received. The $E_T(30)$-probe (2,6-diphenyl-4-(2,4,6-triphenyl-1-pyridinio)phenolate) was kindly provided by Prof. Ch. Reichardt (University of Marburg). Sodium di-*n*-decyl phosphate,[12] sodium *n*-decyl-*n*-octadecyl phosphate,[12] 2,3-bis-*n*-octadecyloxy-propyl)-trimethylammonium chloride and 4-(dioleylmethyl)-1-($PEG_{5000}OCH_3$)-pyridinium bromide[13] were synthesized by Mr. A. Wagenaar.

Doubly distilled water was used for all solutions.

2.2.2 Vesicle Preparation

Stock solutions of approximately 30 mM total amphiphile concentration were prepared by weighing the needed amounts of amphiphile. Water was added to the appropriate volume and the solution was kept in a water bath at 50°C for at least 45 minutes. Then the solution was sonicated using a tip sonicator (Branson Sonifier B15-P) at 50°C for 6 min. (or longer if not all solid material was solubilised). Subsequently, the stock solution was extruded 11 times through a 400 nm filter using a mini-extruder (Avanti Polar Lipids, Alabaster, AL) at 50°C. Finally, the stock solution was diluted to

the desired concentrations and, if required, sodium hydroxide from a 1 M stock solution was added so that the total concentration of sodium hydroxide was 2.25 mM.
In an alternative procedure, stock solutions of approximately 30 mM total amphiphile concentration were prepared by weighing the needed amounts of amphiphile and additive. Chloroform was added in such an amount that the compounds were just dissolved. Chloroform was then evaporated by slowly rotating the sample vial under a stream of nitrogen. Residual amounts of chloroform were removed by storing the sample vial in vacuo for several hours. Then water was added in the appropriate amount and the solution was sonicated as described above.
Certain samples were prepared at different concentrations (*e.g.* some DSC samples were prepared at 2 mM).
Sometimes a larger home-built extruder was used. Up to 10 ml of sample was extruded at least five times through a 200 nm filter. Some solutions were not extruded.
No differences in behaviour between the various preparation methods were observed when various control experiments (DSC, DLS, kinetic experiments (Chapter 3) were performed.
Unless stated otherwise in the text, all samples were prepared following the above described preparation method.

2.2.3 Cryo-Electron Microscopy

A small drop of a 20 mM amphiphile solution was deposited on a glow discharged holey carbon-coated grid. After blotting away the excess of the solution under study, the grids were plunged into liquid ethane. Frozen hydrated specimen were mounted in a GatAn (model 626) cryo-stage and examined in a Philips CM 120 cryo electron microscope operating at 120 kV.

2.2.4 Differential Scanning Microcalorimetry

DSC scans were taken on a VP-DSC apparatus (Microcal, Northampton, MA) with a scan rate of 1°C min^{-1}. The total amphiphile concentration was 2 mM and the total concentration of sodium hydroxide was 2.25 mM. Five scans were performed between 5°C and 100°C. The reference cell was filled with doubly distilled water. The solutions were allowed to equilibrate at 1°C for 90 min. between successive scans. A water scan was subtracted using Microcal Origin software. The first scan was neglected due to the thermal history of the machine, but the other scans were all identical.

2.2.5 Fluorescence and Absorbance Spectroscopy

2.2.5.1 E_T(30) dye

4 µl of a saturated solution of the E_T(30)-probe in acetonitrile was added to a vesicular solution and the wavelength of maximum absorption was measured on a Perkin-Elmer 5 spectrophotometer at least 5 min. after mixing the solutions. Vesicle concentrations were chosen such that λ_{max} did not change with concentration indicating that the E_T(30) probe was fully bound.

2.2.5.2 Pyrene

Pyrene was dissolved in water and filtered at least 1 day after dissolution. This solution was then diluted once. No excimers were present since steady-state fluorescence showed no peak near 450 nm, characteristic of pyrene excimers.[14] Pyrene was present at concentrations lower than 10^{-6} M. Steady-state fluorescence spectroscopic measurements were performed using a SLM SPF-500C spectrofluorometer equipped with a thermostatted cell holder and a magnetic stirring device. Measurements were initiated at least 15 min. after mixing the vesicular and pyrene solution. The instrument settings were as follows: excitation wavelength, 335 nm; slid width 5 nm. The emission spectrum was recorded from 371 nm to 386 nm (slit width, 1 nm; step size 0.20 nm; filter 2). The intensities of the first (around 372 nm) and third peak (around 385 nm) were determined.

2.2.5.3 Nile Red, 1,8-ANS and Laurdan Fluorescence

Nile Red, 1,8-ANS and laurdan fluorescence experiments were performed similar to those for pyrene. Details are given in Table 3.

Table 3. *Experimental Details for Various Fluorescence Experiments*

dye	sol. prep. method	λ_{exc} (nm)	slid width exc. (nm)	slid width em. (nm)	step size (nm)
Nile Red	I[b]	490-590	2	2	4
1,8-ANS	I[b]	380	5	2	4
Laurdan	II[b]	440-490[a]	7.5	2.5	4

[a] λ_{em} (nm) instead of λ_{exc} (nm). [b] See text below.

Solutions were prepared using two methods.
I: The fluorescent dye was added from a concentrated solution in acetonitrile. The amphiphile to dye ratio was 400 or larger. Vesicles were prepared as described in Section 2.2.2.
II: The fluorescent dye was added from a concentrated stock solution in chloroform to a solution of amphiphile and additive in chloroform. The mixture was further processed as described in Section 2.2.2 for solution prepared via the "film" procedure. The amphiphile to dye ratio was 250.
Background scans were performed with vesicles containing no fluorescent dye. The scattering at the wavelength of emission was negligible.

2.2.6 Dynamic Light Scattering

Size distributions were measured using a Malvern Zetasizer 5000 (Malvern, UK). The experiments were performed at a concentration where there is no double scattering (typically < 2.5 mM). The data was analysed using the algorithms provided with the software. A size distribution was accepted as reasonable when several analysis methods yielded similar results.

2.2.7 ζ Potentials

Mobilities were measured using a Malvern Zetasizer 5000 (Malvern, UK). ζ potentials were then calculated using the Smoluchowsky limits.[15] All solutions used contained 5 mM total amphiphile concentration and 2.25 mM NaOH and were prepared as described (Section 2.2.2), except that 5 mM solutions were used and the solutions were not extruded. All experiments were performed around 15°C.

2.2.8 Turbidity Experiments

Turbidity was measured by measuring the absorbance at 410 nm on a Perkin-Elmer λ5 or λ12 spectrophotometer.

2.3 Results and Discussion

2.3.1 Cryo-Electron Microscopy

2.3.1.1 Sodium Di-*n*-Decylphosphate

Vesicles, formed from **$C_{18}C_{18}$+**, are "lens-shaped" (Figure 2.1a),[11,16] *i.e.* vesicles are round when looked from the top, but strongly flattened when looked from aside. The non-spherical shape suggests that packing of these synthetic amphiphiles is less efficient than in their natural analogues (phospholipids).

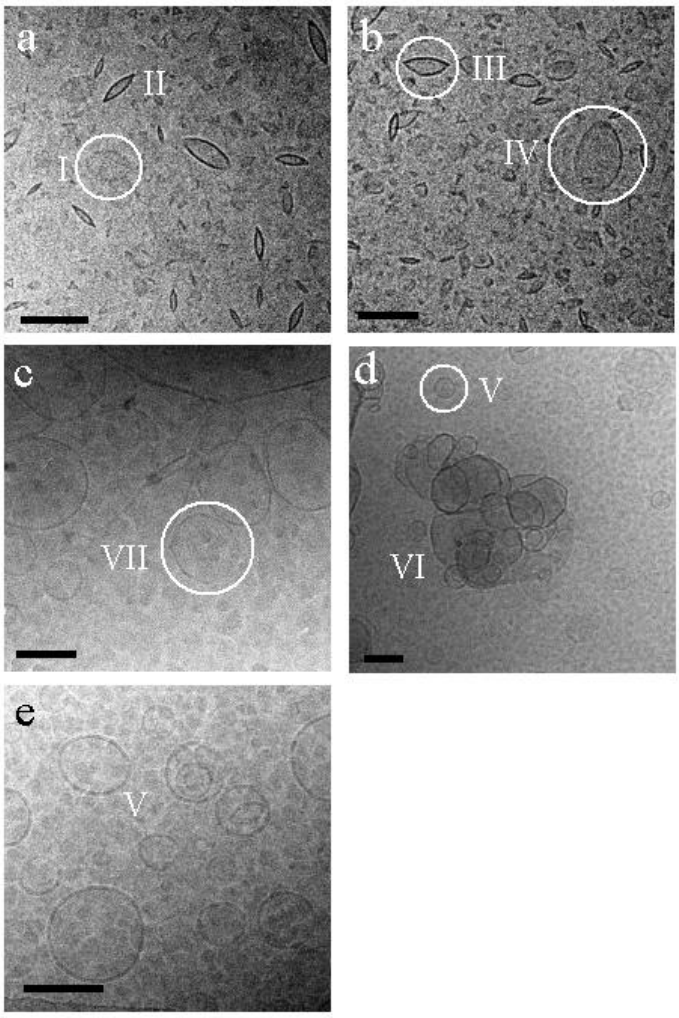

Figure 2.1. *Cryo-EM pictures of mixtures of* **$C_{18}C_{18}$+** *and* **$C_{10}C_{10}$-**. *The letter denotes the percentage of* **$C_{10}C_{10}$-** *as a function of the total amphiphile concentration. (a) 0 mol%; (b) 10 mol%; (c) 40 mol%; (d) 50 mol%; (e) 70 mol%. Explanation of numbers: (I) top view; (II) side view; (III) side view where one "lens" has extra curvature; (IV) top view, but slightly tilted; (V) spherical vesicle; (VI) clustering of vesicles; (VII) angular vesicle. The bar represents 100 nm.*

Upon the addition of 10 mol% of sodium di-*n*-decylphosphate (**$C_{10}C_{10}$-**; Scheme 2.2; Figure 2.1b) the cryo-EM picture shows more or less the same structures, except that sometimes one of the two "lenses" has extra curvature. At 40 mol% of **$C_{10}C_{10}$-** (Figure 2.1c) angular spherical vesicles are observed. This angularity has been observed before[11] and is due to the fact that the vesicles are below their main phase transition temperature (Section 2.3.4) when they are vitrified. This angularity is also observed for 50 mol% of **$C_{10}C_{10}$-** (Figure 2.1d), but now also clustering occurs due to the absence of strong electrostatic repulsion between the vesicles since the vesicles are almost overall neutral. At 70 mol% of **$C_{10}C_{10}$-** (Figure 2.1e) only spherical vesicles are observed.

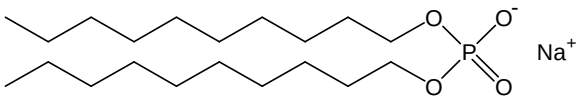

Scheme 2.2. *Sodium di-n-decylphosphate (**$C_{10}C_{10}$-**).*

2.3.2 Vesicle Solubilisation by Nonionic Single-Tailed Surfactants

Single-tailed nonionic surfactants are widely used to solubilise biological membranes in order to obtain cellular content or membrane proteins. But they are also used to reconstitute membrane proteins into model membranes.[17,18] Sugar-based surfactants, oligo-ethylene glycol mono-*n*-alkyl ethers and derivatives of the latter, such as Triton X, are often used as solubilising agent (Scheme 2.3) and therefore their interactions with bilayers have been well studied in the literature.[17] The most commonly used techniques to study vesicular breakdown are turbidity, fluorescence spectroscopy and isothermal titration microcalorimetry (ITC).

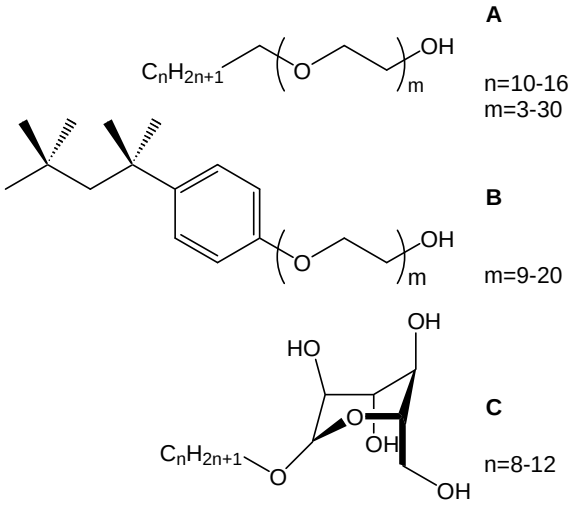

Scheme 2.3. *Examples of commonly used nonionic detergents used to solubilise membranes. A: oligo-ethylene glycol n-alkyl ether (**C_nEO_m**); B: Triton X; C: n-Alkyl glucoside (**C_nGlu**).*

Membrane solubilisation proceeds via a three-step mechanism (Scheme 2.4).[18,19] In the first stage, upon addition of single-tailed surfactants to a vesicular solution, the single-tailed surfactants will partially insert into the bilayer, leading to swelling of the vesicles. This proceeds until the vesicles are saturated with single-tailed surfactant.

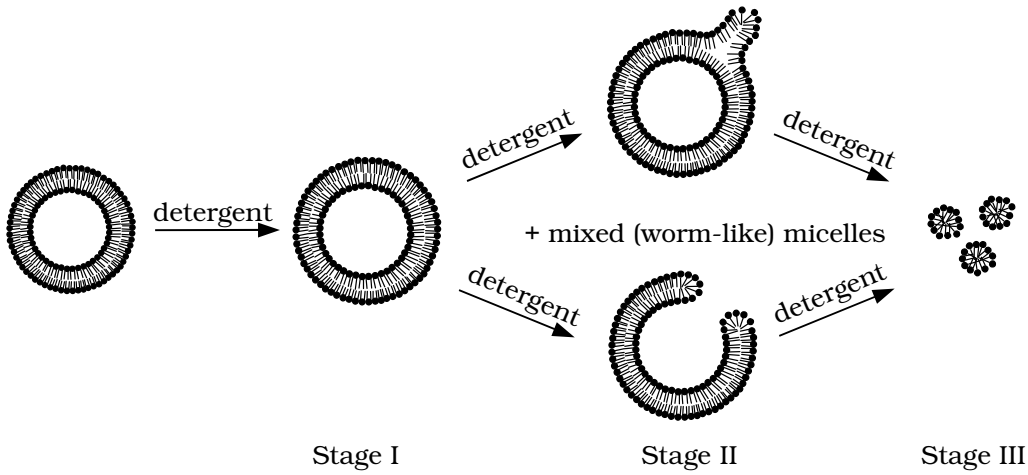

Scheme 2.4. *Schematic representation of the two most commonly accepted mechanisms of vesicle solubilisation.*

At any time of stage I the amount of membrane-bound single-tailed surfactant can be calculated using the molar ratio of bound single-tailed surfactant to the amount of double-tailed amphiphile (R_b). This ratio depends on the binding constant K, as was derived by Schurtenberger *et al.*[20] We will further use the words detergent (det) for single-tailed surfactant and amphiphile (amph) instead of double-tailed amphiphile.

$$R_b \equiv \frac{[\text{det}]_{ves}}{[\text{amph}]} = K[\text{det}]_w \qquad (2.1)$$

In this eq. $[\text{det}]_{ves}$ and $[\text{det}]_w$ are the vesicular and aqueous concentrations of detergent with respect to the total volume, respectively.

An alternative model makes use of the mole fraction partition coefficient P and assumes ideal mixing of amphiphile and detergent.[21] This model makes use of the mole fraction bound detergent in the membrane, rather then the mole ratio. K and P are related via eq. (2.2):[22]

$$K = \frac{P}{[H_2O]_w}(1 + R_b) \qquad (2.2)$$

$[H_2O]_w$ is the concentration of water in the solution and in dilute systems this is 55.6 M. This slightly different approach leads to rather different results, especially at higher detergent concentrations. Experimentally it has been found that a constant K better describes the system than a constant P. A composition-dependent partition coefficient, $P(X_b)$, has been derived using the non-ideality parameter ρ_0 and this approach leads to similar concentrations of bound and unbound detergent as calculated using K. Therefore, we will further use the model of a constant K as derived by Schurtenberger *et al.* [20]

In stage II the breakdown of the vesicles can occur via two mechanisms. Either mixed micelles "escape" from the vesicles, or the vesicle is "eaten up" by the detergent. At the same time mixed (worm-like) micelles coexist. Due to this breakdown, compounds encapsulated

inside the vesicles are released.[23-26] In the third stage all the amphiphiles are dissolved into mixed micelles.

Despite the fact that the vesicle solubilisation is widely used and the general mechanism appears clear, many of the details, such as alternative meachanisms,[27-29] domain formation upon detergent addition[30,31] and vesicle fusion upon detergent addition,[32,33] are still poorly understood.

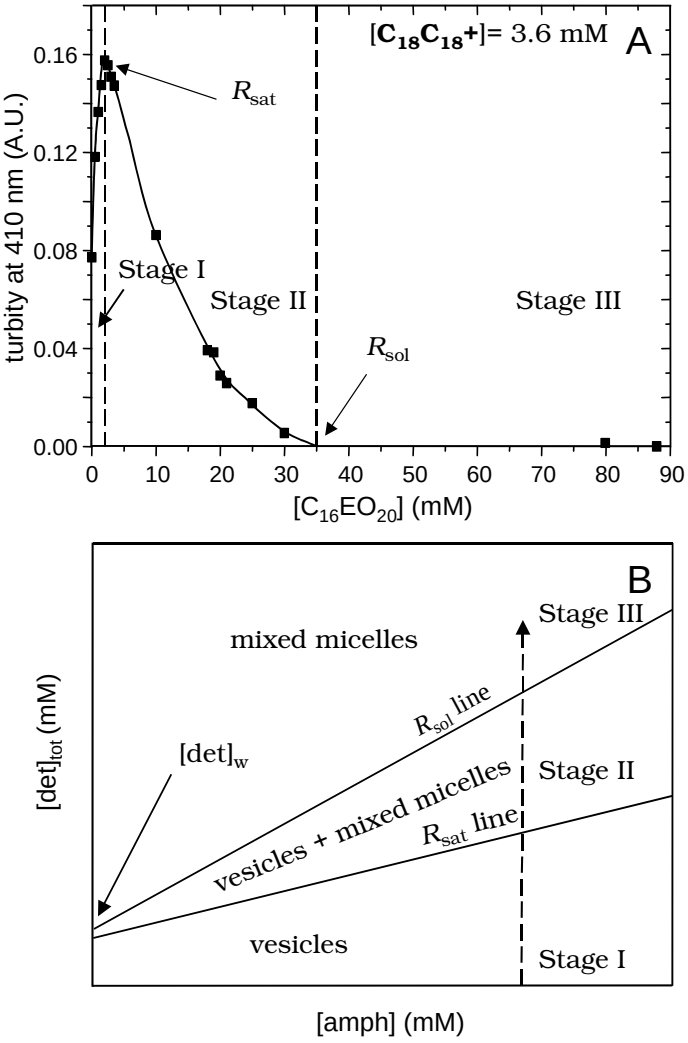

Figure 2.2. *A: Plot of turbidity versus the concentration of added detergent (**$C_{16}EO_{20}$**). Dashed lines separate the different stages. B: Schematic and theoretical representation of a simplified phase diagram of vesicle solubilisation. The dashed arrow is the direction of a solubilisation experiment through the different stages. The reverse direction of the arrow is a membrane reconstitution experiment.*

Measuring the turbidity of a vesicular solution upon detergent addition, initially an increase in turbidity is shown due to the swelling of the vesicles in the first stage (and sometimes due to fusion of vesicles as well; Figure 2.2A).[34,35] A maximum in turbidity is observed when the vesicles are saturated with detergent. The ratio of the concentrations of detergent to amphiphile at which this occurs is called R_{sat} (compare eq. (2.1)). Then the turbidity will decrease since the vesicles are being consumed, and scattering by micelles is negligible.

When all vesicles have disappeared, addition of more detergent will not change the turbidity anymore. The ratio of the concentrations of detergent to amphiphile at which the turbidity becomes constant is called R_{sol}. When this experiment is repeated at several amphiphile concentrations a plot as in Figure 2.2B can be constructed. The intercept of the straight lines through the R_{sat} and R_{sol} values with the y-axis is the amount of free detergent in solution at the saturation and solubilisation point, respectively. Ideally, the R_{sat} and R_{sol} line cross at the y-axis. This concentration is being associated with the critical micellar concentration (CMC) of the detergent.[36] However, usually this point underestimates the CMC. The slope of the R_{sat} and R_{sol} line is related to the amount of bound detergent, as can be seen in eq. (2.3).

$$[\text{det}]_{\text{tot}} = [\text{det}]_{\text{w}} + [\text{det}]_{\text{ves}} = [\text{det}]_{\text{w}} + \frac{[\text{det}]_{\text{ves}}}{[\text{amph}]}[\text{amph}] = [\text{det}]_{\text{w}} + R_{\text{b}}[\text{amph}] \tag{2.3}$$

Taking the ratio of the slope to the intercept of a plot of eq. (2.3) one obtains the value for K (eq. (2.1)) at either the saturation point, or the solubilisation point. However, experimentally this is not so straightforward. Usually, CMC values are rather small (<1 mM) and since the intercept is extrapolated from experimental data the error in the intercept is quite large. Calculation of K requires division by this small value and therefore small fluctuations in the intercept will lead to large deviations in the value for K. In addition, the relationship between the concentrations of amphiphile and detergent usually deviates from linearity close to zero amphiphile concentration.[36]

It is more convenient to use ITC to measure binding constants, since it leads to smaller errors in the binding constant and the value of the binding constant can be obtained in one single experiment. In addition, it also gives information about the enthalpy of binding.[22,37,38]

The binding constant K correlates rather well with the CMC, *i.e.* if K increases, the CMC decreases.[22,39] This is reasonable since both binding to a vesicle and aggregation into micelles proceeds via a similar mechanism (transfer of the hydrophobic tail from water to an apolar pseudophase, release of water from the hydrophobic hydration shell, etc.)

Micellisation is described by the equilibrium given below, and hence is described by the micellar binding constant K_{mic} (in mole fraction).

$$n\,\text{S(aq)} \rightleftharpoons \text{S}_n\text{(mic)}$$

$$K_{\text{mic}} = \frac{[\text{S}]_{\text{mic}}}{[\text{S}]_{\text{w}}} \tag{2.4}$$

In this equation $[S]_{mic}$ and $[S]_w$ are the micellised and aqueous mole fraction of detergent, respectively. The mole fraction $[S]_{mic}$ equals approximately 1, since the number of detergent molecules in the micelle is large relative to the number of water molecules. Considering that above the CMC the concentration of aqueous mole fraction detergent is more or less given by the CMC it follows that K_{mic} is related to the CMC.

$$K_{\text{mic}} = \frac{1}{\text{CMC}_{\text{mole fraction}}} \triangleq \frac{55.6}{\text{CMC}_{\text{molar}}} \tag{2.5}$$

In more detail, if $K\cdot$CMC (in molar) equals 1 the standard Gibbs energy of detergent binding to vesicles (eq. (2.6)) is equal to the standard Gibbs energy of micellisation (eq. (2.7)).[39]

$$\Delta_{\text{binding}}G^0 = -RT\ln(55.6K) \tag{2.6}$$

$$\Delta_{\text{mic}}G^0 = -RT\ln\left(\frac{\text{CMC}}{55.6}\right) \tag{2.7}$$

The factor 55.6 is the molar concentration of water in water and has to be added since ΔG should be calculated in terms of mole fractions rather than concentrations (eq. (2.5)).
For most surfactants this relationship is valid within 2 kJ/mol (factor of *ca.* 2 in K or CMC) and hence K can be predicted rather well once the CMC is known. This approach has been validated in the literature.[40]
It should be noted that turbidity experiments are a rather insensitive method. It is based on a change in measured absorbance due to the scattering of light. Therefore, anything that scatters light significantly will be detected, and hence, anything that has a small scattering ability will not be detected. This means that a small concentration of large vesicles will be readily detected by an increase in turbidity, whereas a moderate concentration of small vesicles, worm-like micelles, or bilayer fragments will not be detected. As a result, reported values for R_{sat} and R_{sol} do not necessarily represent the true point of detergent saturation or solubilisation of the vesicles. Nevertheless, turbidity experiments have led to useful results. More sensitive methods, but yet more elaborate techniques, include ITC[22,37,38] and dynamic light scattering (Section 2.3.3).
Finally, it is important to know whether the detergent binds to both the inner as well as the outer leaflet, or only to the outer leaflet. Ionic detergents are expected to experience a large kinetic barrier for crossing the bilayer since the bilayer interior is rather apolar. However, experiments have shown that nonionic detergents, such as Triton X (Scheme 2.3B), rapidly cross the bilayer.[22,41,42]

2.3.2.1 Eicosa-Ethylene Glycol Mono *n*-Hexadecyl Ether

Eicosa-ethylene glycol mono *n*-hexadecyl ether (**$C_{16}EO_{20}$**; Scheme 2.3A), also known as Brij 58, is not often used in membrane solubilisation. Usually detergents with a shorter alkyl tail and a shorter ethylene glycol head group are used (**C_nEO_m**; n=10-12, m=3-8). Their binding strength has been well studied in the literature.[39,43] Addition of two CH_2 groups to the hydrophobic tail only leads on average to an increase of the binding by a factor of at most 20, whereas addition of 1 ethylene glycol unit leads to a decrease in the binding constant by a factor of 1.6. It is ambitious to derive (extrapolate) the expected binding constant for **$C_{16}EO_{20}$** from these data. The binding constant cannot be measured experimentally using ITC since ITC requires titration of a vesicular solution into a solution containing the detergent below the CMC. The CMC of **$C_{16}EO_{20}$** is approximately 3.9 μM.[44] However, using the relationship $K \cdot \text{CMC} = 1$ (in molar concentration; eqs. (2.6) and (2.7)) the binding constant can be roughly estimated. For **$C_{16}EO_{20}$** it is expected to be around $2.5 \cdot 10^5$ M^{-1}. This means that at any given amphiphile concentration **$C_{16}EO_{20}$** is completely bound.
Figure 2.3 shows the phase diagram for various amphiphile concentrations. As can be seen, above 2 mM **$C_{18}C_{18}$+** there is a linear relationship between the concentrations of **$C_{18}C_{18}$+** and **$C_{16}EO_{20}$** at the phase boundaries. The R_{sat} and R_{sol} values are 0.84 and 12, respectively. The bilayer composition at the saturation point is similar to what has been found when **$C_{18}C_{18}$+** vesicles (R_{sat} *ca.* 1)[45] or phospholipids vesicles (R_{sat}=0.48-0.66) were solubilised by **$C_{12}EO_8$**.[46-48] However, the value of 12 we find at the solubilisation point is much higher than reported in the literature (R_{sol}=1.8-5). Experiments with erythrocyte membranes and a series of **C_nEO_8** surfactants show a decrease in R_{sat} and R_{sol} from 2.23 to

0.03 and from 3.45 to 0.06, respectively, for n=10 to n=18.[43] The largest changes are found going from n=10 to n=12. Apparently, **$C_{16}EO_{20}$** saturates membranes with a R_b similar to that of **$C_{12}EO_8$**, but is much less efficient in completely solubilising them than most other nonionic ethylene glycol detergents. In addition, it should be noted that solubilisation of membranes that are in the gel-like state is more difficult than when they are in the liquid-crystalline state.

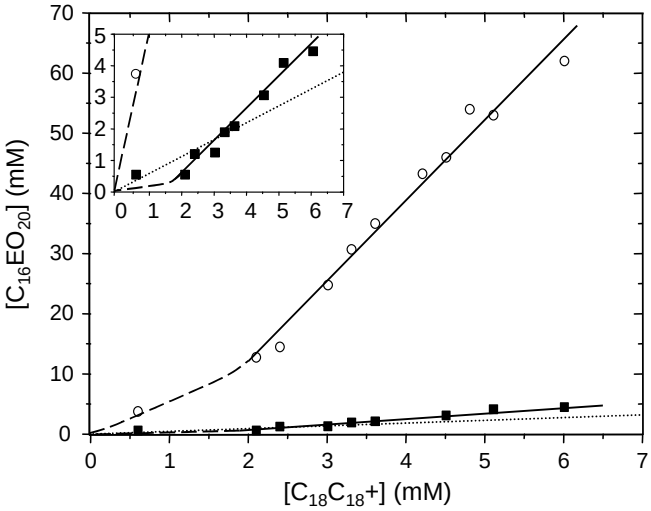

Figure 2.3. *Phase diagram of vesicle solubilisation of* ***$C_{18}C_{18}$+*** *by* ***$C_{16}EO_{20}$****. Solid lines are linear fits through the points of detergent-saturated vesicles (R_{sat}; ■) and fully solubilised vesicles (R_{sol}; ○). Dashed lines are anticipated phase boundaries crossing the y-axis at the CMC of* ***$C_{16}EO_{20}$****. The dotted line represents solutions containing 35 mol% of* ***$C_{16}EO_{20}$****. The inset shows the R_{sat} values in more detail.*

Extrapolation of the R_{sat} and R_{sol} lines to zero amphiphile concentration leads to negative values of the intercept. Since the intercept is related to the free detergent concentration (CMC), this is physically impossible. Usually, the intercept is slightly smaller than the CMC of the detergent.[36] Since the CMC of **$C_{16}EO_{20}$** is small (and K high), the ratio of the slope to the intercept is large. These factors might contribute to the negative value for the intercept, but we have no clear explanation.

In general, vesicular solutions to which micelles are added require time to reach equilibrium, since reorganisation of amphiphile and detergent into different types of aggregates can be slow.[42] Therefore, usually solubilisation experiments are done with vesicles in the liquid-crystalline state. Our experiments were performed below the phase transition temperature, which may lead to further complications.[49] In fact, in several of the solution mixtures we observed partial precipitation after allowing the solution to equilibrate over night, indicating that our samples precipitate after extensive equilibration. However, we note that this process is observed in detergent-free solutions as well, although in those cases the process of precipitation is much slower. We contend that our experiments were done at the optimum time to allow a large extent of equilibration, but with as little precipitation as possible. Experiments involving precipitation were repeated, and all data fitted reasonably on the absorbance versus detergent concentration curves. Solutions prepared by cosonication of detergent and amphiphile should be in the equilibrium state since no re-equilibration should have to take place, besides of course the fact that most vesicles are intrinsically metastable.

2.3.2.2 *n*-Dodecyl-*β*-Maltoside

For membrane solubilisation the disaccharide *n*-dodecyl-*β*-maltoside (**C_{12}Mal**; Scheme 2.5) is not a popular detergent.[19] Usually, for experimental considerations **C_{10}Mal** is preferred. However, in practice more experiments have been performed with monosaccharide octyl glucoside (**C_8Glu**).[33,50-54] An important observation is that sugar-derived detergent can induce vesicle fusion prior to saturation.[33]

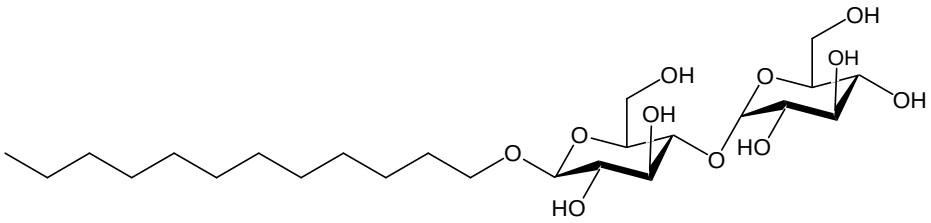

Scheme 2.5. *n-Dodecyl-β-maltoside (**C_{12}Mal**).*

The CMC of **C_{12}Mal** is 150-200 μM,[19,22,55,56] and hence we expected a binding constant of *ca.* 5000-7000 M^{-1}. Using ITC the binding constant has been measured, and a value of 5000 M^{-1} has been reported.[39]

Figure 2.4 shows the phase diagram of mixtures of **$C_{18}C_{18}$+** and **C_{12}Mal**. Due to fewer data points, and somewhat unusual behaviour of these detergent/amphiphile mixtures (Section 2.3.3.4) the pattern is not as clear as that for **$C_{16}EO_{20}$**. Especially, the crossing of the R_{sat} and R_{sol} line is usually not observed. However, this crossing has been observed for solubilisation experiments of phospholipid vesicles by a series of sugar-based surfactants (including **C_{12}Mal**).[57]

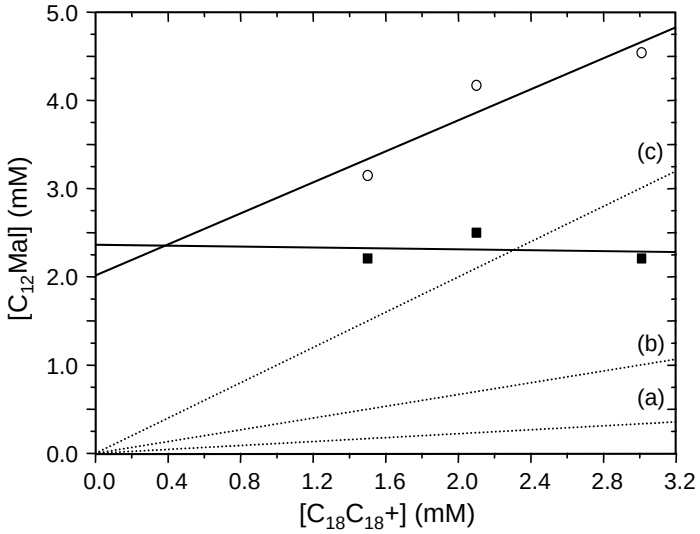

Figure 2.4. *Phase diagram of vesicle solubilisation of **$C_{18}C_{18}$+** by **C_{12}Mal**. Solid lines are linear fits through the points of detergent saturated vesicles (■) and fully solubilised vesicles (○). Dotted lines represent solutions containing 10 (a), 25 (b) and 50 mol% (c) of **C_{12}Mal**.*

For these reasons and "odd" behaviour (Section 2.3.3.4) we decided to refrain from a detailed interpretation. We only note that up to 3 mM of **$C_{18}C_{18}$+** about 2 mM **C_{12}Mal** is needed to saturate the membrane. The slope in the R_{sol} line is 0.88 (lit. 2.34[57]), which is considerable smaller than that found for **$C_{16}EO_{20}$** indicating that **C_{12}Mal** readily solubilises membranes of **$C_{18}C_{18}$+**. In fact, less than one molecule of **C_{12}Mal** is needed per molecule of **$C_{18}C_{18}$+** to solubilise vesicles into mixed micelles.
The remarks made for solutions containing **$C_{18}C_{18}$+** and **$C_{16}EO_{20}$** about the time required to reach equilibrium are also valid for mixtures of **$C_{18}C_{18}$+** and **C_{12}Mal** (Section 2.3.2.1).

2.3.3 Dynamic Light Scattering

2.3.3.1 Theoretical Considerations

Dynamic light scattering (DLS), also known as quasi-elastic light scattering (QELS) and photo correlation spectroscopy (PCS), is a powerful technique to measure the size distribution of aggregates present in solution. DLS is able to report a statistically meaningful size distribution by performing only a single experiment. The time required to perform a DLS experiment on a vesicular solution is less than one hour. However, there are also several drawbacks and considerations that have to be taken into account before performing a DLS experiment, particularly since DLS always reports a size distribution regardless the quality of the experiment and/or the sample under study.
Dynamic light scattering is based on the random diffusion (Brownian motion) of particles in solution. When laser light (in our case 632 nm) enters the solution, particles scatter the light. When the particles are small (<60 nm, *i.e.* $< \lambda_{laser}/10$; Rayleigh scattering) the light is randomly scattered into all directions. When the particles are larger, scattering is no longer random (Mie scattering) and the scattering becomes particle-size and angle-dependent. However, at 90 degrees the scattering intensity is usually acceptably high for most particle sizes.
In the ideal case when only spherical particles with one size are present in solution, the diffusion coefficient of the particle can be calculated from the fluctuations in the light intensity induced by the moving particle. This is done with a photocorrelator that correlates the signal intensity with time. In case of a large particle, the correlation is lost only slowly with time since large particles move only slowly (Figure 2.5A). In case of small particles, the correlation is lost quickly (Figure 2.5B). From the diffusion coefficient the hydrodynamic radius (R_h) can be calculated using the Stokes-Einstein relationship:

$$R_h = \frac{k_B T}{6\pi\eta D} \tag{2.8}$$

In this equation k_B, T, η and D are the Boltzmann constant, absolute temperature, viscosity and diffusion constant, respectively.
In non-ideal cases, *i.e.* when there are particles present with different sizes, there is not one diffusion coefficient and hence the measured diffusion constant has to be split up mathematically. This leads to a size distribution. This splitting up can be carried out using several different algorithms, such as, for example, CONTIN, cumulant analysis, nonnegative least-squares analysis (NNLS), or the "automatic" analysis.[58,59] In most of these fitting

procedures the upper and lower size limit can be set to a certain value. When the particle size distribution is relatively narrow and monodisperse, these algorithms will give more or less the same size distribution. However, when the size distribution is polydisperse and/or multimodal, the different analysis methods will report different results. In this case analysis of the data can become too complicated to ensure reliable values for the size distribution. Consequently, reports in the literature about measured particle sizes are rather meaningless unless the width of the distribution is reported.
In the case of non-spherical particles (Figure 2.5B) diffusion is not equal in all directions, and hence the reported size distribution becomes broader, as if there are particles in solution with the minimum and maximum width of the particle, and all sizes in between. In order to obtain an idea of the extent to which the particles are non-spherical, the angular dependence of the intensity of the scattered light can be measured. Using the Guinier approximation,[60,61] the angular dependence can be described by eq. (2.9):

$$I(\theta) \propto \exp\left(\frac{-q^2 R_g^3}{3}\right), (qR_g \ll 1) \tag{2.9}$$

In this equation R_g is the radius of gyration and q the scattering factor:

$$q = \frac{4\pi n_s}{\lambda_0} \sin(\theta/2) \tag{2.10}$$

In this equation n_s is the refractive index of the solvent and θ_0 is the wavelength of the laser beam. The ratio of R_g/R_h yields then information on the shape of the particle. For example, cylindrical micelles have a value of R_g/R_h of *ca.* 2.[60,62]
We decided to refrain from such an analysis since the results are not required for an understanding of our experimental results described in the other chapters in this thesis.

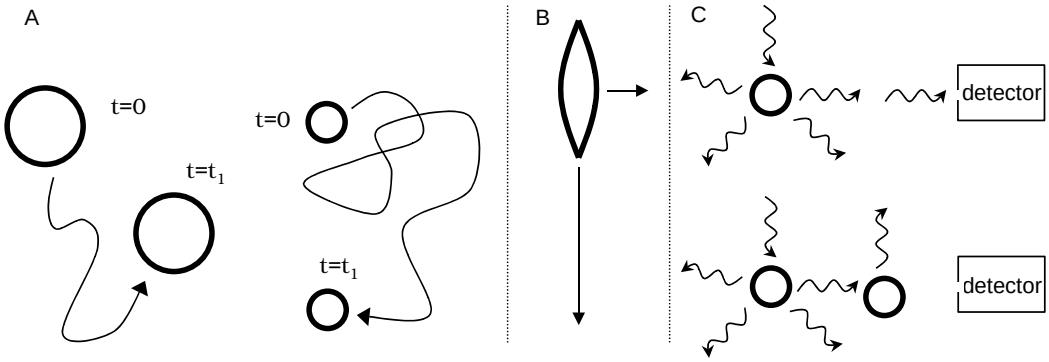

Figure 2.5. *A: Example of random diffusion of a large (left) and a small (right) particle through a solution. B: Diffusion of a non-spherical particle. The arrows denote the relative size of the diffusion constant in that specific direction. C: Example of double scattering due to a high concentration of particles in solution.*

Another drawback of DLS, besides the inability to handle polydisperse and multimodal size distributions, is the strong dependence of the scattering ability on particle size. For a given concentration increasing the particle size ten-fold the scattered intensity will be 10^6 times larger. This makes it difficult to observe the presence of micelles if in the same solution vesicles are present as well, except when the micelles are present in much larger

concentrations. We also note that the presence of dust particles will strongly influence the results.

As a result of the strong dependence of the scattered intensity on particle size, only an intensity-weighted size distribution can be calculated. This means that when there are two different sized particles in solution that differ by a factor of ten in size, and their concentrations are equal, that the peak of the larger particle will be 10^6 times higher than the peak of the smaller particle. Hence, if the two peaks would be equal, this would mean that the concentration of the smaller particle is 10^6 times higher than the concentration of the larger particle.

In concentrated samples scattered light can be scattered again (double scattering), leading to misleading results, since the doubly scattered light will not reach the detector. Therefore, experiments should be performed under conditions that the amount of scattered light is linear with the concentration of the particles.

Large particles (> 1 μm) usually have a tendency to precipitate. Since precipitation is fast relative to the Brownian motion of similar-sized particles, the reported diffusion coefficient will be largely determined by the rate of precipitation. Hence, since the size distribution is calculated from the diffusion coefficient, the size distribution will report a size that is smaller than the actual size distribution.

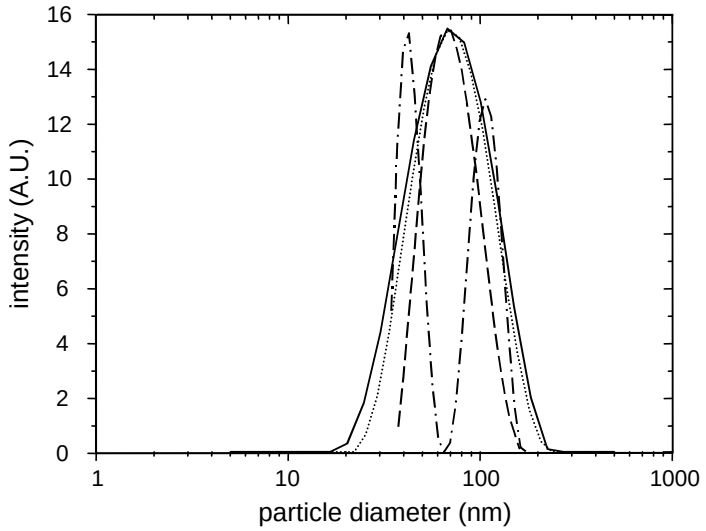

Figure 2.6. *Example of size distribution as calculated with various algorithms (10 mol% of* ***C_{12}Mal****). Solid line CONTIN 5-500 nm; dashed and dashed-dotted line CONTIN autorange; dotted line automatic.*

In Figure 2.6 an example of the results of a DLS experiment is given. The solution contains 0.5 mM **$C_{18}C_{18}$+** cosonicated with 10 mol% of the micelle-forming **C_{12}Mal**. Small micelles have a low scattering intensity (typically 0.1-1 kCounts s^{-1}), whereas that of vesicles is usually much higher (> 50 kCounts s^{-1}). Considering that this solution has a scattered intensity of around 130 kCounts s^{-1}, there are large particles in solution. All the data was analysed using the CONTIN and automatic algorithm. In the automatic algorithm the upper and lower size limits are chosen by the software, in the CONTIN algorithm the upper and lower size limit can both be chosen by the software or manually chosen. The experiment shown in Figure 2.6 was repeated five times on the same solution and two different size distributions were found (dashed and dashed-dotted line) using the CONTIN algorithm,

where the upper and lower limits were automatically chosen such that the upper limit is 100 times larger than the lower limit. One size distribution is monomodal, and the other bimodal. A closer look reveals that the maximum in the monomodal distribution is in between the two maxima of the bimodal distribution. The total width of the distribution is similar for both distributions. Considering that the overlap between the two distributions is rather large, we anticipate that the monomodal distribution is the more likely distribution, since we cannot rationalise why two different vesicle populations should exist. Therefore, we believe that these different distributions are probably due to small variations in the experimental data.
We consider a size distribution to be likely, if under the different fitting conditions the results are similar. For solutions containing 10 mol**%** of **C_{12}Mal** we therefore suggest that they possess a distribution with a maximum around 100 nm, and a width that goes up to 200 nm.

2.3.3.2 Di-*n*-Octadecyldimethylammonium Chloride

In Figure 2.7A the scattered intensity and Z_{ave} as a function of the concentration of **$C_{18}C_{18}$+** are shown. Z_{ave} is the average particle size, assuming that there is no size distribution, *i.e.* there are only particles with a single size. This makes Z_{ave} independent of the size distribution algorithm. Of course, this is highly unrealistic, however, it gives a good idea of the dynamics of the system. Below a concentration of 2.1 mM of **$C_{18}C_{18}$+** the scattered intensity is linearly related to the concentration. In addition, Z_{ave} is independent of the concentration of **$C_{18}C_{18}$+**, except that at higher concentrations the scattering in Z_{ave} is smaller. This proves that in this concentration range there is no double scattering. This is also supported by the independence of the size distribution with concentration.
The scattered intensity and the Z_{ave} value of a 0.5 mM solution of **$C_{18}C_{18}$+** were followed with time (Figure 2.8A). Z_{ave} scatters between 85 nm and 115 nm. In the first 10 hours the scattered intensity fluctuates up and down by about 6%. Then, it steadily decreases. This might indicate precipitation of larger particles. Once precipitated, the apparatus can no longer detect them, and hence a lower scattered intensity is reported. Therefore, after 19 h the solution was stirred, leading to a small increase in scattered intensity. However, neither Z_{ave} nor the size distribution changes after stirring. Then, the scattered intensity gradually increases, but again, Z_{ave} and the size distribution do not change. However, the increase in scattered intensity is rather small, making it difficult to detect subtle changes in the size distribution. Finally, the solution was stirred again after 90 hours, as can be seen in the jump in scattered intensity.
Vesicles formed from **$C_{18}C_{18}$+** are not spherical as was shown by cryo-electron microscopy (Figure 2.1a) and reported in the literature for **$C_{18}C_{18}$+** with bromide counterions.[11,16] As a result, the reported size distribution will be broader relative to spherical vesicles with the same volume. The size reported by DLS is in agreement with the size indicated by cryo-electron microscopy.

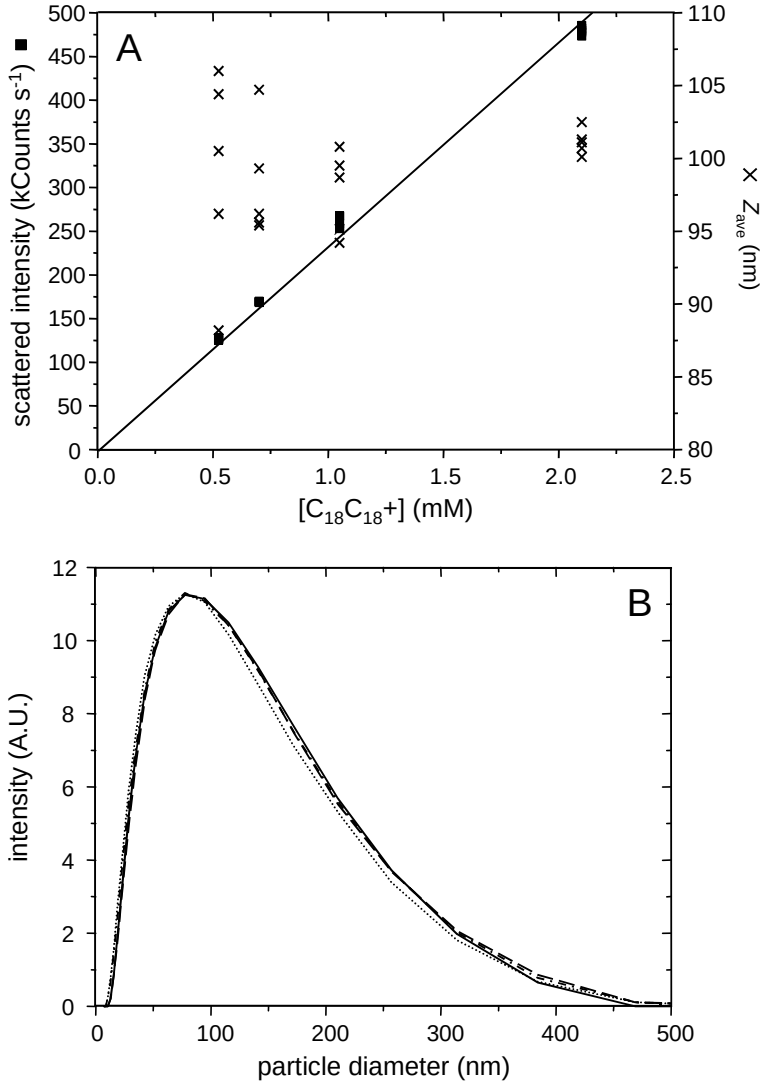

Figure 2.7. *Plots of the stability and size (A) and size distribution (B) of vesicles formed from* ***$C_{18}C_{18}$+*** *at various concentrations (same concentrations as in A). A: scattered intensity (■) and Z_{ave} (×). A: The line is a linear fit of the scattered intensity (forced through zero).*

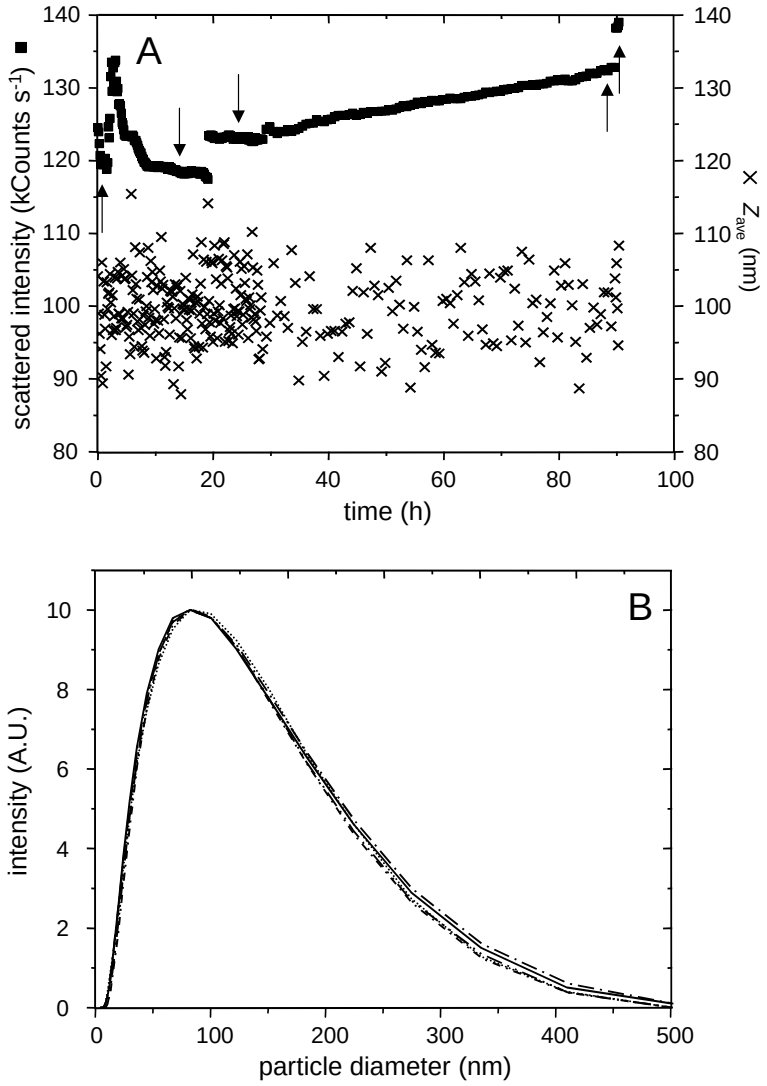

Figure 2.8. *Plot of the stability and size (A) and size distribution (B) of vesicles formed from* $\mathbf{C_{18}C_{18}+}$*. A: scattered intensity (■) and* Z_{ave} *(×). Arrows in A indicate moments for which the size distributions are shown in B.*

2.3.3.3 Eicosa-Ethylene Glycol Mono-*n*-Hexadecyl Ether

Solutions containing various amounts of $\mathbf{C_{16}EO_{20}}$ were prepared in three different ways. In the first procedure amphiphile and detergent were dissolved and sonicated simultaneously at the appropriate ratio. The amphiphile concentration was 30 mM. DLS experiments were performed just after diluting the solution to 0.5 mM $\mathbf{C_{18}C_{18}+}$. In the second procedure vesicles containing $\mathbf{C_{18}C_{18}+}$ and 5 mol% of $\mathbf{C_{16}EO_{20}}$ were prepared, and then to the same sample increasing amounts of $\mathbf{C_{16}EO_{20}}$ were added from a concentrated stock solution (0.5 mM $\mathbf{C_{18}C_{18}+}$). In a third procedure $\mathbf{C_{18}C_{18}+}$ vesicles were prepared, and to different samples containing 2.1 mM $\mathbf{C_{18}C_{18}+}$ various amounts of $\mathbf{C_{16}EO_{20}}$ micelles were added. Solutions were then allowed to equilibrate for 60 h. We decided to follow these different procedures in order to obtain information about the dynamics of the system.

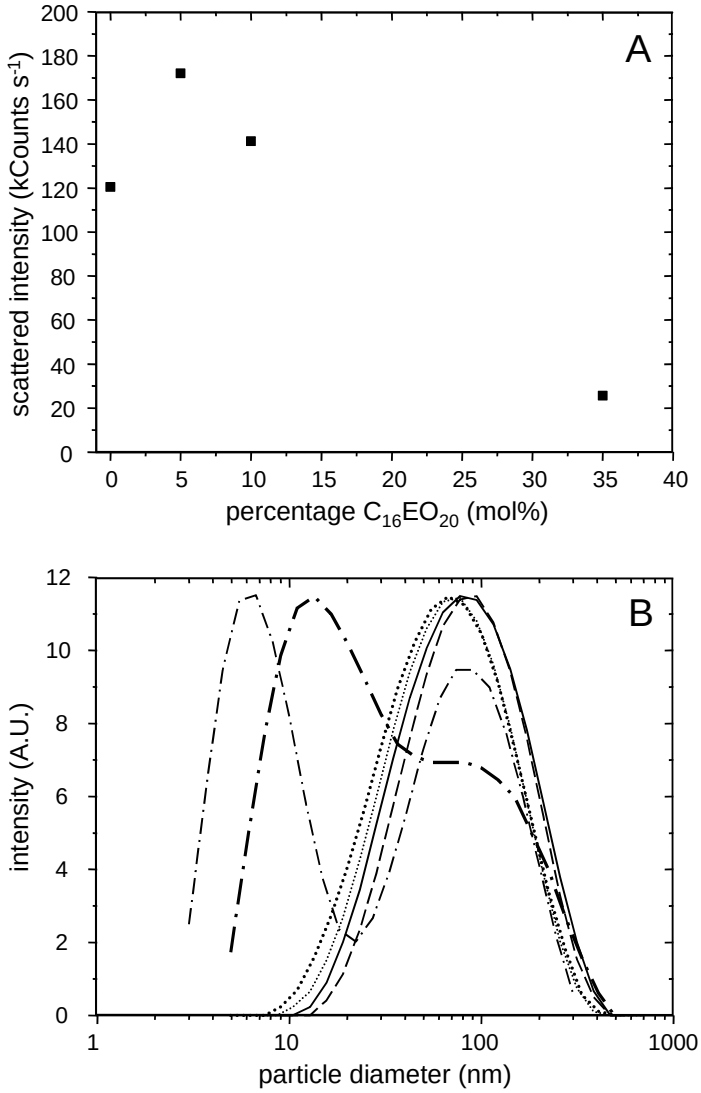

Figure 2.9. *Plot of the scattered intensity (A) and size distribution (B) of vesicles formed from* ***$C_{18}C_{18}$+*** *and* ***$C_{16}EO_{20}$*** *at various mole fractions. Experiments were performed directly after dilution from a 30 mM stock solution, unless stated otherwise. B:* ***$C_{16}EO_{20}$****: 0 mol% (solid line); 5 mol% (dashed line); 10 mol% (dotted line; thick line after 14 h); 35 mol% (dash-dotted line; thick line after 5 h).*

Figure 2.9 shows the results of the first procedure. Initially, upon increasing the concentration of **$C_{16}EO_{20}$** the scattered intensity increases.[40,63] However, already at 10 mol% of **$C_{16}EO_{20}$** the scattered intensity decreases again. The increase is in line with an increase in vesicle size. At 35 mol% it can be seen that micelle formation plays a significant role, since the size distribution shows two peaks (not visible at 10 mol%). One around the original size of the vesicles, and one at about a ten-fold smaller size (7 nm), which agrees with the size of a spherical micelle.[61,62] Because the scattering strongly depends on the size of the aggregate, the fact that we observe micelles, indicates that their concentration is significantly higher than that of the vesicles. Roughly, we can estimate the concentration of

micelles to be about 10^6 times higher, since the peaks are almost equal in intensity (section 2.3.3.1).

When the solutions containing 10 mol% and 35 mol% of **$C_{16}EO_{20}$** are allowed to equilibrate after dilution to 0.5 mM, neither the scattered intensity nor Z_{ave} changes significantly with time (Figure 2.10). In addition, also the size distributions do not change substantially (Figure 2.9B).

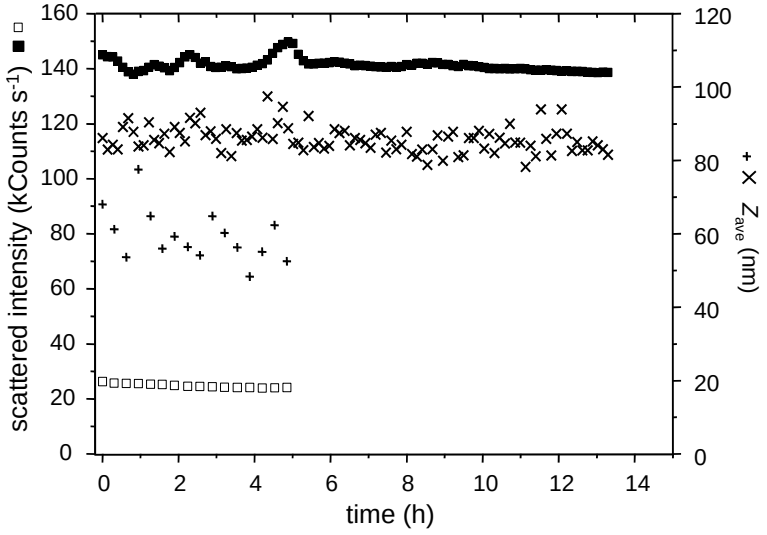

Figure 2.10. *Plot of the scattered intensity and Z_{ave} of vesicles formed from* **$C_{18}C_{18}$+** *and* **$C_{16}EO_{20}$** *at 10 mol% and 35 mol%. Scattered intensity: 10 mol% (■); 35 mol% (□). Z_{ave}: 10 mol% (×); 35 mol% (+).*

It can be concluded that vesicles prepared using the first procedure are stable with time upon dilution (at least 14 h). This effect is not often observed, since upon dilution of a detergent/amphiphile mixture the detergent redistributes over the vesicular/micellar and aqueous phase. Therefore, dilution of these systems leads to reconstitution of vesicles (*i.e.* when the system is in stage II of the solubilisation process; Section 2.3.2), since the amount of detergent bound to the membrane decreases upon dilution. However, due to the large binding constant of **$C_{16}EO_{20}$** (Section 2.3.2.1) redistribution between the two phases does not take place, since all detergent remains vesicular bound.

The second procedure was used to study the dynamics of the mixed detergent/amphiphile system. It can be seen in Figure 2.11 that the scattered intensity increases up to the addition of 65 mol% of **$C_{16}EO_{20}$** that was added within 4 hours. At the same time Z_{ave} increases from 100 nm to 110 nm, as does the maximum of the size distribution (Figure 2.12A). However, at the same time, it can be seen that the scattered intensity decreases in the hour after the addition of a small volume from a concentrated micellar solution of **$C_{16}EO_{20}$**. This indicates that the system does not reach equilibrium, and (substantial and) immediate breakdown of the vesicles only occurs above 65 mol% of **$C_{16}EO_{20}$**. By contrast, when the system is allowed to equilibrate (Figure 2.9A), vesicular breakdown is already seen at 10 mol% of **$C_{16}EO_{20}$** (by a decrease in the scattered intensity).

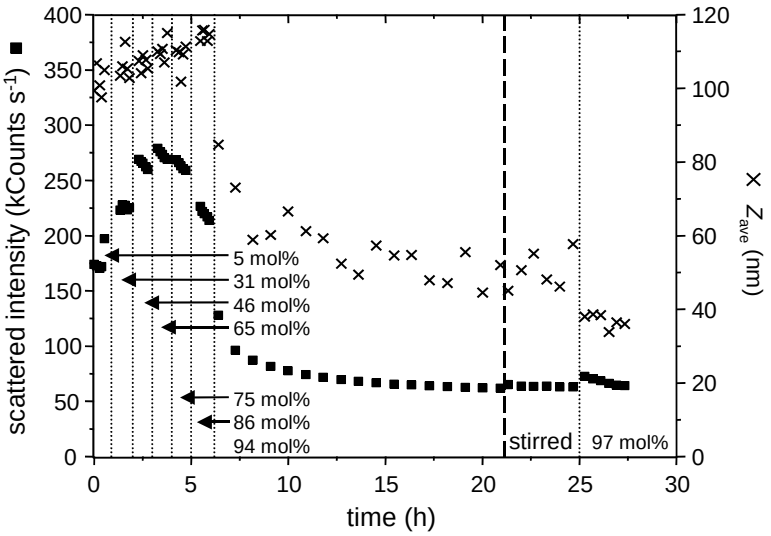

Figure 2.11. *Plots of the scattered intensity (■) and Z_{ave} (×) of vesicles formed from* ***$C_{18}C_{18}$+*** *and* ***$C_{16}EO_{20}$*** *at various mole fractions as a function of time. Experiments were performed by consecutive addition of* ***$C_{16}EO_{20}$*** *micelles from a concentrated solution. Samples were allowed to equilibrate for 15 min. Dotted lines represent the next addition of* ***$C_{16}EO_{20}$*** *micelles. The dashed line represents the time at which the solution was stirred for a few seconds.*

The dynamics of vesicle solubilisation become more clear when the solution to which 94 mol% of **$C_{16}EO_{20}$** was added in 6 h was allowed to equilibrate over night (Figure 2.11). Both the scattered intensity and Z_{ave} decrease until they reach a stable level. At this level there are still vesicles present in solution, as indicated by the still relatively large value of the scattered intensity and Z_{ave}. This assumption is confirmed by the size distributions shown in Figure 2.12B. Directly after addition of 94 mol% of **$C_{16}EO_{20}$** the height of both peaks is more or less similar. After 14 h the height of the peak around 100 nm has significantly decreased.

It can be seen that binding of **$C_{16}EO_{20}$** leads to an increase in size as is shown by the size distribution. Not only the size of the vesicles increases by an increase of the hydrophobic volume, but also because the oligo-ethylene glycol head group increases the hydrodynamic radius. Especially at higher mole fractions of **$C_{16}EO_{20}$** this is probably the result of the oligo-ethylene glycol head group going from a random coil at low mole fraction to a more extended structure at higher molar fraction as a result of steric interactions with each other.

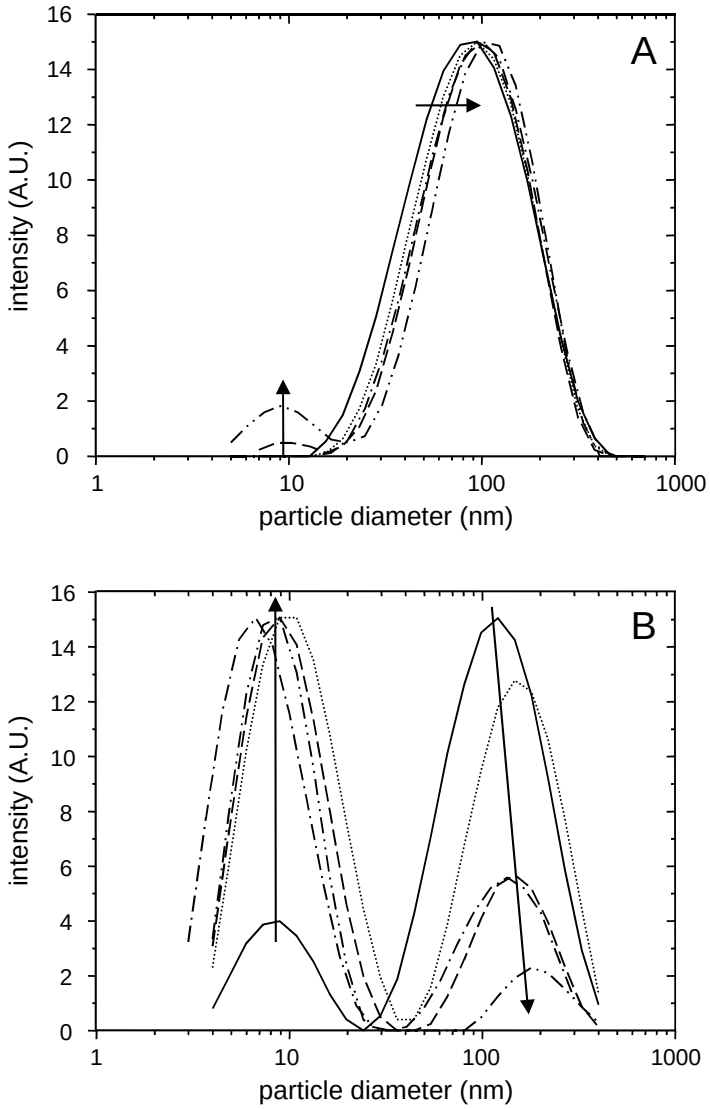

Figure 2.12. *Plot of the size distribution (A+B) of vesicles formed from* $C_{18}C_{18}$+ *and* $C_{16}EO_{20}$ *at various mole fractions. Size distributions correspond to the experiments shown in Figure 2.11. A:* $C_{16}EO_{20}$*: 5 mol% (solid line); 31 mol% (dotted line); 46 mol% (dashed line); 65 mol% (dash-dotted line) and 75 mol% (dash-double-dotted line). B:* $C_{16}EO_{20}$*: 86 mol% (solid line); 94 mol% (dotted line) directly after addition; 94 mol% (dashed line) after 14 h.; 94 mol% (dash-dotted line) after 15 h and stirring; 97 mol% (dash-double-dotted line).*

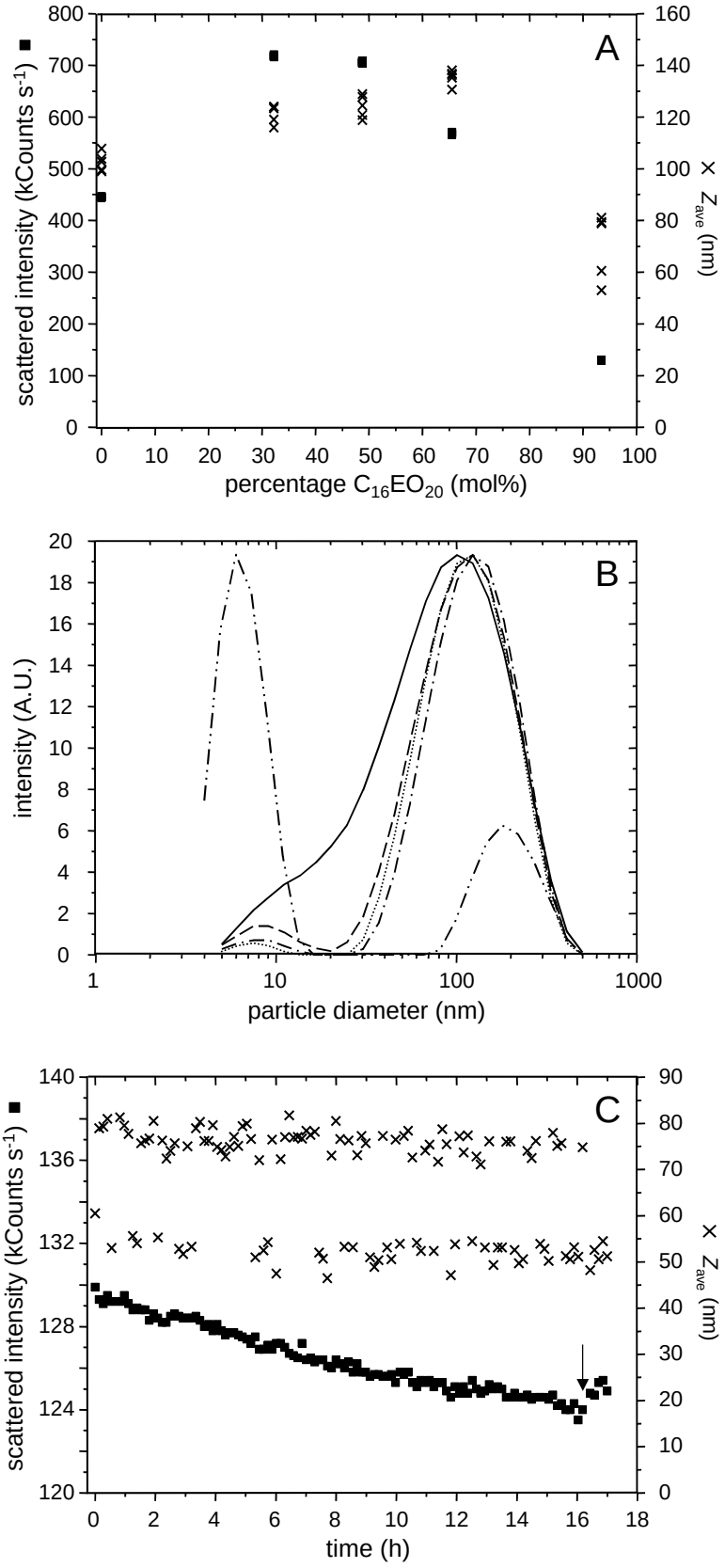
A
scattered intensity (kCounts s-1)
Zave (nm)
percentage C16EO20 (mol%)
B
intensity (A.U.)
particle diameter (nm)
C
scattered intensity (kCounts s-1)
Zave (nm)
time (h)

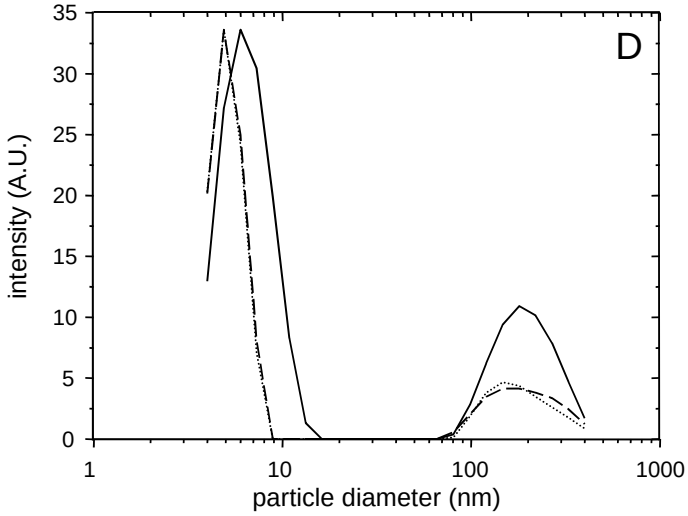

Figure 2.13. *Plot of the scattered intensity and Z_{ave} (A+C) and size distribution (B+D) of vesicles formed from* ***$C_{18}C_{18}$+*** *and* ***$C_{16}EO_{20}$*** *at various mole fractions (A+B), or as a function of the time (C+D). A+C: scattered intensity (■) and Z_{ave} (×). B:* ***$C_{16}EO_{20}$****: 0 mol% (solid line); 32 mol% (dashed line); 49 mol% (dotted line); 66 mol% (dash-dotted line); 93 mol% (dash-double-dotted line). C: 93 mol% of* ***$C_{16}EO_{20}$****. The arrow indicates the time at which the solution was stirred. D: t=0 h (solid line); t=16 h (dotted line); t=17 h and after shaking (dashed line).*

When solutions containing 2.1 mM of **$C_{18}C_{18}$+** with varying amounts of **$C_{16}EO_{20}$** are allowed to equilibrate for 60 h, vesicle saturation is observed below 30 mol% as is indicated by a decrease in scattered intensity (Figure 2.13A). This is in agreement with the turbidity experiments, where samples were prepared following the same procedure as here (Figure 2.3). However, Z_{ave} continues to increase up to 60 mol% of **$C_{16}EO_{20}$** due to incorporation of **$C_{16}EO_{20}$** into the remaining vesicles. Micelles are only detected when their relative concentration is rather high and hence they are only observed above 93 mol% of **$C_{16}EO_{20}$** (Figure 2.13B). This latter solution was examined as a function of time after 60 h of equilibration. Figure 2.13C shows that the scattered intensity is still rather high, and only drops by about 5% in the course of 16 h. Strangely enough, the Z_{ave} values scatter either around 52 nm or around 75 nm, but not in between. They do not vary with time. We have no explanation for this observation, but we can exclude that this results from micelle formation or fluctuations in micelle and vesicle concentrations. This is mainly exemplified by similar size distributions for these different reported Z_{ave} values (data not shown).

In principle, solutions prepared using the first and third procedure should yield similar results, since both solutions are allowed to equilibrate. However, they do not. The mole fraction of saturation and the mole fraction at which micelles are detected are different for both procedures (*ca.* 5 mol% and *ca.* 30 mol% for the first and third procedure, respectively). In addition, scattered intensities and Z_{ave} do not change significantly with time. These complications probably arise from the fact that these systems are metastable, leading potentially to different metastable states, depending on the preparation method. Based on these observations and the results from solutions prepared via the second procedure (Figure 2.11), we propose that trafficking of **$C_{16}EO_{20}$** across the bilayer is rather slow, since otherwise there would be more consistency between the different procedures for vesicle preparation.

2.3.3.4 *n*-Dodecyl-*β*-Maltoside

Stock solutions of about 30 mM **$C_{18}C_{18}$+** were prepared by cosonicating **$C_{18}C_{18}$+** and **C_{12}Mal**, followed by extrusion. These solutions behaved somewhat unusually in their macroscopic behaviour. The solutions with 25 mol% of **C_{12}Mal** became slightly turbid upon standing, but gentle shaking made the solutions transparent with a bluish colour. After about 5 min. they became turbid again. This process was repeatable. After addition of 2.25 mM NaOH from a 1 M stock solution a white precipitate was observed, which disappeared upon vigorous shaking, leading to a transparent bluish solution that was stable overnight (as observed by eye). Precipitation after NaOH addition was also observed for solutions with 50 mol% of **C_{12}Mal**. However, this solution was also rather viscous, which is indicative of the presence of worm-like micelles.[61,62]
When the scattered intensity of these various solutions is considered (Figure 2.14A), it can be seen that above 25 mol% of **C_{12}Mal** the scattered intensity decreases.

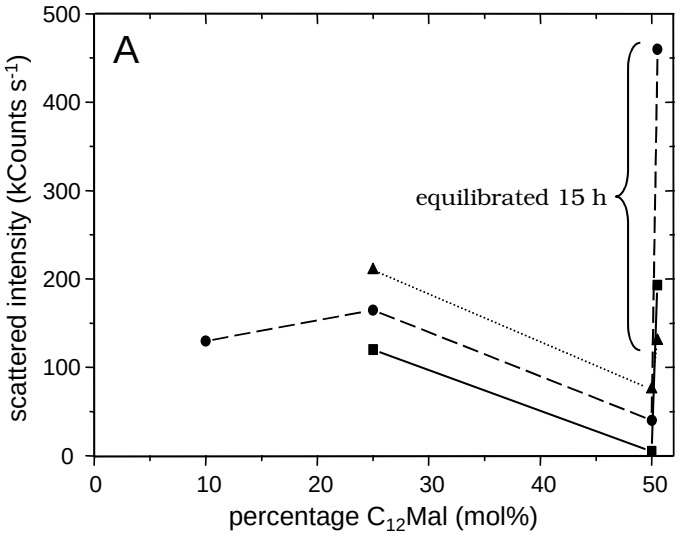

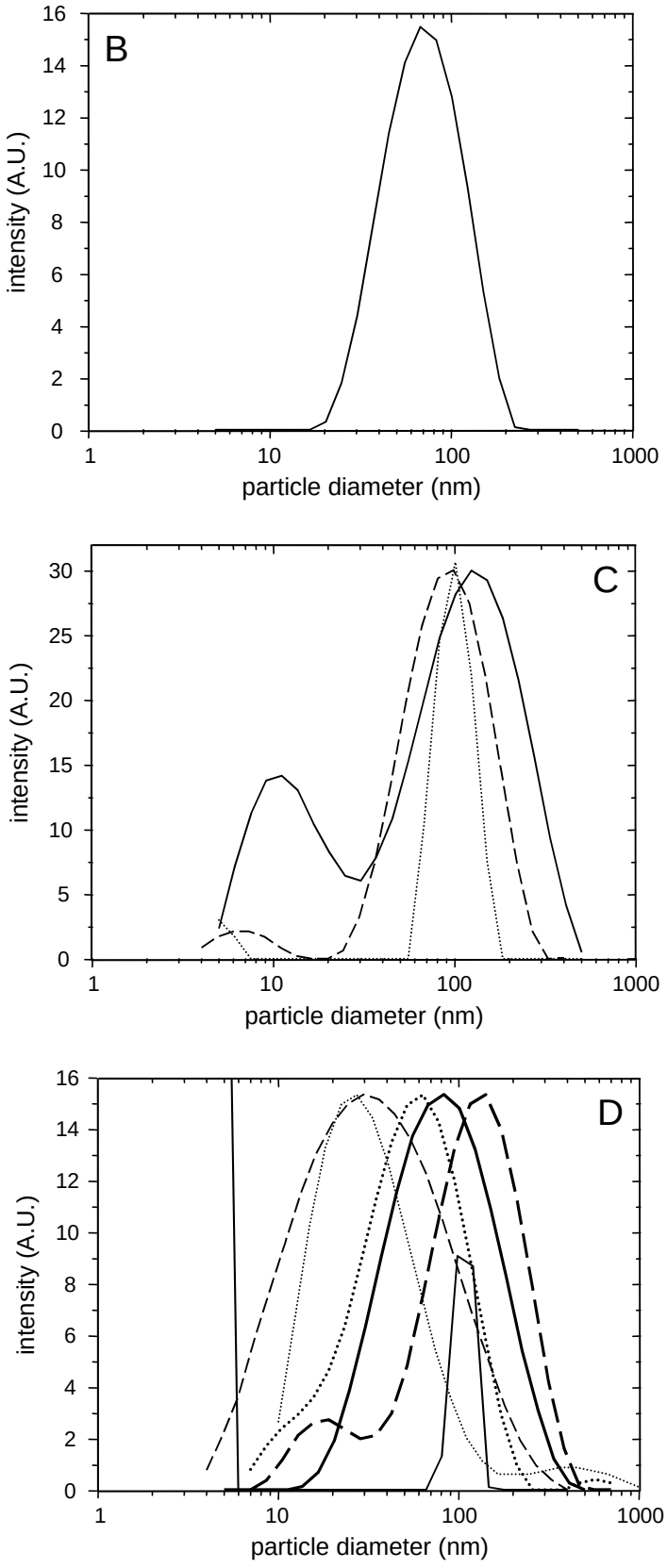

The figure caption can be found on the next page.

Figure 2.14. *A: Plot of scattered intensity versus the mole percentage* ***C_{12}Mal****. No NaOH added (■); 2.25 mM NaOH added (●); diluted from a 30 mM stock solution after visual precipitation upon NaOH addition (▲). B-D: Size distributions for 10 mol% of* ***C_{12}Mal*** *(B), 25 mol% of* ***C_{12}Mal*** *(C) and 50 mol% of* ***C_{12}Mal*** *(D). B: 2.25 mM NaOH. C+D: Solid line no NaOH added; dashed line 2.25 mM NaOH added; dotted line represents the visually precipitated solution. D: thin lines represent data directly after preparation; thick lines after 15 h equilibration.*

DLS experiments were performed using solutions prepared in three different ways. In all three cases the vesicles were prepared as described in the beginning of this paragraph, but then NaOH was either not added, or added to a dilute vesicular solution, or to a concentrated vesicular solution, that was then shaken and subsequently diluted to the same concentration as the other solutions (0.5 mM **$C_{18}C_{18}$+**).

The trend in the scattered intensity going from 25 mol% of **C_{12}Mal** to 50 mol% of **C_{12}Mal** is the same for all three preparation methods. Upon equilibration overnight the scattered intensity of the solution containing 50 mol% of **C_{12}Mal** is increased for all three preparation methods. However, the absolute values are not the same.

The solution containing 10 mol% of **C_{12}Mal** (Figure 2.14B) shows a monomodal distribution comparable to a solution without **C_{12}Mal** (Figure 2.8B), except that the distribution is narrower. At 25 mol% of **C_{12}Mal**, in the absence of NaOH, the distribution is bimodal (maxima at 10 nm and 125 nm), similar as in the presence of 2.25 mM NaOH. However, in the presence of NaOH the distribution is narrower. The small size peak is rather small, but this does not necessarily mean that the concentration of small particles (micelles) is small, since their scattering ability is rather poor. Vesicles from the precipitated solution show an even narrower distribution. At 50 mol% of **C_{12}Mal**, in the absence of NaOH, there is a peak around 100 nm, but a large peak is showing up at sizes smaller than 5 nm. This observation is in agreement with the low scattering intensity and indicates that the solution mainly consists of (worm-like) micelles and a few larger aggregates. Upon the addition of 2.25 mM NaOH smaller sized vesicles are formed (30 nm), but the distribution is rather broad (starting at 4 nm, and ending at 300 nm). Therefore we suggest that this solution contains a broad mixture of large vesicles, worm-like micelles, and perhaps also spherical micelles. For all three solutions containing 50 mol% of **C_{12}Mal** slightly larger vesicles are formed overnight, consistent with large increases in the scattering intensity. At the small-particle side of the graph there is still a small peak indicating that there is still a large number of small aggregates. However, at the large particle-side of the distribution small peaks are appearing indicating that also some large aggregates are formed. In fact, we visually observed on the bottom of the cuvet some precipitated vesicles, which could not be solubilised upon shaking. Growth of vesicles has also been observed in other solubilisation studies.[27-29]

It is difficult to be fully convinced of the presence of small micelles in the previous solutions, since their scattering is usually negligible compared to the scattering from large aggregates. However, if, due to the transformation of vesicles into micelles, the scattered intensity decreases, this must be due to micelle formation. This decrease can be seen by the decrease in scattered intensity going from 25 mol% to 50 mol% of **C_{12}Mal** and therefore we anticipate that significant micelle formation occurs above 25 mol% of **C_{12}Mal**.

In order to study the dynamics of the systems, five solutions containing a fixed concentration of **$C_{18}C_{18}$+** and various amounts of **C_{12}Mal** were prepared. A certain amount of a concentrated stock solution of **C_{12}Mal** was added to a solution containing 2.1 mM **$C_{18}C_{18}$+** and 2.25 mM NaOH. Then they were left for 60 h to equilibrate.

In the turbidity experiments (Figure 2.4) it can be seen that at 2.1 mM **$C_{18}C_{18}$+**, saturation and solubilisation is supposed to occur around 50 mol% and 65 mol% of **C_{12}Mal**, respectively. In fact, at 50 mol% of **C_{12}Mal**, Z_{ave} and the scattered intensity reach a maximum. However, at 65 mol% still not all vesicles have been solubilised into mixed micelles considering the scattered intensity. Even at 80 mol% of **C_{12}Mal** complete solubilisation is not achieved. Apparently, turbidity experiments are not able to detect the remaining vesicles, or bilayer fragments.

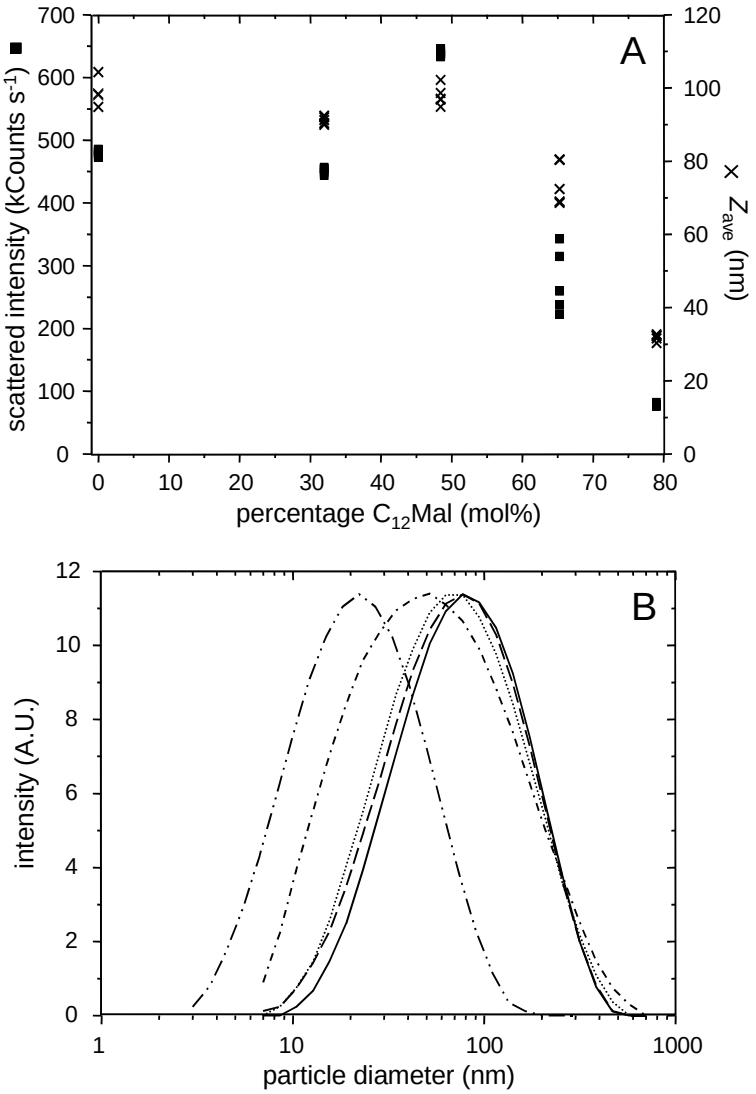

Figure 2.15. *Plot of the scattered intensity and Z_{ave} (A) and size distribution (B) of vesicles formed from **$C_{18}C_{18}$+** and **C_{12}Mal** at various mole fractions. A: scattered intensity (■) and Z_{ave} (×). B: **C_{12}Mal**: 0 mol% (solid line); 32 mol% (dashed line); 48 mol% (dotted line); 65 mol% (dash-dotted line) and 79 mol% (dash-double-dotted line).*

The size distributions shown in Figure 2.15B are in agreement with those shown in Figure 2.14. The most surprising feature is the absence of any indication of micelle formation. The maximum in the size distribution decreases from around 80 nm to 20 nm, but there appears no peak in the spherical micellar region as was observed for **$C_{16}EO_{20}$**.
A shift in the maximum, rather than the appearance of a peak around 5-6 nm has also been observed in the transition from vesicles to worm-like micelles to spherical micelles.[61,62] Therefore, we propose that solubilisation by **C_{12}Mal** proceeds via worm-like micelles, whereas solubilisation by **$C_{16}EO_{20}$** proceeds directly (mainly) to spherical micelles.
We do not fully understand all the processes going on in solutions containing **$C_{18}C_{18}$+** and **C_{12}Mal**. Especially the addition of NaOH leads to substantial changes in the behaviour of the aggregates. It appears that upon addition of NaOH the vesicles tend to grow, but the extent and rate depend on the exact procedure.

2.3.3.5 (2,3-Bis-*n*-Octadecyloxy-Propyl)-Trimethylammonium Chloride

In order to study a molecule more closely related to phospholipids, but without the structural complexities, such as the ester linkage and dipole moment orientation, we decided to study (2,3-bis-*n*-octadecyloxy-propyl)-trimethylammonium chloride (**$C_{18}C_{18}$G+**; Scheme 2.6). This molecule has the same structure as **$C_{18}C_{18}$+**, except that the hydrophobic tails are not directly connected to the head group, but they are connected via a glycerol linker. Contrary to most phospholipids, the tails are connected to the glycerol unit via an ether bond, rather than an ester bond, thereby avoiding complications arising from hydrolysis.

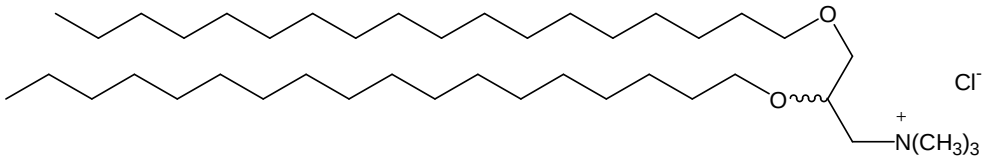

Scheme 2.6. *(2,3-Bis-n-octadecyloxy-propyl)-trimethylammonium chloride (**$C_{18}C_{18}$G+**)*

The solubility of **$C_{18}C_{18}$G+** is rather poor compared to that of **$C_{18}C_{18}$+**. The upper limit of solubilisation is around 25 mM. Figure 2.16 shows the size distribution of a 0.5 mM solution. Rather unexpectedly, besides vesicles with a size of around 100 nm, also micelles are formed (maximum 5-6 nm). This is probably the result of an unfavourable bilayer packing.

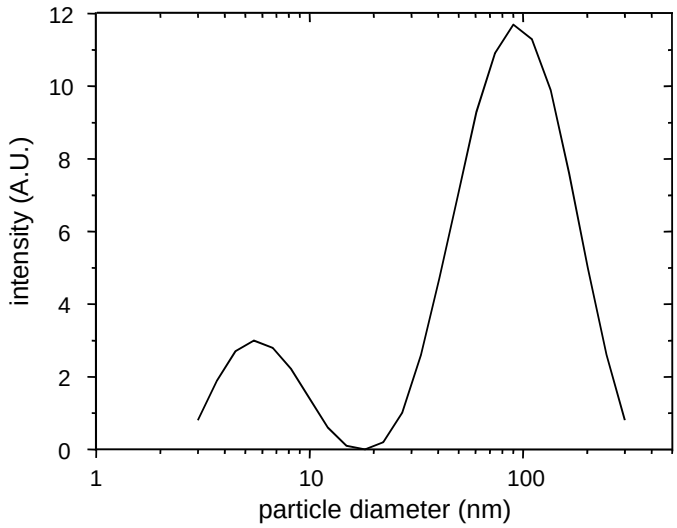

Figure 2.16. *Size distribution of a solution containing 100 mol% of* ***$C_{18}C_{18}G^+$****.*

2.3.4 Differential Scanning Microcalorimetry

2.3.4.1 General Considerations

In Chapter 1 it was discussed that an important feature of vesicles is that alkyl tails of the amphiphiles in membranes usually can reside in two states. At low temperatures the tails are in a highly ordered, rigid (gel-like) state, and at high temperatures the tails are transferred into a more fluid (liquid-crystalline) state. The temperature for this morphological change is typical for each amphiphile and is called the main phase transition temperature (T_m).

Differential scanning microcalorimetry (DSC) is a powerful non-invasive technique for measuring the main phase transition temperature, since it requires no fluorescent or spectroscopic probe.[64] Instead it measures the excess heat that has to be added to the sample cell containing the vesicular solution relative to a reference cell that solely contains water, or buffer, while monotonically increasing the temperature of the cells at a constant rate. This increase is typically 1 degree per minute. Usually, the temperature at which the scan of excess heat versus temperature shows a maximum is taken as the main phase transition temperature. This is, however, in principle incorrect. It is more correct to take the main phase transition temperature at the point where the scan starts to deviate from the base line, since it is at that point that the tails start to go from one phase to the other.[65] In the case of phospholipids the transition is usually rather narrow,[65-75] indicating that all the phospholipid molecules in the membrane go from the gel-like state into the liquid-crystalline in a cooperative way. This is described by the "patch number", which is the number of molecules that go from one phase to the other at the same time.[75] In our system transitions are generally broader, making it more difficult to determine the temperature at which the measured excess heat starts to deviate from the base line. Therefore, we decided to take the maximum of the scans as an indication of the main phase transition temperature.

In addition to the main phase transition, other phase transitions can occur as well. Most of them are transitions to non-lamellar structures, such as inverted hexagonal phases, cubic phases, etc.[76] In membranes the most common additional transition beside the gel-like to liquid-crystalline transition is the transition to the "ripple-phase" (also often referred to as the "pre-transition"),[66,68,70,77-79] which is found in between the gel-like and liquid-crystalline phases. In this phase the membrane adopts a ripple-like structure, where the tails are still in a gel-like conformation. Since this phase is structurally not significantly different from the gel-like state, the enthalpy of this change is usually small leading only to a small peak relative to the main phase transition.

2.3.4.2 Sodium Di-*n*-Decylphosphate

The T_m for **$C_{18}C_{18}$+** vesicles is 40°C (Figure 2.17) which agrees with the literature (37-40°C)[80] and for **$C_{10}C_{10}$-** vesicles 8°C.[12] In Figure 2.17 the scans for pure **$C_{18}C_{18}$+** and mixtures of **$C_{18}C_{18}$+** with **$C_{10}C_{10}$-** are shown. At 10 mol% of **$C_{10}C_{10}$-** a second peak arises around 27°C and this peak becomes more prominent until it reaches a maximum at 50 mol% of **$C_{10}C_{10}$-**. At the same time the peak at 40°C decreases in size and slowly moves towards 30°C, disappearing at 30 mol% of **$C_{10}C_{10}$-**. Above 50 mol% of **$C_{10}C_{10}$-** there is only one peak and upon increasing the amount of anionic amphiphile the peak shifts towards 8°C. Above 75 mol% of **$C_{10}C_{10}$-** it was impossible to perform DSC scans since precipitation took place a few minutes after preparation of the vesicles.

These results can be explained in terms of the presence of neutral microdomains between 10 and 30 mol% of **$C_{10}C_{10}$-**. The peak arising in the range 23-27°C must have a 1:1 cationic:anionic amphiphile ratio since it is the only peak that is observed at 50 mol% of **$C_{10}C_{10}$-**. Therefore we contend that at 10 mol% of **$C_{10}C_{10}$-** neutral microdomains are formed besides a mainly cationic phase. At 30 mol% of **$C_{10}C_{10}$-** these microdomains resolve into a single homogeneous phase again. At the same time as the microdomains are formed, the cationic domains possess an increasing amount of **$C_{10}C_{10}$-** randomly mixed-in since the peak in the DSC scans progressively moves towards lower temperatures.

In principle the appearance of two peaks in the DSC scans could also be due to the presence of two types of vesicles in solution, but this option was ruled out since all cryo-EM pictures show only one type of vesicle present. If there would be two types of vesicles in solution one would expect to see both cationic ("lens"-type vesicles; Figure 2.1a) and catanionic vesicles (aggregates of spherical vesicles; Figure 2.1d) since only the peaks corresponding to these type of bilayers are observed in the DSC scans. Since this is not the case, the peak in the DSC scan at 27°C should belong to neutral microdomains.

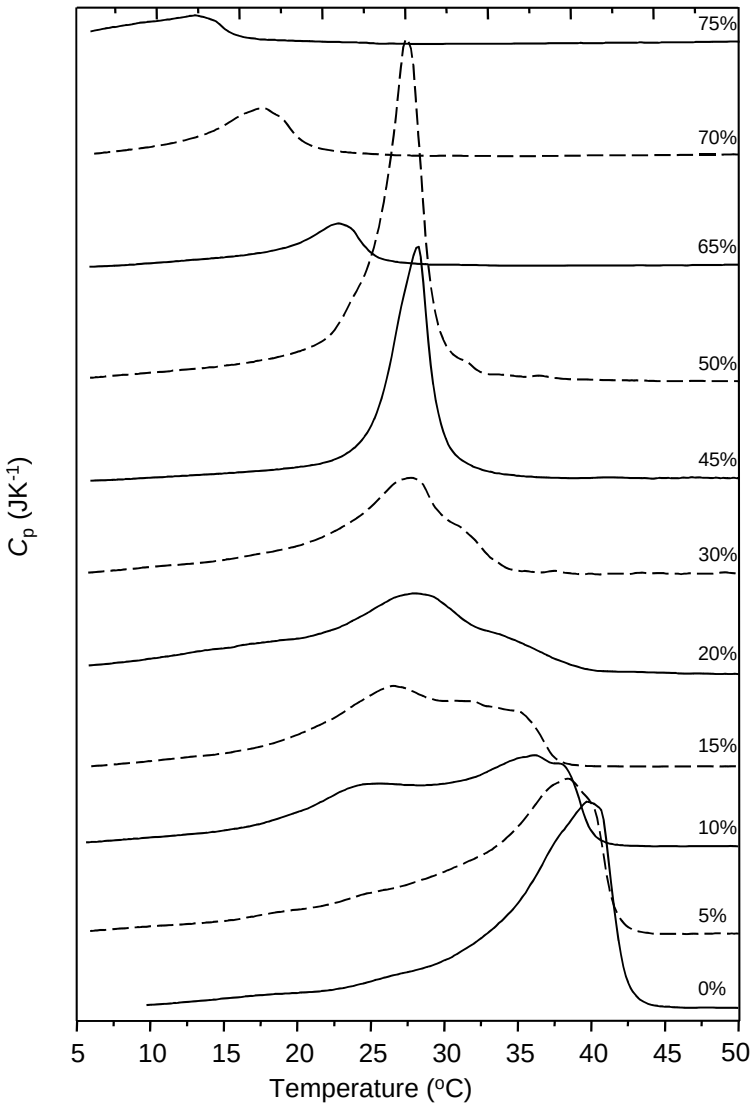

Figure 2.17. *Heating scans for mixtures of* $\mathbf{C_{18}C_{18}}$**+** *and* $\mathbf{C_{10}C_{10}}$**-** *vesicles. The number denotes the mole percentage of* $\mathbf{C_{10}C_{10}}$**-** *as a function of the total amphiphile concentration. Lines have been displaced vertically for clarity.*

2.3.4.3 Sodium *n*-Decyl-*n*-Octadecylphospate

In nature phospholipids with two tails differing significantly in length can be a result of auto-oxidation of unsaturations in one of the tails.[81] The T_m for vesicles formed from the synthetic asymmetric amphiphile sodium *n*-decyl-*n*-octadecylphosphate (**$C_{10}C_{18}$-**) is 21°C.[82]

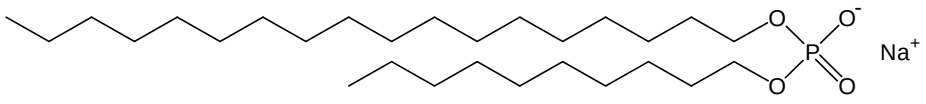

Scheme 2.7. *Sodium n-decyl-n-octadecylphosphate (*$\mathbf{C_{10}C_{18}}$**-**).

This is considerably lower than the T_m of vesicles formed from sodium di-*n*-octadecylphosphate (85°C),[83] but close to that of **$C_{10}C_{10}$-** (11°C).[12] In Figure 2.18 the scans for pure **$C_{18}C_{18}$+** and mixtures of **$C_{18}C_{18}$+** with **$C_{10}C_{18}$-** are shown. Already at 5 mol% of **$C_{10}C_{18}$-** a second peak arises around 34°C and this peak becomes more prominent until it reaches a maximum at 20 mol% of **$C_{10}C_{18}$-**. At the same time the peak at 40°C decreases in size and slowly moves towards 37°C, disappearing at 20 mol% of **$C_{10}C_{18}$-**. This behaviour is similar to what is observed for addition of **$C_{10}C_{10}$-**, except that the peaks appear and disappear at much lower molar ratios. Above 20 mol% of **$C_{10}C_{18}$-** a new peak arises at 36°C that subsequently shifts towards 42°C (at 50 mol% of **$C_{10}C_{18}$-**) being the only peak above 40 mol% of **$C_{10}C_{18}$-**. Above 50 mol% the peak decreases towards the phase transition temperature of 100 mol% of **$C_{10}C_{18}$-**.

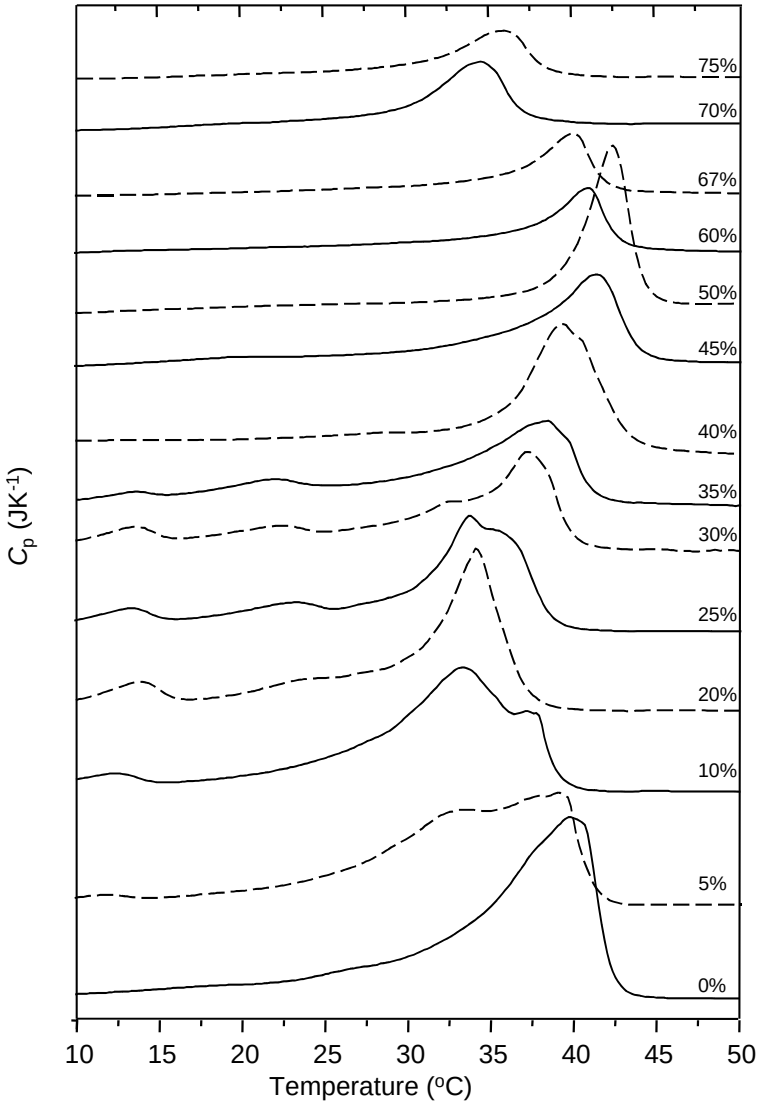

Figure 2.18. *Heating scans for mixtures of* **$C_{18}C_{18}$+** *and* **$C_{10}C_{10}$-** *vesicles. The number denotes the mole percentage of* **$C_{10}C_{10}$-** *as a function of the total amphiphile concentration. Lines have been displaced vertically for clarity.*

It is tempting to conclude that for mixtures of $\mathbf{C_{18}C_{18}^+}$ and $\mathbf{C_{10}C_{18}^-}$ just as for $\mathbf{C_{10}C_{10}^-}$ neutral microdomains are formed. However, mixtures of $\mathbf{C_{18}C_{18}^+}$ and $\mathbf{C_{10}C_{18}^-}$ possess a more complex behaviour (Figure 2.20). For mixtures of $\mathbf{C_{18}C_{18}^+}$ and $\mathbf{C_{10}C_{10}^-}$ the upcoming peak that is related to neutral microdomains has its maximum roughly at the average of the maxima of 100 mol% of $\mathbf{C_{10}C_{10}^-}$ and 100 mol% of $\mathbf{C_{18}C_{18}^+}$. However, in mixtures of $\mathbf{C_{18}C_{18}^+}$ and $\mathbf{C_{10}C_{18}^-}$ the peak that has its maximum at this average disappears above 30 mol%. In addition, at 50 mol% the maximum in the DSC scan is at a higher temperature than for 100 mol% of $\mathbf{C_{18}C_{18}^+}$. Finally, pre-transitions are observed for solutions containing between 5 and 45 mol% of $\mathbf{C_{10}C_{18}^-}$.
These observations make it difficult to assign the peaks to particular phases.

2.3.4.4 Sodium Dimethylphosphate

Sodium dimethylphosphate ($\mathbf{C_{01}C_{01}^-}$; Scheme 2.8) is not an amphiphile since the tails are too short. However, we decided to study mixtures of $\mathbf{C_{18}C_{18}^+}$ and $\mathbf{C_{01}C_{01}^-}$ in order to be able to distinguish between the hydrophobic (tails) and electrostatic (head group) interactions with the cationic amphiphile $\mathbf{C_{18}C_{18}^+}$. The lack of hydrophobic interactions is clear from the near independence of the main phase transition temperature of the concentration $\mathbf{C_{01}C_{01}^-}$ (Figure 2.19). It has been reported that salt can increase the main phase transition with by few degrees, this is usually found only at higher salt concentrations.[84-86] However, the addition of $\mathbf{C_{01}C_{01}^-}$ seems to induce a pre-transition.

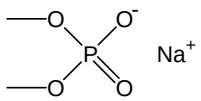

Scheme 2.8. *Sodium dimethylphosphate ($\mathbf{C_{01}C_{01}^-}$).*

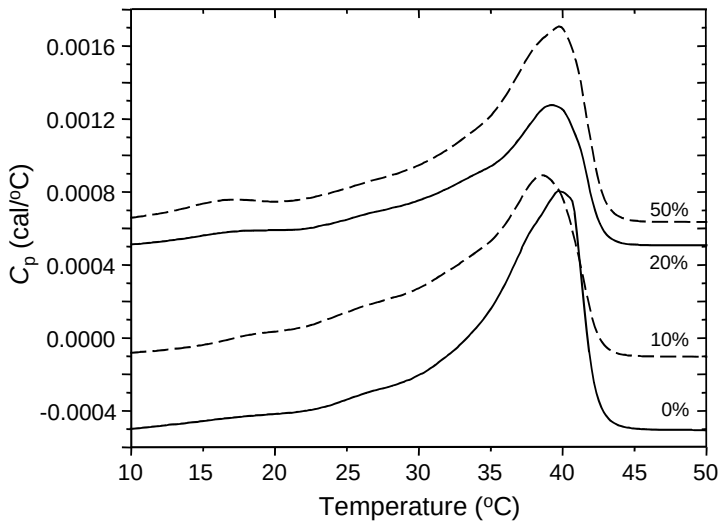

Figure 2.19. *Heating scans for mixtures of $\mathbf{C_{18}C_{18}^+}$ and $\mathbf{C_{01}C_{01}^-}$. The number denotes the mole percentage of $\mathbf{C_{01}C_{01}^-}$ as a function of the total amphiphile concentration. Lines have been displaced vertically for clarity.*

2.3.4.5 Effects of Anionic Double-Tailed Amphiphiles. A Summary

Figure 2.20 shows an overview of the temperatures at which the peaks are observed in the thermograms of mixtures of $\mathbf{C_{18}C_{18}}$**+** with $\mathbf{C_{10}C_{10}}$**-**, $\mathbf{C_{10}C_{18}}$**-** and $\mathbf{C_{01}C_{01}}$**-**. The different effects induced by the three different anionic amphiphiles are clear. The anionic "amphiphile" $\mathbf{C_{01}C_{01}}$**-** has no influence on the phase transition temperature, as anticipated for an inert ion.

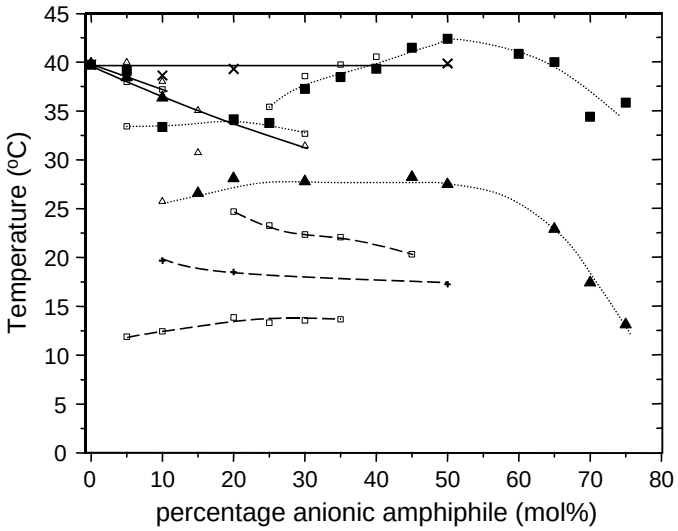

Figure 2.20. *Maxima in the DSC scans as a function of the bilayer composition. Closed symbols indicate the major peak; open symbols are for the minor peaks.* $\boldsymbol{C_{10}C_{10}}$*- (▲);* $\boldsymbol{C_{10}C_{18}}$*- (■);* $\boldsymbol{C_{01}C_{01}}$*- (×; +). Solid lines follow the trend of the initial major peak, dotted lines follow the trend of upcoming peaks and dashed lines follow the trend of pre-transitions.*

In the literature only a few studies concerning mixtures of double-tailed cationic and double-tailed anionic amphiphiles with respect to the influence on the phase transition temperature are known.[70,87] This is not unexpected since these types of mixtures readily form non-lamellar phases.[88-90] We made an endeavour to form stable vesicles from mixtures of $\mathbf{C_{18}C_{18}}$**+** with sodium di-*n*-octadecylphosphate (**$\mathbf{C_{18}C_{18}}$-**) and sodium dioleylphosphate (**$\mathbf{C_{18:1}C_{18:1}}$-**; Scheme 2.9). However, already at 5 mol% of anionic amphiphile precipitation was observed.

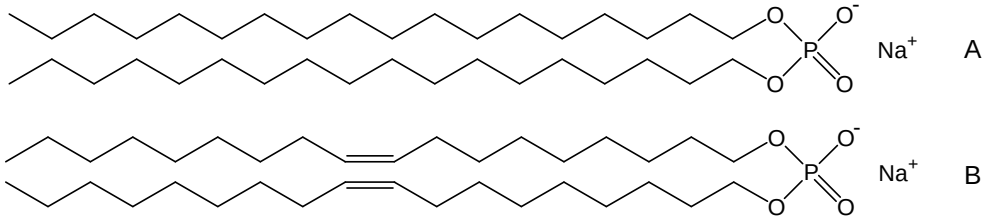

Scheme 2.9. *A: Sodium di-n-octadecylphosphate (*$\boldsymbol{C_{18}C_{18}}$*-). B: Sodium dioleylphosphate (*$\boldsymbol{C_{18:1}C_{18:1}}$*-).*

In a 65:35 molar ratio mixture of several cationic amphiphiles and an anionic amphiphile (Scheme 2.10) the main phase transition temperature was significantly higher for the mixture than for the pure components.[70,87] Depending on the exact structure the peaks are either narrow, or broad showing several maxima. The increase in the main phase transitions temperature was mainly attributed to the electrostatic interaction between the head groups, since the phase behaviour of mixtures of the anionic amphiphile with the fully *N*-methylated amphiphile is similar to that for the tertiary amine amphiphile (**$C_{16}C_{16}$+**).[70] Other work suggests that hydrogen bonding plays a more important role.[87]

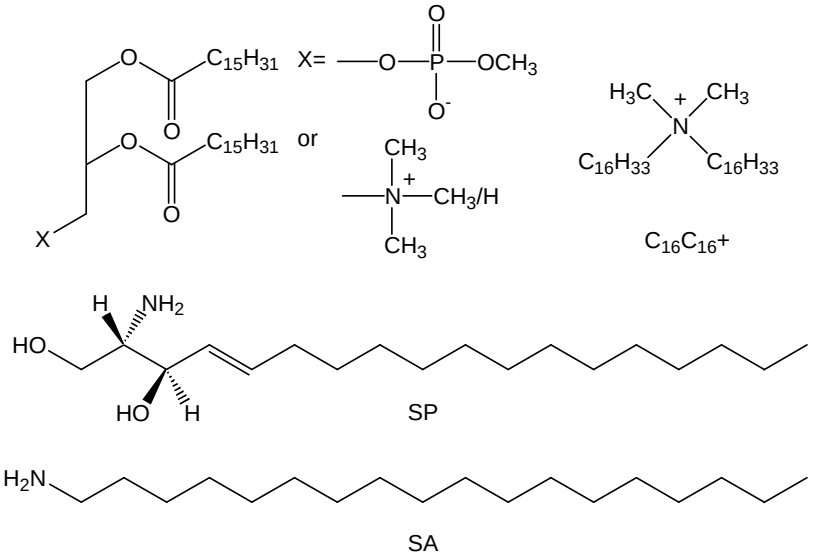

Scheme 2.10. *Cationic and anionic synthetic phospholipid analogues (three compounds in the top), sphingosine (SP) and stearylamine (SA)*

More is known about the phase behaviour with respect to the phase transition temperatures of mixtures of cationic and anionic amphiphiles, where one of the amphiphiles has only one tail. Mixtures of a negatively charged phospholipid (DPPS) with sphingosine (the only natural occurring cationic surfactant[91]) and with stearylamine (Scheme 2.10) were studied at different molar ratios and pH values.[71] The DSC scans show at low pH (when all SP and SA is protonated) that only thermograms with a single peak are observed in the (near) single-component region or when both components are present in (nearly) equal amounts. In addition, at any given molar ratio the T_m is higher than the T_m of the single components, reaching a maximum at the equimolar ratio. The latter results were also found for synthetic analogues.[92] As for mixtures of double-tailed cationic and anionic amphiphile mixtures the effect is attributed to the electrostatic attraction resulting in a tighter packing of the amphiphiles. However, mixtures of SA and the zwitterionic phospholipid DPPC also show that at low pH the T_m increases.[93] The maximum increase only amounts to *ca.* 5 degrees, whereas in the case of negatively charged amphiphile this effect is about 12 degrees, suggesting that hydrogen bonding plays only a partial role.

In the case of double-tailed cationic ammonium amphiphiles and an anionic single-tailed surfactant that are not capable of forming hydrogen bonds, a large (*ca.* 20°C) increase in T_m relative to the T_m of the ammonium amphiphiles is also observed. The mixture reaches its maximum at the equimolar ratio.[86,92,94,95] However, the thermograms often show multiple

and/or broad maxima that are not always reproducible for the subsequent heating scans, indicating a dynamic metastable system.[95]

Despite the large structural differences between the amphiphiles it can be concluded that in most cases, described in the current literature of mixtures of cationic and anionic amphiphiles, the phase transition temperature increases, when vesicles are formed from oppositely charged amphiphiles, reaching a maximum at the equimolar ratio. The thermograms often show multiple and/or broad peaks, indicating that there are different domains or various transitions in the bilayer and that those can be highly dynamic and metastable. The increase in T_m is due to electrostatic and, if possible, hydrogen-bond interactions, that leads to a tighter packing of the alkyl tails. With this in mind, it is remarkable that mixtures of **$C_{18}C_{18}$+** and **$C_{10}C_{10}$-** do not show a maximum in the phase transition temperature at the equimolar ratio. We speculate that this is due to the large hydrophobic mismatch in the alkyl tails inhibiting an efficient packing of the tails. This mismatch even leads to worse packing relative to pure **$C_{18}C_{18}$+**. Similar behaviour was found when negatively charged phospholipids (with *n*-dodecyl tails) were mixed with a series of *n*-alkyltrimethylammonium bromides.[96,97] The T_m was depressed for an *n*-octyl tail, but increased for a *n*-tetradecyl tail. Both *n*-decyl- and *n*-dodecyl-tailed surfactants showed biphasic behaviour, *i.e.* at low mole fraction an increase in T_m and at high mole fraction a decrease in T_m. Probably, for these mixtures, initially due to favourable charge interactions lead to more efficient chain packing, whereas at higher concentration the large number of single-tailed surfactants in the bilayer counteracts this favourable interaction. We anticipate that similar behaviour is to be expected when amphiphiles with opposite charge are mixed and at least one of the tails contains an unsaturation. However, no such an example is present in the current literature. Mixtures of **$C_{18}C_{18}$+** and **$C_{10}C_{18}$-** show at low mole fraction similar behaviour as mixtures with **$C_{10}C_{10}$-**, but at higher mole fractions the main phase transition temperatures increase again. Apparently, the mismatch is not pronounced enough to inhibit efficient packing in mixtures with **$C_{10}C_{18}$-**. This can also be seen in the phase transition temperature of pure **$C_{10}C_{10}$-** that is also lower than that of **$C_{10}C_{18}$-**.

2.3.4.6 Long Linear Alcohols

Addition of small amounts (<20 mol%) of saturated *n*-octadecyl alcohols to cationic vesicles of **$C_{18}C_{18}$+** leads to a decrease of maximum 5 degrees in the main phase transition temperature. At higher mole fractions the main phase transition temperature increases, but much more rapidly and to a higher temperature for *n*-octadecanol (**C_{18}OH**; Scheme 2.11C) than for batyl alcohol (**C_{18}GOH**; Scheme 2.11D). At 50 mol% the main phase transition temperature is 60°C and 45°C for **C_{18}OH** and **C_{18}GOH**, respectively. Addition of *n*-decanol (**C_{10}OH**; Scheme 2.11A) leads to a decrease to 30°C at 30 mol% and it only increases again above 50 mol% to reach a temperature of 33°C at 66 mol%.[65] Finally, addition of oleyl alcohol (**$C_{18:1}$OH**; Scheme 2.11B) leads to a similar pattern as for **C_{10}OH**, except that the peaks are becoming much broader, indicating that the transition becomes much less cooperative.

These results are in agreement with literature reports where *n*-alcohols behave like amphiphiles leading to a decrease in the phase transition temperature for alcohols with short (< C_{10}) chains and an increase for alcohols with a long (> C_{10}) chain.[66-69,98-100] Also broadening of peaks has been observed.[66,67,69] Experiments with linear carboxylic acids show similar trends.[66,68]

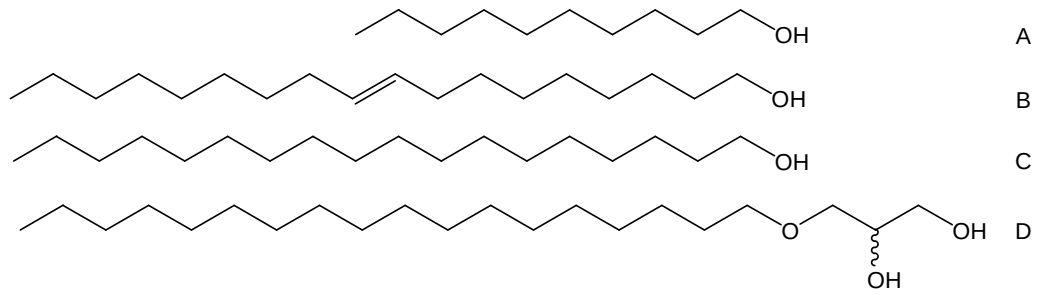

Scheme 2.11. *A. n-Decanol (**C_{10}OH**); B. Oleylalcohol (**$C_{18:1}$OH**); C. n-Octadecanol (**C_{18}OH**); A. Batyl alcohol (**C_{18}GOH**).*

In fact, the DSC scans are more complex than described above. Several control experiments were performed to check the reproducibility. Unfortunately, the reproducibility in certain mixtures is not too high (*e.g.* 20 mol% of **C_{18}OH**; Figure 2.21B), indicating that the vesicles are metastable and that their exact structure depends on the time between preparation and experiment, the procedure that was followed to make the vesicles, and probably some more variables. Also, the fact that many scans show more than one peak indicates that there is either more than one transition or that the alcohol and amphiphile are not homogeneously mixed, or both. Similar effects were seen for alcohol/phospholipids mixtures.[98] This is especially the case for the mixtures with **C_{18}OH** and **$C_{18:1}$OH**, and to a much lesser extent for **C_{10}OH** and **C_{18}GOH**.

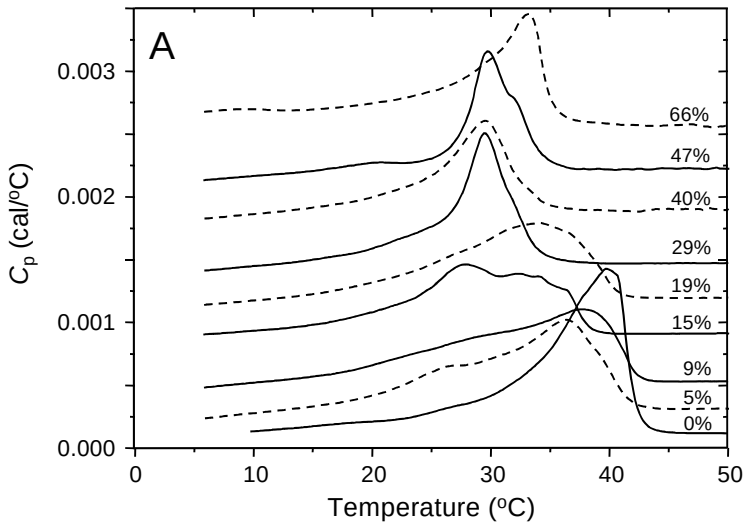

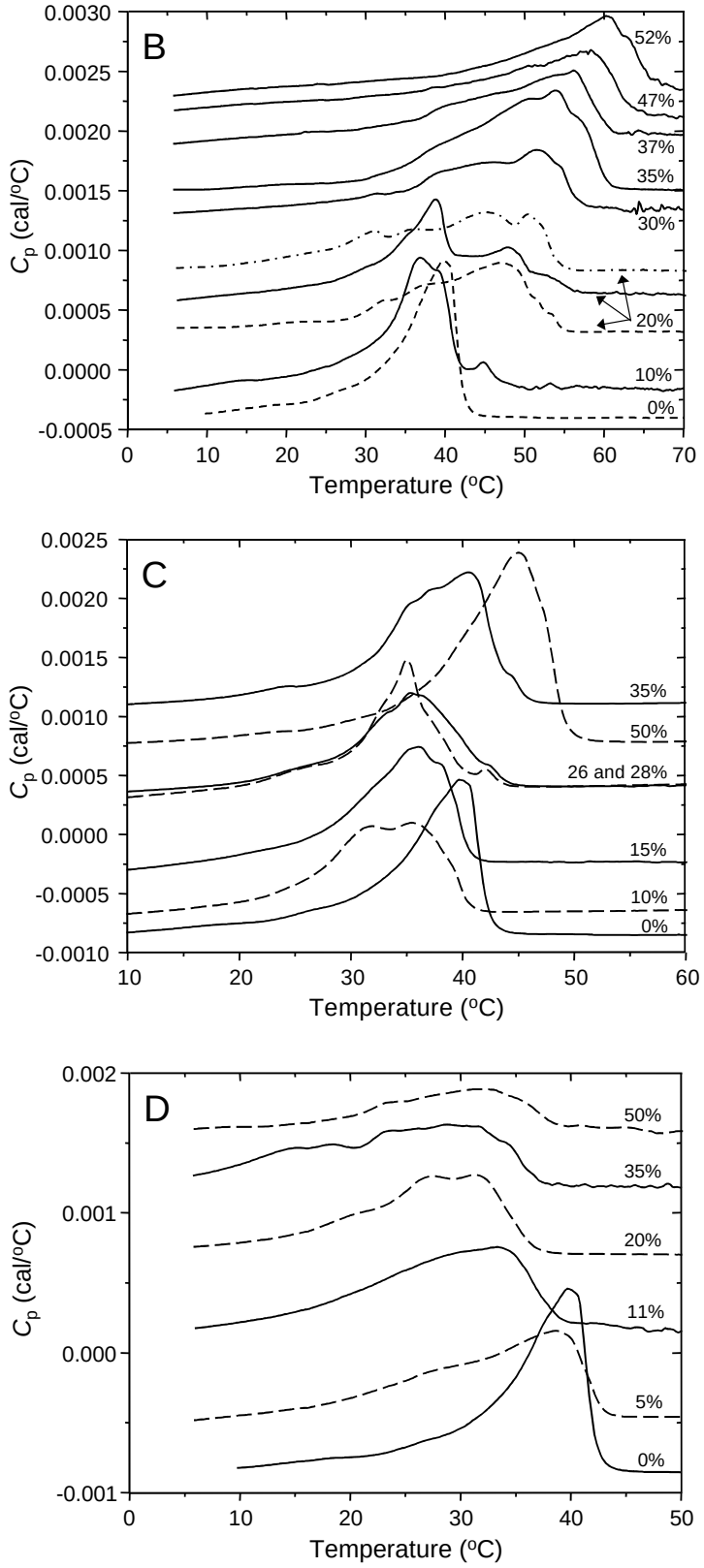

Figure 2.21. *Heating scans for mixtures of* ***$C_{18}C_{18}$+*** *with* ***$C_{10}OH$*** *(A),* ***$C_{18}OH$*** *(B),* ***$C_{18}GOH$*** *(C) and* ***$C_{18:1}OH$*** *(D). The number denotes the mole percentage of alcohol as a function of the total amphiphile concentration. In C the heating scan for 26 mol% is represented by the dashed line. Lines have been displaced vertically for clarity.*

The reason for this multiple phase formation might come from the high melting point of **C_{18}OH** and **C_{18}GOH**. In combination with the unfavourable packing parameter of **C_{18}OH** (>1), this leads to a situation where **C_{18}OH** dissolution in membranes of **$C_{18}C_{18}$+** is rather unfavourable. Crystallisation of small domains rich in **C_{18}OH** within the membrane might occur. **C_{18}GOH** has a larger hydrophilic moiety, leading to a more favourable packing parameter and therefore it might lead to a better dissolution in the membrane making crystallisation in the membrane less favourable. The large increase in the phase transition temperature in the presence of **C_{18}OH** is in agreement with the observation that there is an increase in ordering in the bilayer.[100] Phospholipids with unsaturation in the tails have usually a phase transition temperature below 0°C, since these unsaturations disrupt the bilayer and make efficient packing difficult. Likewise, in the dry state phospholipids with unsaturation are usually more wax-like than their saturated analogues. Therefore it is a bit surprising to notice that addition of **$C_{18:1}$OH** does not lead to a larger decrease in phase transition temperature than observed here. The broadening of the peaks is anticipated on the basis of the literature.

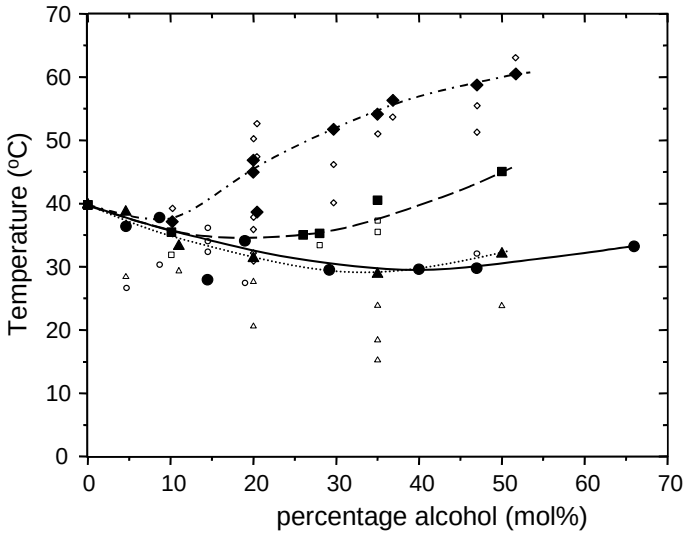

Figure 2.22. *Phase transitions of* ***$C_{18}C_{18}$+*** *vesicles with added alcohols. Closed symbols are major peaks and open symbols are minor peaks.* ***C_{10}OH*** *(●);* ***C_{18}OH*** *(◆);* ***C_{18}GOH*** *(■);* ***$C_{18:1}$OH*** *(▲). Lines are only drawn to guide the eye.*

2.3.4.7 Nonionic Single-tailed Surfactants

As can be seen in Figure 2.23A-C the addition of additives with a larger hydrophilic part compared to that of the alcohols leads to a lowering of the main phase transition temperature. In fact, these single-tailed surfactants destabilise vesicles (disturb the packing of the bilayer, section 2.3.3.4). Linear alcohols can, in principle, destabilise vesicles as well. However, due to their small hydrophilic moiety their packing parameter is larger than 1, whereas single-tailed surfactants generally have a packing parameter around $^1/_3$. Therefore the alcohols are not able to solubilise the vesicles into mixed micelles. With this in mind the decrease in the main phase transition temperature is not surprising, since the main phase transition temperature for a great deal reflects the packing efficiency of the tails,[101]

which is disturbed by the addition of single-tailed surfactants. A decrease in the main phase transition temperature was also observed for phospholipid and cationic vesicles with cationic, anionic and nonionic surfactants.[92,96,97,102-104]

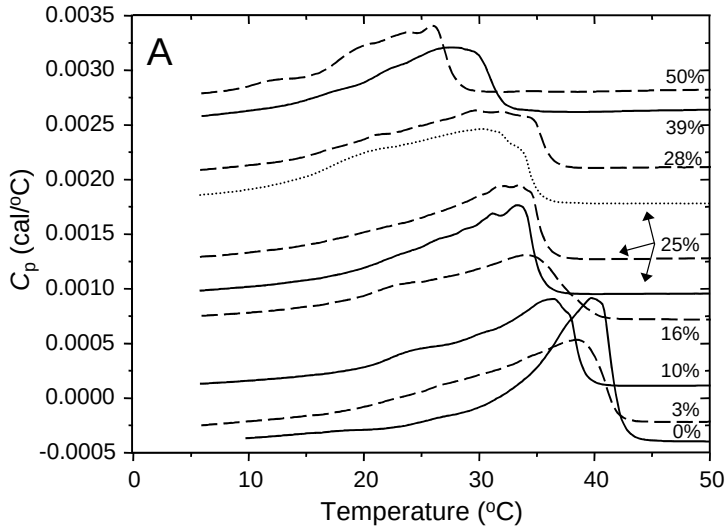

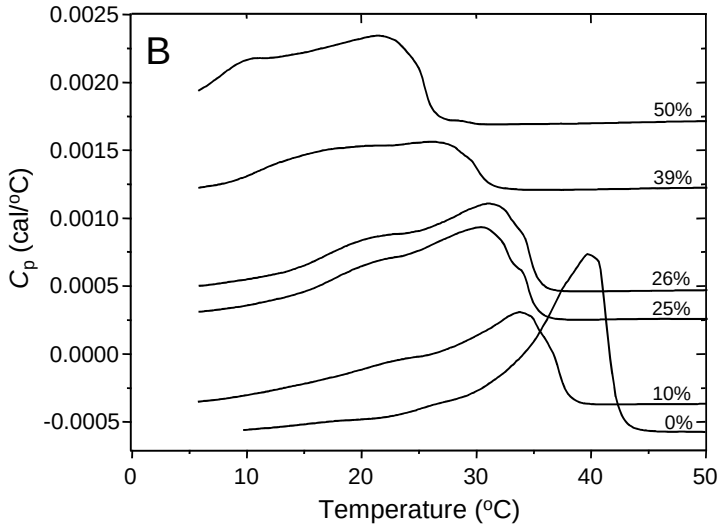

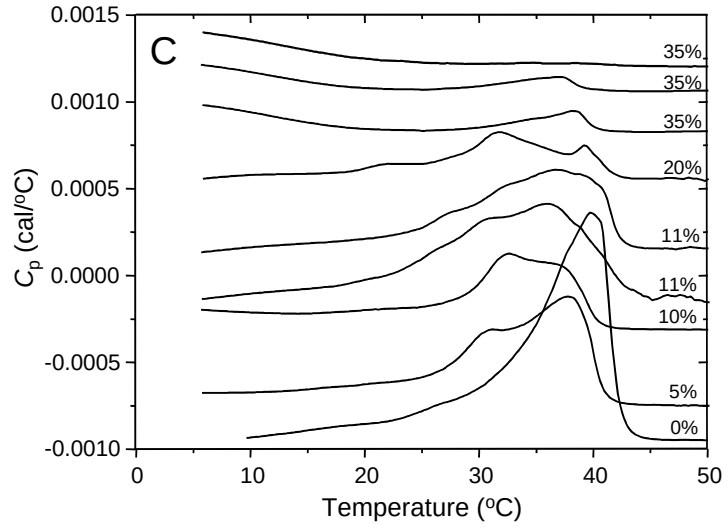

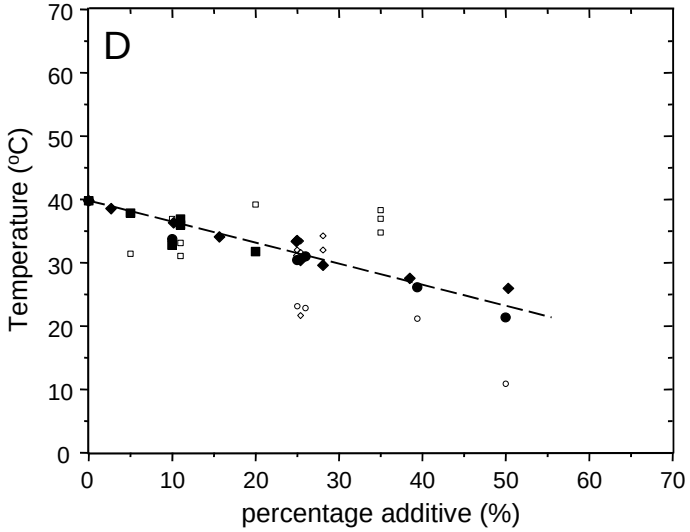

Figure 2.23. *Heating scans for mixtures of* ***$C_{18}C_{18}$+*** *and* ***C_{12}Mal*** *(A),* ***C_{12}Glu*** *(B),* ***$C_{16}EO_{20}$*** *(C). The number denotes the mole percentage of alcohol as a function of the total amphiphile concentration. Lines have been displaced vertically for clarity. A: dotted line is a solution prepared by mixing a vesicular solution of* ***$C_{18}C_{18}$+*** *with a micellar solution of* ***C_{12}Mal****. D: Maxima in the DSC scans as a function of the bilayer composition. Closed symbols are the major peaks; open symbols are minor peaks.* ***C_{12}Mal*** *(♦);* ***C_{12}Glu*** *(●);* ***$C_{16}EO_{20}$*** *(■). The line is only drawn to guide the eye.*

Figure 2.23D shows an overview of the maxima in the peaks. Surprisingly, the different additives more or less have a similar influence on the phase transition temperatures. At higher mole fractions the number of additional transitions increases, which is in line with the potential appearance of other morphologies than vesicular bilayers. This is especially the case upon the addition of **$C_{16}EO_{20}$**. At 35 mol% the solution contains a mixture of vesicles and mixed (worm-like) micelles, as is shown by both turbidity experiments (Section 2.3.2.1) and dynamic light scattering (Section 2.3.3.4).

2.3.4.8 4-(Dioleylmethyl)-1-($PEG_{5000}OCH_3$)-Pyridinium Bromide

4-(Dioleylmethyl)-1-($PEG_{5000}OCH_3$)-pyridinium bromide (SAINT-44; Scheme 2.12) is similar to **$C_{16}EO_{20}$** with respect to the head group. Both molecules have a large ethylene glycol head group, but the size of the head group is over two times as large for SAINT-44. In addition, SAINT-44 is cationic, has a bromide counterion and has two oleyl tails (approximately 20% trans).

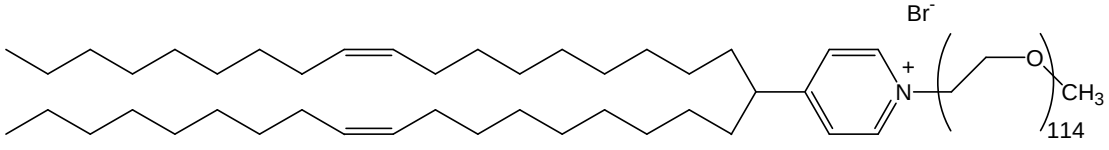

Scheme 2.12. *4-(Dioleylmethyl)-1-($PEG_{5000}OCH_3$)-pyridinium bromide (SAINT-44)*

In water SAINT-44 forms micelles with a CMC in the micromolar range.[105] Therefore, its binding efficiency towards vesicles formed from **$C_{18}C_{18}$+** is high (Section 2.3.2), resulting in almost complete binding. Unfortunately, SAINT-44 has a bromide counterion, and therefore we have to compare the results with vesicles formed from 95 mol% of **$C_{18}C_{18}$+** and 5 mol% of dimethyldi-*n*-octadecylammonium bromide (**$C_{18}C_{18}$+Br-**). In Figure 2.24 the heating scans for the mixed vesicular systems are shown. Surprisingly, upon the addition of 5 mol% of **$C_{18}C_{18}$+Br-** the main phase transition temperature is decreased, which disagrees with the literature where the T_m is a few degrees higher for 100 mol% of **$C_{18}C_{18}$+Br-** than for **$C_{18}C_{18}$+**.[11,106-109] An even lower T_m is found when 5 mol% of SAINT-44 is added. This is not unlikely since micelle-forming surfactants lower the T_m (Section 2.3.4.7) and the tails have unsaturations that further disturb the packing of the bilayer. In fact, the effect is quite large considering that the other additives do not have such a large effect at 5 mol%.

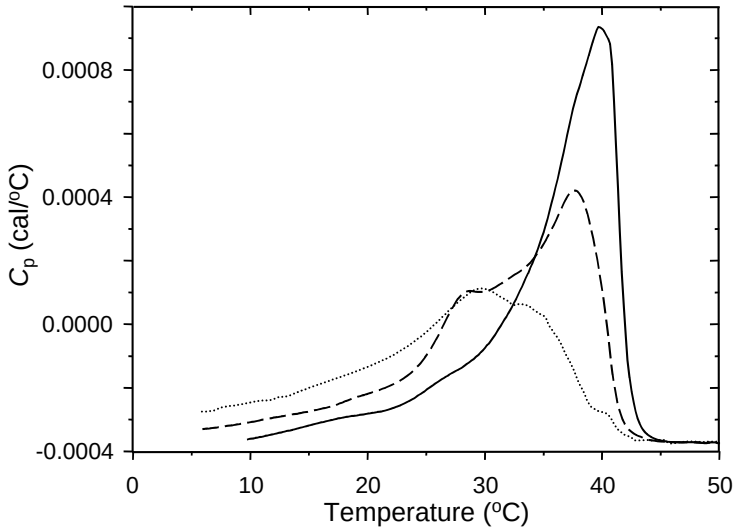

Figure 2.24. *Heating scans for* **$C_{18}C_{18}$+** *(solid line), 5 mol% of* **$C_{18}C_{18}$+Br-** *(dashed line) and 5 mol% of SAINT-44 (dotted line).*

2.3.4.9 (2,3-Bis-*n*-Octadecyloxy-Propyl)-Trimethylammonium Chloride

The heating scan for vesicles formed from **$C_{18}C_{18}$G+** (Scheme 2.6) is shown in Figure 2.25. The main phase transition temperature is 56.8°C, which is about 17 degrees higher than that for vesicles formed from **$C_{18}C_{18}$+**. Apparently the packing of the tails is much more efficient. This is probably a result from the presence of the glycerol linker. This linker is also found in phospholipids.

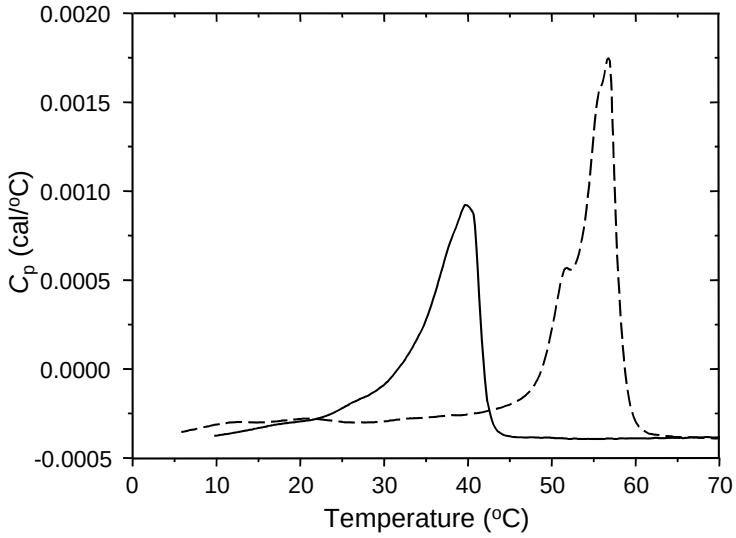

Figure 2.25. *Heating scan for* ***$C_{18}C_{18}$+*** *(solid line) and* ***$C_{18}C_{18}$G+*** *(dashed line).*

2.3.5 Membrane Polarity

2.3.5.1 Theoretical Considerations

With the aim to understand the influence of various additives on the properties of vesicles it is necessary to study the polarity of the polar-apolar interface both as a function of the type of additive and as a function of the mole fraction of additive in the bilayer. The polarity can be probed using several different dye molecules. A few commonly used dyes are shown in Scheme 2.13. However, their way of reporting the polarity, or better, their sensitivity towards changes in the chemical structure of solvents or changes in the composition of solvent mixtures is quite different, and this has led to different polarity scales for different dyes.[110] For example, the wavelength of maximum fluorescence of Prodan shifts from 400 nm in cyclohexane to 530 nm in water.[111] The fluorescence spectrum of pyrene, on the contrary, has several maxima, and the wavelengths of these maxima are rather insensitive upon a change in solvent. However, the relative intensity of the first and third peak (I_1/I_3) is sensitive for solvent polarity, leading to a value of I_1/I_3 of 0.62 and 1.80 for *n*-hexane and water, respectively.[112] It becomes more interesting when different classes of solvents are considered (hydrocarbons, alcohols, amines, etc.). Within a class there is usually a trend between the structural variation and the reported polarity. However, between classes a relationship between structure and reported polarity is not necessarily present. The origin of this effect comes from the different interactions that the dyes are sensitive to. Prodan and the $E_T(30)$ dye are, for example, sensitive to hydrogen bonding, whereas pyrene is not. In solvent mixtures preferential solvation becomes important. These properties make it difficult to design a universal polarity scale, since the intermolecular forces (hydrogen bonds, dispersion forces, etc.) depend strongly upon both probe and solvent. However, the general features are usually similar, *i.e.* water is at the polar side of the scale and *n*-hexane on the apolar side. Reichardt has reviewed the literature about a number of solvatochromic

probes and several (empirical) models to describe the interactions between these dyes and solvents.[110]

It should be noted that not all polarity scales are established using fluorescence spectroscopy. The $E_T(30)$ probe, for example, reports its local polarity through a change in the maximum UV/vis absorbance.

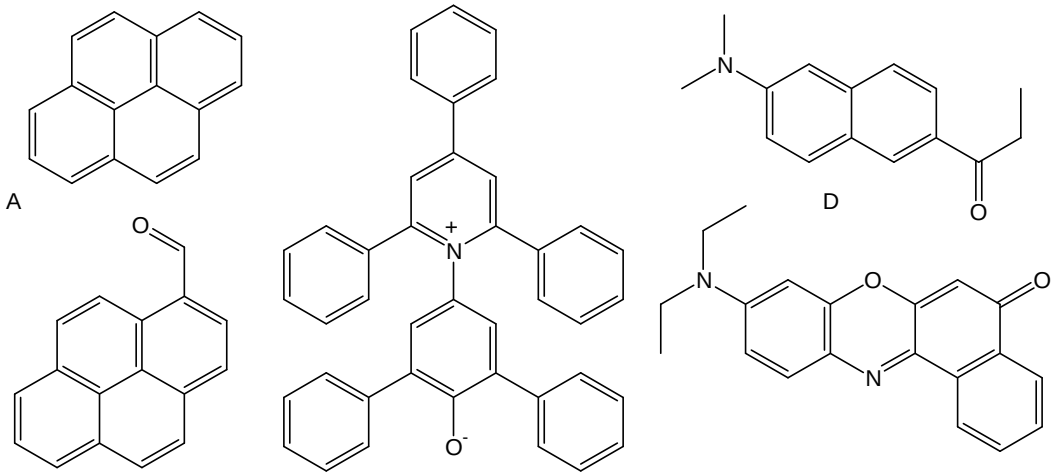

Scheme 2.13. *Some examples of commonly used probes for measuring solvent polarity. (A) Pyrene; (B) Pyrene-3-Carboxaldehyde; (C) $E_T(30)$; (D) Prodan ;(E) Nile Red.*

In order to explain the observations discussed above, intramolecular energy transfer and specific dye-solvent interactions in fluorescent dyes have to be considered.[113] When a dye molecule is excited from its ground state to an excited state, it usually rapidly decays (10^{-12} s) to the first singlet state (S_1). Often the dipole moment is increased upon excitation, leading to fast solvent relaxation (10^{-11}–10^{-10} s) in low-viscosity media[114] and in polar solvents this leads to a lowering in the excited state energy. From this state, the locally excited state (LE), a photon can be emitted (10^{-8} s). The more polar the solvent, the lower the excited state energy and hence, the longer the wavelength of emission. This effect of the solvent is called the general solvent effect. If specific dye-solvent interactions can occur, for example, through hydrogen bonding, the excited state can be further stabilised, and the wavelength is red-shifted. In addition to these two interactions the dye can form an internal charge-transfer state (ICT), or a twisted internal charge-transfer state (TICT). From the ICT and TICT also radiationless decay via electron transfer can occur, which makes the fluorescence yield in polar solvents for certain dyes low. Examples of such behaviour are ANS (Scheme 2.15) and Nile Red fluorescence in water. It should be noted that emission is always from the lowest-energy excited state. This means that in a series of solvents a change in mechanism of photon emission can occur. This is the reason that there are different polarity scales, since changes in fluorescence mechanism are dye-dependent. This is best seen in Lippert plots, where the difference in wavenumber of maximum absorption and emission is plotted against the orientation polarisability (Δf).[115] If there is no change in fluorescence mechanism this plot yields a straight line that is related to the squared difference of the dipole moment in the ground and excited state. A change in emission mechanism is usually accompanied by a change in dipole moment of the excited state and hence the slope in the Lippert plot will change. A change in mechanism can also be

observed in other ways.[116] Specific interactions are also the reason that certain dyes are sensitive towards changes in the polar solvent region, whereas they are not very sensitive in the apolar solvent region.

Some fluorescent dyes exhibit several peaks in their emission spectrum. This is the case when fluorescence occurs from different vibrational levels within one excited state.[117] This means that the path to the ground level does not proceed exclusively via solvent relaxation, but partly directly from the vibronic level to which the dye was excited. Of course, partial relaxation to lower energy states cannot be excluded in all cases. The relative intensity of the peaks depends on the vibronic level of the preferred excited state. This type of fluorescence mechanism is shown by pyrene, but also by Nile Red fluorescence in very apolar solvents.

In micellar and vesicular aggregates the interpretation of the data becomes even more troublesome. The probes are sometimes rather large and their presence can induce local structural changes in the aggregates or even aggregation.[118-120] The $E_T(30)$ probe, for example, is quite large compared to a micelle. But also for large aggregates the exact binding location of the probe is uncertain. Some probes seem to have different binding sites within micelles,[121] other probes have more well-defined binding sites.[122] This problem has partially been overcome by designing probes that are covalently bound to surfactants fixing the location of the probe. In other cases incomplete binding of the probe has to be taken into account, so that the measured signal is sometimes an average of the fluorescence spectra of the probe in water and in the aggregate. Moreover, additional interactions between the probe and the surfactant have to be considered.[123-125]

These considerations make it difficult to assign a well-defined polarity to bilayers. However, by employing different dyes that are sensitive for different interactions, and by looking at trends, rather than absolute values, still useful information can be deduced from the experiments.

In order to have some way of comparing the different polarity scales the probes that report a wavelength of maximum fluorescence or absorbance the energy of the transition (E_T) can be calculated and subsequently normalised. The E_T transition (in kcal mol^{-1}) is calculated according to eq. (2.11):[110]

$$E_T = hc\tilde{\nu}_{max}N_A = \frac{28591}{\lambda_{max}} \qquad (2.11)$$

In this equation h, c and N_A are Planck's constant, the speed of light and Avogadro's number, respectively. λ_{max} and ν_{max} are the wavelength (in nm) and frequency of the maximum absorption of the dye, respectively.

Usually, the normalised E_T is then calculated by taking the E_T value of tetramethylsilane (TMS) and water and adjusting them to 0 and 1, respectively, by employing eq. (2.12)

$$E_T^N = \frac{E_T(\text{solvent})\text{-}E_T(\text{TMS})}{E_T(\text{water})\text{-}E_T(\text{TMS})} = \frac{\lambda^{-1}_{\text{max,solvent}} - \lambda^{-1}_{\text{max,TMS}}}{\lambda^{-1}_{\text{max,water}} - \lambda^{-1}_{\text{max,TMS}}} \qquad (2.12)$$

For our purposes we normalised against water and 1,4-dioxane, since we anticipate that differences between the vesicles with the various additives are much smaller than the change from water to TMS. The normalised polarity $P^{w/d}$ can then be calculated via eq. (2.13).

$$P^{w/d} = \frac{\lambda^{-1}_{\text{max,mixt}} - \lambda^{-1}_{\text{max,dioxane}}}{\lambda^{-1}_{\text{max,water}} - \lambda^{-1}_{\text{max,dioxane}}} \qquad (2.13)$$

2.3.5.2 Laurdan Fluorescence

Laurdan has a similar structure as Prodan (Scheme 2.13D), except that the ethyl group is replaced by an undecanol group (Scheme 2.14). This ensures its full binding to aggregates possessing hydrophobic binding sites. The fluorescence spectrum of Laurdan in vesicles is independent of the structure of the head group, but depends on the phase of the tails.[126,127] The fluorescence spectrum has two peaks. When the tails are in the gel-like state, the peak on the blue side of the spectrum (*ca.* 440 nm) is larger than the peak at the red side (*ca.* 490 nm). When the tails are in the liquid-crystalline state the peak on the red side is the largest peak. This change in the spectrum originates from the possibility of water molecules near the fluorescent probe to reorient on the time scale of the lifetime of the excited state when the tails are in the liquid-crystalline state. This reorientation is not possible when the tails are in the more rigid gel-like state.[113,126]
When 360 nm is chosen as excitation wavelength laurdan molecules residing in gel-like domains are mainly excited, whereas when 390 nm is chosen mainly laurdan molecules residing in liquid-crystalline domains are excited. Hence, the excitation spectrum can also be used to probe the phase of the tails. In principle, both the excitation and emission spectra lead to similar results. However, the excitation spectrum shows two clear peaks, whereas for the same sample the second peak in the emission spectrum is much less pronounced.

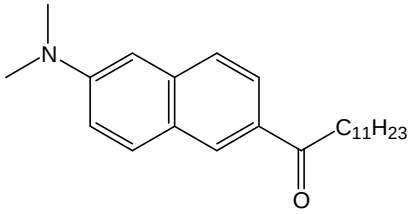

Scheme 2.14. *Laurdan.*

The excitation or emission spectra of the same sample at various temperatures show a change at the main phase transition temperature. This change can be quantified by calculating the generalized polarization (*GP*):

$$GP = \frac{I_{\text{blue}} - I_{\text{red}}}{I_{\text{blue}} + I_{\text{red}}} \qquad (2.14)$$

From a mathematical point of view it makes more sense to use the excitation spectrum, since this spectrum shows two clear peaks, whereas in the emission spectrum one of the peaks is usually just a small bump in the curve. When two clear peaks are present the peaks can be deconvoluted (Figure 2.26B) and the *GP* can be calculated using the fitted intensity at the maxima. This gives better values for *GP* than taking the measured intensities at fixed wavelengths. Contrastingly, in the literature usually the experimental intensity at fixed wavelengths is taken.[126,128-135] Unfortunately, the calculated *GP* from the deconvoluted spectra depends on the wavelengths between which the experimental data is fitted, illustrating the general problem that is encountered when two overlapping peaks are being deconvoluted.
In our set of experiments we are interested in the (relative) change of the state of the tails as a function of the type and molar ratio of additives at a fixed temperature (15°C). Therefore the trend in the calculated *GP* is important, rather than the absolute value.

The excitation spectra were recorded following the fluorescence at 440 nm and 490 nm (Figure 2.27) in order to study the influence of selective excitation of laurdan molecules that are present in liquid-crystalline domains and gel-like domains. The *GP* values were calculated using fits between 318 nm and 408 nm. The *GP* is independent of the bilayer composition and emission wavelength for the range of additives studied here, despite the large structural variation in additives. The results are in agreement with our observation using differential scanning microcalorimetry, where we concluded that all phase transition temperatures are above 15°C. In addition, the wavelength of maximum excitation for both peaks is independent of the bilayer composition (data not shown). This wavelength has been suggested to be a measure for bilayer polarity.[129] The large scattering in the data of Figure 2.27A compared to Figure 2.27B comes from the lower intensity (quantum yield) in the excitation spectrum, which makes it more difficult to deconvolute the peaks.

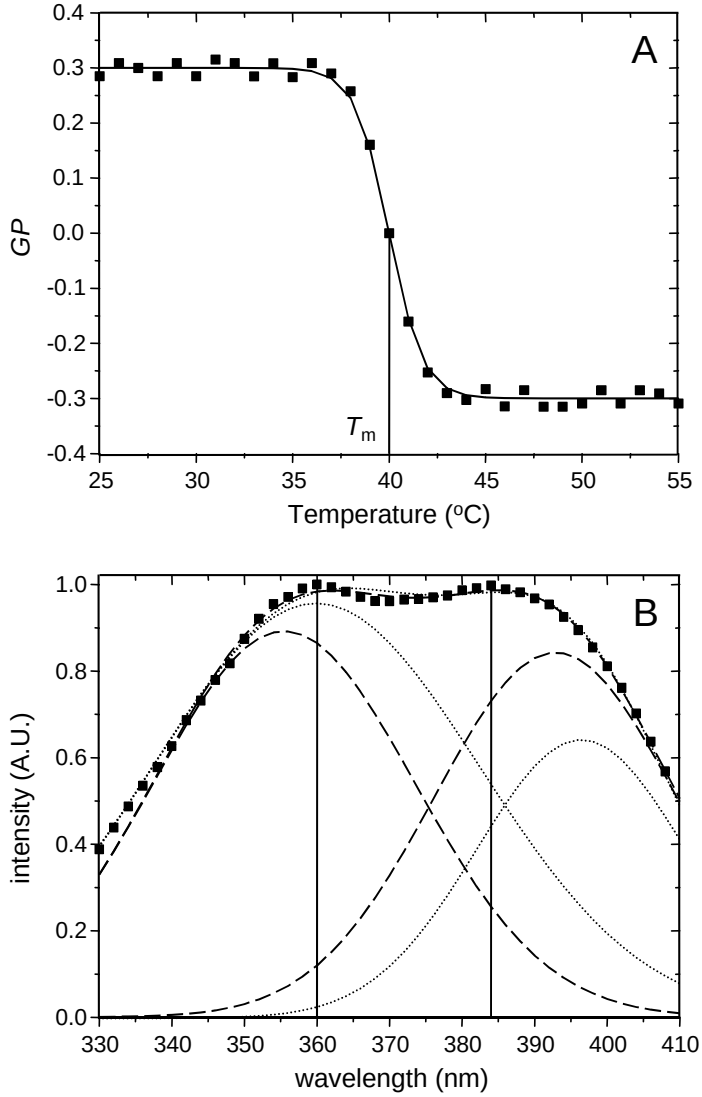

Figure 2.26. *Typical plot of GP versus temperature using fictional data (A) and laurdan excitation spectrum followed from the emission at 490 nm (B). Solid squares are experimental data points. Solid lines are at the wavelength of maximum fluorescence, dashed lines are the deconvoluted peaks, when fitted between 338 nm and 408 nm, dotted lines when fitted between 318 nm and 408 nm.*

From eq. (2.14) it can be seen that the value of *GP* is 1 when all the amphiphiles are in the gel-like state, and -1 when in the liquid-crystalline state. These values are usually not reported in the literature since the peaks at 440 nm and 490 nm are rather broad. Also in this study the value of 1 or -1 is not reported suggesting that the bilayers are not fully in one type of state. The average value of *GP* of all the data points in Figure 2.27A and B are 0.32 and 0.25, respectively, indicating that in Figure 2.27B laurdan reports a slightly more fluid-like bilayer, which is in agreement with a better excitation of laurdan molecules present in liquid-crystalline domains. This approach assumes the presence of distinct liquid-crystalline and gel-like domains that are co-existing in bilayers. This assumption is also used for the calculation of patch numbers (Section 2.3.4.1)

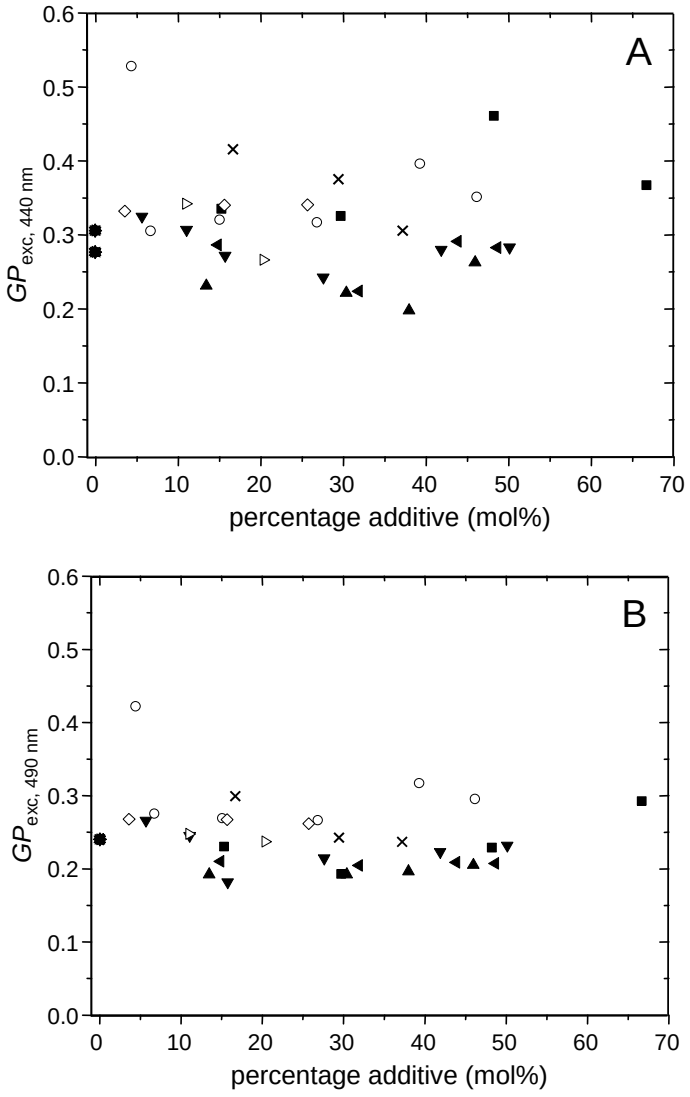

Figure 2.27. *Plot of GP_{exc} versus bilayer composition. Emission followed at (A) 440 nm and (B) 490 nm.* ***$C_{10}OH$*** *(■);* ***$C_{18}OH$*** *(▲);* ***$C_{18}GOH$*** *(◀);* ***$C_{18:1}OH$*** *(▼);* ***$C_{12}Glu$*** *(○);* ***$C_{12}Mal$*** *(◇);* ***$C_{16}EO_{20}$*** *(▷);* ***$C_{10}C_{10}$*** *(×).*

2.3.5.3 E_T(30) Absorbance

The E_T(30) probe (Scheme 2.13) is an excellent solvatochromic dye to probe the polarity of solvents, and solvent mixtures.[110] The wavelength of maximum absorbance shifts from 930 nm to 453 nm going from TMS to water, which makes it a very sensitive probe. For most dyes upon increasing the polarity of the solvent the wavelength of maximum absorbance shifts towards longer wavelength. However, for those dyes the ground state has a smaller dipole moment than the excited state, whereas for the E_T(30) dye it is the other way around. This means that in polar solvents the ground state of the E_T(30) dye in stabilised relative to the excited state , and in apolar solvents the E_T(30) dye is destabilised. In addition, hydrogen bond donation stabilises the ground state. The absorbance is due to an intramolecular charge transfer from the negatively charged oxygen to the positively charged pyridinium ring leading to a diradical species.

Unfortunately, due to its size it is less suitable for measuring the polarity of micellar and vesicular surfaces. As can be seen in Figure 2.28 the reproducibility is rather poor. This can originate from several possibilities: 1. The probe might not be fully bound. We checked this by adding more E_T(30), but this did not change the E_T(30) value. 2. The structure of the aggregate might change. This is a well-known problem. Vesicles are metastable and their size, shape and stability depend on the preparation method. Hence, with time the structure of the bilayer aggregate changes. Depending on the molecular structure the rate of this may be highly variable. Addition of the large E_T(30) probe might induce morphological changes, and depending on the history of the sample, this might lead to different structures.

Despite these problems, within the two series (initial and duplo experiments) there is a good correlation between the different data points, suggesting that upon the addition of the various additives the measured local polarity does not change too much. The average value of the normalised polarity ($P^{w/d}$) is 0.68, which corresponds to a polarity similar to methanol (0.72). This is consistent with an almost constant E_T(30) value for several CTAB/alcohol micellar solutions.[136]

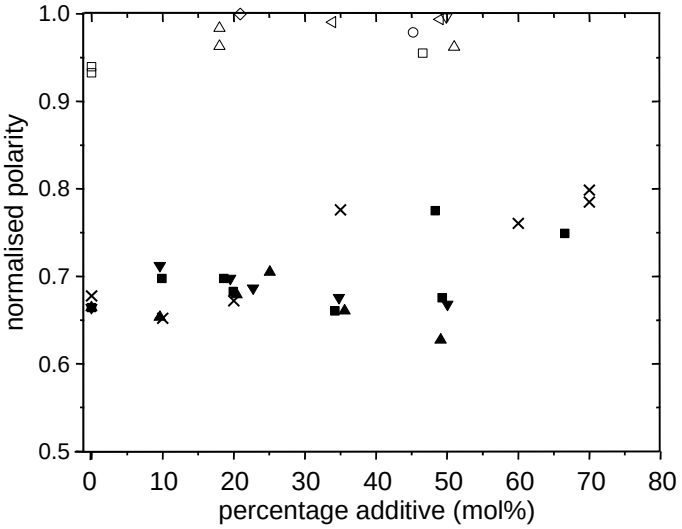

Figure 2.28. *Plots of normalised polarity ($P^{w/d}$) as measured by E_T(30) versus bilayer composition. Closed symbols are initial experiments, open symbols are duplo experiments.* ***C_{10}OH*** *(■);* ***C_{18}OH*** *(▲);* ***C_{18}GOH*** *(◁);* ***$C_{18:1}$OH*** *(▼);* ***C_{12}Glu*** *(○);* ***C_{12}Mal*** *(◇);* ***$C_{10}C_{10}$-*** *(×).*

2.3.5.4 Pyrene Fluorescence

Pyrene has been used already since the late 1970s for measuring solvent polarity and the polarity of micellar aggregates.[112] The fluorescence spectrum shows several vibronic peaks of which the intensity depends on solvent polarity. The ratio of the first and third peak is usually taken as a measure of polarity. Hydrocarbon solvents generally have an I_1/I_3 value around 0.6, aromatic solvents between 1.0 and 1.3 and simple polar solvents between 1.3 and 2.0 (water: 2.0)

The wavelengths of the peaks in the fluorescence spectrum are hardly sensitive towards solvent polarity, which is reasonable since pyrene has no dipole moment in the ground state and only a small dipole moment in the locally excited state (LE).[113] In the excited state it exhibits an LE state, with several vibronic levels. In water excitation is mainly to the first vibronic level leading to a relatively high intensity of I_1, and hence a large value of I_1/I_3. In more apolar media the energy minimum of the LE state is shifted with respect to the ground state minimum. As a result excitation is mainly to and emission is mainly from the third vibronic level, and hence I_1/I_3 becomes smaller.

Despite the lack of functional groups in pyrene, we anticipate that it binds in the Stern region, since arenes are known to bind near the interface of micelles.[123,125,137]

An experimental problem in employing pyrene fluorescence in probing vesicular polarity is the background scattering. The background scattering is rather independent of the wavelength between 370 to 390 nm. This is the region of the first and third emission peak. The intensity of the background scattering depends both on the size and concentration of the vesicles. In practice the background scattering leads to a lowering of the value of I_1/I_3.

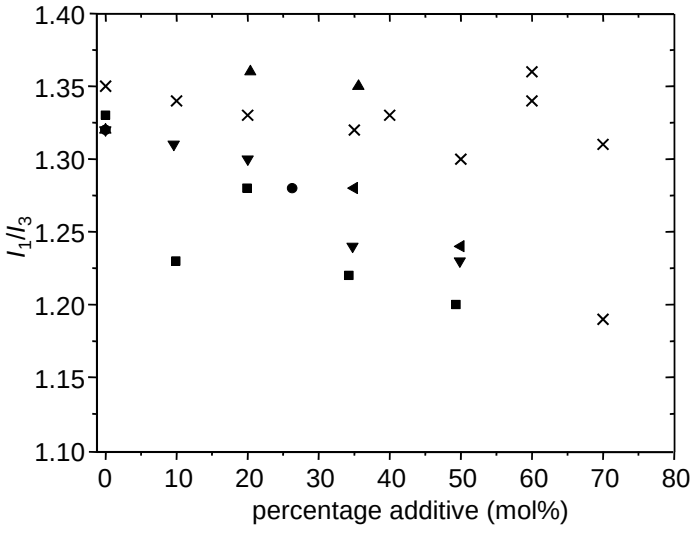

Figure 2.29. *Plots of I_1/I_3 versus bilayer composition.* ***$C_{10}OH$*** *(■);* ***$C_{18}OH$*** *(▲);* ***$C_{18}GOH$*** *(◄);* ***$C_{18:1}OH$*** *(▼);* ***$C_{12}Glu$*** *(●);* ***$C_{10}C_{10}$*** *(×).*

Plots of I_1/I_3 versus bilayer composition are shown in Figure 2.29. The value of I_1/I_3 varies between 1.2 and 1.35, which is comparable to a change from methanol to THF (1.33 and 1.20, respectively). There seems to be a trend that the addition of alcohol and pyranoside

leads to a more apolar environment. Addition of **$C_{10}C_{10}$-** does not lead to a change in polarity, except that at 70 mol% there is quite some scattering. The value of 1.2-1.35 is similar to that which has been observed for cationic and nonionic micelles of DeTAB (1.28), CTAC (1.35), Triton-X100 (1.32) and **C_{12}Mal** (1.24),[138] but slightly higher than that for anionic micelles such as sodium *n*-dodecanoate (1.04) and SDS (1.14).[112] Overall, it can be concluded that the change in polarity as sensed by pyrene does not change significantly in the presence of the additives.

2.3.5.5 ANS Fluorescence

The fluorescent behaviour of 1,8-ANS (Scheme 2.15) and its derivatives in solution has been studied in some detail in the literature.[116,139-146] In water the fluorescence intensity of ANS is rather poor due to a preferred radiationless electron transfer from the lowest-energy excited state (ICT). However, bound to a hydrophobic binding site the fluorescence readily increases. In addition, the emission spectrum is sensitive to the local polarity making it a popular probe to study subtle changes in the surface polarity of liposomes or biological membranes. In water and 1,4-dioxane its wavelength of maximum emission is at 555 nm and 472 nm, respectively.[146] This change in wavelength of maximum emission can be explained by a general solvent effect and a specific solvent-dye interaction leading to an intramolecular charge transfer mechanism, depending on the solvent, or binding site.[116,139-142,146] In solvents of higher viscosity the spectra are blue shifted.

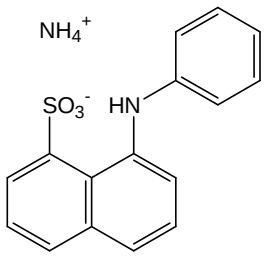

Scheme 2.15. *1-Anilinonaphthalene-8-sulfonate ammonium salt.*

In Figure 2.30 the normalised polarity ($P^{w/d}$) is shown for vesicular solutions containing the additives. The experiments were performed in the absence (A) and in the presence (B) of 2.25 mM NaOH. The general trend is not different in the presence of NaOH, but the absolute value varies slightly. In general there seems to be a slight trend towards higher values of $P^{w/d}$ upon increasing the amount of additive. It should be noted that the changes in $P^{w/d}$ are significantly smaller than those shown in Figure 2.28. Special attention should be drawn to **$C_{16}EO_{20}$** and **C_{18}OH**. At 20 mol% of **$C_{16}EO_{20}$** and 50 mol% of **C_{18}OH** $P^{w/d}$ is significantly higher than for the other data points, suggesting water penetration into the bilayer. For **$C_{16}EO_{20}$** this is reasonable since this surfactant is able to solubilise vesicles.

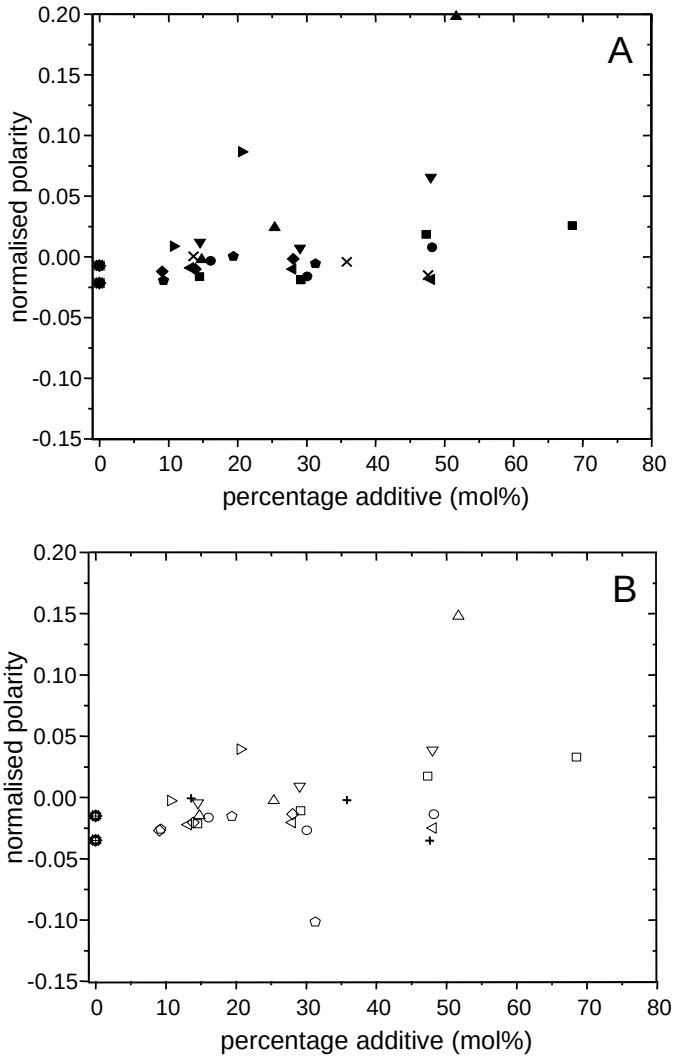

Figure 2.30. *Plot of normalised polarity ($P^{w/d}$) as measured by ANS versus bilayer composition. A is for solutions without added NaOH, B is for solutions with added NaOH (2.25 mM).* ***$C_{10}OH$*** *(■);* ***$C_{18}OH$*** *(▲);* ***$C_{18}GOH$*** *(◀);* ***$C_{18:1}OH$*** *(▼);* ***$C_{12}Glu$*** *(●);* ***$C_{12}Mal$*** *(◆);* ***$C_{16}EO_{20}$*** *(▶);* ***$C_{10}C_{10}$-*** *(×; +); Cholesterol (⬟).*

The value of $P^{w/d}$ is 0.01 and –0.01 in the absence and presence of NaOH, respectively. This value of around zero suggests that the local polarity is comparable to that of 1,4-dioxane. However, these values are not far off for the value of methanol (0.07).[139] $P^{w/d}$ in cationic vesicles of di-*n*-dodecyldimethylammonium bromide is comparable to what we observe here (0.02).[147] The bilayers formed from **$C_{18}C_{18}$+** are in general less polar compared to biological membranes (0.08-0.28),[146,148-151] and membranes formed from natural or synthetic phospholipids (-0.06-0.27).[152-155] In some of the biological membranes still some membrane protein is present, which has binding sites for ANS as well.[149-151] Binding to membranes is, however, more favourable than to enzymes.[151] The wavelength of maximum fluorescence depends on the temperature. In sarcolemma vesicles $P^{w/d}$ drops from 0.28 to 0.22 when the temperature is lowered from 25°C to 15°C.[150] This might explain why the average value of $P^{w/d}$ that we measured for our cationic vesicles is slightly lower than what is reported for the $E_T(30)$ probe.

2.3.5.6 Nile Red Fluorescence

Both the absorption and fluorescence spectrum of Nile Red (also known as Nile Blue A oxazone) are sensitive to changes in solvent polarity. The wavelength of maximum absorbance shifts from 591 nm to 484 nm going from water to *n*-heptane, respectively, whereas the wavelength of maximum fluorescence shifts from 657 nm to 529 nm for the same solvents.[156] This effect is typical for dyes that are more polar in their excited state than in their ground state, and in fact, the dipole moment of the excited state is approximately 7 D larger.[157,158] Both the absorption and fluorescence emission spectra show a significant shift in the wavelength of maximum absorption or fluorescence upon a change in polarity. This makes it possible to preferentially excite dye molecules residing in domains of different polarity, such as is the case in microemulsions.[159,160161] The mechanism of fluorescence is similar to that for ANS (Section 2.3.5.5), except that the intramolecular charge-transfer state is replaced by a twisted intramolecular charge-transfer (TICT) state. Hydrogen bonding plays an important role in the emission from the TICT state,[157,158] leading to potential electron transfer and hence only little fluorescence is observed in water. In long linear *n*-alkanes the fluorescence spectrum shows two peaks, probably due to emission from two vibronic levels.[158,159]

In an initial study the fluorescence behaviour of Nile Red in several solvents and solvent mixtures was measured as a function of the excitation wavelength. The wavelength of maximum emission was in all cases well within 1 nm of each other indicating that the excitation wavelength has no influence on the emission wavelength in pure solvents and solvent mixtures. The normalised polarity as measured by Nile Red is plotted against the normalised polarity as measured by the $E_T(30)$ dye (Figure 2.31A).[110] A linear relationship between the normalised polarity as sensed by $E_T(30)$ and Nile Red was found, except in the region of very apolar solvents. This provides evidence that both Nile Red and the $E_T(30)$ dye sense their environment in a similar fashion in this polarity region. In fact, in the literature a more extensive set of solvents was used and a deviation from linearity was only observed below an $E_T(30)$ value of 40 (less polar than CH_2Cl_2).[160] This observation indicates that the $E_T(30)$ dye is less sensitive in very apolar solvents than Nile Red.

In microemulsions the fluorescence emission spectrum is a sum (of log normal plots) of the dye located in the different phases (hydrocarbon region, micellar interface and water).[160] Due to quenching of the fluorescence in water the dye in the aqueous phase is usually not observed. The wavelength of maximum fluorescence of the dye located at the aqueous/hydrocarbon interface is usually somewhere between the value of water and that of a liquid surfactant. In solutions with large hydrocarbon content the wavelength of maximum fluorescence depends on the excitation-wavelength, indicating that the dye is selectively excited. However, in solutions with low hydrocarbon content the excitation wavelength dependence is not present. Therefore, it is anticipated that this is due to a preference of the Nile Red dye to bind at the interface.

In Figure 2.31B the excitation-wavelength depended fluorescence in vesicles with different additives is shown. $P^{w/d}$ increases with increasing excitation wavelength. This is in agreement with an increase in maximum absorbance and fluorescence with increasing polarity. This means that upon increasing the excitation wavelength, dye molecules that are located at more polar binding sites are relatively better excited, and, as a consequence, an

average (slightly) higher polarity is reported. We anticipate that in vesicles there is no selective excitation, but a preferred excitation, since our system lacks a true hydrocarbon phase (as in microemulsions), and, since Nile Red has a preference for the interface, the relative number of Nile Red molecules present deep in the bilayer is small. Consequently their contribution is relatively small.

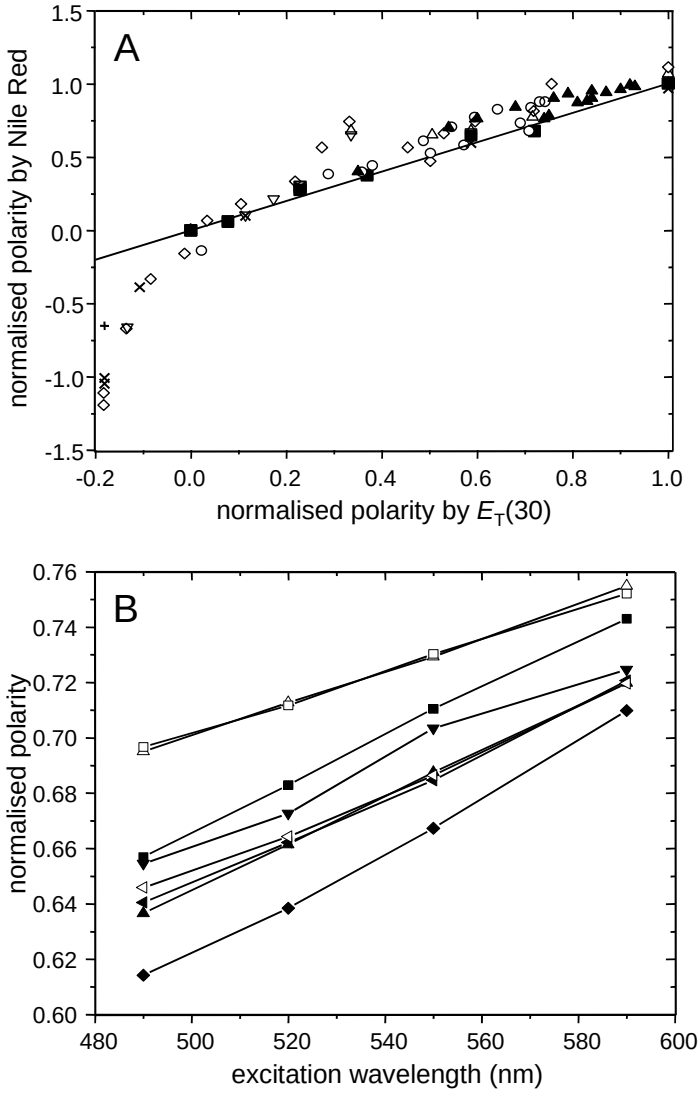

Figure 2.31. *A: Plot of normalised polarity measured by Nile Red fluorescence versus the normalised polarity as measured by $E_T(30)$ for several solvents and solvent mixtures. The excitation wavelength was 490 nm (□) and 590 nm (■). Mixtures of water and 1,4-dioxane or acetonitrile (590 nm; ▲). Data from literature was included for comparison: Greenspan[156] (×); Sackett[162] (△); Sarkar[157] (○); Oliveira[159] (+); Boldrini[163] (▽); Hungerford[160] (◇). The line is the linear relationship between the normalised polarities of $E_T(30)$ and Nile Red (slope=1). B: Plot of normalised polarity as measured by Nile Red fluorescence versus excitation wavelength for vesicles of* ***$C_{18}C_{18}$+*** *with, from top to bottom, 50 mol% of* ***C_{10}OH*** *(□), 20 mol% of* ***C_{18}OH*** *(△), 40 mol% of* ***C_{10}OH*** *(■), 5 mol% of* ***$C_{18:1}$OH*** *(▼), 25 mol% of* ***C_{18}GOH*** *(◁), 10 mol% of* ***C_{18}GOH*** *(◀), 10 mol% of* ***C_{18}OH*** *(▲) and 40 mol% of* ***C_{12}Mal*** *(◆). Lines are only drawn to guide the eye.*

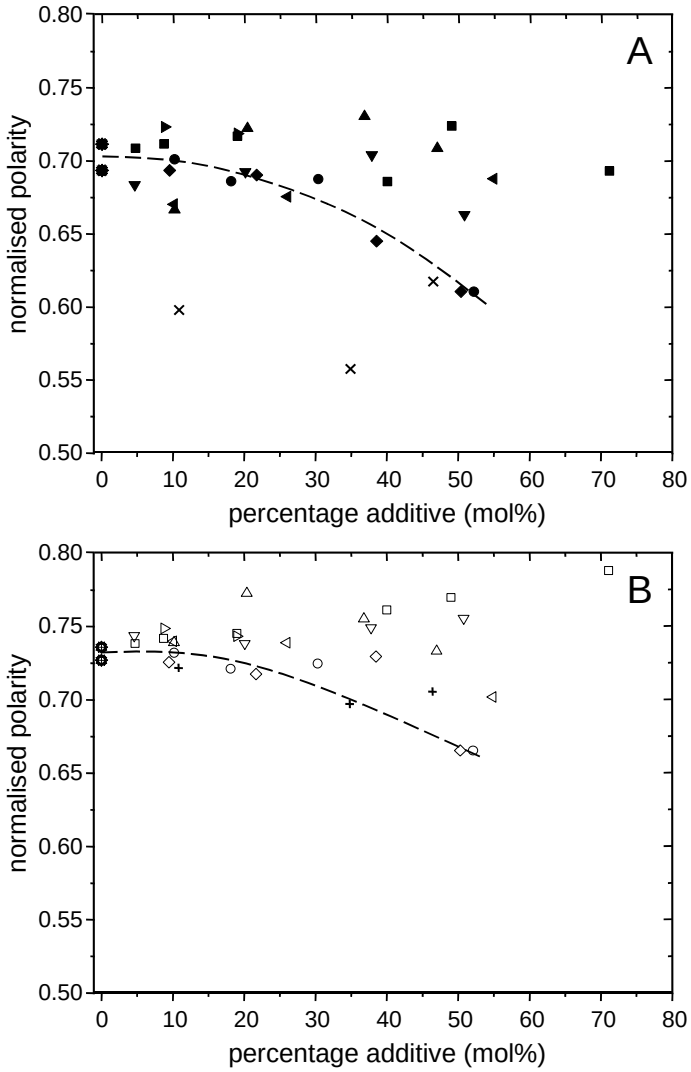

Figure 2.32**. Plot of normalised polarity ($P^{w/d}$) as measured by Nile Red fluorescence versus bilayer composition. Excition wavelength 490 nm (A) and 590 nm (B).* ***C_{10}OH *(■);* ***C_{18}OH*** *(▲);* ***C_{18}GOH*** *(◄);* ***$C_{18:1}$OH C_{12}Glu*** *(●);* ***C_{12}Mal*** *(♦);* ***$C_{16}EO_{20}$*** *(►);* ***$C_{10}C_{10}$-*** *(×;+). Dashed lines are drawn to guide the eye through vesicular solutions containing alkyl pyranosides.*

As can be seen in Figure 2.32A and B $P^{w/d}$ is more or less constant. In Figure 2.32A and B $P^{w/d}$ is on average 0.68 and 0.73, respectively. This value is close to the value of methanol (0.70). We refrain from a more detailed comparison since the value of $P^{w/d}$ is only an average of the dye molecules that are preferentially excited. However, trends are still informative, assuming that the distribution of Nile Red is not affected by changes in bilayer composition. When the excitation wavelength is 490 nm the reported value for $P^{w/d}$ in vesicles with **$C_{10}C_{10}$-** is lower than that reported for vesicles with other additives. However, this difference is not apparent when excitation occurs at 590 nm. Upon the addition of alcohols $P^{w/d}$ remains constant, whereas upon the addition of the alkyl pyranosides $P^{w/d}$ decreases slightly.[164] This effect could originate from a dehydration of the vesicle/water interface, making it less polar, as was observed for mixed micelles of SDS and *n*-dodecylmalono-bis-*N*-methylglucamide. Below a mole fraction of SDS of 0.3 the head group region is completely

dehydrated, since the sugar units have replaced all the water molecules in the interfacial region.[165] However, at this stage the counterion binding is still about 40%. In addition, nonionic micelles containing **C_{12}Mal** or **C_{12}Glu** have an interface that is "aqueous-like" in nature,[55] *i.e.* the effective dielectric constant (ε_{eff}) is larger than that for nonionic micelles with an oligo ethylene oxide head group (but the ε_{eff} of sugar-based surfactants is lower than the ε_{eff} of water). These two observations suggest a situation that the polarity, as sensed by Nile Red, is slightly lower in cationic vesicles with alkyl pyranosides. However, we stress that the change in $P^{w/d}$ is not large, which complicates the interpretation of the experimental data.

The values of $P^{w/d}$ that are reported here are slightly higher than what has been measured for egg PC vesicles (0.58-0.65; λ_{exc}=550 nm)[156,166] and DPPC (0.51 (estimate); λ_{exc}=550 nm).[167]

2.3.5.7 Summary of Membrane Polarity Experiments

The different results for pyrene, laurdan, ANS and Nile Red fluorescence and $E_T(30)$ absorbance are consistent with each other. The reported values of $P^{w/d}$, I_1/I_3 and the wavelength of maximum fluorescence in the spectrum of laurdan in vesicles are mostly independent of the bilayer composition. However, for certain dyes in some vesicular systems there seems to be a slight deviation from this general trend.

The absolute value of $P^{w/d}$ varies from dye to dye. The value of $P^{w/d}$ reported by Nile Red and $E_T(30)$ is about 0.7 (Figure 2.28 and Figure 2.32), whereas ANS reports a value around 0 (Figure 2.30). Despite these differences in absolute value they reflect a difference in interaction between dye and its environment rather than a difference in polarity. This is apparent when the values of $P^{w/d}$ are compared with the value of methanol as sensed by these dyes (0.72, 0.70 and 0.07, respectively). This is reasonable considering that our choice of taking 1,4-dioxane as a reference is arbitrary and the sensitivity of these dyes towards 1,4-dioxane is not necessarily the same. The observation that in aqueous aggregates the polarity is similar to the polarity in methanol has been observed before.[147,168] Also the polarity as sensed by pyrene is similar in vesicles as in methanol (1.20-1.35 and 1.33, respectively).

It should be noted that in order to minimise scattering from the vesicles the fluorescence experiments were done on solutions containing at most 0.5 mM **$C_{18}C_{18}$+**. Control experiments were performed in the absence of fluorescent dye. Except for pyrene background scattering was negligible. However, in the case of vesicular solutions containing **C_{12}Mal** the amphiphile concentration of 0.5 mM leads to incomplete binding of **C_{12}Mal**, and therefore at the same mole fraction, but higher amphiphile concentration, the observed changes in polarity might be larger.

In general, it can be concluded that the local polarity of the membrane interface as reported by the dyes used in this study is only slightly affected by the addition of double-tailed anionic amphiphiles, single-tailed nonionic surfactants, and long linear alcohols.

2.3.6 ζ Potential

2.3.6.1 Theoretical Considerations

A charged particle that diffuses through a solution interacts with its counterions and other charged particles. Depending on the surface charge and the counterion concentration a certain number of counterions will be in close proximity of the charged particle. The amount of counterions that compensate for the charges on the surface is often described by the fraction of counterion binding β. This parameter is part of the pseudophase model derived by Romsted.[169] In this model there are two pseudophases, a vesicular pseudophase and an aqueous pseudophase. The concentration of ions in the vesicular pseudophase is determined by the counterion binding β, and the aqueous ion concentration is simply given by the total ion concentration minus the concentration bound to the surface. Since the model assumes two phases, at the border of the vesicular and aqueous pseudophase there is a sharp change in ion concentration.
A more realistic, yet also more complex, description of the ability to bind counterions is given by the Poisson-Boltzmann equation. This model describes the distribution of ions as a function of the potential at a certain distance from the surface of a spherical particle and depends on the surface charge density and total ion concentration.
The Poisson-Boltzmann equation is described by eq. (2.15):

$$\frac{1}{r^2}\frac{\mathrm{d}}{\mathrm{d}r}\left(r^2\frac{\mathrm{d}\psi_r}{\mathrm{d}r}\right)=\frac{-F}{\varepsilon_0\varepsilon_r}c_0\mathrm{e}^{\frac{-ze\psi_r}{k_bT}},R<r\le b \qquad (2.15)$$

In this equation F, ε_0, ε_r, k_b, e and z are the well-known physical constants: Faraday constant, vacuum permittivity, the relative permittivity, Boltzmann constant, elementary charge, and the sign of the charge (+1 or −1), respectively. T is the absolute temperature, and the potential at a distance r from the centre of a particle with radius R is given by ψ_r. b is the distance at which the potential approaches 0 mV. This equation is solved under the boundary conditions, *i.e.* $\mathrm{d}\psi/\mathrm{d}r|_b = 0$ and $\mathrm{d}\psi/\mathrm{d}r|_R = -\sigma/\varepsilon_0\varepsilon_r$, where σ is the surface charge density. These conditions specify that the potential at infinite distance from the charged surface is zero and that the potential at the surface is linearly related to the surface charge density.
Experimentally it is difficult to measure the surface potential. It is easier to measure the ζ potential (Scheme 2.16), although this parameter is not entirely free from ambiguity.[170] The ζ potential is measured at the slipping plane of a charged particle that is moving through a solution. The location of slipping plane is difficult to measure and it depends on many variables, *e.g.* temperature, salt concentration, pH, etc. In a typical experiment to measure the ζ potential, a voltage is applied over a capillary containing a solution with charged particles. Due to this voltage there will be a flow in the cell. However, since the flow is circular (going into one direction in the middle of the capillary and back along the cell walls) at 14.6% and 85.4 % from the cell wall there is no voltage-induced flow. This is called the stationary phase. There, the particles move entirely due to the voltage applied and their ζ potential. From the measured electrophoretic mobility the ζ potential can be calculated via the Henry equation (eq. (2.16)), although other equations and empirical relationships exist to calculate the ζ potential.[171,172] Differences between these models originate for experiments under other conditions, or just different approaches. Below a potential of *ca.* |50| mV differences are usually smaller than 10%.

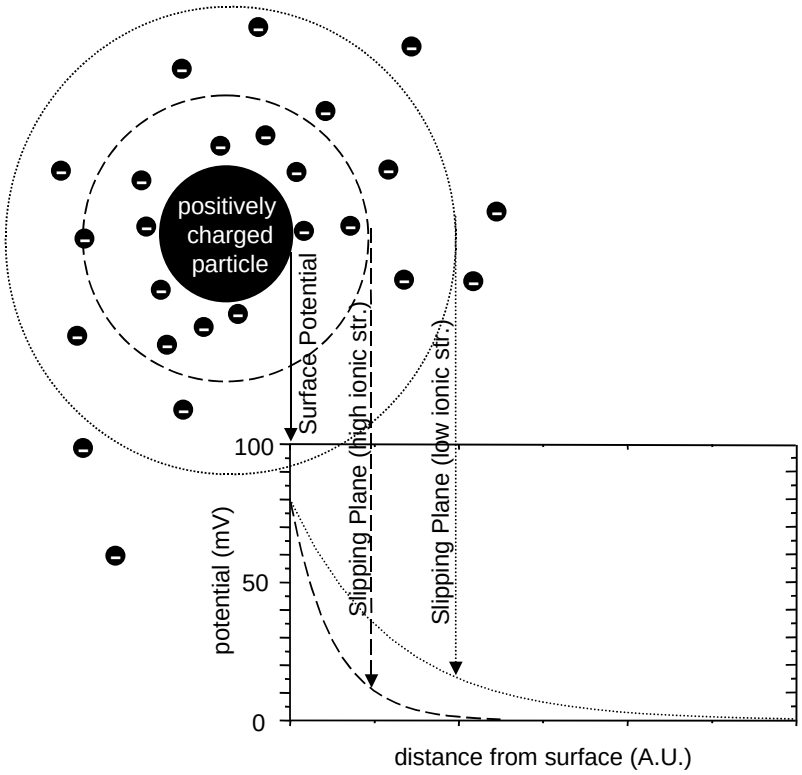

Scheme 2.16. *Schematic representation of the potential at a certain distance from a charged particle in solution.*

$$\zeta = \frac{3\eta\mu}{2\varepsilon_0\varepsilon_r f(\kappa, R)} \tag{2.16}$$

In this equation is η the viscosity, μ the electrophoretic mobility and f(κ,*R*) is a function of the inverse of the Debye length and the radius of the particle.

In practice, the ζ potential is often used as a measure for colloidal stability. Below a potential of 30 mV the electrostatic repulsion between particles becomes too small and they tend to aggregate as a result of Van der Waals interactions. However, this threshold value is rather arbitrary.

2.3.6.2 Dimethyldi-*n*-Octadecylammonium Chloride and Sodium Di-*n*-Decylphosphate

In Figure 2.33 the ζ potential is shown for mixed vesicles containing **$C_{18}C_{18}$+** and increasing amounts of **$C_{10}C_{10}$-**. The ζ potential only slightly decreases with increasing **$C_{10}C_{10}$-** content up to 50 mol%. Then the sign of the ζ potential is reversed.

The value we find for 100 mol% of **$C_{18}C_{18}$+** is also found in the literature,[173] but also a value of 84.8 mV has been reported.[174] However, several remarks have to be made. Vesicles formed from **$C_{18}C_{18}$+** are not spherical. The preparation method has a large influence on the mobility. Not only because it might lead to a different size distribution for the vesicles, but also because residual organic solvent (used in the literature reports) might be present.[175]

Finally, also the concentration plays a role. Therefore, comparison with the literature is difficult. In addition, we used 2.25 mM NaOH, which leads to a lowering of the ζ potential. One might anticipate that upon the addition of **$C_{10}C_{10}$-** the ζ potential should decrease more strongly since the surface potential is decreased upon the addition of more **$C_{10}C_{10}$-**. However, at the same time also the salt concentration is increased and therefore the ζ potential is measured closer to the vesicular surface. Apparently, these two effects compensate each other, and the ζ potential is only slightly decreased.
Special attention should be drawn to the ζ potential for 50 mol% of **$C_{10}C_{10}$-**. For this solution the ζ potential is approximately 30 mV indicating that the outer leaflet is positively charged and the aggregates are colloidally stable. This observation is in disagreement with the cryo-EM pictures (Section 2.3.1.1), indicating aggregation of vesicles. Apparently, 30 mV is in our case not large enough to prevent aggregation.

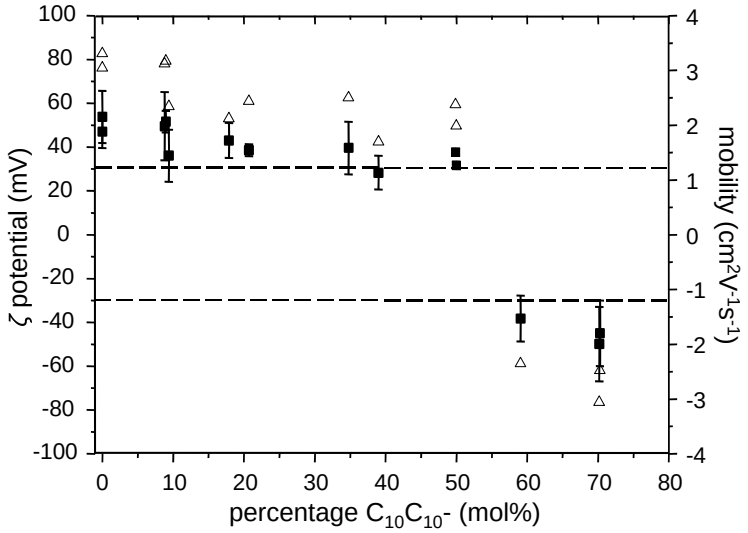

Figure 2.33. *Plot of the ζ potential (■) and electrophoretic mobility (△) as a function of the bilayer composition. The error bars denote the widths of the ζ potential peak. Dashed lines are drawn to show the colloidally stable region (ζ potential).*

2.3.7 General Overview

It is surprising to notice that addition of **C_{10}OH** and **C_{18}GOH** to vesicles formed from **$C_{18}C_{18}$+** has little influence on the general properties. The main phase transition temperature is only slightly affected up to 50 mol%, and fluorescence spectroscopy using various dyes does not reveal significant changes in measured polarity. Similar results apply when **$C_{18:1}$OH** and **C_{18}OH** are added, except that addition of **C_{18}OH** leads to a significant increase in the main phase transition above 20 mol% of **C_{18}OH**. Addition of more than 20 mol% of **$C_{18:1}$OH** leads to severe broadening of the main phase transition. Both observations are reasonable since the packing of the tails has a large influence on the main phase transition temperature. Hence, addition of **C_{18}OH** leads to a better packing, whereas addition of **$C_{18:1}$OH** leads a worse packing.

Upon increasing the size of the hydrophilic part of the additive, the packing parameter of the additives is severely changed. Whereas for the alcohols the packing parameter is larger than 1, for **C_{12}Mal**, **C_{12}Glu** and **$C_{16}EO_{20}$** the packing parameter is about $^1/_3$, leading to micelle formation when dissolved in pure water. **C_{12}Glu** does not dissolve in water, due to a high Krafft temperature, which is observed more often for these types of surfactants.[56,176] **C_{12}Mal** and **$C_{16}EO_{20}$** are able to solubilise vesicles into micelles. The point where the surfactants saturate the membrane is readily achieved, and this is also the case for the point of complete solubilisation by **C_{12}Mal**. A large mole fraction is required to completely solubilise vesicles by **$C_{16}EO_{20}$**. However, to reach an equilibrium state in mixtures of **$C_{18}C_{18}$+** and **C_{12}Mal** or **$C_{16}EO_{20}$** (when micelles are added to vesicles of **$C_{18}C_{18}$+**) requires at least 15 h. In addition, the phase behaviour of mixtures of **$C_{18}C_{18}$+** and **C_{12}Mal** in the presence of NaOH shows precipitation and reorganisation into larger aggregates. We do not fully understand this behaviour, but considering that sugar-based surfactants have anomalous behaviour with respect to other nonionic[177] or charged surfactants, this is not surprising. This anomalous solution behaviour includes a complex phase diagram (strongly dependent with respect to the α or β anomer),[176,178,179] binding of hydroxide ions (unknown mechanism),[56,61,62,180-184] a relatively low effective dielectric constant,[55] dehydration of the polar shell[165,185,186] and weak carbohydrate-carbohydrate interactions (under debate).[187-195]
Polarity experiments also reveal no or little changes in polarity upon the addition of **C_{12}Glu**, **C_{12}Mal** and **$C_{16}EO_{20}$**. However, measurements were performed under conditions where no or small amounts of micelles were formed.
In vesicles formed from the cationic **$C_{18}C_{18}$+** and the anionic **$C_{10}C_{10}$-** amphiphile the main phase transition temperature is lowered, but the DSC scans show that between 10 mol% and 35 mol% of **$C_{10}C_{10}$-** neutral microdomains are formed. Surprisingly, at 50 mol% of **$C_{10}C_{10}$-** no increase in the main phase transition temperature is seen, although this is usually the case in catanionic surfactant mixtures. This latter behaviour is observed when **$C_{18}C_{18}$+** is mixed with the asymmetric **$C_{10}C_{18}$-**. We anticipated a dehydration of the Stern region due to charge compensation by the head groups, but this is not indicated by the fluorescent dyes, except perhaps Nile Red when excited at 490 nm. It should be noted that at 490 nm mainly dye molecules residing in the hydrophobic interior of the bilayer are excited.
In general, addition of a wide variety of additives leads to relatively small changes in the properties of the formed vesicles. The major effects are found in changes of the main phase transition temperature, and the (partial) solubilisation of the vesicles by **C_{12}Mal** and **$C_{16}EO_{20}$**.

2.4 Conclusions

Addition of linear 1-alcohols, anionic double-tailed amphiphiles and nonionic single-tailed surfactants to vesicles formed from **$C_{18}C_{18}$+** leads to little or no changes in measured surface polarity as shown by (fluorescent) dyes, such as 1,8-ANS, Nile Red, pyrene, the E_T(30)-dye and laurdan. On the contrary, the main phase transition temperature can be increased or decreased to quite a large extent. In addition, (neutral) microdomain formation has been observed as well. An increase in the phase transition temperature (at mole

fractions over 0.2) is observed for saturated linear alcohols, where the extent of the increase is larger with increasing carbon atom content in the alcohol. Transitions are broadened extensively upon addition of **$C_{18:1}$OH**, or disappear completely at higher mole fractions due to micelle formation as observed for **C_{12}Mal** and **$C_{16}EO_{20}$**. In the case of the addition of **$C_{10}C_{10}$-** or **$C_{10}C_{18}$-** (neutral) microdomain formation is observed.

C_{12}Mal and **$C_{16}EO_{20}$** solubilise the vesicles into mixed micelles, but the process is rather slow.

Vesicles containing **C_{12}Mal** exhibit somewhat unusual phase behaviour. In a mixed system containing **$C_{18}C_{18}$+** and **C_{12}Mal** "reversible" precipitation is observed upon the addition of small amounts of NaOH. Upon shaking this precipitate disappears. Dynamic light scattering experiments show that size distributions are not greatly effected, upon addition of NaOH. Overnight the vesicles tend to grow, whereas they do not grow in size in the absence of NaOH. This type of behaviour is not observed in mixed systems with **C_{12}Glu**, since **C_{12}Glu** is insoluble in water at 15°C due to its high Krafft temperature.

2.5 Acknowledgements

Dr. Marc Stuart is acknowledged for taking the cryo-EM pictures and fruitful discussions on solvatochromic dyes. Marco Scarzello is also thanked for discussions on solvatochromic dyes

2.6 References

(1) Zubay, G. *Biochemistry*; Addison-Wesley Publishing Company: Reading (USA), **1983**.
(2) Gennis, R. B. In *Biomembranes: Molecular Structure and Function*; Springer-Verlag: New York, **1989**; pp 20-35.
(3) Darnell, J.; Lodish, H.; Baltimore, D. In *Molecular Cell Biology*; Scientific American Books: New York, **1990**; pp 491-499.
(4) Alberts, B.; Bray, D.; Lewis, J.; Raff, M.; Roberts, K.; Watson, J. D. In *Molecular Biology of the Cell*; Garland Publishing: New York, **1994**; pp 477-485.
(5) De Kruyff, B.; Van Deenen, L. L. M.; Demel, R. A. *Biochim.Biophys.Acta* **1972**, *255*, 331-347.
(6) Demel, R. A.; Van Deenen, L. L. M.; Geurts van Kessel, W. S. *Biochim.Biophys.Acta* **1972**, *266*, 26-40.
(7) Demel, R. A.; De Kruijff, B. *Biochim.Biophys.Acta* **1976**, *457*, 109-132.
(8) Clejan, S.; Bittman, R.; Deroo, P. W.; Isaacson, Y. A.; Rosenthal, A. F. *Biochemistry* **1979**, *18*, 2118-2125.
(9) Carmona-Ribeiro, A. M.; Yoshida, L. S.; Sesso, A.; Chaimovich, H. *J.Colloid Interface Sci.* **1984**, *100*, 433-443.
(10) Carmona-Ribeiro, A. M.; Yoshida, L. S.; Chaimovich, H. *J.Phys.Chem.* **1985**, *89*, 2928-2933.
(11) Andersson, M.; Hammerström, L.; Edwards, K. *J.Phys.Chem.* **1995**, *99*, 14531-14538.
(12) Wagenaar, A.; Rupert, L. A. M.; Engberts, J. B. F. N.; Hoekstra, D. *J.Org.Chem.* **1989**, *54*, 2638-2642.
(13) Rejman, J.; Wagenaar, A.; Engberts, J. B. F. N.; Hoekstra, D. *Biochim.Biophys.Acta* **2004**, *1660*, 41-52.
(14) Berlman, I. B. *Handbook of Fluorescence Spectra of Aromatic Molecules*; Academic Press: New York, **1965**.
(15) Egorova, E. M. *Colloids Surf.A* **1998**, *131*, 19-31.
(16) Jung, M.; Hubert, D. H. W.; van Veldhoven, E.; Frederik, P. M.; Blandamer, M. J.; Briggs, B.; Visser, A. J. W. G.; van Herk, A. M.; German, A. L. *Langmuir* **2000**, *16*, 968-979.
(17) *Biochim. Biophys. Acta* devoted a special issue on membrane solubilisation and reconstitution: **2000**, *1508*, 1-251

(18) Lichtenberg, D.; Robson, R. J.; Dennis, E. A. *Biochim.Biophys.Acta* **1983**, *737*, 285-304.
(19) Kragh-Hansen, U.; le Maire, M.; Møller, J. V. *Biophys.J.* **1998**, *75*, 2932-2946.
(20) Schurtenberger, P.; Mazer, N.; Kanzig, W. *J.Phys.Chem.* **1985**, *89*, 1042-1049.
(21) Tanford, C. *The Hydrophobic Effect: Formation of Micelles and Biological Membranes*; Wiley: New York, **1980**.
(22) Heerklotz, H.; Seelig, J. *Biochim.Biophys.Acta* **2000**, *1508*, 69-85.
(23) Edwards, K.; Almgren, M. *Langmuir* **1992**, *8*, 824-832.
(24) Nagawa, Y.; Regen, S. L. *J.Am.Chem.Soc.* **1992**, *114*, 1668-1672.
(25) Liu, Y. P.; Regen, S. L. *J.Am.Chem.Soc.* **1993**, *115*, 708-713.
(26) Memoli, A.; Annesini, M. C.; Petralito, S. *Int.J.Pharm* **1999**, *184*, 227-235.
(27) Nilsson, K.; Almgren, M.; Brown, W.; Jansson, M. *Mol.Cryst.Liq.Cryst.* **1987**, *152*, 181-203.
(28) Edwards, K.; Almgren, M. *Prog.Colloid Polym.Sci.* **1990**, *82*, 190-197.
(29) Babnik, B.; Miklavcic, D.; Kandušer, M.; Hägerstrand, H.; Kralj-Iglic, V.; Iglic, A. *Chem.Phys.Lipids* **2003**, *125*, 123-138.
(30) Heerklotz, H. *Biophys.J.* **2002**, *83*, 2693-2701.
(31) Heerklotz, H.; Szadkowska, H.; Anderson, T.; Seelig, J. *J.Mol.Biol.* **2003**, *329*, 793-799.
(32) Edwards, K.; Almgren, M.; Bellare, J.; Brown, W. *Langmuir* **1989**, *5*, 473-478.
(33) Seras, M.; Edwards, K.; Almgren, M.; Carlson, G.; Ollivon, M.; Lesieur, S. *Langmuir* **1996**, *12*, 330-336.
(34) This effect is due to a better ability to scatter light when particles increase in size.
(35) Goñi, F. M.; Alonso, A. *Biochim.Biophys.Acta* **2000**, *1508*, 51-68.
(36) Lichtenberg, D.; Opatowski, E.; Kozlov, M. M. *Biochim.Biophys.Acta* **2000**, *1508*, 1-19.
(37) Heerklotz, H.; Lantzsch, G.; Binder, H.; Klose, G.; Blume, A. *Chem.Phys.Lett.* **1995**, *235*, 517-520.
(38) Heerklotz, H.; Lantzsch, G.; Binder, H.; Klose, G.; Blume, A. *J.Phys.Chem.* **1996**, *100*, 6764-6774.
(39) Heerklotz, H.; Seelig, J. *Biophys.J.* **2000**, *78*, 2435-2440.
(40) López, O.; Cócera, M.; Parra, J. L.; De la Maza, A. *Colloids Surf.A* **2001**, *193*, 221-229.
(41) le Maire, M.; Møller, J. V.; Champeil, P. *Biochemistry* **1987**, *26*, 4803-4810.
(42) Alonso, A.; Urbaneja, M. A.; Goñi, F. M.; Carmona, F. G.; Cánovas, F. G.; Gómez-Fernández, J. C. *Biochim.Biophys.Acta* **1987**, *902*, 237-246.
(43) Prete, P. S. C.; Gomes, K.; Malheiros, S. V. P.; Meirelles, N. C.; de Paula, E. *Biophys.Chem.* **2002**, *97*, 45-54.
(44) Van Os, N. M.; Haak, J. R.; Rupert, L. A. M. *Physico-Chemical Properties of Selected Anionic, Cationic and Nonionic Surfactants*; Elsevier: Amsterdam, **1993**.
(45) Barreleiro, P. C. A.; Olofsson, G.; Brown, W.; Edwards, K.; Bonassi, N. M.; Feitosa, E. *Langmuir* **2002**, *18*, 1024-1029.
(46) Johnsson, M.; Edwards, K. *Langmuir* **2000**, *16*, 8632-8642.
(47) Levy, D.; Gulik, A.; Seigneuret, M.; Rigaud, J. L. *Biochemistry* **1990**, *29*, 9480-9488.
(48) Edwards, K.; Almgren, M. *J.Colloid Interface Sci.* **1991**, *147*, 1-21.
(49) Schnitzer, E.; Lichtenberg, D.; Kozov, M. M. *Chem.Phys.Lipids* **2003**, *126*, 55-76.
(50) Paternostre, M.; Meyer, O.; GrabielleMadelmont, C.; Lesieur, S.; Ghanam, M.; Ollivon, M. *Biophys.J.* **1995**, *69*, 2476-2488.
(51) Opatowski, E.; Kozlov, M. M.; Lichtenberg, D. *Biophys.J.* **1997**, *73*, 1448-1457.
(52) Wenk, M. R.; Alt, T.; Seelig, A.; Seelig, J. *Biophys.J.* **1997**, *72*, 1719-1731.
(53) Keller, M.; Kerth, A.; Blume, A. *Biochim.Biophys.Acta* **1997**, *1326*, 178-192.
(54) Wenk, M. R.; Seelig, J. *J.Phys.Chem.B* **1997**, *101*, 5224-5231.
(55) Drummond, C. J.; Warr, G. G.; Grieser, F.; Ninham, B.; Evans, D. F. *J.Phys.Chem.* **1985**, *89*, 2103-2109.
(56) Balzer, D. *Langmuir* **1993**, *9*, 3375-3384.
(57) Caussanel, F.; Andre-Barrès, C.; Lesieur, S.; Rico-Lattes, I. *Colloids Surf.B* **2001**, *22*, 193-203.
(58) van der Meeren, P.; van Laethem, M.; Vanderdeelen, J.; Baert, L. *J.Lipos.Res.* **1992**, *2*, 23-42.
(59) The "automatic" analysis is provided with the Malvern Zetasizer 5000 software. Using this algorithm the software chooses the analysis algorithm itself.
(60) Schurtenberger, P.; Cavaco, C. *Langmuir* **1994**, *10*, 100-108.
(61) Johnsson, M.; Wagenaar, A.; Engberts, J. B. F. N. *J.Am.Chem.Soc.* **2003**, *125*, 757-760.
(62) Johnsson, M.; Wagenaar, A.; Stuart, M. C. A.; Engberts, J. B. F. N. *Langmuir* **2003**, *19*, 4609-4618.
(63) de la Maza, A.; Coderch, L.; López, O.; Parra, J. L. *Micron* **1998**, *29*, 175-182.
(64) Lee, A. G. *Biochim.Biophys.Acta* **1977**, *472*, 237-281.
(65) Kamaya, H.; Matubayasi, N.; Ueda, I. *J.Phys.Chem.* **1984**, *88*, 797-800.
(66) Eliasz, A. W.; Chapman, D.; Ewing, D. F. *Biochim.Biophys.Acta* **1976**, *448*, 220-230.
(67) Lee, A. G. *Biochemistry* **1976**, *15*, 2448-2454.

(68) Mabrey, S.; Sturtevant, J. M. *Biochim.Biophys.Acta* **1977**, *486*, 444-450.
(69) Jain, M. K.; Wu, N. M. *J.Membrane Biol.* **1977**, *34*, 157-201.
(70) Silvius, J. R. *Biochim.Biophys.Acta* **1991**, *1070*, 51-59.
(71) López-García, F.; Micol, V.; Villalaín, J.; Gómez-Fernández, J. C. *Biochim.Biophys.Acta* **1993**, *1153*, 1-8.
(72) Lin, H. N.; Li, S. S.; Brumbaugh, E. E.; Huang, C. H. *Arch.Biochem.Biophys.* **1995**, *319*, 408-412.
(73) Madler, B.; Binder, H.; Klose, G. *J.Colloid Interface Sci.* **1998**, *202*, 124-138.
(74) Svitova, T. F.; Hill, R. M.; Radke, C. J. *Langmuir* **1999**, *15*, 7392-7402.
(75) Blandamer, M. J.; Briggs, B.; Cullis, P. M.; Irlam, K. D.; Engberts, J. B. F. N.; Streefland, L. *Thermochim.Acta* **2000**, *364*, 173-179.
(76) Koynova, R.; Caffrey, M. *Chem.Phys.Lipids* **2002**, *115*, 107-219.
(77) Woodward, J. T.; Zasadzinski, J. A. *Biophys.J.* **1997**, *72*, 964-976.
(78) Leidy, C.; Kaasgaard, T.; Crowe, J. H.; Mouritsen, O. G.; Jorgensen, K. *Biophys.J.* **2002**, *83*, 2625-2633.
(79) Kaasgaard, T.; Leidy, C.; Crowe, J. H.; Mouritsen, O. G.; Jorgensen, K. *Biophys.J.* **2003**, *85*, 350-360.
(80) Feitosa, E.; Barreleiro, P. C. A.; Olofsson, G. *Chem.Phys.Lipids* **2000**, *105*, 201-213.
(81) Ali, S.; Bittman, R. *J.Lipid Res.* **1996**, *37*, 2305-2309.
(82) Blandamer, M. J.; Briggs, B.; Cullis, P. M.; Engberts, J. B. F. N.; Wagenaar, A.; Smits, E.; Hoekstra, D.; Kacperska, A. *J.Chem.Soc., Faraday Trans.* **1994**, *90*, 2709-2715.
(83) Blandamer, M. J.; Briggs, B.; Cullis, P. M.; Engberts, J. B. F. N.; Wagenaar, A.; Smits, E.; Hoekstra, D.; Kacperska, A. *Langmuir* **1994**, *10*, 3507-3511.
(84) Sapia, P.; Coppola, L.; Ranieri, G.; Sportelli, L. *Colloid Polym.Sci.* **1994**, *272*, 1289-1294.
(85) Sturtevant, J. M. *Chem.Phys.Lipids* **1998**, *95*, 163-168.
(86) Marques, E. F.; Khan, A.; Lindman, B. J. *Thermochim.Acta* **2002**, *394*, 31-37.
(87) Eibl, H.; Wooley, P. *Biophys.Chem.* **1979**, *10*, 261-271.
(88) Lewis, R. N. A. H.; McElhaney, R. N. *Biophys.J.* **2000**, *79*, 1455-1464.
(89) Hafez, I. M.; Ansell, S.; Cullis, P. R. *Biophys.J.* **2000**, *79*, 1438-1446.
(90) Tarahovsky, Y. S.; Arsenault, A. L.; MacDonald, R. C.; McIntosh, T. J.; Epand, R. M. *Biophys.J.* **2000**, *79*, 3193-3200.
(91) Merrill, A. H.; Stevens, V. L. *Biochim.Biophys.Acta* **1989**, *1010*, 131-139.
(92) Blandamer, M. J.; Briggs, B.; Cullis, P. M.; Engberts, J. B. F. N.; Kacperska, A. *J.Chem.Soc., Faraday Trans.* **1995**, *91*, 4275-4278.
(93) Castelli, F.; Panico, A.; Pignatello, R.; Mazzone, P. *J.Colloid Interface Sci.* **1995**, *175*, 289-292.
(94) Blandamer, M. J.; Briggs, B.; Cullis, P. M.; Engberts, J. B. F. N. *Chem.Soc.Rev.* **1995**, *24*, 251-257.
(95) Kacperska, A. *J.Therm.Anal.* **2000**, *61*, 63-73.
(96) Inoue, T.; Iwanaga, T.; Fukushima, K.; Shimozawa, R. *Chem.Lett.* **1988**, 277-280.
(97) Inoue, T.; Iwanaga, T.; Fukushima, K.; Shimozawa, R.; Suezaki, Y. *Chem.Phys.Lipids* **1988**, *48*, 189-196.
(98) Hui, F. K.; Barton, P. G. *Biochim.Biophys.Acta* **1973**, *296*, 510-517.
(99) Lee, A. G. *Biochim.Biophys.Acta* **1977**, *472*, 285-344.
(100) Zavoico, G. B.; Chandler, L.; Kutchai, H. *Biochim.Biophys.Acta* **1985**, *812*, 299-312.
(101) Other factors that can contribute to the temperature of the main phase transition are head group interactions, salt effects, and the presence of small organic additives (organic solvents).
(102) Inoue, T.; Miyakawa, K.; Shimozawa, R. *Chem.Phys.Lipids* **1986**, *42*, 261-270.
(103) Inoue, T.; Fukushima, K.; Shimozawa, R. *Bull.Chem.Soc.Jpn.* **1988**, *61*, 1565-1569.
(104) Carion-Taravella, B.; Lesieur, S.; Chopineau, J.; Lesieur, P.; Ollivon, M. *Langmuir* **2002**, *18*, 325-335.
(105) Johnsson, M. *unpublished results*
(106) Blandamer, M. J.; Briggs, B.; Cullis, P. M.; Green, J. A.; Waters, M.; Soldi, G.; Engberts, J. B. F. N.; Hoekstra, D. *J.Chem.Soc., Faraday Trans.* **1992**, *88*, 3431-3434.
(107) Feitosa, E.; Brown, W. *Langmuir* **1997**, *13*, 4810-4816.
(108) Barreleiro, P. C. A.; Olofsson, G.; Alexandridis, P. *J.Phys.Chem.B* **2000**, *104*, 7795-7802.
(109) Benatti, C. R.; Feitosa, E.; Fernandez, R. M.; Lamy-Freund, M. T. *Chem.Phys.Lipids* **2001**, *111*, 93-104.
(110) Reichardt, C. *Chem.Rev.* **1994**, *94*, 2319-2358.
(111) Brewer, G. J. *Biochemistry* **1992**, *31*, 1809-1815.
(112) Kalyanasundaram, K.; Thomas, J. K. *J.Am.Chem.Soc.* **1977**, *99*, 2039-2044.
(113) Lakowicz, J. R. In *Principles of Fluorescence Spectroscopy*; Kluwer Academic: New York, **1999**; pp 185-210.
(114) Kosower, E. M.; Dodiuk, H. *J.Am.Chem.Soc.* **1974**, *96*, 6195-6196.
(115) The orientational polarisibility is a function of the dielectric constant, refractive index, the radius of the cavity in which the dye resides and some physical constants.

(116) Kosower, E. M.; Kanety, H. *J.Am.Chem.Soc.* **1983**, *105*, 6236-6243.
(117) Strictly speaking this is not correct. Excitation can also occur to different excited states, but this is rare.
(118) Amire, S. A.; Burrows, H. D. *J.Chem.Soc., Faraday Trans.1* **1982**, *78*, 2033-2040.
(119) Wang, G. J.; Engberts, J. B. F. N. *Langmuir* **1994**, *10*, 2583-2587.
(120) Capek, I. *Adv.Colloid Interface Sci.* **2002**, *97*, 89-149.
(121) Cang, H.; Brace, D. D.; Fayer, M. D. *J.Phys.Chem.B* **2001**, *105*, 10007-10015.
(122) Kachel, K.; Asuncion-Punzalan, E.; London, E. *Biochim.Biophys.Acta* **1998**, *1374*, 63-76.
(123) Fendler, J. H.; Fendler, E. J.; Infante, G. A.; Shi, P.-S.; Patterson, L. K. *J.Am.Chem.Soc.* **1974**, *97*, 89-95.
(124) Matzinger, S.; Hussey, D. M.; Fayer, M. D. *J.Phys.Chem.B* **1998**, *102*, 7216-7224.
(125) Gallivan, J. P.; Dougherty, D. A. *Proc.Natl.Acad.Sci.USA* **1999**, *96*, 9459-9464.
(126) Parasassi, T.; Destasio, G.; Ravagnan, G.; Rusch, R. M.; Gratton, E. *Biophys.J.* **1991**, *60*, 179-189.
(127) Bagatolli, L. A.; Parasassi, T.; Fidelio, G. D.; Gratton, E. *Photochem.Photobiol.* **1999**, *70*, 557-564.
(128) Parasassi, T.; Destasio, G.; Dubaldo, A.; Gratton, E. *Biophys.J.* **1990**, *57*, 1179-1186.
(129) Parasassi, T.; Distefano, M.; Loiero, M.; Ravagnan, G.; Gratton, E. *Biophys.J.* **1994**, *66*, 763-768.
(130) Bagatolli, L. A.; Maggio, B.; Aguilar, F.; Sotomayor, C. P.; Fidelio, G. D. *Biochim.Biophys.Acta* **1997**, *1325*, 80-90.
(131) Bagatolli, L. A.; Gratton, E.; Fidelio, G. D. *Biophys.J.* **1998**, *75*, 331-341.
(132) Hirsch-Lerner, D.; Barenholz, Y. *Biochim.Biophys.Acta* **1999**, *1461*, 47-57.
(133) Zubiri, D.; Domecq, A.; Bernik, D. L. *Colloids Surf.B* **1999**, *13*, 13-28.
(134) Campbell, R. B.; Balasubramanian, S. V.; Straubinger, R. M. *Biochim.Biophys.Acta* **2001**, *1512*, 27-39.
(135) Harris, F. M.; Best, K. B.; Bell, J. D. *Biochim.Biophys.Acta* **2002**, *1565*, 123-128.
(136) Muñoz, M.; Graciani, M. D. M.; Rodríguez, A.; Moyá, M. L. *J.Colloid Interface Sci.* **2003**, *266*, 208-214.
(137) Almgren, M.; Grieser, F.; Thomas, J. K. *J.Am.Chem.Soc.* **1979**, *101*, 279-291.
(138) Aoudia, M.; Zana, R. *J.Colloid Interface Sci.* **1998**, *206*, 158-167.
(139) Stryer, L. *J.Mol.Biol.* **1965**, *13*, 482-495.
(140) Stryer, L. *Science* **1968**, *162*, 526-533.
(141) Brand, L.; Gohlke, J. R. *Ann.Rev.Biochem.* **1972**, *41*, 843-868.
(142) Robinson, G. W.; Robbins, R. J.; Fleming, G. R.; Morris, J. M.; Knight, A. E. W.; Morrison, R. J. S. *J.Am.Chem.Soc.* **1978**, *100*, 7145-7150.
(143) Turner, D. C.; Brand, L. *Biochemistry* **1968**, *7*, 3381-3390.
(144) Kosower, E. M.; Dodiuk, H. *J.Am.Chem.Soc.* **1978**, *100*, 4173-4179.
(145) Kosower, E. M.; Dodiuk, H.; Kanety, H. *J.Am.Chem.Soc.* **1978**, *100*, 4179-4188.
(146) Slavik, J. *Biochim.Biophys.Acta* **1982**, *694*, 1-25.
(147) Rupert, L. A. M.; Engberts, J. B. F. N.; Hoekstra, D. *J.Am.Chem.Soc.* **1986**, *108*, 3920-3925.
(148) Lanyi, J. K. *Biochim.Biophys.Acta* **1974**, *356*, 245-256.
(149) Zierler, K.; Rogus, E. *Biochim.Biophys.Acta* **1978**, *514*, 37-53.
(150) Zierler, K.; Rogus, E. *Biochim.Biophys.Acta* **1979**, *551*, 389-405.
(151) Slavik, J.; Horák, J.; Rihová, L.; Kotyk, A. *J.Mol.Biol.* **1982**, *64*, 175-179.
(152) Gulik-Krzywicki, T.; Shechter, E.; Iwatsubo, M.; Ranck, J. L.; Luzzati, V. *Biochim.Biophys.Acta* **1970**, *219*, 1-10.
(153) Zingsheim, H. P.; Haydon, D. A. *Biochim.Biophys.Acta* **1973**, *298*, 755-768.
(154) Bashford, C. L.; Morgan, C. G.; Radda, G. K. *Biochim.Biophys.Acta* **1976**, *426*, 157-172.
(155) Teissié, J.; Baudras, A. *Biochimie* **1977**, *59*, 693-703.
(156) Greenspan, P.; Fowler, S. D. *J.Lipid Res.* **1985**, *26*, 781-789.
(157) Sarkar, N.; Das, K.; Nath, D. N.; Bhattacharyya, K. *Langmuir* **1994**, *10*, 326-329.
(158) Dutta, A. K.; Kamada, K.; Ohta, K. *J.Photochem.Photobiol.A* **1996**, *93*, 57-64.
(159) Oliveira, M. E. C. D. R.; Hungerford, G.; Da Graça Miguel, M.; Burrows, H. D. *J.Mol.Struct.* **2001**, *563*, 443-447.
(160) Hungerford, G.; Castanheira, E. M. S.; Oliveira, M. E. C. D. R.; Da Graça Miguel, M.; Burrows, H. *J.Phys.Chem.B* **2002**, *106*, 4061-4069.
(161) Stuart, M.C.A.; Van de Pas, J.C.; Engberts, J.B.F.N. J. Colloid Interface Sci. submitted
(162) Sackett, D. L.; Wolff, J. *Anal.Biochem.* **1987**, *167*, 228-234.
(163) Boldrini, B.; Cavalli, E.; Painelli, A.; Terenziani, F. *J.Phys.Chem.A* **2002**, *106*, 6286-6294.
(164) In Figure 1.32A the normalised polarity was calculated using the wavelength of maximum fluorescence of water and 1,4-dioxane as measured when excited with light of 490 nm. In Figure 1.31B it was calculated using the average of the wavelength of maximum fluorescence as measured by excitation at 490 nm and 590 nm. This slightly different approach leads to

slightly different values of the same experimental data in Figures 1.31B and 1.32A. This is also the case in Figure 1.32B.
(165) Griffiths, P. C.; Pettersson, E.; Stilbs, P.; Cheung, A. Y. F.; Howe, A. M.; Pitt, A. R. *Langmuir* **2001**, *17*, 7178-7181.
(166) Krishna, M. M. G. *J.Phys.Chem.A* **1999**, *103*, 3589-3595.
(167) Coutinho, P. J. G.; Castanheira, E. M. S.; Rei, M. C.; Oliveira, M. E. C. D. R. *J.Phys.Chem.B* **2002**, *106*, 12841-12846.
(168) Klijn, J. E.; Kevelam, J.; Engberts, J. B. F. N. *J.Colloid Interface Sci.* **2000**, *226*, 76-82.
(169) Romsted, L. S. In *Micellization, Solubilization and Microemulsions*; Mittal, K. L., ed., Plenum Press: New York, **1977**; pp 509-530.
(170) Hiemenz, P. C. In *Principles of Colloid and Surface Chemistry*; Marcel Dekker, Inc.: New York, **1977**; pp 453-487.
(171) O'Brien, R. W.; White, L. R. *J.Chem.Soc., Faraday Trans.2* **1978**, *74*, 1607-1626.
(172) Ohshima, H.; Healy, T. W.; White, L. R. *J.Chem.Soc., Faraday Trans.2* **1983**, *79*, 1613-1628.
(173) Nascimento, D. B.; Rapuano, R.; Lessa, M. M.; Carmona-Ribeiro, A. M. *Langmuir* **1998**, *14*, 7387-7391.
(174) Carmona-Ribeiro, A. M.; Midmore, B. R. *J.Phys.Chem.* **1992**, *96*, 3542-3547.
(175) Vieira, D. B.; Carmona-Ribeiro, A. M. *J.Colloid Interface Sci.* **2001**, *244*, 427-431.
(176) Boyd, B. J.; Drummond, C. J.; Krodkiewska, I.; Grieser, F. *Langmuir* **2000**, *16*, 7359-7367.
(177) Shinoda, K.; Carlsson, A.; Lindman, B. *Adv.Colloid Interface Sci.* **1996**, *64*, 253-271.
(178) Söderman, O.; Johansson, I. *Curr.Opin.Colloid Interface Sci.* **1999**, *4*, 391-401.
(179) Hoffmann, B.; Platz, G. *Curr.Opin.Colloid Interface Sci.* **2001**, *6*, 171-177.
(180) Bergeron, V.; Waltermo, A.; Claesson, P. M. *Langmuir* **1996**, *12*, 1336-1342.
(181) Waltermo, A.; Claesson, P. M.; Simonsson, S.; Manev, E.; Johansson, I.; Bergeron, V. *Langmuir* **1996**, *12*, 5271-5278.
(182) Sierra, M. L.; Svensson, M. *Langmuir* **1999**, *15*, 2301-2306.
(183) Baba, T.; Zheng, L. Q.; Minamikawa, H.; Hato, M. *J.Colloid Interface Sci.* **2000**, *223*, 235-243.
(184) Zheng, L. Q.; Shui, L. L.; Shen, Q.; LI, G. Z.; Baba, T.; Minamikawa, H.; Hato, M. *Colloids Surf.A* **2002**, *207*, 215-221.
(185) Bales, B. L.; Howe, A. M.; Pitt, A. R.; Roe, J. A.; Griffiths, P. C. *J.Phys.Chem.B* **2000**, *104*, 264-270.
(186) Bales, B. L.; Ranganathan, R.; Griffiths, P. C. *J.Phys.Chem.B* **2001**, *105*, 7465-7473.
(187) Klotz, I. M.; Franzen, J. S. *J.Am.Chem.Soc.* **1962**, *84*, 3461-3466.
(188) Venkatesan, P.; Cheng, Y.; Kahne, D. *J.Am.Chem.Soc.* **1994**, *116*, 6955-6956.
(189) Simons, K.; Ikonen, E. *Nature* **1997**, *387*, 569-572.
(190) Veiga, M. P.; Goñi, F. M.; Alonso, A.; Marsh, D. *Biochemistry* **2000**, *39*, 9876-9883.
(191) Pincet, F.; Le Bouar, T.; Zhang, Y. M.; Esnault, J.; Mallet, J. M.; Perez, E.; Sinaÿ, P. *Biophys.J.* **2001**, *80*, 1354-1358.
(192) Sugahara, M.; Uragami, M.; Tokutake, N.; Yan, X.; Regen, S. L. *Langmuir* **2002**, *18*, 981-983.
(193) Bazito, R. C.; El Seoud, O. A. *Langmuir* **2002**, *18*, 4362-4366.
(194) Schneider, M. F.; Zantl, R.; Gege, C.; Schmidt, R. R.; Rappolt, M.; Tanaka, M. *Biophys.J.* **2003**, *84*, 306-313.
(195) Santacroce, P. V.; Basu, A. *Angew.Chem.,Int.Ed.Engl.* **2003**, *42*, 95-98.

CHAPTER 3

EFFECTS OF CATANIONIC DOUBLE-TAILED VESICLES ON THE KEMP ELIMINATION REACTION

*The rate-determining deprotonation of 5-nitrobenzisoxazole (Kemp elimination) by hydroxide ions is efficiently catalysed by vesicles formed from dimethyldi-n-octadecylammonium chloride (**$C_{18}C_{18}$+**). Gradual addition of sodium di-n-decylphosphate (**$C_{10}C_{10}$-**) or sodium n-decyl-n-octadecylphosphate (**$C_{10}C_{18}$-**) leads to the formation of catanionic vesicles. Increasing percentages of **$C_{10}C_{10}$-** or **$C_{10}C_{18}$-** in the vesicular bilayers decrease the catalysis of the Kemp elimination. A detailed kinetic analysis, supported by consideration of substrate binding site polarities and counterion binding percentages, suggest that the catalytic effects of **$C_{18}C_{18}$+/$C_{10}C_{10}$-** and **$C_{18}C_{18}$+/$C_{10}C_{18}$-** catanionic vesicles are primarily determined by the binding of catalytically active hydroxide ions to the vesicular surface area. The formation of neutral microdomains in the bilayer, as revealed by DSC (Chapter 2), is not apparent from the catalytic effects found for these vesicles. Interestingly, the catalytic effects observed for 50 mol% of **$C_{10}C_{10}$-** in the catanionic vesicles indicate that cationic domains must be present in the bilayer leaflets.*

*The non-amphiphilic sodium dimethylphosphate (**$C_{01}C_{01}$-**) is able to replace hydroxide ions from the Stern region with the same relative strength as chloride ions.*

The overall kinetic results illustrate that a highly complex mix of factors determines the catalytic effects on reactions occurring in biological cell membranes.

3.1 Introduction

As discussed in Chapter 1 the biological membrane is an extremely complex mixture of various lipids, steroid and proteins. However, not only the mixture is complex, also the molecular structure and properties of the lipids themselves are complex since they can undergo various interactions with each other. Therefore, as a first step we decided to study mixtures of double-tailed amphiphiles. An important interaction between (zwitterionic) lipids is the electrostatic interaction between the cationic ammonium group and the anionic phosphate group, which are present in most phospholipids.

In this chapter, in order to elucidate the influence of electrostatic interactions between amphiphile head groups, the influence of increasing amounts of the first class of additives, anionic double-tailed amphiphiles with a phosphate head group, incorporated into cationic vesicles formed from dimethyldi-*n*-octadecylammonium chloride on the vesicle-catalysed reaction of 5-nitrobenzisoxazole (**1**; Scheme 3.1) with hydroxide ions was studied. In Chapter 1 it was shown that the reaction is sensitive towards changes in the local polarity[1-5] and the concentration of hydroxide ions. Especially this latter dependence is expected to be important, since the anionic amphiphiles will expel hydroxide ions from the Stern region, since they are excellent counterions themselves.

Sodium di-*n*-decylphosphate and sodium *n*-decyl-*n*-octadecylphosphate were chosen in order to study not only the influence of the phosphate head group, but also influence of asymmetry in the tails. The effects of sodium dimethylphosphate on the catalysis was studied in order to obtain more detailed information on the ammonium phosphate interactions.

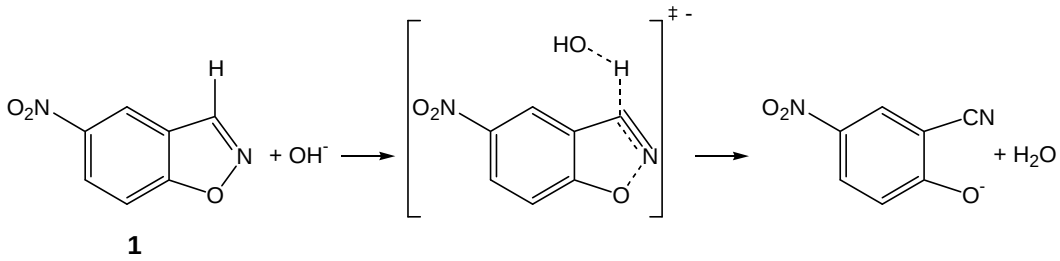

1

Scheme 3.1. *Kemp elimination reaction.*

In Chapter 2 it has been shown that the mixed vesicles formed from cationic and anionic double-tailed amphiphiles segregate into domains. In mixed vesicles with $\mathbf{C_{10}C_{10}}$- these domains are rich in either the cationic amphiphile, or rich in 1:1 complexes of both amphiphiles. The size of the domains is unknown. In mixed vesicles with $\mathbf{C_{10}C_{18}}$- the DSC scans exhibit even more complex behaviour.

3.2 Experimental

3.2.1 General

Materials, the vesicle preparation and the fluorescence and the absorbance spectroscopic measurements have been described in Chapter 2.

3.2.2 Kinetic experiments

Kinetic experiments were performed using an Applied Photophysics SX-18MV Stopped-Flow Reaction Analyzer (Leatherhead, UK) thermostatted with a Neslab RTE-111 water bath. The deprotonation reaction was followed at 380 nm. The temperature was 15.0 ± 0.1°C unless stated otherwise. Before the kinetic run was started, the alkaline vesicular solution and solution containing **1** were allowed to cool to 15.0°C for at least 15 minutes. Control experiments were performed to see whether "aging" of the solution was a factor of importance, but no effect was found over a period of 15 hours. Stock solutions of **1** were prepared by dissolving 0.33 mg of **1** in 100 ml of water ($2\cdot 10^{-5}$ M). For each stock solution the UV/vis spectra before and after reaction were recorded to check the concentration and purity.

In all the kinetic runs the concentration of hydroxide ions was 2.25 mM and the concentration of **1** was $1\cdot 10^{-5}$ M (please note that in the stopped-flow apparatus one volume unit with **1** is mixed with one volume unit of the alkaline vesicular solution).

It is assumed that the reaction takes place both at the inner and outer leaflet of the vesicles with equal rate constants, since hydroxide ions are known to cross the bilayer fast on the time scale of the reaction (and therefore OH^- crossing is not the rate-limiting step).[6-9] This is in agreement with our observation that the observed rate constant does not change over a period of 15 hours and literature observations on the kinetics in solutions containing $\mathbf{C_{18}C_{18}}$+.[10,11] No difference in rate constant has been found for the endo- and exovesicular leaflet for a hydroxide-ion catalysed hydrolysis reactions.[12] Distribution of **1** over the leaflets is considered to be fast since **1** is a small and nonionic molecule.[13]

3.3 Results and Discussion

3.3.1 Characterisation of the Vesicle-Catalysed Reaction

The mechanism of the Kemp elimination reaction has been thoroughly studied and has been found to proceed via a base-catalysed E2 elimination.[1-3] The standard molar Gibbs energy of activation ($\Delta^{\ddagger}G^{\ominus}$) of a reaction is related to the rate constant (k_w) by eq. (3.1).[14]

$$k_w = \frac{k_B T}{h} e^{\frac{-\Delta^{\ddagger}G^{\ominus}}{RT}} \tag{3.1}$$

In this equation h, k_B and R are Planck's, Boltzmann's and the gas constant, respectively. T is the temperature. Since the standard molar Gibbs energy is related to the standard molar enthalpy and entropy of activation via $\Delta^{\ddagger}G^{\ominus} = \Delta^{\ddagger}H^{\ominus} - T\Delta^{\ddagger}S^{\ominus}$, it is possible to rewrite eq. (3.1) into a linear equation (eq. (3.2)). Then the activation parameters can be obtained via an Eyring plot by measuring the rate constant at various temperatures under the assumption that $\Delta^{\ddagger}H^{\ominus}$ and $\Delta^{\ddagger}S^{\ominus}$ are independent of temperature.

$$\ln\left(\frac{k_w h}{k_B T}\right) = -\frac{\Delta^{\ddagger}H^{\ominus}}{R}\frac{1}{T} + \frac{\Delta^{\ddagger}S^{\ominus}}{R} \tag{3.2}$$

The isobaric activation parameters were calculated using rate constants obtained between 6°C and 60°C, and a linear dependence between $\ln(k_w/T)$ and $1/T$ is found (Figure 3.1A; k_w is the bimolecular aqueous rate constant for the reaction with hydroxide ions). No corrections were necessary to compensate for the presence of H^+ ions or a shift in the auto-ionisation equilibrium as a result of the change in temperature.[15] Usually k_w is used for the reaction with water, and not with hydroxide ions. However, the rate constant with water is very small ($<10^{-8}$ s^{-1}),[2] and we prefer to assign k_w to the rate constant with hydroxide ions in the aqueous phase of a vesicular solution, since we compare the base-catalysed reaction proceeding in the aqueous and vesicular pseudophases (Section 3.3.2) rather than between the reaction with water and hydroxide ions.

From the slope and intercept in Figure 3.1A we calculated $\Delta^{\ddagger}H^{\ominus}$ and $T\Delta^{\ddagger}S^{\ominus}$ to be 69 ± 1 kJ mol^{-1} and 2.4 ± 0.4 kJ mol^{-1}at 288 K, respectively. Since calculation of $T\Delta^{\ddagger}S^{\ominus}$ requires extrapolation to the intercept with the y-axis, alternatively, $T\Delta^{\ddagger}S^{\ominus}$ can be calculated more accurately from a given k_w at a certain temperature. At 15°C $T\Delta^{\ddagger}S^{\ominus}$ is then calculated to be 2.2 ± 0.1 kJ mol^{-1}. These values are different from those reported in the literature for this reaction ($\Delta^{\ddagger}H^{\ominus}$=48 kJ mol^{-1}; $T\Delta^{\ddagger}S^{\ominus}$=-5.4 kJ mol^{-1}).[2] Unfortunately, no experimental details were given, besides that the experiments were performed in the presence of 100 mM KCl. Interpretation of activation parameters is difficult since they depend on many factors that are not easily separated. In general, bimolecular reactions in water involving an organic substrate and a small (hydrated) ion have a large enthalpic contribution (typically $\Delta^{\ddagger}H^{\ominus}$=50-110 kJ mol^{-1}) and a smaller entropic contribution (typically $T\Delta^{\ddagger}S^{\ominus}$ *ca.* -20 kJ mol^{-1}).[2,16-19] The negative entropy probably arises from the fact that entropy is lost upon bringing the two reagents together. This makes it surprising that we find $T\Delta^{\ddagger}S^{\ominus} > 0$. For the alkaline hydrolysis of Ellman's reagent (breaking of a disulfide bond) also a positive entropic contribution was found ($T\Delta^{\ddagger}S^{\ominus}$=14 kJ mol^{-1}), whereas the enthalpic contribution is similar as described before ($\Delta^{\ddagger}H^{\ominus}$=46 kJ mol^{-1}).[10]

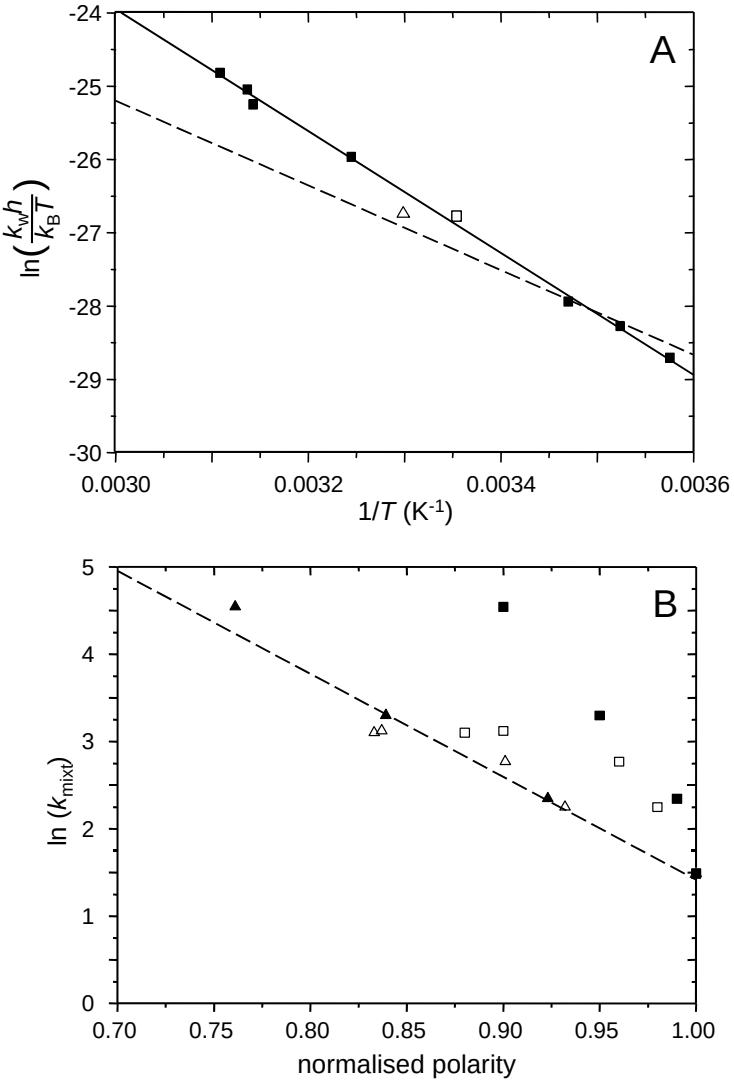

Figure 3.1. *A: Eyring plot for the reaction of 5-nitrobenzisoxazole with hydroxide ions in water (■). Literature: Pérez-Juste[5] (□); Kemp[2] (△; dashed line). The solid line is a linear fit to the experimental data. B: Plot of the natural logarithm of the observed rate constant versus the normalised polarity as measured by the E_T(30) (■) and Nile Red dye (▲) in mixtures of water-1,4-dioxane (closed symbols) and water-acetonitrile (open symbols).*

To further characterise the Kemp elimination reaction the rate constants were measured in aqueous mixtures of acetonitrile and 1,4-dioxane. These values were plotted against the normalised polarity (eq. (2.13)) as measured by Nile Red and the E_T(30) dye. Despite the similar response to medium changes in solvent (mixtures) more polar than dichloromethane by Nile Red and the E_T(30) dye (Figure 2.31A), only Nile Red fluorescence is linearly related to the natural logarithm of the observed rate constant in the two sets of solvent mixtures. This result indicates that the Kemp elimination reaction and Nile Red fluorescence are sensitive to similar medium changes.

In order to obtain a better understanding of the origin of the changes in the rate constants, the Gibbs energies of transfer from water to the system under study of the reagents and the

activated complex have to be considered. Studies on the Gibbs energy of transfer of a hydroxide ion from water into mixtures of water and an organic solvent ($\Delta_{tr}G(OH^-)$) have been scarce.[20] However, since fluoride and hydroxide are isoelectronic and similar in size (ionic radius) it seems reasonable to use the data of the fluoride ion as an indication of the trend in $\Delta_{tr}G(OH^-)$ to aqueous mixtures. And in fact, there is reasonable agreement between $\Delta_{tr}G(OH^-)$ and $\Delta_{tr}G(F^-)$.[21] However, the $\Delta_{tr}H(F^-)$ and $\Delta_{tr}S(F^-)$ to mixtures of water and acetonitrile or methanol fluctuate strongly depending on the mole fraction of water. This indicates that many (compensating) factors play a role in this, at first sight, simple process. Despite these complications $\Delta_{tr}G(OH^-)$ and $\Delta_{tr}G(F^-)$ are always positive and increase with decreasing polarity. Transfer of **1** to solvent mixtures leads to a negative $\Delta_{tr}G(\mathbf{1})$, as is common for small neutral organic molecules.[22-25] As for small ions the transfer of the activated complex to solvent mixtures will have a positive $\Delta_{tr}G(\mathbf{1}\text{--}OH^-)$. However, as confirmed by our kinetic observations, we anticipate that $\Delta_{tr}G(\mathbf{1}\text{--}OH^-) < \Delta_{tr}G(\mathbf{1}) + \Delta_{tr}G(OH^-)$, since in the activated complex the negative charge is delocalised. Analogously to this, halide ions follow the trend $\Delta_{tr}G(F^-) > \Delta_{tr}G(Cl^-) > \Delta_{tr}G(Br^-) > \Delta_{tr}G(I^-)$.[21,26] In Scheme 3.2 a schematic overview of the changes in Gibbs energy is shown as we propose for the reaction going from water to a water/organic solvent mixture. Mixtures of water and organic solvents have their relevance for understanding micellar and vesicular catalysis. Despite the fact that the vesicular surface is far more complex in composition, which cannot be mimicked by these simple mixtures, still valuable information can be obtained from these mixtures.

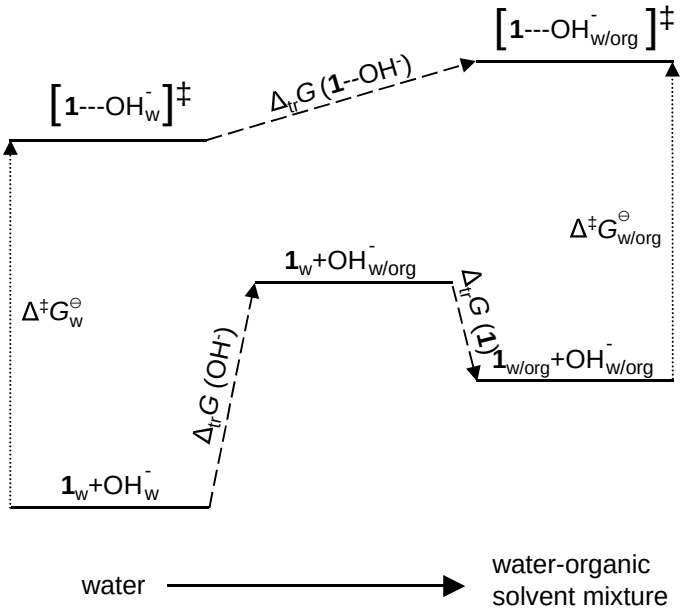

Scheme 3.2. *Schematic representation of the changes in activation Gibbs energy going from water to an aqueous binary mixture.*

Reactions of hydrophilic ions with an organic substrate in various water-organic solvent mixtures have been studied in some detail.[27-30] Most of them involve S_N2 reactions, and only few concern E2 elimination reactions. Especially literature data concerning reactions of hydroxide ions are scarce. Dehydration of the hydroxide ion is an important factor that can lead to large rate accelerations. At low organic solvent contents stabilisation of larger

organic substrates can be more important than dehydration of the anion leading to rate retardation.[29,30] The reaction of **1** with hydroxide ion in water-organic solvent mixtures does not exhibit such a trend, indicating that dehydration of the hydroxide ion has the largest influence.

3.3.2 Kinetic Analysis.

The Kemp elimination is efficiently catalysed by vesicles formed from dimethyldi-*n*-octadecylammonium chloride (**$C_{18}C_{18}$+**). At 15°C and in the presence of 2.25 mM of sodium hydroxide, the observed rate is increased by a factor of *ca.* 1000 relative to the observed rate constant in water. In a typical experiment upon increasing the total amphiphile concentration ($[amph]_{tot}$) there is initially a sharp increase of the observed rate constant (k_{obs}) to a maximum value, whereas k_{obs} then slowly decreases. This type of behaviour is characteristic for micellar and vesicular catalysis of bimolecular reactions.[31,32]
This rate profile can be analysed in terms of the pseudophase model with ion exchange developed by Menger[31] and Romsted (Scheme 3.3).[32] The principles of this model have been discussed in Chapter 1, but for clarity, before introducing the mathematical equations, the most important considerations will be briefly summarised. In this model there are two pseudophases; an aqueous pseudophase and a vesicular pseudophase. In the apolar vesicular pseudophase the rate constant is much higher than in the aqueous pseudophase. Since **1** prefers to be in the vesicular pseudophase, and the base prefers to bind to the cationic surface, the two reagents are efficiently brought together.

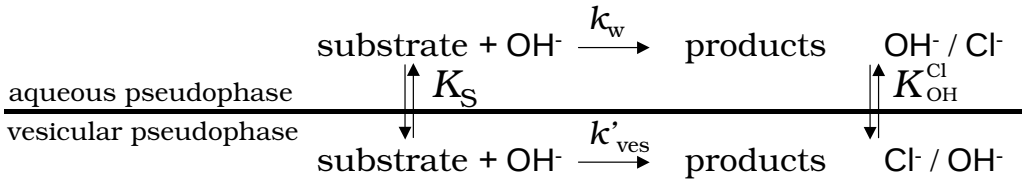

Scheme 3.3. *Schematic representation of the kinetic model used. K_S is the binding constant of the organic substrate to the vesicular pseudophase, k_w is the rate constant in water, k'_{ves} is the vesicular rate constant and K_{OH}^{Cl} represents the competition between OH^- and Cl^- to bind to the vesicular pseudophase.*

The observed rate of the reaction can be described by the sum of the rate in the aqueous and vesicular pseudophases:

$$k_{obs}[P]_{tot} = k_w[OH]_w[P]_w + k'_{ves}[OH]_{ves}[P]_{ves} \quad (3.3)$$

In this equation $[P]_{tot}$, $[P]_w$ and $[P]_{ves}$ are the total, aqueous and vesicular concentrations of **1**, respectively. The total probe concentration is equal to the sum of probe concentrations in the aqueous and vesicular phase. k_{obs} is the observed rate constant. k_w and k'_{ves} are the rate constants with hydroxide ions in the aqueous and the vesicular pseudophase, respectively. $[OH^-]_w$ and $[OH^-]_{ves}$ are the hydroxide concentrations in the aqueous and the vesicular phase. The total hydroxide concentration follows the mass balance via eq. (3.4):

$$[OH^-]_{tot} = [OH^-]_w + [OH^-]_{ves} \quad (3.4)$$

The binding constant K_S (eq. (3.5)) of **1** to the vesicles is expressed in terms of the total amphiphile concentration ($[amph]_{tot}$), *i.e.* the sum of the concentration of cationic and anionic amphiphiles.

$$K_S = \frac{[P]_{ves}}{[P]_w[amph]_{tot}} \tag{3.5}$$

Combining and rewriting eqs. (3.3), (3.4) and (3.5) with eqs. (3.6) and (3.7) gives eq. (3.8).[11]

$$k_{ves} = k'_{ves}[amph]_{tot} \tag{3.6}$$

$$m_{OH} = \frac{[OH^-]_{ves}}{[C_{18}C_{18}+]_{excess}} \tag{3.7}$$

$$k_{obs} = \frac{k_w[OH^-]_{tot} + (k_{ves}K_S - k_w)m_{OH}[C_{18}C_{18}+]_{excess}}{1+K_S[amph]_{tot}} \tag{3.8}$$

$[\mathbf{C_{18}C_{18}+}]_{excess}$ is the concentration of $\mathbf{C_{18}C_{18}+}$ that is present in the bilayer in excess to the amount of anionic amphiphile (Sections 3.3.5 and 3.3.6) and can be described by eq. (3.9).

$$[C_{18}C_{18}+]_{excess} = (1-2\alpha)[amph]_{tot} \tag{3.9}$$

In this eq. α is the ratio of anionic amphiphile to the total amphiphile concentration.

Since one cannot measure the vesicular hydroxide concentration (m_{OH}), it can be calculated considering the counterion binding to the excess of $\mathbf{C_{18}C_{18}+}$ (β_{excess}; eq. (3.10)), the ion exchange constant (K_{OH}^{Cl}; eq. (3.11)) and mass balance (eqs. (3.4) and (3.12)).

$$\beta_{excess} = \frac{[OH^-]_{ves}+[Cl^-]_{ves}}{[C_{18}C_{18}+]_{excess}} = \frac{[OH^-]_{ves}}{[C_{18}C_{18}+]_{excess}} + \frac{[Cl^-]_{ves}}{[C_{18}C_{18}+]_{excess}} = m_{OH} + m_{Cl} \tag{3.10}$$

$$K_{OH}^{Cl} = \frac{[Cl^-]_{ves}[OH^-]_w}{[Cl^-]_w[OH^-]_{ves}} \tag{3.11}$$

$$[Cl^-]_{tot} = [Cl^-]_w + [Cl^-]_{ves} \tag{3.12}$$

Combining the eqs. above leads to eq. (3.13).

$$m_{OH}^2 + m_{OH}\left[\frac{[OH^-]_{tot} + K_{OH}^{Cl}[Cl^-]_{tot}}{(K_{OH}^{Cl}-1)[C_{18}C_{18}+]_{excess}} + \beta_{excess}\right] - \left[\frac{\beta_{excess}[OH^-]_{tot}}{(K_{OH}^{Cl}-1)[C_{18}C_{18}+]_{excess}}\right] = 0 \tag{3.13}$$

The *total* counterion binding (β_{tot}) includes the binding of $\mathbf{C_{10}C_{10}-}$ to the total amount of cationic amphiphiles and is given by eq. (3.14):

$$\beta_{tot} = \frac{[OH^-]_{ves}+[Cl^-]_{ves}+\alpha[amph]_{tot}}{[C_{18}C_{18}+]_{tot}} = \frac{\alpha + \beta_{excess}(1-2\alpha)}{1-\alpha} \tag{3.14}$$

An important assumption is that the counterion binding remains constant over the total amphiphile concentration range. This approximation has been validated for micelles,[33] and we assume this is also valid for vesicular solutions.

3.3.3 Parameter Compensation

In eqs. (3.8) and (3.13) there are four parameters that are, in principle, unknown (k_{ves}, K_S, K_{OH}^{Cl} and β_{excess}). However, in the literature one can usually find reasonable values for these parameters for systems that only contain a few well-studied components (*e.g.* water and amphiphiles). In the case of a more complex mixture the data analysis becomes more difficult. If one compares two of these kinetic curves to each other it is usually possible to fit

both curves reasonably well by adjusting just *randomly one* of the four parameters. This means that although the parameters have different physical meaning they compensate each other to a large extent.[34-39]

It can be directly seen in eq. (3.8) that for small values of K_S the bottom part of the equation does not change too much. Under those circumstances, and if k_w is also very small, K_S and k_{ves} can perfectly compensate each other. An example is shown in Figure 3.2A. As long as K_S is smaller than 25 M^{-1}, the lower part of eq. (3.8) stays around 0.9 and the product of K_S and k_{ves} scales linearly with the observed rate constant. Deviation from linearity is only observed when K_S is larger than 30 M^{-1}.

In order to use a more general method to examine parameter compensation and, as a result, to get a better insight into the meaning of all the fitted values of the parameters, we calculated the error in these parameters by calculating χ^2.[40]

$$\chi^2 = \sum_{i=1}^{i=n} \frac{(k^i_{calc} - k^i_{obs})^2}{(\sigma^i_{k_{obs}})^2} \qquad (3.15)$$

In this equation n is the number of data points, k^i_{calc} the calculated rate constant for the n^{th} data point and σ^i_{kobs} is the estimated experimental error for that data point. χ^2 is the sum of the squared difference between the experimental and calculated value relative to the experimental error of all experimental data points. If the difference between an experimental and calculated data point is larger than the experimental error its contribution to χ^2 is larger than 1, whereas it is smaller than 1 if the difference is smaller than the experimental error. Since the square of the difference is taken χ^2 increases quickly in magnitude when data point fall outside the experimental error. If now one parameter in eqs. (3.8) or (3.13) is systematically slightly varied, and χ^2 is minimised by allowing a second parameter to vary, one obtains a new value for χ^2. If for a certain variation in the systematically varied parameter, the new value of χ^2 is exactly equal to the original value than the parameter that was allowed to vary can perfectly compensate the parameter that was systematically varied. In case that the new value of χ^2 is just slightly higher, then the second parameter can just partially compensate the first parameter. In an ideal case the new value of χ^2 is much larger than the original value and then parameter compensation is (nearly) absent.

By systematically changing one parameter, the parabola as shown in Figure 3.2B is obtained and hence the error as a function of another parameter can be calculated by calculating the width of the parabola at a value of χ^2+1. In this way the error in a parameter can be calculated as a function of any other parameter in the equations. The χ^2 values do not necessarily form a parabola, but usually this is quite a reasonable approximation.

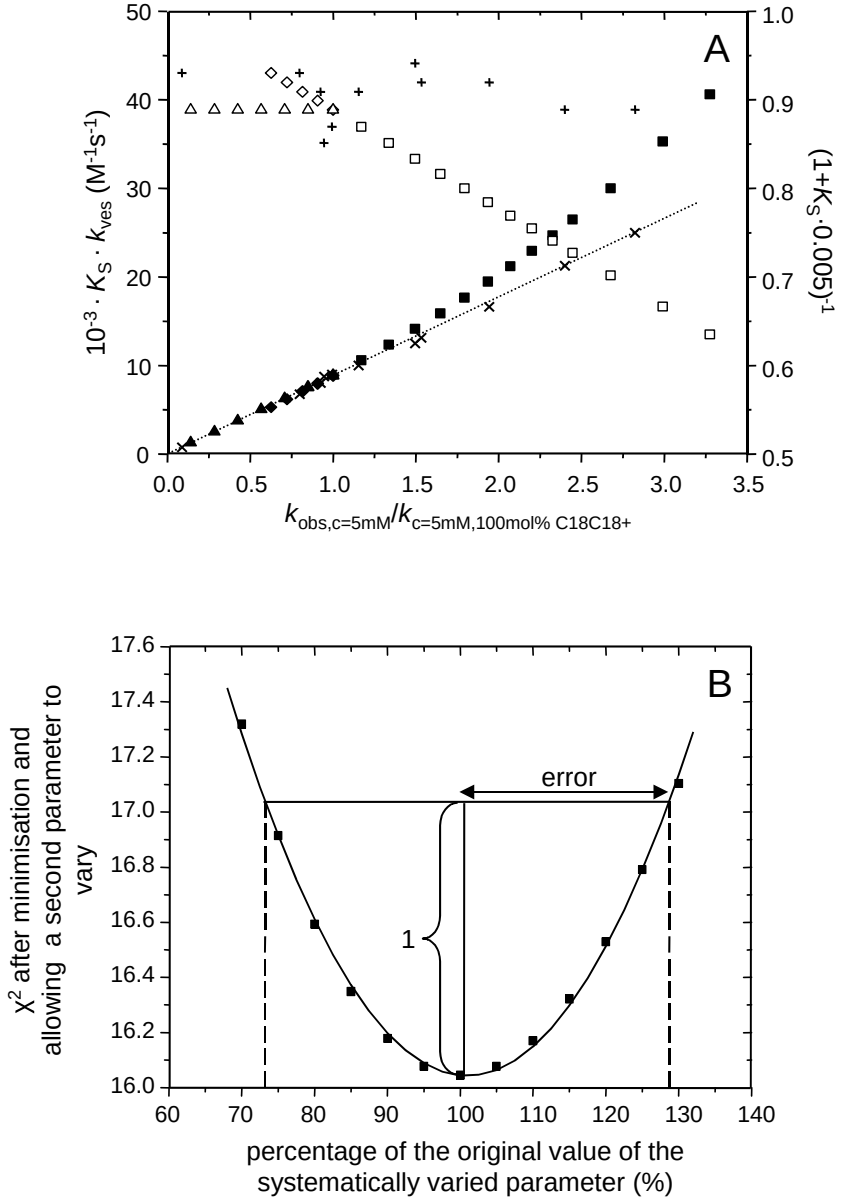

Figure 3.2. *A: Example of compensation of K_S and k_{ves}. Plot of $K_S \cdot k_{ves}$ (left axis, closed symbols) and $1/(1+K_S[amph]_{tot})$ (right axis, open symbols) versus the relative observed rate constant at 5 mM amphiphile concentration. K_S varied from 12.5 to 25 M^{-1} and k_{ves} = 350 s^{-1} (◆,◇); K_S = 25 M^{-1} and k_{ves} varied from 50 to 350 s^{-1} (▲,△); random variation with K_S varied between 12.5 to 25 M^{-1} and k_{ves} varied between 50 and 1000 s^{-1} (×,+); K_S varied from 30 to 125 M^{-1} and k_{ves} = 350 s^{-1} (■,□). The dotted line is a linear fit through the data points where K_S < 25 M^{-1}. Please note that for the solid symbols (left axis) deviation from the dotted straight line is only observed when the open symbols (right axis) deviate significantly from a value of 0.9, which is the situation for which k_{ves} and K_S do not compensate each other. B: Example of calculating the error of a parameter as a function of another parameter (100 mol% of* ***$C_{18}C_{18}$+****).*

As can be seen in Table 3.1 the interdependence of the different parameters is in certain cases quite large, which has been observed before.[34,36-39] This means that for this set of equations, parameter compensation is quite large. For example, an increase in k_{ves} can be quite well compensated by a decrease in counterion binding, since the error in this case is 34%. Likewise a change in K_S or β_{excess}, respectively, can be compensated by changes in k_{ves} (34% and 28%). In this analysis the absolute error depends on the experimental error. If the experimental error is twice as small, the absolute errors will be twice as well, but the dependence of the parameters on each other is *not* affected. In our example of the addition of 100 mol% of **$C_{18}C_{18}$+** we estimated the experimental error to be 1 s^{-1} for all data points. Most data points are within 1 s^{-1} from the fitted curve justifying our choice of 1 s^{-1}.

Table 3.1. *Errors in the parameters as a function of the other parameters for 100 mol% of* ***$C_{18}C_{18}$+****.*

	value	error$_{kves}$	error$_{KS}$	error$_{\beta}$	error$_{KS+kves}$ [a)]
k_{ves}	350	--	118 (34%)	118 (34%)	--
K_S	25.0	8.6 (34%)	--	4.7 (19%)	--
β_{excess}	0.890	0.25 (28%)	0.12 (13%)	--	1.98 ± 2.47

[a)] *See text.*

The plots of χ^2 versus the percentage of varied parameter did not all give a nice parabola. The increase in χ^2 with decreasing k_{ves} was larger than the increase in χ^2 with increasing k_{ves}. This means that K_S and β_{excess} compensate k_{ves} to a larger extent at larger values of k_{ves} than at smaller values.

Since we took a reasonable value for β_{excess} from the literature, rather than a fitted value, another problem arises from this arbitrary choice. The reason for taking a literature value for this parameter was that when all three parameters (β_{excess}, K_S and k_{ves}) were allowed to vary this yields unrealistic values of $\beta_{excess} > 1$. This can be seen in Table 3.1, where the minimum of χ^2 is found at a value of β_{excess}=1.98, when both K_S and k_{ves} were allowed to vary. In addition, parameter compensation is larger as can be seen from the large error (125%).

If one minimises χ^2 with an arbitrary chosen value of β_{excess} the obtained value of χ^2 is not a global minimum. If one then systematically varies one parameter and then wants to calculate the error as a function of the other two parameters the minimum of the parabola is not at 100%, but at a different percentage.

3.3.4 Ion Exchange Constant

The ion exchange constant K_{OH}^{Cl} can be calculated by measuring the observed rate constant at various chloride concentrations. The chloride ions will expel the hydroxide ions from the Stern region determined solely by the relative strength of both ions to bind to the vesicles.
Ruan *et al.*[41] derived that when the conditions in eqs. (3.16) and (3.17) are met, m_{OH} (eq. (3.18)) can be calculated with these assumptions via simplification of eq. (3.13).

$$\frac{[OH^-]_{tot}+K_{OH}^{Cl}[Cl^-]_{tot}}{(K_{OH}^{Cl}-1)[C_{18}C_{18}+]_{excess}} \gg \beta_{excess} \tag{3.16}$$

$$\left(\frac{[OH^-]_{tot}+K_{OH}^{Cl}[Cl^-]_{tot}}{(K_{OH}^{Cl}-1)[C_{18}C_{18}+]_{excess}}\right)^2 \gg \frac{4\beta_{excess}[OH^-]_{tot}}{(K_{OH}^{Cl}-1)[C_{18}C_{18}+]_{excess}} \tag{3.17}$$

$$m_{OH} = \frac{\beta_{excess}[OH^-]_{tot}}{[OH^-]_{tot} + K_{OH}^{Cl}[Cl^-]_{tot}} \tag{3.18}$$

Substituting eq. (3.18) into eq. (3.8) and considering that the contribution of the observed vesicular rate constant is much higher than the observed aqueous rate constant,[42] eq. (3.8) can be rewritten as eq. (3.19).

$$\frac{1}{k_{obs}} = \frac{1 + K_S[C_{18}C_{18}+]_{excess}}{k_{ves}K_S[C_{18}C_{18}+]_{excess}\beta_{excess}} + \frac{(1 + K_S[C_{18}C_{18}+]_{excess})K_{OH}^{Cl}}{k_{ves}K_S[C_{18}C_{18}+]_{excess}\beta_{excess}[OH^-]_{tot}}[Cl^-]_{tot} \tag{3.19}$$

The ion exchange constant can now be calculated by taking the ratio of the slope to the intercept in a plot of $1/k_{obs}$ versus $[Cl^-]_{tot}$ and multiplication of that ratio with $[OH^-]_{tot}$. (eq. (3.20)).

$$K_{OH}^{Cl} = \frac{\text{slope}}{\text{intercept}} \times [OH^-]_{tot} \tag{3.20}$$

Since obeying to the conditions (eqs. (3.16) and (3.17)) requires the knowledge of the ion exchange constant, it should be checked afterwards, whether the conditions are still met. For K_{OH}^{Cl} equals 1.6, the conditions are met if $[C_{18}C_{18}+]_{excess}$ < 0.23 mM and $[Cl^-]_{tot}$ > 2.5 mM, or if $[C_{18}C_{18}+]_{excess}$ < 0.5 mM and $[Cl^-]_{tot}$ > 4.5 mM (maximum of 3% deviation in m_{OH}). These conditions were applied in our experiments.
As can be seen in Figure 3.3A, the main problem with these fits is the small value of the intercept compared to the slope and scattering. This problem originates from several considerations: (1) vesicles are thermodynamically metastable and several different structures close in Gibbs energy coexist. Therefore depending on time and the exact preparation method there can be slightly different vesicles, leading to slightly different vesicular rate constants; (2) at lower temperatures, at which most of the experiments have been performed, reproducibility becomes more troublesome (compare the kinetic curve for 100 mol% of **$C_{18}C_{18}$+** at 15°C and 25°C, Figure 3.4A and Figure 3.9A, respectively; (3) the conditions require that we use a low amphiphile concentration. In this region small changes in amphiphile concentration lead to a relatively large change in the observed rate constant; (4) the conditions also require a high salt concentration. This means that the line has to be extrapolated to zero salt concentration; (5) we used 2.25 mM NaOH. The use of more NaOH would in principle lead to a smaller value of the slope, while the intercept does not change. However, large hydroxide concentrations might induce changes in the vesicular shape.[43]

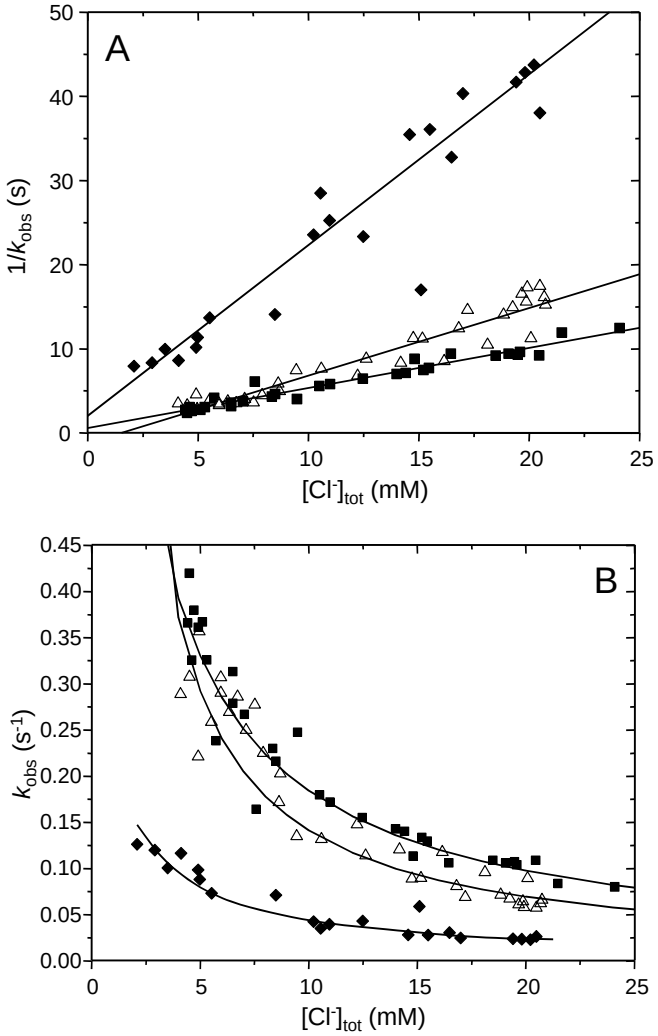

Figure 3.3. *Linear (A) and non-linear (B) plots used to calculate K_{OH}^{Cl}. The percentage denotes the percentage of* **$C_{10}C_{10}^-$** *as a function of the total amphiphile concentration. (■) 0 mol%; (△) 20 mol%; (♦) 35 mol%. Lines are fits to the data.*

In order to get more reliable values out of the fit, the same data has been plotted, but instead of fitting to a linear equation the data has been fitted to the inverse of a linear equation (y=1/(a+bx)). In this way the scattering in the data points at high chloride concentrations is of less importance. The results are shown in Table 3.2.

Table 3.2. *Values of K_{OH}^{Cl} obtained from linear and non-linear fits.*

Solution	slope	intercept	K_{OH}^{Cl} [a]	slope	intercept	K_{OH}^{Cl} [b]
100% **$C_{18}C_{18}^+$**	477±19	0.58±0.06	1.8 ± 0.2	480±21	0.62±0.17	1.7 ±0.5
20% **$C_{10}C_{10}^-$** [c]	803±43	-1.2±0.4	-1.5 ± 0.4	731±23	-0.23±0.18	-7.0 ±5.4
35% **$C_{10}C_{10}^-$**	2029±105	2.0±1.8	2.3 ± 2.1	1986±79	2.7±0.5	1.7 ± 0.3
CTAB[d]	(6.0±0.1) $\times10^{-3}$	(2.2±0.0) $\times10^{-5}$	12.8 ± 0.2	(5.9±0.1) $\times10^{-3}$	(2.2±0.2) $\times10^{-5}$	12.5 ± 2.4

[a] From a linear fit. [b] From a non-linear fit. [c] Large scattering in experimental data (Figure 3.3). [d] Experimental data for K_{OH}^{Br} in CTAB micelles from Ruan *et al.*[41]

From the values of K_{OH}^{Cl} and the corresponding error (ΔK_{OH}^{Cl}) for 100 mol% of **$C_{18}C_{18}$+** and 35 mol% of **$C_{10}C_{10}$-** of both the linear and non-linear fits, the weight-averaged value for K_{OH}^{Cl} at 15°C was calculated using eq. (3.21). The error was calculated as the square root of the sum of the squared errors.

$$\overline{K}_{OH}^{Cl} = \frac{\sum_{i=1}^{i=n} \frac{K_{OH,i}^{Cl}}{\Delta K_{OH,i}^{Cl}}}{\sum_{i=1}^{i=n} \frac{1}{\Delta K_{OH,i}^{Cl}}} \qquad (3.21)$$

The value for K_{OH}^{Cl} is 1.8 ± 2.2. This value is on the lower limit of values found in the literature at 25°C (1.2-11).[11,34,44-49] However, for all but two studies[11,48] these values have been measured for non-vesicular systems. It is not too surprising that the value of K_{OH}^{Cl} is independent of bilayer composition since this has also been observed for mixed micelles of CTAB and pentanol.[50]

We used K_{OH}^{Cl} = 1.6 in all our fits of vesicular catalysis, since this is the average of all the experiments we performed in this thesis (Chapter 4, 5 and 6) and this value has been obtained for vesicles of **$C_{18}C_{18}$+** in the literature.[11] The change from 1.8 to 1.6 only has a minor effect on the fitted parameters. For example for 100% **$C_{18}C_{18}$+**, k_{ves} and K_S change from 295 s^{-1} to 300 s^{-1} and from 31.8 M^{-1} to 32.6 M^{-1}, respectively.

3.3.5 Sodium Di-*n*-Decylphosphate

Figure 3.4 shows the plots of the observed rate constant versus the total amphiphile concentration. The scattering in the experimental data is large compared to the scattering observed for micellar solutions, but this is quite common for vesicular media,[49,51-53] especially at lower temperatures. As can be seen clearly, the maximum observed rate constant decreases with increasing **$C_{10}C_{10}$-** content. Remarkably, the observed rate constant for the solution containing 50 mol% of **$C_{10}C_{10}$-** still shows an *increase* with increasing amphiphile concentration. This indicates that there must be positively charged domains, since otherwise inhibition should occur. These domains cannot be too large since otherwise in the DSC scans there should be two peaks (Chapter 2).

In principle the increase in observed rate constant for 50 mol% of **$C_{10}C_{10}$-** could be a salt effect on the reaction proceeding in the aqueous pseudophase since we use the sodium salt of **$C_{10}C_{10}$-** and the chloride salt of **$C_{18}C_{18}$+**. However, the data in Figure 3.5 clearly shows that salt does not increase the observed rate constant for the Kemp elimination.

Considering that the increase in observed rate constant for 50 mol% of **$C_{10}C_{10}$-** is modest compared to that for 45 mol% of **$C_{10}C_{10}$-**, it appears that the excess of **$C_{18}C_{18}$+** in the positively charged domains is only in the range of 1 to 2 mol% (considering the observed rate constants at 45 mol% of **$C_{10}C_{10}$-** relative to the observed aqueous rate constant).

Inhibition, as a consequence of the lack of binding of hydroxide ions to anionic vesicles, is observed for 70 mol% of **$C_{10}C_{10}$-** (Figure 3.4) for which eq. (3.8) simplifies to eq. (3.22). Consequently, knowledge of three of the four unknown parameters (k_{ves}, β_{excess} and K_{OH}^{Cl}) is not required, and the value of the remaining unknown parameter (K_S) can be obtained.

$$k_{obs} = \frac{k_w[OH^-]_{tot}}{1 + K_S[amph]_{tot}} \qquad (3.22)$$

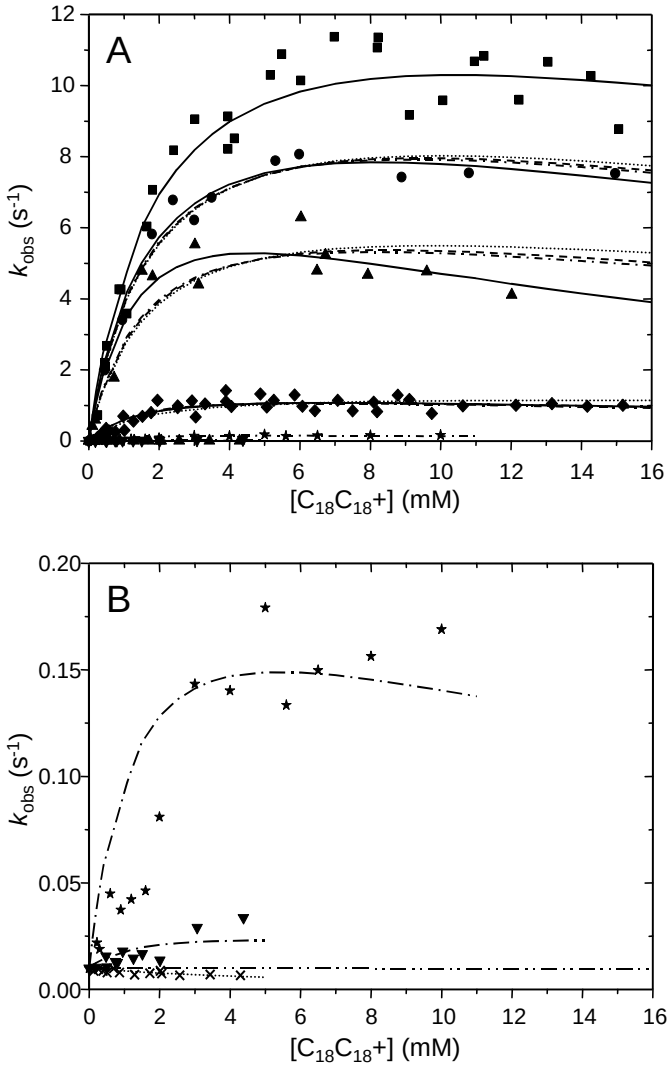

Figure 3.4. *A+B: Plots of observed rate constants versus the concentration of* $\mathbf{C_{18}C_{18}}$+ *for* $\mathbf{C_{18}C_{18}}$+ *vesicles with* $\mathbf{C_{10}C_{10}}$-*: 0 mol% (■); 10 mol% (●); 20 mol% (▲); 35 mol% (◆); 45 mol% (★); 50 mol% (▼); 70 mol% (×). Solid lines are fits allowing* k_{ves} *and* K_S *to vary; dotted lines are fits allowing* K_S *to vary; dashed lines are fits allowing* k_{ves} *to vary; dash-dotted lines are fits allowing* β_{excess} *to vary. The dot-dot-dashed line is the aqueous observed rate constant (B).*

Since the deprotonation reaction is general-base catalysed, the phosphate head group might catalyse the reaction as well. However, this is ruled out for two reasons: (1) we do not observe any catalysis by anionic vesicles; (2) the pK_a of water and dialkyl phosphate is 15 and 2 (rough estimate)[54], respectively. Given that the Brønsted β value for the kinetic probe in this study is 0.74[2] this leads a factor of at least $10^{9.6}$ in rate difference between the phosphate-catalysed reaction and the hydroxide-ion catalysed reaction. Thus the phosphate-catalysed reaction can be neglected.

The data for 45 mol% of $\mathbf{C_{10}C_{10}}$- and 50 mol% of $\mathbf{C_{10}C_{10}}$- were not fitted to eq. (3.8), since the experimental profiles only show the beginning of the rate profile, resulting in an unreliable fit. Performing the kinetic experiments at higher amphiphile concentration was not possible because of solubility problems.

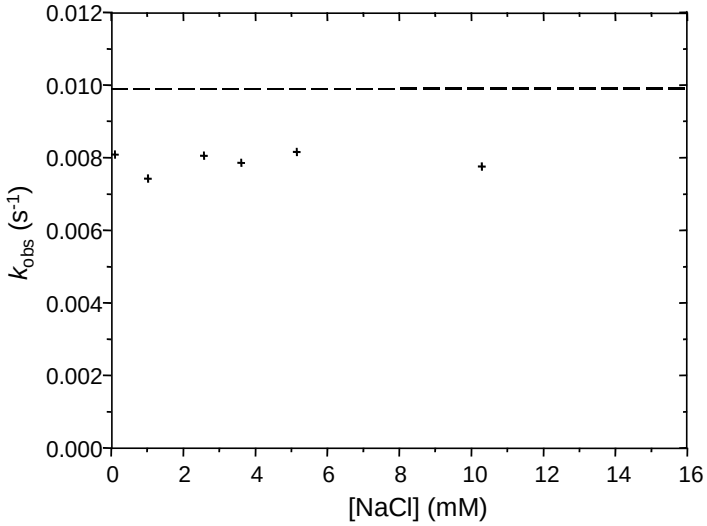

Figure 3.5. *Observed rate constant (+) as a function of [NaCl]. The dashed line is the observed rate constant in pure water.*

We fitted the data of 100 mol% of **$C_{18}C_{18}$+**, 10 mol% of **$C_{10}C_{10}$-**, 20 mol% of **$C_{10}C_{10}$-**, 35 mol% of **$C_{10}C_{10}$-** and 70 mol% of **$C_{10}C_{10}$-** using K_{OH}^{Cl} =1.6. The fits are shown in Figure 3.4. The values of the fitted parameter can be found in Figure 3.6. Figure 3.6A shows the parameters where the binding constant (K_S) and vesicular rate constant (k_{ves}) were allowed to vary. The excess counterion binding (β_{excess}) was kept constant at 0.89.[5] Figure 3.6B shows β_{excess} and β_{tot} as a function of the amount of **$C_{10}C_{10}$-**, whereas k_{ves} and K_S are kept constant.

For 100 mol% of **$C_{18}C_{18}$+** the fitted curve has a maximum rate constant of 10.3 s^{-1}. This means that the maximum *observed catalysis* ($k_{obs,max}/k_{w,obs}$) is about 1000. This is close to the number of 850 found at 25°C[5] and also close to a value of another base (hydroxide) and vesicle (**$C_{18}C_{18}$+**) catalysed reaction.[55] In order to calculate the catalysis from the second-order aqueous and vesicular rate constants, knowledge of the molar volume is required. Values reported in literature vary between 0.44 M^{-1} to 0.58 M^{-1}.[55,56] We took a value of 0.58 M^{-1} and using the pseudo-first-order vesicular rate constant (295 s^{-1}) from the fit the *catalytic rate acceleration* was calculated to be a factor of 50.

The alkaline hydrolyses of *N*-methyl-*N*-nitroso-*p*-toluenesulfonamide and *p*-nitrophenyl octanoate in vesicles of **$C_{18}C_{18}$+** were catalysed (3700-47000 and 59 times, respectively) with respect to the observed rate constant, but inhibition (10 and 5 fold, respectively) was found with respect to the catalytic rate acceleration.[11,48] The observed catalysis depends not only on the vesicular rate constant, but also on the binding efficiency of the two reagents. That means that the observed catalysis is large when the local concentration for both reagents is high. Increasing the aggregate concentration leads to more binding of reagents and this has a beneficial effect on the observed rate constant. However, upon increasing the aggregate concentration the effective reaction volume is also increased diluting the reagents and this lowers the observed rate constant. At the aggregate concentration where these two effects cancel each other, the plot of observed rate constant versus aggregate concentration exhibits a maximum. The height of the maximum is only partially determined by the vesicular rate constant. The catalytic rate acceleration, on the contrary, is solely determined

by the bimolecular rate constants, and therefore this parameter yields direct information on the relative reactivity of the reagents in the aqueous and vesicular pseudophase.
The rate increase for the reaction of **1** with hydroxide is probably a result from dehydration of the hydroxide ion, similar to what is observed in water-organic solvent mixtures (Section 3.3.1). In fact, several attempts have been made to simulate the Stern region by mixtures of water, organic solvents and high salt concentrations.[19,57-59] However, different mixtures mimicking the Stern Region were found, depending on the type of reaction employed.

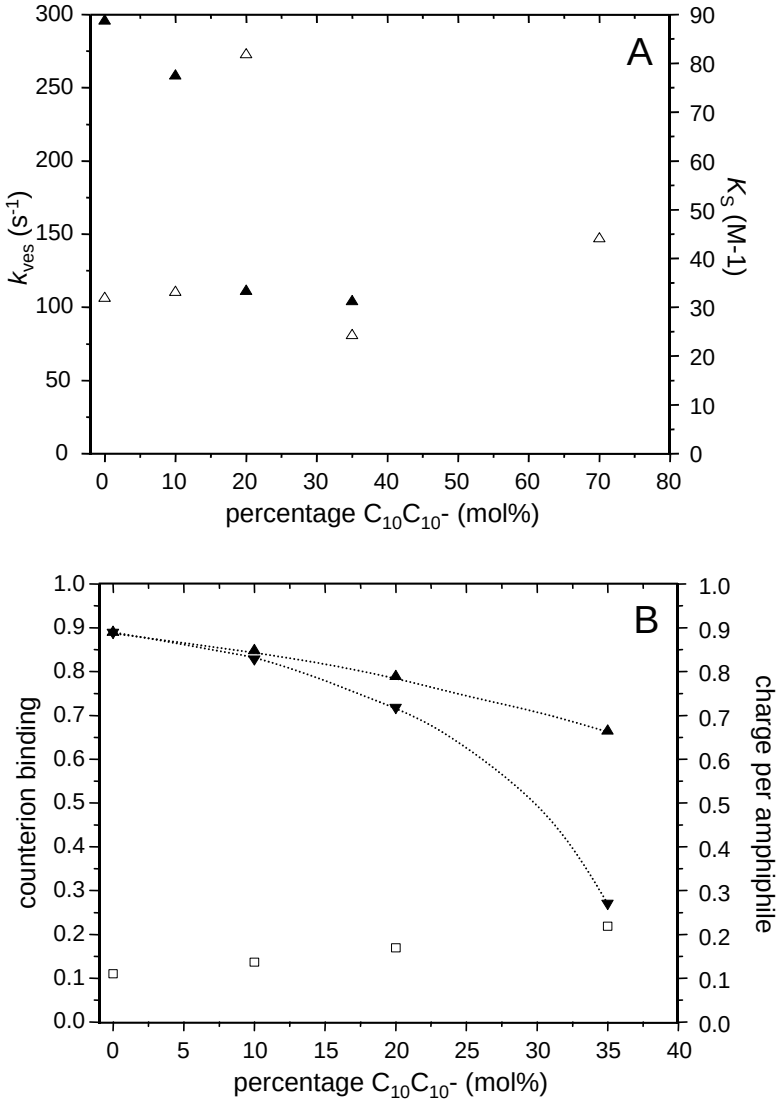

Figure 3.6. *A: Plot of k_{ves} (▲; left axis) and K_S (△; right axis) as a function of bilayer composition. B: Plot of the total counterion binding (▲), the excess counterion binding (▼) on the left axis and charge per total amphiphile concentration (□) on the right axis as a function of bilayer composition. Lines are drawn to guide the eye.*

In Figure 3.6A the fitted parameters are shown. The binding constant of the kinetic probe between up to 70 mol% of **$C_{10}C_{10}$-** stays roughly the same (considering the scattering in the data), while the vesicular rate constant decreases strongly.[60] This is remarkable since the vesicular rate constant depends mainly on the polarity of the vesicular reaction medium. As

was shown in Chapter 2 the polarity of the bilayer does not change significantly with increasing **$C_{10}C_{10}$-** content. In addition, parameter compensation has to be taken into account as well, as has been discussed before (Section 3.3.3). Therefore it is anticipated that the counterion binding changes rather than the vesicular rate constant. This is in agreement with the literature. Kinetic studies on S_N2 reactions where a bromide ion acts as a nucleophile show that in cationic micelles the micellar rate constant does not vary much upon the addition of butanol,[61,62] pentanol[50] or $C_{10}E_4$.[63] Instead, the decrease in *observed* rate constant is attributed to a decrease in counterion binding. This decrease in counterion binding is confirmed for mixed micelles of anionic surfactants and alcohols[64] and nonionic surfactants.[65] However, care has to be taken since certain nonionic surfactants increase the micellar rate constant via partial dehydration of the bromide ion.[66,67]

In Figure 3.6B the data was fitted again, but now keeping constant the vesicular rate constant and the binding constant (using the data from the fit of 100 mol% of **$C_{18}C_{18}$+**), thus allowing β_{excess} (eq. (3.10)) to vary. This can be rationalized by the fact that the counterion binding for aggregates with only one type of amphiphile (positive or negative) is high, because there is a high local charge density. When cationic and anionic amphiphiles are mixed in unequal amounts, the overall local charge density, and therefore the counterion binding, is lowered. Figure 3.6B shows the *excess* counterion binding as a function of the **$C_{10}C_{10}$-** content. The calculated *total* counterion binding (β_{tot}; eq. (3.14)) is shown as well. Surprisingly, this total counterion binding is only slightly affected by the addition of **$C_{10}C_{10}$-**. By contrast, the *excess* counterion binding is significantly decreased upon addition of **$C_{10}C_{10}$-** and we contend that the kinetic data shown in Figure 3.4 are primarily determined by this factor. The excess counterion binding for 35 mol% of **$C_{10}C_{10}$-** is quite low (0.27), but reasonable compared to that for mixed micelles of CTAB and nonionic amphiphiles[63,66,67] or butanol.[61]

The results are further rationalised by considering the surface charge density of the vesicles with different amounts of **$C_{10}C_{10}$-**. The surface charge density is related to the charge per total amphiphile concentration (e_{amph}; eq. (3.23)) since the surface charge arises from cationic amphiphiles that do not have a counterion or adjacent anionic amphiphile in their vicinity to compensate their charge.

$$e_{amph} = \frac{(1-\beta_{excess})(1\text{-}2\alpha)[amph]_{tot}}{[amph]_{tot}} = (1-\beta_{excess})(1\text{-}2\alpha) \qquad (3.23)$$

The calculated charge per total amphiphile concentration (Figure 3.6B) increases only slightly between 0 mol% and 35 mol% of **$C_{10}C_{10}$-**. This observation relates nicely to the slight decrease of the ζ potential (Chapter 2).

At this stage we note that the formation of microdomains at 10-30 mol% of **$C_{10}C_{10}$-** (as indicated by DSC, Chapter 2) will influence the composition-dependent observed rate constants shown in Figure 3.4. However, we refrain from a further analysis of this effect in the absence of more detailed information about the sizes of these domains.

3.3.6 Sodium *n*-Decyl-*n*-Octadecylphosphate

As discussed in Chapter 2 the phase transition temperatures in mixtures of $\mathbf{C_{10}C_{18}}$- and $\mathbf{C_{18}C_{18}}$+ show a different behaviour as compared to mixtures of $\mathbf{C_{10}C_{10}}$- and $\mathbf{C_{18}C_{18}}$+. The mole fractions at which there are two different phases is much smaller (between 5 and 20 mol%) for mixtures with $\mathbf{C_{10}C_{18}}$- and approaching 50 mol% of $\mathbf{C_{10}C_{18}}$- the packing of the amphiphile mixture is more efficient as indicated by the increase in the phase transition temperature. Below 40 mol% of $\mathbf{C_{10}C_{18}}$- there is also a pretransition around 13°C. Since the DSC scans, and hence also the structure of vesicles, are always sensitive towards the exact preparation procedure for the vesicles, it is not surprising to see that for 5 mol% of $\mathbf{C_{10}C_{18}}$- the scattering in the data is quite large (Figure 3.7A).

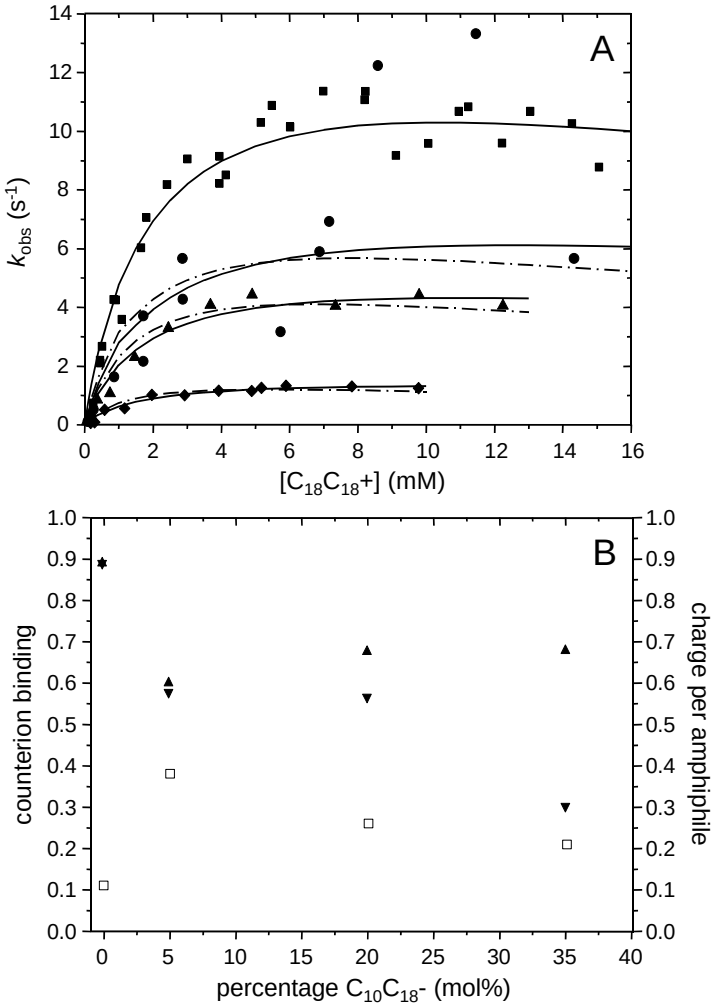

Figure 3.7. *A: Plot of observed rate constant versus* $\mathbf{C_{18}C_{18}}$+ *concentration for* $\mathbf{C_{18}C_{18}}$+ *vesicles with* $\mathbf{C_{10}C_{18}}$-*: 0 mol% (■); 5 mol% (●); 20 mol% (▲); 35 mol% (◆). Solid lines are fits allowing* k_{ves} *and* K_S *to vary and dash-dotted lines are fits allowing* β_{excess} *to vary. B: Plot of the total counterion binding (▲; left axis), the excess counterion binding (▼; left axis) and charge per total amphiphile concentration (□; right axis) as a function of bilayer composition.*

The data was fitted in the same way as for **$C_{10}C_{10}$-**. Considering the complexity of the phase transitions and the relatively small number of data points, the errors in the fits are relatively large. In the first method k_{ves} and K_S were allowed to vary, and in the second method β_{excess} was allowed to vary. Despite the different structure of **$C_{10}C_{18}$-** and the different phase behaviour, the second method leads to similar results as for **$C_{10}C_{10}$-**. For example at 35 mol% the excess counterion binding is 30% and 27% for **$C_{10}C_{18}$-** and **$C_{10}C_{10}$-**, respectively. As for **$C_{10}C_{10}$-** the charge per amphiphile is more or less constant at 0.2.

In Table 3.3 the fitted parameters using the first method (β_{excess} is fixed, K_S and k_{ves} are allowed to vary) are shown.[68] Unlike for **$C_{10}C_{10}$-**, where a decrease in k_{ves} was the major factor influencing the observed rate constant, for **$C_{10}C_{18}$-** K_S is the parameter that is changing most significantly. However, as for **$C_{10}C_{10}$-** we anticipate that the major factor influencing the observed rate constants is a decrease in the counterion binding and not a change in the binding constant or rate constant.

Table 3.3. *Fitted parameters for* ***$C_{10}C_{18}$-.***

Solution	k_{ves} (s^{-1})	K_S (M^{-1})
100 mol% **$C_{18}C_{18}$+**	295	32
5 mol% **$C_{10}C_{18}$-**	325	16
20 mol% **$C_{10}C_{18}$-**	335	15
35 mol% **$C_{10}C_{18}$-**	350	7

Since K_S is smaller than 25 the lower part of eq. (3.8) is close to 1, so that K_S and k_{ves} can compensate each other to a large extent (Section 3.3.3). Figure 3.8 suggests a linear dependence of k_{obs} (at a certain concentration) on the product $K_S \cdot k_{ves}$. Therefore a change in K_S can be compensated by a change in k_{ves}, and the other way around. We refrain from further interpretation of the results from the fit by the first method.

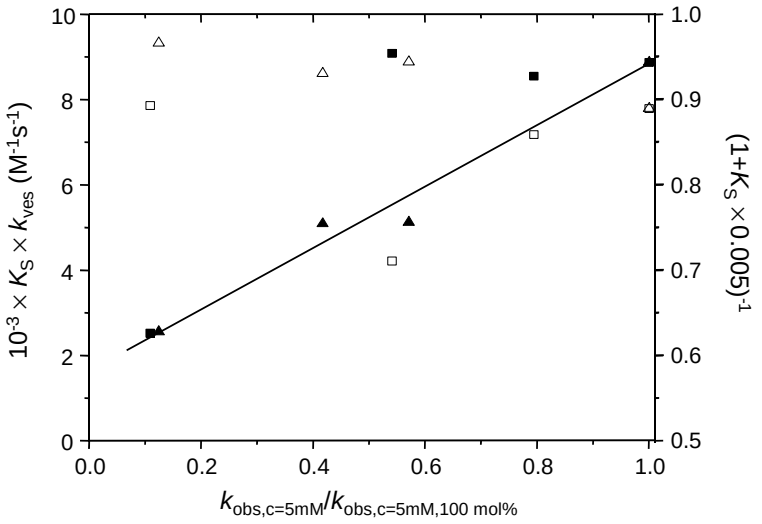

Figure 3.8. *Parameter compensation as shown by plotting $K_S \cdot k_{ves}$ (left axis; ■,▲) and $(1+K_S \cdot 0.005)^{-1}$ (right axis; □,△) versus $k_{obs,c=5mM}/k_{obs,\ c=5mM,100\ mol\%}$.* ***$C_{10}C_{10}$-*** *(▲);* ***$C_{10}C_{18}$-*** *(■). The line is drawn to guide the eye.*[69]

3.3.7 Sodium Dimethylphosphate

To study the influence of the anionic phosphate head group alone, cationic vesicles were studied by measuring the observed rate constants in the presence of $\mathbf{C_{01}C_{01}}$-. The pseudophase model with ion exchange takes into account two types of ions. Introduction of a third (inert) ion leads to mathematical problems. Therefore, instead of K_{OH}^{Cl}, we introduced an apparent ion exchange constant, $K_{OH}^{\Sigma X}$. ΣX stands for the sum of the inert ions present in solution that are in competition with the hydroxide ion to bind to the membrane. This apparent ion exchange constant is then an ion composition average strength of the inert ions to expel hydroxide from the Stern region.

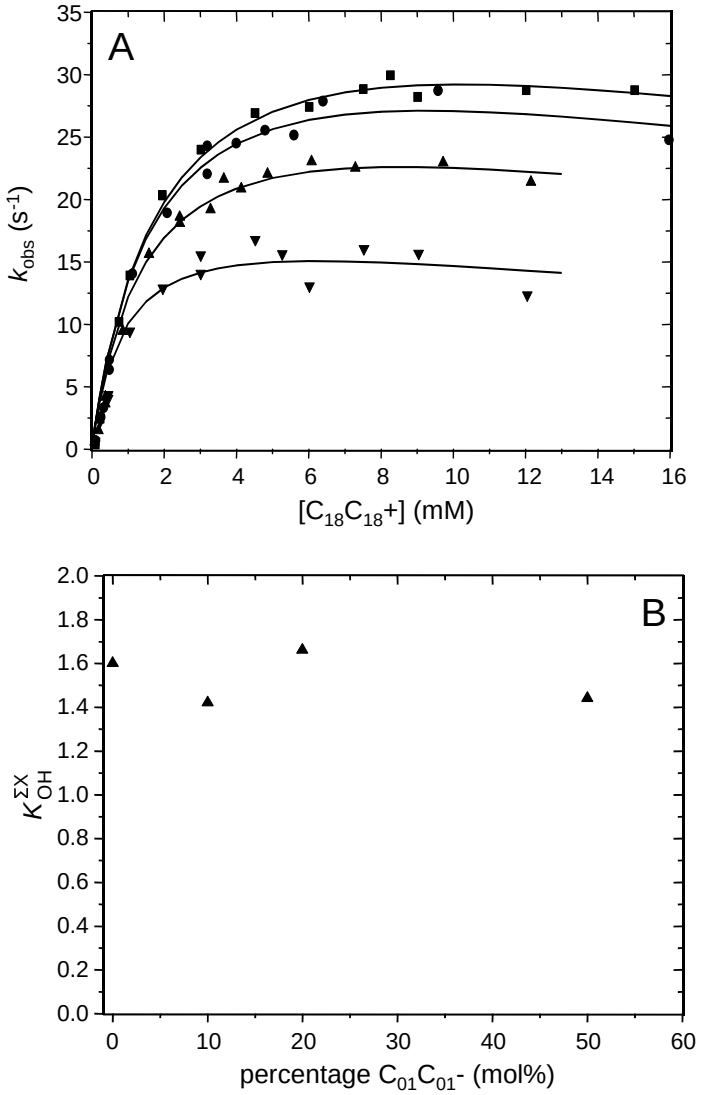

Figure 3.9. *A: Kinetic curves for vesicles with* $\mathbf{C_{01}C_{01}}$*-: 0% (■); 10% (●); 20% (▲); 50% (▼). Solid lines are fits allowing* $K_{OH}^{\Sigma X}$ *to vary. B: Fitted values of* $K_{OH}^{\Sigma X}$ *as a function of the amount of* $\mathbf{C_{01}C_{01}}$*- added.*

As can be seen in Figure 3.9A, the observed rate constants decrease upon the addition of **$C_{01}C_{01}$-**. The kinetic experiments were performed at 25°C. There are fewer data points for 100 mol% of **$C_{18}C_{18}$+** than in Figure 3.4A. However, the scattering in the data points is also less. In Chapter 2 it was shown that the presence of **$C_{01}C_{01}$-** does not change the phase transition temperature. The data was fitted by setting α (eq. (3.9)) to zero and by not accounting for **$C_{01}C_{01}$-** in the total amphiphile concentration. K_{OH}^{Cl} was replaced by $K_{OH}^{\Sigma X}$ and $[Cl^-]_{tot}$ by ($[Cl^-]_{tot}$ + $[\mathbf{C_{01}C_{01}}\text{-}]_{tot}$) in eq. (3.13). The value of $K_{OH}^{\Sigma X}$ does not change significantly up to the addition of 1 equivalent of **$C_{01}C_{01}$-**. This indicates that **$C_{01}C_{01}$-** is just as good as chloride in competing with hydroxide ions to bind to the Stern Region. From the observed rate constants it can be concluded that **$C_{01}C_{01}$-** is less efficient than **$C_{10}C_{10}$-** (data not shown) in reducing the maximum observed rate constant, especially at 50 mol%. This mainly results from both incomplete binding of **$C_{01}C_{01}$-** to the vesicular surface and the inability of **$C_{01}C_{01}$-** to decrease the local charge density by forming amphiphile pairs with **$C_{18}C_{18}$+**. **$C_{01}C_{01}$-** therefore truly acts as an inert counterion.

3.3.8 Summary of the Influence of Anionic Double-Tailed Amphiphiles

We have examined how the observed pseudo-first-order rate constant (k_{obs}, s^{-1}) for deprotonation of **1** in vesicles formed from **$C_{18}C_{18}$+** responds to a gradual addition of anionic bilayer-forming double-tailed amphiphiles, such as **$C_{10}C_{10}$-** and **$C_{10}C_{18}$-**. The combination of a cationic amphiphile with long tails and an anionic amphiphile with at least one short tail was chosen to avoid precipitation of the catanionic mixture.[70] The strength of the phosphate binding to the ammonium head group (as measured by the addition of **$C_{01}C_{01}$-**) is comparable to the binding of chloride ions. However, alkyl tails greatly improve the binding ability. As anticipated on the basis of the decreasing positive surface charge potential of the vesicles, the maximum observed rate constants decrease with increasing concentration of **$C_{10}C_{10}$-** or **$C_{10}C_{18}$-**. Although the main phase transition temperature changes differently for mixtures containing **$C_{10}C_{10}$-** or **$C_{10}C_{18}$-**, analysis of the kinetic data does not show significantly different behaviour. Assuming that k_{ves} and K_S do not change much upon the addition of anionic amphiphiles it is found that the charge per amphiphile increases with the same extent (approximately from 0.1 at 100 mol% of **$C_{18}C_{18}$+** to 0.2 at 35 mol% anionic amphiphile).

In principle, k_{ves} should not be kept constant upon addition of anionic amphiphile, but instead the bimolecular vesicular rate constant corrected for the (change in) molar volume should be kept constant. However, correcting for the molar volume is tedious,[19] since we have no information on the molar volumes of **$C_{10}C_{10}$-** and **$C_{10}C_{18}$-**, let alone in mixtures with **$C_{18}C_{18}$+**. In addition, it is more appropriate to take into account the reaction volume in which the reaction is taking place. Therefore, correcting for the reaction volume introduces similar uncertainties as we have if we do not correct for these changes. As a result, we prefer to refrain from such an analysis.

3.4 Conclusions

Vesicles prepared from **$C_{18}C_{18}^+$** efficiently catalyse the Kemp elimination. The observed catalysis amounts to a factor of *ca.* 1000 relative to the observed aqueous rate constant. The experimental data can be analysed using the pseudophase model with ion exchange, although care has to be taken with respect to parameter compensation. The fit to the data of 100 mol% of **$C_{18}C_{18}^+$** shows that the vesicular rate constant is approximately 50 times larger than the aqueous rate constant. Upon the introduction of increasing amounts of **$C_{10}C_{10}^-$** or **$C_{10}C_{18}^-$** into the bilayer, the observed catalysis (maximum observed rate constant) is decreased. Based on the observations in Chapter 2, it was concluded that the vesicular rate constant and the binding constant of the kinetic probe to the bilayer remain constant. The kinetic data are fitted using these observations. From these fits it is concluded that the counterion binding to the excess cationic amphiphiles is decreased as a result of a decrease in the local charge density. The catalytic efficiency upon adding **$C_{10}C_{10}^-$** or **$C_{10}C_{18}^-$** to the cationic vesicle primarily responds to this decrease of the excess counterion binding. At 50 mol% of **$C_{10}C_{10}^-$** small positively charged domains exist in the leaflets as is indicated by the fact that these vesicles still show catalysis. Inhibition is observed for negatively charged vesicles, as for example for vesicles containing 70 mol% of **$C_{10}C_{10}^-$**.

Addition of **$C_{01}C_{01}^-$** also leads to a decrease in the observed rate constant, however to a lesser extent than for **$C_{10}C_{10}^-$** or **$C_{10}C_{18}^-$**. The data was analysed assuming that the phosphate anion just acts as an inert anion only competing with hydroxide and chloride ions to bind to the cationic charges. The efficiency of binding of **$C_{01}C_{01}^-$** is comparable with that of the chloride ion as was concluded from the constant value of the apparent ion exchange constant K_{OH}^{X} upon increasing the relative amounts of **$C_{01}C_{01}^-$**.

In the present study we have made an attempt to identify the kinetic complexities which arise in the kinetic data when vesicles formed from a single bilayer-forming amphiphile are replaced by vesicles containing variable amounts of another bilayer forming amphiphile of opposite charge-type. This approach represents a first step towards examining bilayer compositions that are more akin to those found in biological membranes.

3.5 Acknowledgements

We thank Prof. L.S. Romsted (State University of New Jersey, New Jersey, USA) for fruitful discussions. Mr A. Wagenaar is thanked for the synthesis of **$C_{10}C_{10}^-$** and **$C_{10}C_{18}^-$**. Theo Rispens is thanked for fruitful discussions.

3.6 References

(1) Casey, M. L.; Kemp, D. S.; Paul, K. G.; Cox, D. D. *J.Org.Chem.* **1973**, *38*, 2294-2301.
(2) Kemp, D. S.; Casey, M. L. *J.Am.Chem.Soc.* **1973**, *95*, 6670-6680.
(3) Kemp, D. S.; Cox, D. D.; Paul, K. G. *J.Am.Chem.Soc.* **1975**, *97*, 7312-7318.
(4) Hollfelder, F.; Kirby, A. J.; Tawfik, D. S. *Nature* **1996**, *383*, 60-63.
(5) Pérez-Juste, J.; Hollfelder, F.; Kirby, A. J.; Engberts, J. B. F. N. *Org.Lett.* **2000**, *2*, 127-130.
(6) Tran, C. D.; Klahn, P. L.; Romero, A.; Fendler, J. H. *J.Am.Chem.Soc.* **1978**, *100*, 1622-1624.
(7) Nichols, J. W.; Deamer, D. W. *Proc.Natl.Acad.Sci.USA* **1980**, *77*, 2038-2042.
(8) Kaiser, S.; Hoffmann, H. *J.Colloid Interface Sci.* **1996**, *184*, 1-10.
(9) Kachel, K.; Asuncion-Punzalan, E.; London, E. *Biochim.Biophys.Acta* **1998**, *1374*, 63-76.
(10) Fendler, J. H.; Hinze, W. L. *J.Am.Chem.Soc.* **1981**, *103*, 5439-5447.
(11) Hervés, P.; Leis, J. R.; Mejuto, J. C.; Pérez-Juste, J. *Langmuir* **1997**, *13*, 6633-6637.
(12) Cuccovia, I. M.; Kawamuro, M. K.; Krutman, M. A. K.; Chaimovich, H. *J.Am.Chem.Soc.* **1989**, *111*, 365-366.
(13) Heerklotz, H.; Seelig, J. *Biochim.Biophys.Acta* **2000**, *1508*, 69-85.
(14) Maskill, H. *The Physical Basis of Organic Chemistry*; Oxford University Press: Oxford, **1990**.
(15) Weast, R. B. *Handbook of Chemistry and Physics*; CRC Press: Cleveland, **1977**.
(16) Saunders, W. H.; Williams, R. A. *J.Am.Chem.Soc.* **1957**, *79*, 3712-3716.
(17) Garcia-Rio, L.; Leis, J. R.; Peña, M. E.; Iglesias, E. *J.Phys.Chem.* **1992**, *96*, 7820-7823.
(18) de Souza, E. F.; Ionescu, L. G. *Colloids Surf.A* **1999**, *149*, 609-615.
(19) Tada, E. B.; Ouarti, N.; Silva, P. L.; Blagoeva, I. B.; El Seoud, O. A.; Ruasse, M. F. *Langmuir* **2003**, *19*, 10666-10672.
(20) Marcus, Y. *Pure Appl.Chem.* **1990**, *62*, 899-940.
(21) Hefter, G. T. *Pure Appl.Chem.* **1991**, *63*, 1749-1758.
(22) Goffredi, M.; Liszi, J.; Nemeth, B.; Liveri, V. T. *J.Sol.Chem.* **1983**, *12*, 221-231.
(23) Brisset, J. L. *J.Chem.Eng.Data* **1985**, *30*, 381-383.
(24) Wimley, W. C.; White, S. H. *Biochemistry* **1992**, *31*, 12813-12818.
(25) Kyte, J. *Biophys.Chem.* **2003**, *100*, 193-203.
(26) Hefter, G. T.; Mclay, P. J. *J.Sol.Chem.* **1988**, *17*, 535-546.
(27) Parker, A. J. *Chem.Rev.* **1969**, *69*, 1-32.
(28) Buncel, E.; Wilson, H. *Acc.Chem.Res.* **1979**, *12*, 42-48.
(29) Bunton, C. A.; Gillitt, N. D.; Kumar, A. *J.Phys.Org.Chem.* **1996**, *9*, 145-151.
(30) Bunton, C. A.; Gillitt, N. D.; Kumar, A. *J.Phys.Org.Chem.* **1997**, *10*, 221-228.
(31) Menger, F. M.; Portnoy, C. E. *J.Am.Chem.Soc.* **1967**, *89*, 4698-4703.
(32) Romsted, L. S. In *Micellization, Solubilization and Microemulsions*; Mittal, K. L., ed., Plenum Press: New York, **1977**; pp 509-530.
(33) Keiper, J.; Romsted, L. S.; Yao, J.; Soldi, V. *Colloids Surf.A* **2001**, *176*, 53-67.
(34) Al-Lohedan, H.; Bunton, C. A.; Romsted, L. S. *J.Phys.Chem.* **1981**, *85*, 2123-2129.
(35) Al-Lohedan, H.; Bunton, C. A. *J.Org.Chem.* **1982**, *47*, 1160-1166.
(36) Rodenas, E.; Vera, S. *J.Phys.Chem.* **1985**, *89*, 513-516.
(37) Bunton, C. A.; Cuenca, A. *Can.J.Chem.* **1986**, *64*, 1179-1183.
(38) Broxton, T. J.; Christie, J. R.; Sango, X. *J.Org.Chem.* **1987**, *52*, 4814-4817.
(39) Khan, M. N.; Ismail, E. *J.Chem.Soc., Perkin Trans.2* **2001**, *8*, 1346-1350.
(40) Kreyszig, E. *Advanced Engineering Mathematics*; John Wiley & Sons: New York, **1999**.
(41) Ruan, K.; Zhao, Z.; Ma, J. *Colloid Polym.Sci.* **2001**, *279*, 813-818.
(42) In the original paper it was stated that k_{ves} should be much larger than k_w, and not $k_{ves}[OH^-]_{ves} >> k_w[OH^-]_w$. In our system this is true as well, but this in principle not correct since the observed rate constant in the aqueous pseudophase should be smaller than the observed rate constant in the vesicular pseudophase and not the respective second-order rate constants.
(43) Clancy, S. F.; Steiger, P. H.; Tanner, D. A.; Thies, M.; Paradies, H. H. *J.Phys.Chem.* **1994**, *98*, 11143-11162.
(44) Plaisance, M.; Ter-Minassian-Saraga, L. *J.Colloid Interface Sci.* **1976**, *56*, 33-41.
(45) Chaimovich, H.; Bonilha, J. B. S.; Politi, M. J.; Quina, F. H. *J.Phys.Chem.* **1979**, *83*, 1851-1854.
(46) Bartet, D.; Gamboa, C.; Sepúlveda, L. *J.Phys.Chem.* **1980**, *84*, 272-275.
(47) Romsted, L. S. In *Surfactants in Solution*; Mittal, K. L., Lindman, B., eds., Plenum Press: New York, **1984**; pp 1017-1065.
(48) Kawamuro, M. K.; Chaimovich, H.; Abuin, E. B.; Lissi, E. A.; Cuccovia, I. M. *J.Phys.Chem.* **1991**, *95*, 1458-1463.
(49) Garcia-Rio, L.; Hervés, P.; Leis, J. R.; Mejuto, J. C.; Pérez-Juste, J. *J.Phys.Org.Chem.* **1998**, *11*, 584-588.

(50) Rodríguez, A.; Muñoz, M.; Graciani, M. D. M.; Moyá, M. L. *J.Colloid Interface Sci.* **2002**, *248*, 455-461.
(51) Moss, R. A.; Swarup, S. *J.Org.Chem.* **1988**, *53*, 5860-5866.
(52) Brinchi, L.; di Profio, P.; Germani, R.; Marte, L.; Savelli, G.; Bunton, C. A. *J.Colloid Interface Sci.* **2001**, *243*, 469-475.
(53) Khan, M. N.; Ismail, E.; Misran, O. *J.Mol.Liq.* **2002**, *95*, 75-86.
(54) Serjeant, E. P.; Dempsey, B. *Ionisation Constants of Organic Acids in Aqueous Solution*; Pergamon Press: Oxford, **1979**.
(55) Fendler, J. H.; Hinze, W. L. *J.Am.Chem.Soc.* **1981**, *103*, 5439-5447.
(56) Lim, Y.; Fendler, J. H. *J.Am.Chem.Soc.* **1979**, *101*, 4023-4029.
(57) Buurma, N. J.; Herranz, A. M.; Engberts, J. B. F. N. *J.Chem.Soc., Perkin Trans.2* **1999**, *5*, 113-119.
(58) Rispens, T.; Engberts, J. B. F. N. *J.Org.Chem.* **2003**, *68*, 8520-8528.
(59) Buurma, N. J.; Serena, P.; Blandamer, M. J.; Engberts, J. B. F. N. *J.Org.Chem.* **2004**, *69*, 3899-3906.
(60) The binding constant for 20 mol% of $\mathbf{C_{10}C_{10}^-}$ is very high. This is a result of few, and poorly reproducible, data points. Setting the binding constant to 30 M^{-1}, gives k_{ves}=233 s^{-1}, which fits nicely into the trend.
(61) Bertoncini, C. R. A.; Nome, F.; Cerichelli, G.; Bunton, C. A. *J.Phys.Chem.* **1990**, *94*, 5875-5878.
(62) Bertoncini, C. R. A.; Neves, M. D. S.; Nome, F.; Bunton, C. A. *Langmuir* **1993**, *9*, 1274-1279.
(63) Bunton, C. A.; Wright, S.; Holland, P. M.; Nome, F. *Langmuir* **1993**, *9*, 117-120.
(64) Bravo, C.; Leis, J. R.; Peña, M. E. *J.Phys.Chem.* **1992**, *96*, 1957-1961.
(65) Rathman, J. F.; Scamehorn, J. F. *J.Phys.Chem.* **1984**, *88*, 5807-5816.
(66) Blaskó, A.; Bunton, C. A.; Toledo, E. A.; Holland, P. M.; Nome, F. *J.Chem.Soc., Perkin Trans.2* **1995**, 2367-2373.
(67) Foroudian, H. J.; Bunton, C. A.; Holland, P. M.; Nome, F. *J.Chem.Soc., Perkin Trans.2* **1996**, 557-561.
(68) The data of 5 mol% of $\mathbf{C_{10}C_{18}^-}$ scatters too much. Therefore k_{ves} was set to 225 s^{-1} and K_S was allowed to vary.
(69) The deviation of the data point at an x-axis value of 0.6 (20 mol% $\mathbf{C_{10}C_{18}^-}$) originates from a set of relatively poor experimental data points leading to a large (most likely erroneous) value of K_S. This leads to a value of K_S·[amph]$_{tot}$ that is in the order of magnitude of 1 and hence the value of the right y-axis of that data point is relatively small. Consequently, parameter compensation of K_S and k_{ves}, observed in general in the system under study, does not occur here.
(70) Adding sodium di-*n*-octadecylphosphate or sodium dioleylphosphate to $\mathbf{C_{18}C_{18}^+}$ leads to precipitation.

CHAPTER 4

EFFECTS OF VARIOUS LONG-TAILED ALCOHOLS ON THE VESICLE-CATALYSED KEMP ELIMINATION REACTION

*Gradual addition of long-tailed linear alcohols, such as n-decanol (**$C_{10}OH$**), n-octadecanol (**$C_{18}OH$**) and batyl alcohol (**$C_{18}GOH$**) to vesicles formed from dimethyldi-n-octadecylammonium chloride leads to a decrease in the observed catalysis of the Kemp elimination. By contrast, gradual addition of oleyl alcohol (**$C_{18:1}OH$**) increases the catalytic efficiency. A detailed kinetic analysis, taking into account substrate binding site polarities, counterion binding percentages and binding affinity of the kinetic probe, suggests that the catalytic changes depend strongly on subtle changes in the structure of the additive. Besides a gradual decrease in the counterion binding, thereby keeping the surface charge density of the vesicular surface constant, changes in the vesicular rate constant and the binding constant should be taken into account. These latter two parameters change to a different extent for the different alcohols.*

The overall kinetic results suggest that in biological membranes variations in the structure of additives can lead to similar effects on the catalysis occurring in cell membranes.

4.1 Introduction

In Chapter 1 it has been discussed that the structural diversity of lipid molecules is very large and consists over a 1000 different structures.[1-3]

Long linear alcohols can be present in membranes as a result of degradation of lipids. Selective degradation plays an important role in signalling as second messenger or bioregulator. For example, in the brain phospholipase A_1, A_2, C and D generate, among other molecules, *sn*-1,2-diacylglycerol as second messenger.[4] Therefore in most cell membranes it is very likely that several different alcohols are present. In fact, 1-*O*-alkylglycerols are known to be taken up by cells from dietary sources like milk or shark liver oil[5] and used for phospholipids synthesis. Shark liver oil contains about 50% of 1-*O*-alkylglycerol. It is also claimed that they are beneficial in cancer treatment and are beneficial for several other medical applications.[5,6]

In Chapter 2 the effect of the addition of the second class of additives, long linear alcohols, to vesicles on the main phase transition temperature has been discussed. From studies on model (phospholipid) membranes with added alcohols it is known that addition of *n*-alcohols leads to a decrease in the main phase transition temperature for alcohols with short (< C_{10}) chains and an increase for alcohols with a long (> C_{10}) chain.[7-12] Also broadening of peaks or multiple peaks in DSC experiments have been observed.[8,9,11] In Chapter 2 it was shown that for cationic vesicles formed from dimethyldi-*n*-octadecylammonium chloride (**$C_{18}C_{18}$+**) in the presence of linear alcohols a similar type of

behaviour was observed. The only difference was that at low mole fraction, irrespective of the alcohol, a slight decrease in the main phase transition temperature was observed.
Compared to lipids, and common single-tailed surfactants, the long tails of alcohols are connected to a very small and relatively apolar "head group" which makes their packing parameter (eq. (1.1)) very different from ordinary surfactants. Therefore, it is stressed that their behaviour when incorporated into bilayer membranes, can be different compared to single-tailed surfactants.

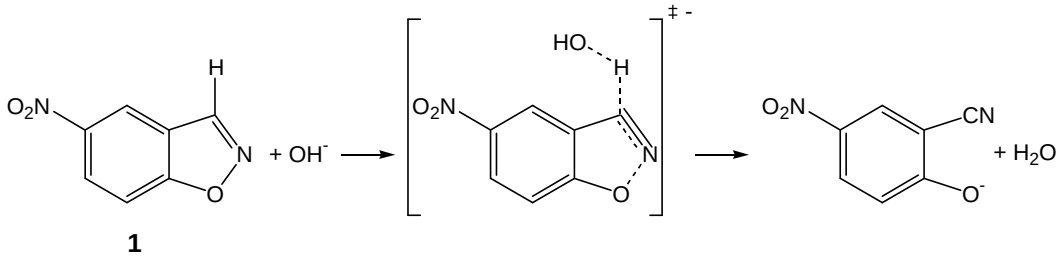

1

Scheme 4.1. *Kemp elimination reaction.*

Based on the above-mentioned properties of membrane-bound linear alcohols we decided to examine the influence of linear alcohols on the catalytic properties of cationic vesicles. As stressed in Chapter 1, the additives (Scheme 4.2) were selected not so much to mimic the overall properties of cell membranes, but rather in an attempt to identify the factors that play a role in determining the properties of cell membranes as reaction media. *n*-Decanol (**$C_{10}OH$**) and *n*-octadecanol (**$C_{18}OH$**) were selected since they have a considerable mismatch and match, respectively, with the chain length of the amphiphile. Oleyl alcohol (**$C_{18:1}OH$**) and batyl alcohol (**$C_{18}GOH$**) were chosen in order to study the influence of the unsaturation in the tail and of the presence of additional hydroxyl groups, respectively.
The bimolecular base-catalysed deprotonation reaction of 5-nitrobenzisoxazole (**1**; Scheme 4.1) has been studied in some detail (Chapter 1 and 3). The reaction is sensitive to the local reaction environment and the local hydroxide-ion concentration. In apolar environments the second-order rate constant is much higher than in polar environments. This makes it a good kinetic probe reaction to study the influence of the alcohols on the **$C_{18}C_{18}$+**-catalysed reaction.

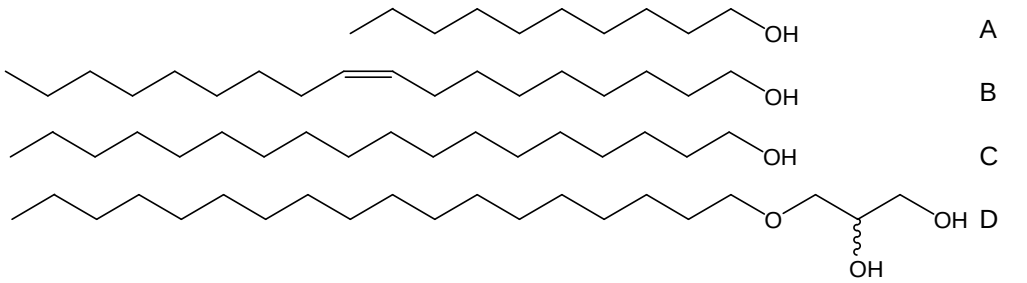

Scheme 4.2. *A. n-Decanol (**$C_{10}OH$**); B. Oleyl alcohol (**$C_{18:1}OH$**; cis:trans=75:25); C. n-Octadecanol (**$C_{18}OH$**); D. Batyl alcohol (**$C_{18}GOH$**).*

4.2 Experimental

Materials and the vesicle preparation have been described in Chapter 2, kinetic experiments in Chapter 3.

4.3 Results and Discussion

4.3.1 Kinetic Analysis

The observed rate constants were analysed using a slightly modified version of the pseudophase model with ion exchange developed by Menger[13] and Romsted[14] and which we used in Chapter 3. Since we have in this chapter no charge compensation we can rewrite the previously used eqs (3.8) and (3.13) to afford eqs (4.1) and (4.2).

$$k_{obs} = \frac{k_w[OH^-]_{tot} + (k_{ves}K_S - k_w)m_{OH}[C_{18}C_{18}+]}{1+K_S[amph]_{tot}} \tag{4.1}$$

$$m_{OH}^2 + m_{OH}\left[\frac{[OH^-]_{tot} + K_{OH}^{Cl}[Cl^-]_{tot}}{(K_{OH}^{Cl}-1)[C_{18}C_{18}+]} + \beta\right] - \left[\frac{\beta[OH^-]_{tot}}{(K_{OH}^{Cl}-1)[C_{18}C_{18}+]}\right] = 0 \tag{4.2}$$

In these equations k_{obs}, k_w and k_{ves} are the observed, aqueous and vesicular rate constant, respectively. K_S is the binding constant of the kinetic probe to the bilayer (amphiphile and additives). K_{OH}^{Cl} is the exchange constant for binding of hydroxide and chloride ions to the bilayer and β is the total counterion binding to the bilayers. $[OH^-]_{tot}$ is the total hydroxide-ion concentration and m_{OH} is the ratio of concentrations of bound hydroxide ions and cationic amphiphiles.

The ion exchange constant K_{OH}^{Cl} can be calculated under the assumptions mentioned in Chapter 3 via eq. (4.3):

$$\frac{1}{k_{obs}} = \frac{1 + K_S[C_{18}C_{18}+]_{tot}}{k_{ves}K_S[C_{18}C_{18}+]_{tot}\beta} + \frac{(1 + K_S[C_{18}C_{18}+]_{tot})K_{OH}^{Cl}}{k_{ves}K_S[C_{18}C_{18}+]_{tot}\beta[OH^-]_{tot}}[Cl^-]_{tot} \tag{4.3}$$

4.3.2 Kinetic Experiments and Fitted Parameters

4.3.2.1 Ion Exchange Constant

As in Chapter 3, the competition between hydroxide and chloride ions to bind to cationic vesicles formed from **$C_{18}C_{18}$+** was measured by externally increasing the concentration of chloride ions.

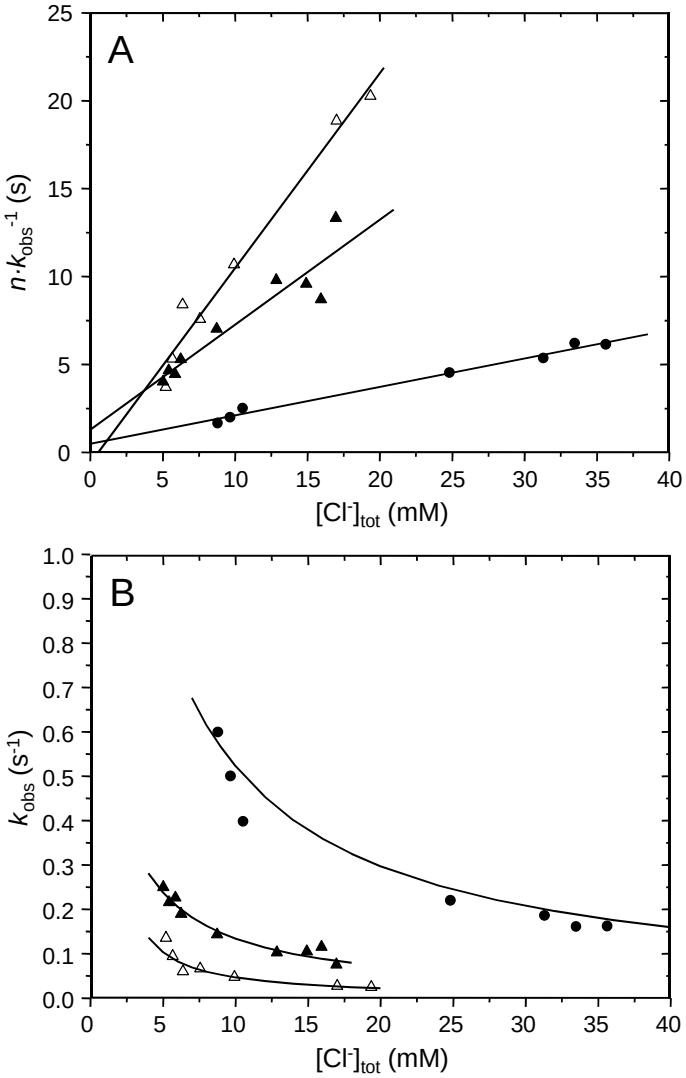

Figure 4.1. *Linear (A) and non-linear (B) plots used to calculate K_{OH}^{Cl}. 20 mol% of* ***C_{18}OH*** *(▲); 50 mol% of* ***C_{18}OH*** *(△); 20 mol% of* ***$C_{18:1}$OH*** *(●). A: n=0.5 for 50 mol% of* ***C_{18}OH****. Lines are best fits.*

In Figure 4.1 the observed rate constants versus the total chloride concentration are shown. The calculated values for K_{OH}^{Cl} from the fits are given in Table 4.1. Despite the good correlation between the experimental data, only reasonable values are found from the linear and non-linear fit for 20 mol% of **C_{18}OH**. The intercept for the solution of 50 mol% of **C_{18}OH** is negative leading to a negative value for K_{OH}^{Cl}. Based on indications in the literature where the ion exchange constant did not change upon the addition of various alcohols, we decided to use a value of 1.6 as we did in Chapter 3, 5 and 6 (average of the reasonable values in these chapters).[15,16] A change in the ion exchange is only expected if the hydration of one of the two ions is changed.

Table 4.1. *Values of K_{OH}^{Cl} obtained from linear and non-linear fits.*

Solution	slope	intercept	K_{OH}^{Cl} a)	slope	intercept	K_{OH}^{Cl} b)
100% **$C_{18}C_{18}$+**	477 ± 19	0.58 ± 0.06	1.8 ± 0.2	480 ± 21	0.62 ± 0.17	1.7 ±0.5
20% **C_{18}OH**	600 ± 84	1.3 ± 0.9	1.1 ± 0.8	650 ± 190	0.97 ± 0.63	1.5 ± 1.1
50% **C_{18}OH**	2224 ± 167	-1.3 ± 3.7	-4 ± 12	2368 ± 523	-2.1 ± 1.8	-2.5 ± 2.2
20% **$C_{18:1}$OH**	162 ± 8	0.48 ± 0.04	0.75 ± 0.08	164 ± 43	0.46 ± 0.33	0.8 ± 0.6

[a] From a linear fit. [b] From a non-linear fit.

4.3.3 Catalytic Effects Induced by the Addition of Various Linear Long-Tailed Alcohols

4.3.3.1 Experimental Observations

The addition of up to 66 mol% of saturated linear alcohols, like **C_{10}OH**, **C_{18}OH** and **C_{18}GOH**, to vesicles of **$C_{18}C_{18}$+** leads in all ratios to a *decrease* in the catalysis by these vesicles (Figure 4.2A-C). However, the extent of the decrease depends on both the length of the tail and the nature of the "head group", although the effect of the tail is more important. For example, addition of 50 mol% of **C_{10}OH** leads to a modest decrease of 8% in the maximum observed rate constant whereas addition of 50 mol% of **C_{18}OH** and **C_{18}GOH** leads to a lowering by 62% and 36%, respectively. Strikingly, the addition of 35 mol% of **$C_{18:1}$OH** leads to an *increase* of the maximum observed rate constant by 140% (Figure 4.2D).

The observed rate constants for 20 mol% of **C_{18}OH** are higher than those for 10 mol% of **C_{18}OH**. This result is odd, but reproducible. We speculate that it might be related to different packing or domain formation at 20 mol% of **C_{18}OH**.

Some care has to be taken with respect to the reaction of alcohols with **1** or formed nitrile, since imines and nitriles are reactive towards alcohols. However, we anticipate that this is unlikely in this case since the carbon atom adjacent to the nitrogen is deactivated.

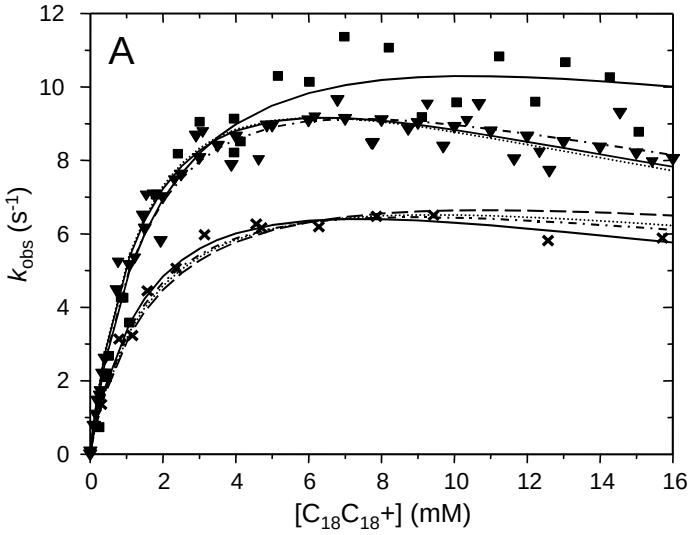

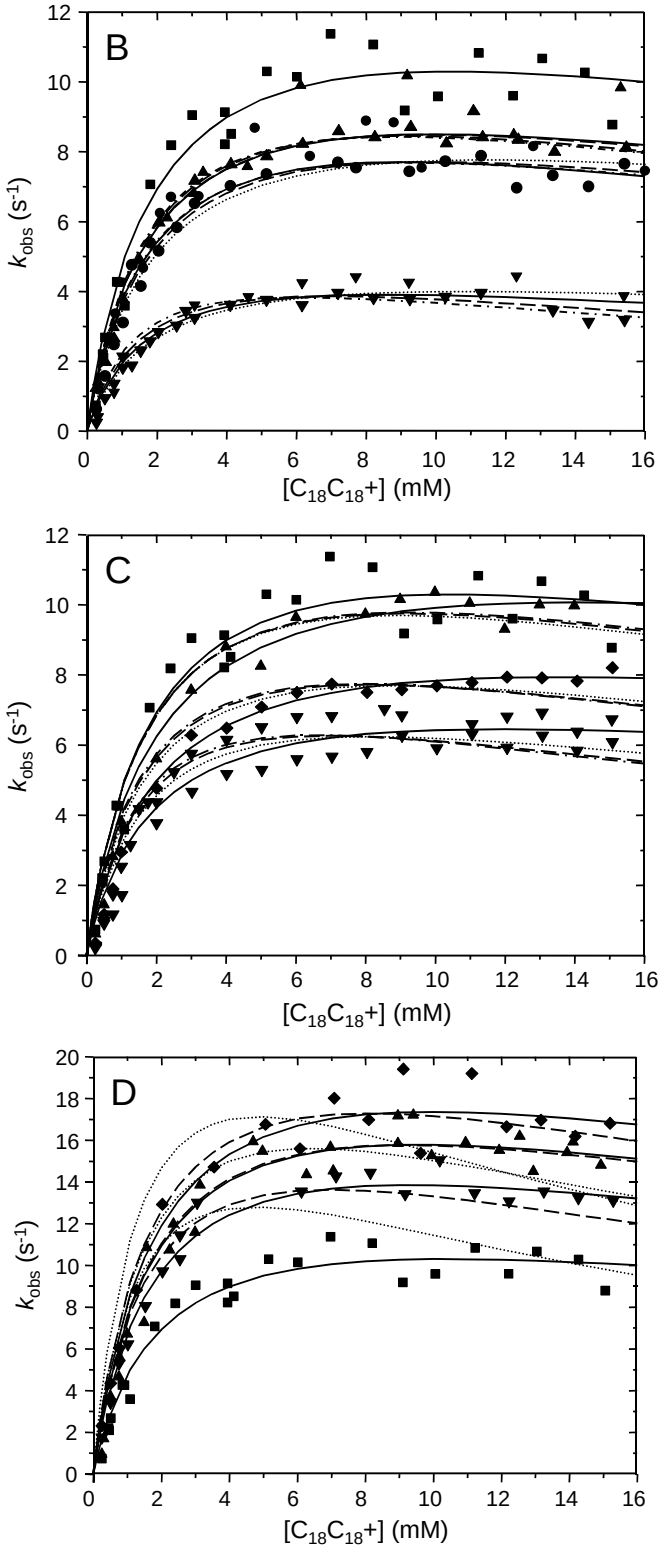

Figure 4.2. *Plots of k_{obs} versus the concentration of* ***$C_{18}C_{18}$+*** *for* ***$C_{18}C_{18}$+*** *vesicles with* ***$C_{10}OH$*** *(A),* ***$C_{18}OH$*** *(B),* ***$C_{18}GOH$*** *(C) and* ***$C_{18:1}OH$*** *(D), where the additive is present in 0 mol % (■), 10 mol% (●), 20 mol% (▲), 35 mol% (◆), 50 mol% (▼) and 66 mol% (×). Solid lines are fits allowing k_{ves} and K_S to vary, dotted lines are fits allowing K_S to vary, dashed lines are fits allowing k_{ves} to vary and dash-dotted lines are fits allowing β to vary. In A to D β was varied as described in the text.*

4.3.3.2 Fitting Procedures

Considering both parameter compensation (Chapter 3) and the complexity of the solution, we decided to fit the data in four different ways. In the first case (method I) we fixed K_{OH}^{Cl},[16] k_{ves} and K_S as for 100% **$C_{18}C_{18}$+** and allowed β to vary. In Figure 4.3A it is apparent that the counterion binding decreases in the order **C_{18}OH** > **C_{18}GOH** > **C_{10}OH**. The data for **$C_{18:1}$OH** could not be fitted in this way since it would lead to a counterion binding larger than 1. The values found for the alcohols with *n*-octadecyl tails are comparable with the total counterion binding we observed for mixed vesicles of **$C_{18}C_{18}$+** and **$C_{10}C_{10}$-** in Chapter 3. However, this does not take into account that **$C_{10}C_{10}$-** has a larger cross-sectional head group area than **C_{18}OH** and **C_{18}GOH**.

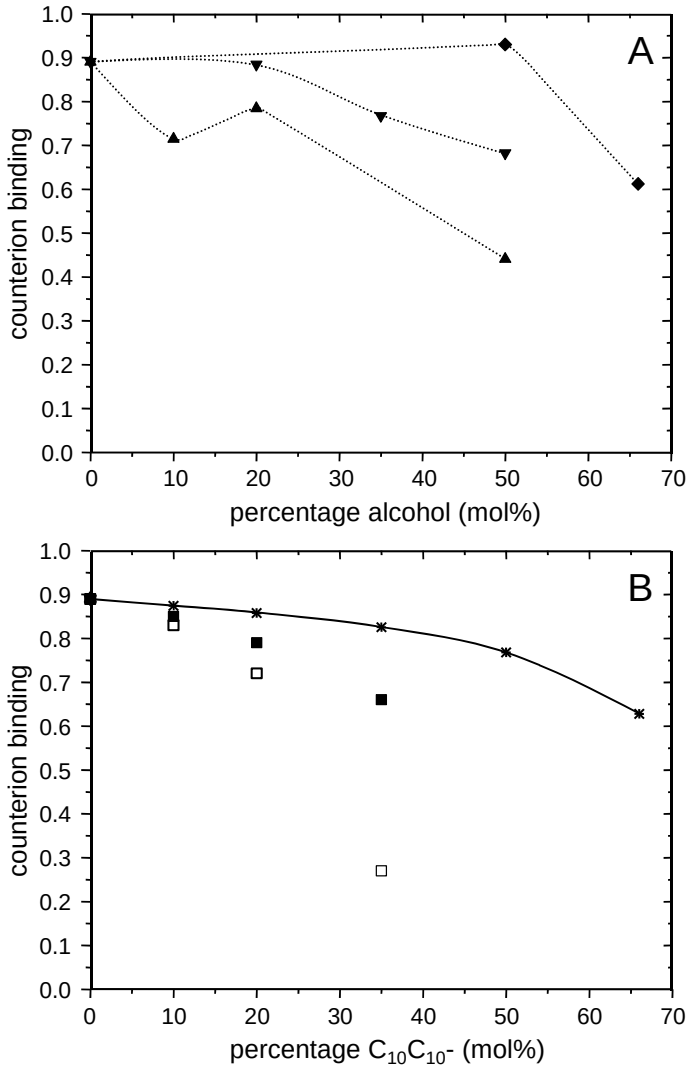

Figure 4.3. *Plot of the counterion binding (fraction) as a function of the bilayer composition. A:* ***C_{10}OH*** *(◆);* ***C_{18}OH*** *(▲);* ***C_{18}GOH*** *(▼). Lines are drawn to guide the eye. B: Excess (□) and total (■) counterion binding as a function of the mole fraction of* ***$C_{10}C_{10}$-*** *(from Chapter 3) and the counterion binding used for method II-IV (✳; see text).*

In Chapter 3 it was concluded that for mixed vesicles of **$C_{18}C_{18}$+** and **$C_{10}C_{10}$-** the charge per surface area remained about constant upon increasing the **$C_{10}C_{10}$-** content. Similar observations were found for mixed vesicles of **$C_{18}C_{18}$+** and **$C_{10}C_{18}$-** (Chapter 3). Therefore we decided to fit the data again, but assuming that four alcohol molecules have the same head group area as one molecule **$C_{10}C_{10}$-** and one molecule **$C_{18}C_{18}$+** (Scheme 4.3). In this way the surface charge density will be similar as that in the systems studied in Chapter 3.
It might appear that this approach does not account for differences in (electrostatic, Van der Waals) interactions between the additives and the amphiphile. However, as long as the head group area is roughly similar for all alcohols, the surface charge density of the vesicular surface will be independent of the structure of the alcohol. Hence, upon increasing amounts of alcohol the counterion decreases similarly for all alcohols. Differences in packing efficiency due to the size of the hydrophobic tail(s) or other differences will be apparent from the vesicular rate constant and binding constant.

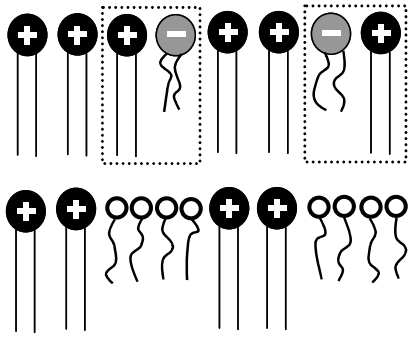

Scheme 4.3. *Schematic representation of how four alcohol molecules fit into the same surface space occupied by* **$C_{10}C_{10}$-** *and* **$C_{18}C_{18}$+** *leading to a similar decrease in counterion binding. Please note that the counterion binding at 25 mol% of* **$C_{10}C_{10}$-** *(2/8) leads to the same counterion binding at 67 mol% of alcohol (8/12).*

Figure 4.3B shows the counterion binding (∗) as used for the method II-IV. In method II, k_{ves} was allowed to vary and in method III K_S was allowed to vary. K_{OH}^{Cl} was 1.6 and K_S (method II) and k_{ves} (method III) were kept constant with respect to the values found for 100 mol% of **$C_{18}C_{18}$+**. It is obvious from Figure 4.4 that both methods lead to the same results considering the trends for the various mixed vesicular solutions. In addition, the trends are also similar to those found for the counterion binding. This is expected since we vary only one parameter. Unfortunately, a closer look at the experimental data and the fits reveals that despite the quite different values obtained for the parameters, the fits are in most cases similar in shape to each other (*e.g.* **C_{18}OH**), whereas some fits do not fit the data very well (*e.g.* **$C_{18:1}$OH**). Similar fits for different values for the parameters make interpretation of the obtained parameters difficult. For those sets of fits intrinsically one cannot discriminate between the fits, unless one has independently measured one or more of these parameters. Unfortunately, despite serious attempts we were not able to measure one of these parameters independently.
The best fits were obtained with method IV where both k_{ves} and K_S were allowed to vary. The ion exchange constant was fixed at 1.6. As can be seen in Figure 4.5 the trends for k_{ves} and K_S are opposite, *i.e.* k_{ves} increases and K_S decreases. The exception to this trend are vesicles formed in the presence of **C_{10}OH** in the sense that the fitted parameters do not change

much upon increasing the **C_{10}OH** content. For both **C_{18}OH** and **$C_{18:1}$OH** the binding constant of the kinetic probe decreases to a similar extent upon the addition of alcohol (at most by a factor of *ca.* 2), whereas for **C_{18}GOH** the binding constant is lowered to a larger extent (at most by a factor of *ca.* 4). At the same time the vesicular rate constant increases for the solutions containing **C_{18}GOH** and **$C_{18:1}$OH** (at most by a factor of *ca.* 4), whereas k_{ves} remains constant for solutions containing **C_{18}OH**.

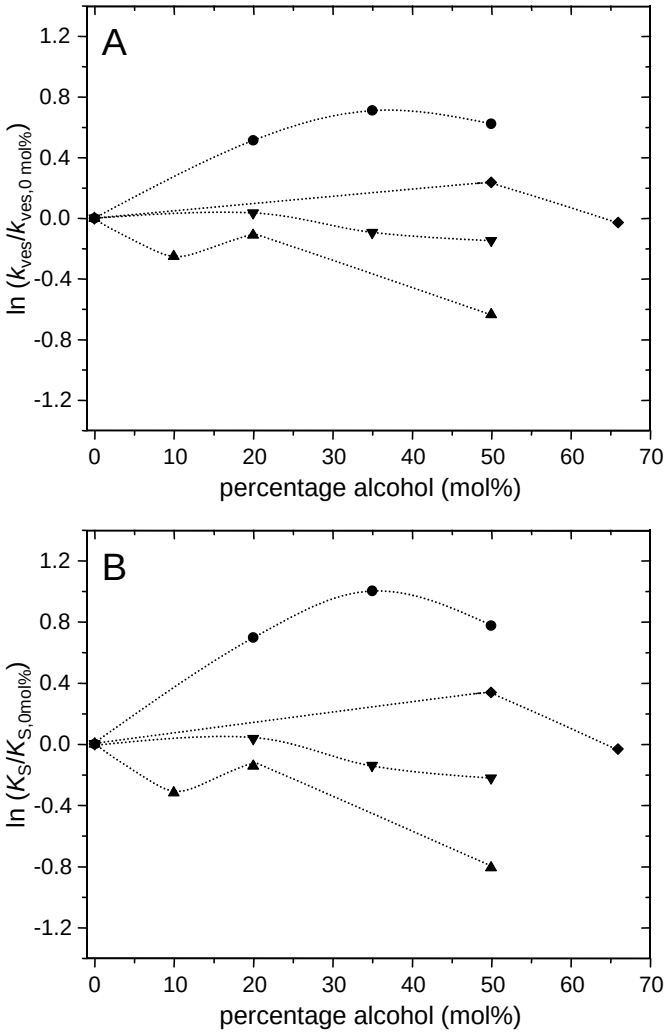

Figure 4.4. *Plot of ln ($k_{ves}/k_{ves,0\%}$) (A) and ln ($K_S/K_{S,0\%}$) (B) versus the mol% of the added alcohol. Fits were obtained by allowing both k_{ves} and K_S vary.* ***C_{10}OH*** *(◆);* ***C_{18}OH*** *(▲);* ***C_{18}GOH*** *(▼);* ***$C_{18:1}$OH*** *(●). Lines are only drawn to guide the eye.*

The trends in the maximum observed rate constants upon increasing amounts of alcohol depend largely on the product $k_{ves} \cdot K_S$ (eq (4.1)), and hence, in principle, a decrease in K_S can be compensated by an increase in k_{ves}. This is, for example, apparent from the fits of **$C_{18:1}$OH** and **C_{18}OH**. For both vesicular solutions K_S decreases to a similar extent. However, since addition of **$C_{18:1}$OH** increases k_{ves}, and addition of **C_{18}OH** does not, the maximum observed rate constant increases upon the addition of **$C_{18:1}$OH**, whereas it decreases upon the addition of **C_{18}OH**. However, we stress that the changes in the parameters are small, which makes it difficult to assign the molecular origin of the observed effects.

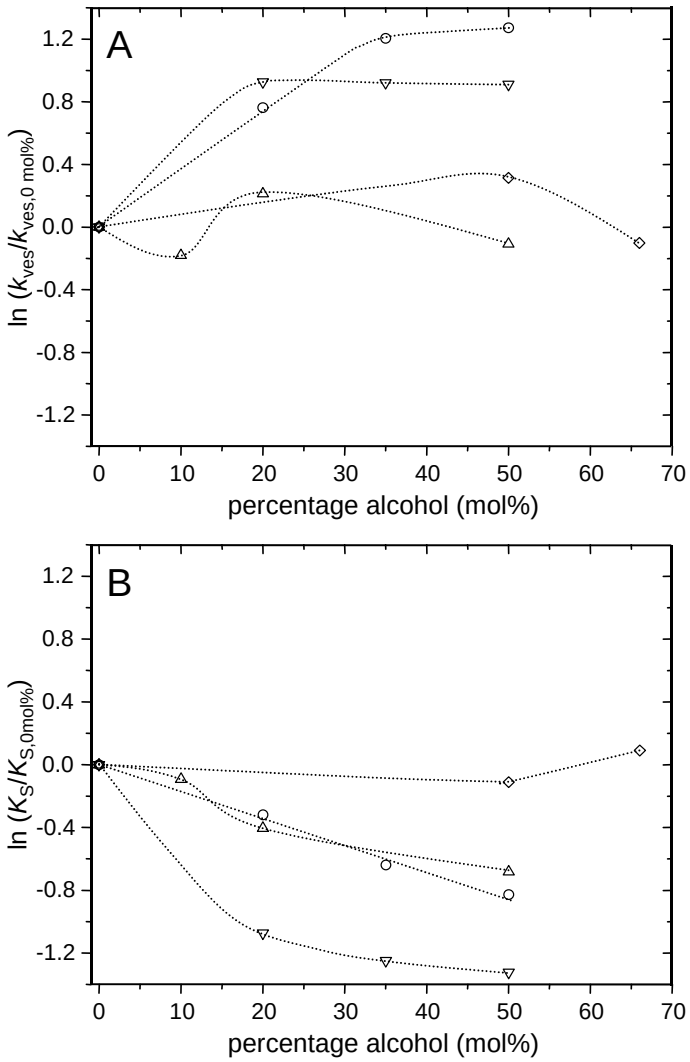

Figure 4.5. *Plot of ln ($k_{ves}/k_{ves,0\%}$) (A) and ln ($K_S/K_{S,0\%}$) (B) versus the mol% of the added alcohol. Fits were obtained by allowing both k_{ves} and K_S to vary.* ***$C_{10}OH$*** *(◇);* ***$C_{18}OH$*** *(△);* ***$C_{18}GOH$*** *(▽);* ***$C_{18:1}OH$*** *(○). Lines are only drawn to guide the eye.*

4.3.4 Kinetic Consequences of Changes in Membrane Properties

In Chapter 2 the properties of cationic vesicles formed in the presence of **$C_{10}OH$**, **$C_{18}OH$**, **$C_{18:1}OH$** and **$C_{18}GOH$** were studied with respect to their main phase transition temperature and membrane polarity. All kinetic experiments were performed at 15°C, which is well below the main phase transition temperature of the vesicles with additives. This is confirmed by the constant positive *GP* value as sensed by laurdan (Chapter 2). However, the DSC scans also reveal that addition of small amounts of alcohols lead to less efficient packing of the tails. This effect is the largest for the alcohols that are liquid in their pure form at room temperature (**$C_{10}OH$** and **$C_{18:1}OH$**). However, at higher content addition of alcohols leads to more efficient packing. This effect is the largest for **$C_{18}OH$** and **$C_{18}GOH$**, whereas also the reduction of the maximum observed rate constants is the largest upon the addition of these alcohols.

The experiments performed to reveal the change in (normalised) polarity in the bilayer upon the addition of linear alcohols show that the polarity changes only slightly. The slight changes are fluorescent- and absorbance-dye dependent. This is reasonable since the probes are sensitive towards different intermolecular interactions. For example, the $E_T(30)$ dye is particularly sensitive towards hydrogen-bond donation, whereas pyrene is not. The differences between the fitted parameters for the alcohols are relatively small, although the differences between the observed rate constants are more pronounced. Most probably the changes in membrane polarity are large enough to be detected kinetically, but too small to be measured using a dye.

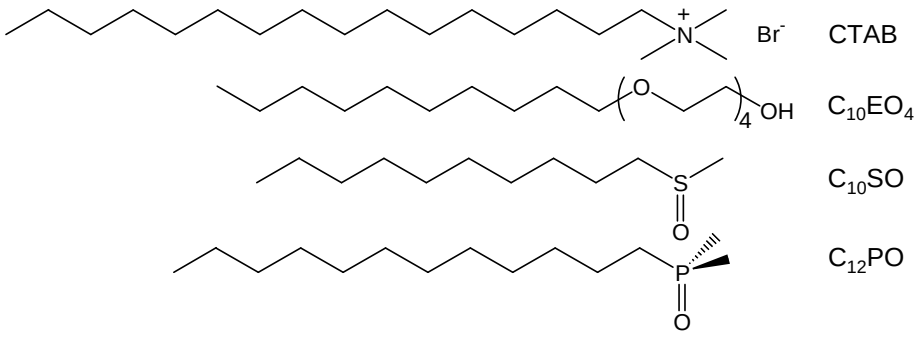

Scheme 4.4. *Cetyltrimethylammonium bromide (CTAB) and three nonionic cosurfactants.*

For S_N2 reactions in mixed micelles of CTAB and short alcohols (less than 6 carbons), K_S and β decrease relative to CTAB micelles, whereas the micellar rate constant does not change.[15-19] The decrease in K_S can be attributed to a stabilisation of the kinetic probes in the aqueous pseudophase due to the presence of non-micellar bound alcohols in this phase. Similar observations were made in micellar CTAB solution containing poly-ethylene glycol in the aqueous pseudophase.[20] However, in our system the concentration of alcohol in the aqueous phase is expected to be extremely low, considering the hydrophobicity of the alcohols. In systems of mixed micelles of CTAB and nonionic surfactants (Scheme 4.4) also a decrease in counterion binding was observed (Figure 4.6).[21-23] This effect is attributed to dilution of the charged head groups upon more alcohol/cosurfactant incorporation. It is striking that the counterion binding is linearly related to the mole fraction irrespective of the structure of the additive and only depends on the counterion binding of the pure ionic micelle (cationic or anionic).[24,25] This behaviour has been approximated mathematically and fits the experimental data quite reasonably.[26,27] In addition, it shows that deviation from linearity is only found above 80 mol% of additive.

In our system, by *only* allowing the counterion binding to vary, we do not obtain such a result (Figure 4.3A). The decrease in counterion binding of CTAB/butanol micelles was confirmed by chemical trapping experiments.[28] These experiments show that addition of butanol leads to an increase in butanol concentration and a decrease in water and bromide concentration in the interfacial region. For 870 mM butanol the local concentration of butanol, bromide and water in the interfacial region are 10 M, ~0.1 M and 38 M, respectively. This means that the counterion binding drops from 75% to 30%, and that the concentration of water drops by about 25%. In conclusion, it seems reasonable to assume

a constant decrease in the counterion binding and further incorporate a change in K_S and/or k_{ves} to account for the rest of the effect, as we did in fitting procedures II-IV.
As in Chapter 3, we choose not to correct k_{ves} for the change in molar volume of the amphiphiles and alcohols, since molar volumes are not known for some of the alcohols used in this study. However, we stress that the molar volumes of the alcohols with 18 carbons in the chain will not be significantly different since the molar volume is mainly determined by the number of carbon atoms in the alcohol, rather than the exact structure of the molecule.[15]

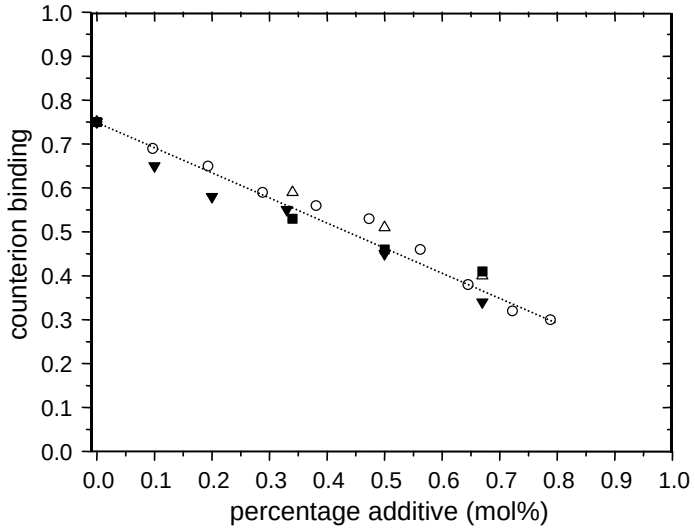

Figure 4.6. *Plot of the counterion binding to mixed micelles of CTAB as a function of the mole fraction additive.* ***$C_{10}EO_4$*** *(■);[21]* ***$C_{12}PO$*** *(△);[22]* ***$C_{10}SO$*** *(▼);[23] butanol (○).[17] The line is drawn to guide the eye.*

4.4 Conclusion

The observed catalysis of the Kemp elimination is decreased upon the addition of **$C_{10}OH$**, **$C_{18}OH$** and **$C_{18}GOH$** to the **$C_{18}C_{18}+$** vesicles, although the extent of the decrease depends on the exact structure of the additive. The observed catalysis is increased upon the addition of **$C_{18:1}OH$**, reaching a maximum at 35 mol% of **$C_{18:1}OH$**. The data can be best fitted using a decreasing counterion binding with increasing additive content and an ion exchange constant fixed at 1.6, leading to realistic values for k_{ves} and K_S. The analysis shows that for **$C_{10}OH$**, **$C_{18}OH$** and **$C_{18:1}OH$**, k_{ves} and K_S only change slightly (at most a factor of around four).

4.5 References

(1) Gennis, R. B. In *Biomembranes: Molecular Structure and Function*; Springer-Verlag: New York, **1989**; pp 20-35.
(2) Darnell, J.; Lodish, H.; Baltimore, D. In *Molecular Cell Biology*; Scientific American Books: New York, **1990**; pp 491-499.
(3) Alberts, B.; Bray, D.; Lewis, J.; Raff, M.; Roberts, K.; Watson, J. D. In *Molecular Biology of the Cell*; Garland Publishing: New York, **1994**; pp 477-485.
(4) Farooqui, A. A.; Horrocks, L. A.; Farooqui, T. *Chem.Phys.Lipids* **2000**, *106*, 1-29.
(5) Hichami, A.; Duroudier, V.; Leblais, V.; Vernhet, L.; LeGoffic, F.; Ninio, E.; Legrand, A. *Eur.J.Biochem.* **1997**, *250*, 242-248.
(6) Gopinath, D.; Ravi, D.; Rao, B. R.; Apte, S. S.; Rambhau, D. *Int.J.Pharm* **2002**, *246*, 187-197.
(7) Hui, F. K.; Barton, P. G. *Biochim.Biophys.Acta* **1973**, *296*, 510-517.
(8) Eliasz, A. W.; Chapman, D.; Ewing, D. F. *Biochim.Biophys.Acta* **1976**, *448*, 220-230.
(9) Lee, A. G. *Biochemistry* **1976**, *15*, 2448-2454.
(10) Mabrey, S.; Sturtevant, J. M. *Biochim.Biophys.Acta* **1977**, *486*, 444-450.
(11) Jain, M. K.; Wu, N. M. *J.Membrane Biol.* **1977**, *34*, 157-201.
(12) Zavoico, G. B.; Chandler, L.; Kutchai, H. *Biochim.Biophys.Acta* **1985**, *812*, 299-312.
(13) Menger, F. M.; Portnoy, C. E. *J.Am.Chem.Soc.* **1967**, *89*, 4698-4703.
(14) Romsted, L. S. In *Micellization, Solubilization and Microemulsions*; Mittal, K. L., ed., Plenum Press: New York, **1977**; pp 509-530.
(15) Bravo, C.; Leis, J. R.; Peña, M. E. *J.Phys.Chem.* **1992**, *96*, 1957-1961.
(16) Rodríguez, A.; Muñoz, M.; Graciani, M. D. M.; Moyá, M. L. *J.Colloid Interface Sci.* **2002**, *248*, 455-461.
(17) Bertoncini, C. R. A.; Nome, F.; Cerichelli, G.; Bunton, C. A. *J.Phys.Chem.* **1990**, *94*, 5875-5878.
(18) Muñoz, M.; Rodríguez, A.; Graciani, M. D. M.; Moyá, M. L. *Langmuir* **1999**, *15*, 1588-1590.
(19) Muñoz, M.; Graciani, M. D. M.; Rodríguez, A.; Moyá, M. L. *J.Colloid Interface Sci.* **2003**, *266*, 208-214.
(20) Graciani, M. D. M.; Rodriguez, A.; Muñoz, M.; Moyá, M. L. *Langmuir* **2003**, *19*, 8685-8691.
(21) Bunton, C. A.; Wright, S.; Holland, P. M.; Nome, F. *Langmuir* **1993**, *9*, 117-120.
(22) Blaskó, A.; Bunton, C. A.; Toledo, E. A.; Holland, P. M.; Nome, F. *J.Chem.Soc., Perkin Trans.2* **1995**, 2367-2373.
(23) Foroudian, H. J.; Bunton, C. A.; Holland, P. M.; Nome, F. *J.Chem.Soc., Perkin Trans.2* **1996**, 557-561.
(24) Rathman, J. F.; Scamehorn, J. F. *J.Phys.Chem.* **1984**, *88*, 5807-5816.
(25) Griffiths, P. C.; Pettersson, E.; Stilbs, P.; Cheung, A. Y. F.; Howe, A. M.; Pitt, A. R. *Langmuir* **2001**, *17*, 7178-7181.
(26) Maeda, H. *J.Colloid Interface Sci.* **2003**, *258*, 390-395.
(27) Akisada, H. *J.Colloid Interface Sci.* **2001**, *240*, 323-334.
(28) Chaudhuri, A.; Romsted, L. S. *J.Am.Chem.Soc.* **1991**, *113*, 5052-5053.

CHAPTER 5

EFFECTS OF ETHYLENE GLYCOL SURFACTANTS AND A PHOSPHOLIPID ANALOGUE ON THE VESICLE-CATALYSED KEMP ELIMINATION REACTION

*The general-base catalysed reaction of 5-nitrobenzisoxazole with hydroxide ions in vesicles formed from dimethyldi-n-octadecylammonium chloride (**$C_{18}C_{18}$+**) is affected upon the addition of surfactants functionalised with an ethylene glycol head group. However, the magnitude of the effect depends on the exact structure of the added surfactant. Addition of 5 mol% of a cationic PEG-ylated double-tailed amphiphile (SAINT-44) leads to an increase in the observed rate constants of about 20 %. Contrastingly, the addition of a nonionic single-tailed surfactant with an oligo-ethylene glycol head group does not lead to a change in the observed rate constant, until the formation of micelles becomes significant at 35 mol%. At that point a decrease in the observed rate constant is observed. A detailed kinetic analysis indicates that upon the addition of both ethylene glycol surfactants the binding constant of the kinetic probe to the vesicles is increased.*

*Due to micelle formation, the phospholipid analogue (**$C_{18}C_{18}$G+**) does not very efficiently catalyse the reaction.*

5.1 Introduction

In vivo drug targeting vehicles usually require a steric stabiliser to reduce adhesion and adsorption of these vehicles to plasma proteins and cellular surfaces (mainly to liver cells, spleen and bone marrow).[1-3] Commonly used steric stabilisers are natural phospholipids with a synthetic poly(ethylene glycol) head group.[1] Due to their large head group and high curvature of these amphiphiles prefer to form micelles. When mixed with a phospholipid that has a negative curvature, such as DOPE, they are able to induce lamellar phases.[4] PEG-ylated lipids that are added in small amounts (< 10 mol%) to liposomes do not break up the lamellar phase,[5-7] and at a low molar ratio the polymer chains are in the "mushroom" conformation, whereas at higher molar ratio the chains interact and therefore undergo a transition into a "brush" conformation.[1] In addition, PEG-ylated liposomes tend to make liposomes less permeable towards certain encapsulated molecules.[7] The extent of the decreased permeability depends on the average degree of polymerisation of the ethylene glycol head group. However, when single-tailed PEG-surfactants are added, the overall picture becomes more complex and the extent of the increase or decrease in permeability depends not only on the average degree of polymerisation, but also on the size of the hydrophobic tail and the linker (ester, ether, amide, etc.).[8] The ability of the linker to form hydrogen bonds with the phospholipids seems to be an important factor in reducing the permeability.

Single-tailed oligo-ethylene glycol alkyl ethers ($C_nH_{2n+1}EO_m$) or derivatives such as Triton X-100, are often used in order to solubilise membranes.[9-12] Their binding strength to membranes increases when the hydrophobic tail is elongated,[11,13,14] an increase in the size of the head group opposes this effect. Contrary to charged single-tailed surfactants flip-flop from the outer leaflet to the inner leaflet and vice versa is fast.[11,15]

To our knowledge the influence of the presence of poly-ethylene glycol in the Stern region on vesicular catalysis has not yet been studied. However, nonionic micelles of **$C_{12}EO_{23}$** and **$C_{12}EO_{10}$** inhibit the alkaline hydrolyses of phenyl benzoate[16] and securinine[17] by effectively separating the organic substrate from the hydroxide ions. Contrastingly, nonionic micelles catalyse the reaction of I_3^- with an organic substrate.[18,19] This effect is probably due to dehydration of the soft I_3^- which favours the rate of the micellar reaction despite the fact that there is no electrostatic attraction between the micelle and the ion. However, catalysis by other inorganic ions (hydroxide, bromide, etc.) and organic substrates has not been found, unless CTAB is added to these micelles.[16,17,20-22] However, the observed rate constants are higher when the nonionic cosurfactant is absent since nonionic surfactants lower the charge density and therefore the counterion binding. Competition between chloride and bromide ions to bind to mixed cationic/nonionic micelles is not affected by the micellar composition.[23] The exact size of the hydrophobic and hydrophilic part of the molecule seems to have little effect on the micellar rate constant for a 1,3-dipolar cycloaddition reaction.[24] In micelles of **$C_{12}EO_{23}$** the pK_a of phenyl salicylate is 1.5 units lower relative to water, whereas CTAB micelles do not lower the pK_a.[25] The above-mentioned catalytic effects reveal that the presence of ethylene glycol units in the Stern region can induce unexpected results, although the exact mechanism is not always clear.

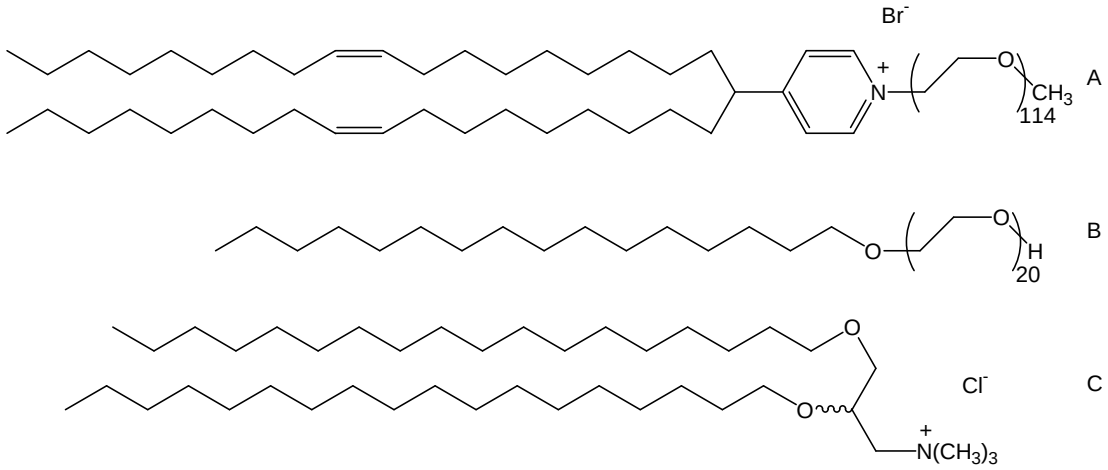

Scheme 5.1. *SAINT-44 (A),* ***$C_{16}EO_{20}$*** *(B) and* ***$C_{18}C_{18}G+$****.*

Based on the above-mentioned considerations we decided to study the kinetic effects of the third class of additives, single- and a double-tailed ethylene glycol surfactant (Scheme 5.1), bound to cationic vesicles of dimethyldi-*n*-octadecylammonium chloride (**$C_{18}C_{18}+$**) on the general-base catalysed reaction of 5-nitrobenzisoxazole (Scheme 5.2). The single-tailed surfactant (eicosa ethylene glycol *n*-hexadecyl ether; **$C_{16}EO_{20}$**; Scheme 5.1B) has its relevance for membrane solubilisation (Chapter 2). The double-tailed compound SAINT-44 (Scheme 5.1A) has previously been used for stabilising lipoplexes in *in vivo* experiments,[26] but its use can be generalised to drug delivery vehicles as well.

In addition, we like to point at the ability of these additives to act as multiple hydrogen bond acceptor, as a result of the number of ether bonds in the head group. This latter point and the observation that **$C_{16}EO_{20}$** can solubilise membranes has its relation to the fourth class of additives, sugar-based surfactants, that will be studied in Chapter 6, since both groups of molecules are single-tailed surfactants.
Finally, also a double-tailed amphiphile with a glycerol linker between the cationic head group and the alkyl tails was used in kinetic studies to verify the influence of the glycerol linker (**$C_{18}C_{18}G+$**; Scheme 5.1C).

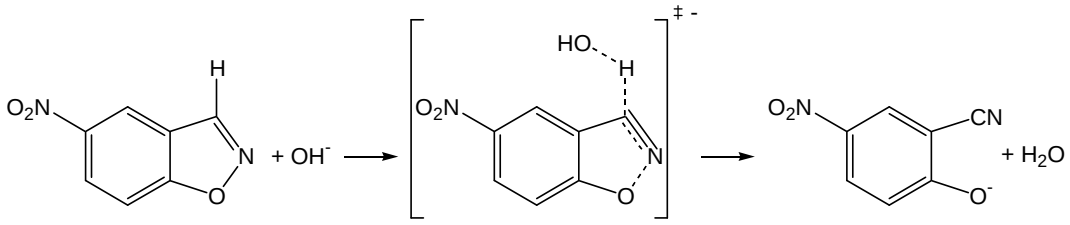

1

Scheme 5.2. *Kemp elimination reaction.*

5.2 Experimental

Materials and the vesicle preparation have been described in Chapter 2, kinetic experiments in Chapter 3.

5.3 Results and Discussion

5.3.1 Kinetic Analysis

The kinetic data was analysed as before (Chapter 4), but for clarity the equations are shown below.

$$k_{obs} = \frac{k_w[OH^-]_{tot} + (k_{ves}K_S - k_w)m_{OH}[C_{18}C_{18}+]}{1+K_S[amph]_{tot}} \tag{5.1}$$

$$m_{OH}^2 + m_{OH}\left[\frac{[OH^-]_{tot} + K_{OH}^{Cl}[Cl^-]_{tot}}{(K_{OH}^{Cl}-1)[C_{18}C_{18}+]} + \beta\right] - \left[\frac{\beta[OH]_{tot}}{(K_{OH}^{Cl}-1)[C_{18}C_{18}+]}\right] = 0 \tag{5.2}$$

In these equations k_{obs}, k_w and k_{ves} are the observed, aqueous and vesicular rate constant, respectively. K_S is the binding constant of the kinetic probe to the bilayer (amphiphile and additives). K_{OH}^{Cl} is the exchange constant for binding of hydroxide and chloride ions to the bilayer and β is the total counterion binding to the bilayers. $[OH]_{tot}$ is the total hydroxide concentration and m_{OH} is the ratio of concentrations of bound hydroxide ions and cationic amphiphiles.
The ion exchange constant K_{OH}^{Cl} can be calculated under the assumptions mentioned in Chapter 3 via eq. (5.3):

$$\frac{1}{k_{obs}} = \frac{1 + K_S[C_{18}C_{18}+]_{tot}}{k_{ves}K_S[C_{18}C_{18}+]_{tot}\beta} + \frac{(1 + K_S[C_{18}C_{18}+]_{tot})K_{OH}^{Cl}}{k_{ves}K_S[C_{18}C_{18}+]_{tot}\beta[OH^-]_{tot}}[Cl^-]_{tot} \tag{5.3}$$

5.3.2 Kinetic Experiments and Fitted Parameters

5.3.2.1 Ion Exchange Constant

The ion exchange constants were calculated by measuring the rate constants as a function of increasing amounts of chloride ions. Upon increasing amounts of chloride ions the hydroxide ions are expelled from the Stern region and hence the observed rate constants decrease. The extent of the decrease is determined by the relative strength of binding of the chloride ions. Figure 5.1 shows a plot of the experimental data and the data was fitted using eq. (5.3). The calculated values from the fits are shown in Table 5.1. The scattering around the fitted lines is rather small. The experimental data for the solution containing 5 mol% of SAINT-44 has somewhat smaller values that for 100 mol% of **$C_{18}C_{18}$+**. This is due to the fact that this solution was measured at an amphiphile concentration of 0.28 mM, whereas the rates for 100 mol% of **$C_{18}C_{18}$+** were measured at 0.51 mM.

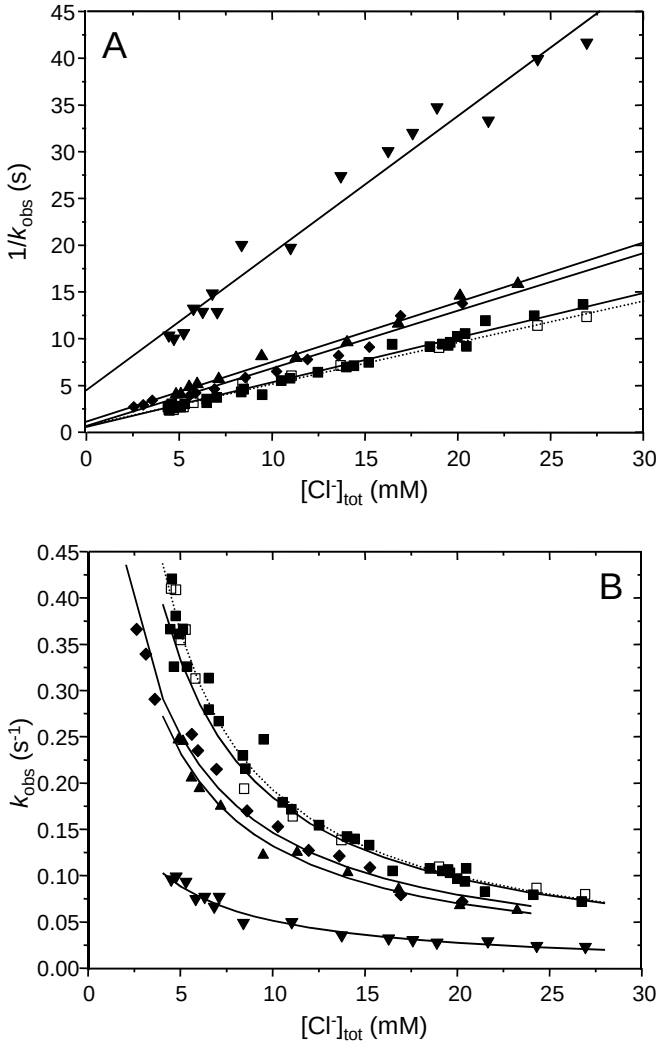

Figure 5.1. *Linear (A) and non-linear (B) plots used to calculate K_{OH}^{Cl}. 100 mol% of* ***$C_{18}C_{18}$+*** *(■); 5 mol% of* ***$C_{18}C_{18}$+Br-*** *(□);5 mol% of SAINT-44 (▲); 35 mol% of* ***$C_{16}EO_{20}$*** *(◆); 100 mol% of* ***$C_{18}C_{18}$G+*** *(▼). Lines are best fits.*

Table 5.1. *Values of K_{OH}^{Cl} obtained from linear and non-linear fits.*

Solution	slope	intercept	K_{OH}^{Cl} a)	slope	intercept	K_{OH}^{Cl} b)
100% **$C_{18}C_{18}$+**	477 ± 19	0.58 ± 0.06	1.8 ± 0.2	480 ± 21	0.62 ± 0.17	1.7 ±0.5
5% **$C_{18}C_{18}$+Br-**	444 ± 14	0.71 ± 0.04	1.4 ± 0.1	483 ± 34	0.36 ± 0.25	3.0 ± 2.1
5% **S44**	639 ± 23	1.14 ± 0.09	1.3 ± 0.1	649 ± 52	1.07 ± 0.42	1.4 ± 0.6
35% **$C_{16}EO_{20}$**	616 ± 34	0.70 ± 0.14	2.0 ± 0.4	565 ± 34	1.09 ± 0.21	1.1 ± 0.2
100% **$C_{18}C_{18}$G+**	1465 ± 68	4.48 ± 0.96	0.8 ± 0.2	1586 ± 101	3.31 ± 0.87	1.1 ± 0.3

a) From a linear fit. b) From a non-linear fit.

The replacement of 5 mol% of **$C_{18}C_{18}$+** by **$C_{18}C_{18}$+Br-** has little influence on the slope and intercept of the fit and on the ion exchange constant. This is reasonable for two reasons: (1) 5 mol% is a small amount, especially with respect to solutions with added NaCl; (2) The ion exchange constant for bromide and hydroxide ions is in the order of 2.1 to 31,[27-34] and therefore only slightly higher than literature values of K_{OH}^{Cl} (1.2-11).[27-29,31,33,35-37] The value of K_{OH}^{Cl} for 100 mol% of **$C_{18}C_{18}$G+** is somewhat smaller than expected. The value of 0.8 suggests that hydroxide binding is preferred over chloride binding, which we find rather unexpected.

The average ion exchange constant was calculated according to eq. (3.19). Taking all the values into account, it is calculated to be 1.4 ± 2.3. The error is quite large due to the large value in the non-linear fit for 5 mol% of **$C_{18}C_{18}$+Br-**. If we leave this value out of the average, and also neglect the value of 0.8 we find a value of 1.4 ± 0.9. As discussed before in Chapter 3 and 4 we will use a value of 1.6 for all vesicular solutions.

5.3.2.2 Eicosa-Ethylene Glycol Mono *n*-Hexadecyl Ether

Addition of 35 mol% of **$C_{16}EO_{20}$** decreases the observed catalysis by about 30%. The addition of **$C_{16}EO_{20}$** leads to micelle formation as was discussed in Chapter 2. Turbidity experiments reveal that at 35 mol% of **$C_{16}EO_{20}$** solubilisation of the membrane is only occurring below 3 mM **$C_{18}C_{18}$+.** This is partially confirmed by DLS experiments, where the size distribution of a solution containing 35 mol% of **$C_{16}EO_{20}$** directly after dilution from 30 mM to 0.5 mM, has its main peak below 10 nm, with only a minor peak at 80 nm. Overnight the intensity of the large particles decreases. Since its reorganisation seems slow, and considering the large dependence of scattered intensity on particle size, this means that in all solutions containing 35 mol% of **$C_{16}EO_{20}$** most of the **$C_{16}EO_{20}$** and **$C_{18}C_{18}$+** are present in micelles. Below 10 mol% of **$C_{16}EO_{20}$** no micelles are detected by both turbidity and DLS experiments.

In terms of the observed rate constant (k_{obs}), modification of eq. (5.1) is required where not only a vesicular pseudophase is taken into account, but also a micellar pseudophase. In addition, adaptation of the model also requires correction for relative amounts of **$C_{16}EO_{20}$** and **$C_{18}C_{18}$+** that are present in the respective pseudophases. However, mathematically it is not possible to set up such a model and obtain fitted parameters that are not subjected to extensive parameter compensation. Therefore, we decided to fit the experimental data to eq. (5.1) and we take into account that both k_{ves} and K_S will report a location-averaged value of

the "true" k_{ves} and k_{mic} and $K_{S,ves}$ and $K_{S,mic}$, respectively. The subscript "mic" stands for the rate constant in or binding constant to the micellar pseudophase.

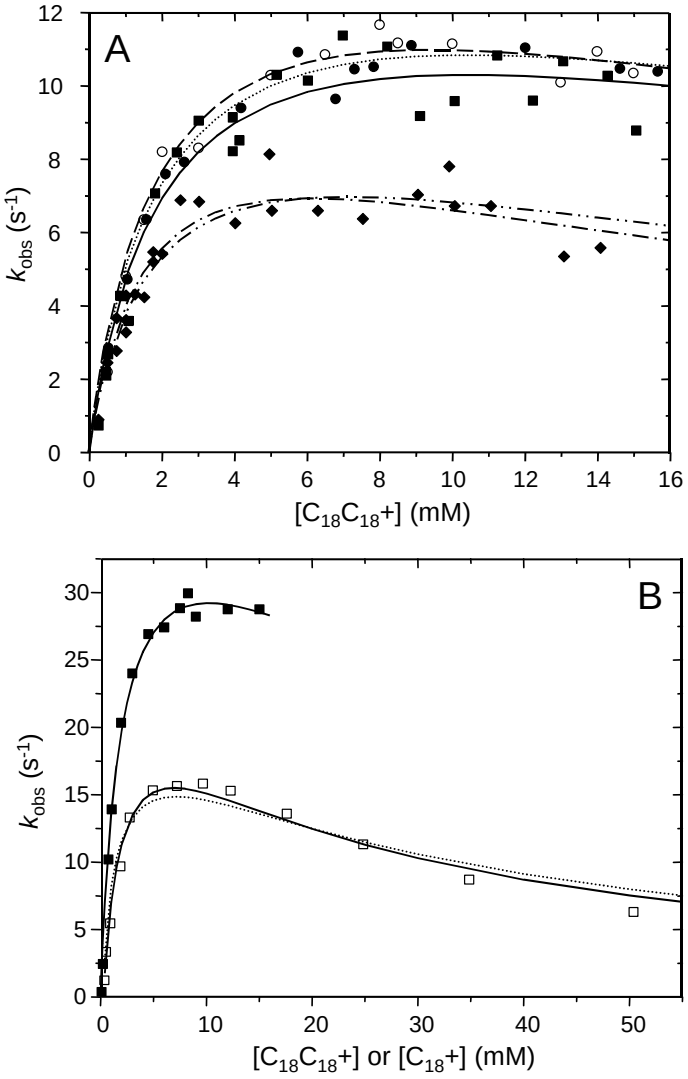

Figure 5.2. *Kinetic curves for various vesicular and mixed-micellar solutions. A: 100 mol% of* $\mathbf{C_{18}C_{18}+}$ *(■; solid line); 5 mol% of* $\mathbf{C_{16}EO_{20}}$ *(○; dashed line); 10 mol% of* $\mathbf{C_{16}EO_{20}}$ *(●; dotted line); 35 mol% of* $\mathbf{C_{16}EO_{20}}$ *(◆; dash-dotted line and dash-double-dotted line (fixing* K_S *at 25* M^{-1}*)). Lines are fits allowing* k_{ves} *and* K_S *to vary. B: Kinetic curves for* $\mathbf{C_{18}C_{18}+}$ *(vesicles; ■) and* $\mathbf{C_{18}+}$ *(micelles; □) at 25°C. Solid lines* $K_{OH}^{Cl} = 1.6$ *and dotted line* $K_{OH}^{Cl} = 10$.

The kinetic data for solutions containing $\mathbf{C_{18}C_{18}+}$ and $\mathbf{C_{16}EO_{20}}$ can be found in Figure 5.2A. The data was fitted using eq. (5.1) and the obtained values can be found in Table 5.2. As can be seen, addition of small amounts of $\mathbf{C_{16}EO_{20}}$ does not lead to a change in the observed rate constants.

A detailed interpretation of the fitted parameters is a bit unrewarding due to parameter compensation (Chapter 3). However, it is worthwhile to discuss a number of observations from the fitted parameters and the literature.

Table 5.2. *Fitted parameters for several vesicular solutions and a micellar solution.*

Solution	β	K_{OH}^{Cl}	k_{ves} (s^{-1})	K_S (M^{-1})
100 mol% **$C_{18}C_{18}^+$** [a]	0.89	1.6	295	32
5 mol% **$C_{16}EO_{20}$** [a]	0.88	1.6	345	29
10 mol% **$C_{16}EO_{20}$** [a]	0.87	1.6	430	22
35 mol% **$C_{16}EO_{20}$** [a]	0.83	1.6	195	43
35 mol% **$C_{16}EO_{20}$** [b]	0.83	1.6	240	32
100 mol% **$C_{18}C_{18}^+$** [a,c]	0.89	1.6	975	26
100 mol **C_{18}^+** [a,c]	0.80	1.6	340	54
100 mol **C_{18}^+** [a,c]	0.80	10	976	41

[a] k_{ves} and K_S allowed to vary. [b] Only k_{ves} varied [c] at 25°C.

Only small changes in k_{ves} and K_S are observed (less than a factor of at most 2), up to 10 mol% of **$C_{16}EO_{20}$**. At 35 mol% of **$C_{16}EO_{20}$** the maximum observed rate constant is about 30% lower relative to that for 100 mol% of **$C_{18}C_{18}^+$**. Keeping the binding constant fixed at 32, the vesicular rate constant is only lowered by about 20%. Changes in aggregate structure are expected to affect the observed and vesicular or micellar rate constant, as has been observed for changes from spherical micelles to worm-like micelles and vesicles.[38,39] The change observed for 35 mol% of **$C_{16}EO_{20}$** is small compared to what is expected for a change from a vesicular solution to a solution mainly containing micelles for the reaction of **1** with hydroxide ions.[40] In Figure 5.2B vesicles of **$C_{18}C_{18}^+$** are compared with micelles formed from *n*-octadecyltrimethylammonium chloride (**C_{18}^+**; experimental data taken from Pérez-Juste *et al.*[40]). The observed catalysis of **$C_{18}C_{18}^+$** at 25°C relative to the aqueous rate constant amounts to a factor of about 890, whereas the observed catalysis by **C_{18}^+** is only a factor of about 470. In order to calculate the *catalytic rate acceleration* (Chapter 3), values for the molar volume are required. We took 0.58 M^{-1} for **$C_{18}C_{18}^+$**.[40-42] For **C_{18}^+** we extrapolated the value of DTAB (*n*-dodecyltrimethylammonium bromide) and CTAB (*n*-hexadecyltrimethylammonium bromide) to **C_{18}^+** and corrected for the change in counterion.[43-45] The molar volume of **C_{18}^+** was then calculated to be approximately 0.37 M^{-1}. The catalytic rate acceleration then amounts to 8.5 and 39 for **C_{18}^+** and **$C_{18}C_{18}^+$**, respectively. If we use K_{OH}^{Cl} = 10 for the micellar solution, which seems more reasonable for micellar solutions,[27-29,31,33,35-37] the catalytic rate acceleration is about a factor of 24, which is still less than that for the catalytic rate acceleration of vesicles.

The *increase* in K_S going from vesicles to micelles is somewhat surprising since vesicles are expected to bind small organic molecules better than micelles, although the opposite trend has also been observed.[24] This trend is also observed going to the mixed micellar/vesicular solution containing 35 mol% of **$C_{16}EO_{20}$**, although the data can be satisfactorily fitted by keeping K_S constant at 32 M^{-1}. At lower percentages the increase in K_S is not apparent, but this is the result of the fact that for these solutions the observed effects are too small.

The role of the ethylene glycol head group has to be considered as well. Solubilisation experiments have shown that small organic molecules dissolve at up to a factor of three better in aqueous solutions containing polyethylene glycol (PEG) than in its absence.[46,47] In a study concerning a micellar solution and PEG in the aqueous pseudophase a decrease in

the micellar binding constant of an organic substrate was found upon an increase in the concentration of PEG.[48] The effect was attributed to a decreased polarity of the aqueous phase. In contrast, micelles with an ethylene glycol head group might therefore experience a more hydrophobic Stern region, and hence binding of small organic molecules might be improved.

An important conclusion can be drawn from the vesicular solutions containing 5 and 10 mol% of **$C_{16}EO_{20}$**, since no mixed micelles are present under these conditions. As discussed in Chapter 1, and noted in the experimental sections of Chapter 3 and 4, the reaction of **1** with hydroxide ions can proceed with different rates and/or rate constants at the inner and outer leaflet of the bilayer. Different rates for the leaflets are observed when permeation of the reactants is the rate-limiting step. In Section 5.1 it was pointed out that single-tailed surfactants are known to decrease the packing of the membrane in the absence of favourable interactions between amphiphile and single-tailed surfactant (*e.g.* hydrogen bonding).[8] As a result, permeation of reactants through the bilayer should be faster when **$C_{16}EO_{20}$** is incorporated into the bilayer. Considering that no changes in the observed rate constants as a function of the amphiphile concentration are found upon incorporation of 5 and 10 mol% of **$C_{16}EO_{20}$**, it can be concluded that permeation of **1** and/or hydroxide ions is not the rate-limiting step in the deprotonation reaction in the absence **$C_{16}EO_{20}$**. From these experiments it cannot be concluded whether the reaction proceeds at both leaflets with different rate constants.

5.3.2.3 SAINT-44 and $C_{18}C_{18}G+$

In Figure 5.3 the kinetic profiles are shown for a solution containing **$C_{18}C_{18}+$** and 5 mol% of SAINT-44. Since SAINT-44 has a bromide counterion, a solution containing **$C_{18}C_{18}+$** and 5 mol% of **$C_{18}C_{18}+$** with a bromide ion in stead of a chloride counterion (**$C_{18}C_{18}+Br-$**) has been studied as well. Addition of 5 mol% of **$C_{18}C_{18}+Br-$** leads to a slight lowering in the observed rate constants, which is reasonable considering the small amount of bromide ions. In addition, binding of bromide ions is slightly preferred over binding of chloride and hydroxide ions. On the contrary, addition of 5 mol% of SAINT-44 improves the observed catalysis by about 20%. However, due to few data points at higher concentrations and the relatively small change, it is difficult to assign this effect to a change in k_{ves} or K_S. In the case that it would be mainly due to a change in K_S, this can be rationalised in terms of a decrease in polarity of the Stern region, as discussed before (Section 5.3.2.2). However, in the case of SAINT-44 the effect of the ethylene glycol is now already observed at 5 mol%. It should be noted that SAINT-44 has a degree of polymerisation of 114, whereas that for **$C_{16}EO_{20}$** is only 20. However, despite the structural difference the same trend in K_S is observed.

In addition, it should be noted that the tails of SAINT-44 contain unsaturations. As in the case of **$C_{18:1}OH$** (Chapter 4) this could give rise to an increase in observed rate constants as well.

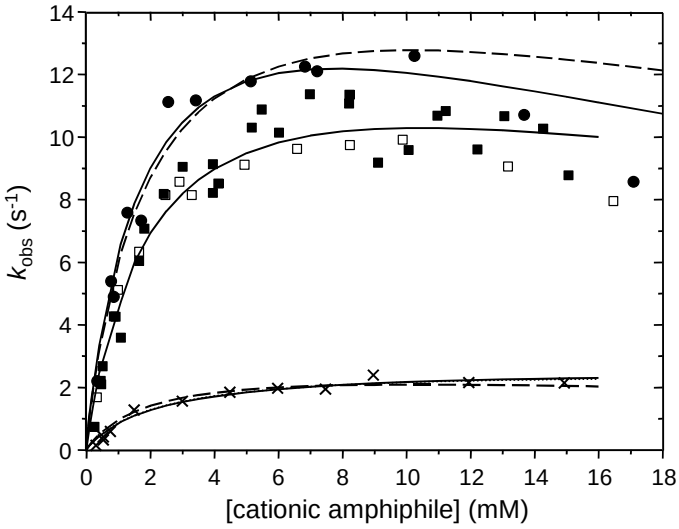

Figure 5.3. *Kinetic curves for vesicular solutions. 100 mol% of* ***$C_{18}C_{18}$+*** *(■); 5 mol% of* ***$C_{18}C_{18}$+Br-*** *(□); 5 mol% of SAINT-44 (●); 100 mol% of* ***$C_{18}C_{18}$G+*** *(×). Solid lines are fits allowing k_{ves} and K_S to vary, dotted lines are fits allowing K_S to vary, dashed lines are fits allowing k_{ves} to vary and dash-dotted lines are fits allowing β to vary.*

Due to parameter compensation, analysis of the data for **$C_{18}C_{18}$G+** is not possible. As was shown in Chapter 3 for small values of K_S, K_S and k_{ves} are readily able to compensate each other (eq. (5.2)). Under these conditions the observed rate constant scales linearly with the value of the product of K_S and k_{ves}. Therefore it is not possible to interpret the fitted parameters and draw conclusions about the origin of the relatively small observed catalytic efficiency. However, a detailed characterisation (Chapter 2) reveals a solution of **$C_{18}C_{18}$G+** that consists of large structures of about 120 nm, but also smaller aggregates are present. In combination with the high intensity of the scattered light this indicates that besides vesicles also micelles, and/or bilayer fragment are present. This result is not very surprising if one considers the solubility limit of the amphiphile and the high phase transition temperature (65°C). It is difficult to derive the relative populations of amphiphiles in vesicles and micelles/bilayer fragments from DLS, but considering the large dependence of the scattered intensity on the particle size, we anticipate that most of the amphiphiles are present in micelles or small bilayer fragments.

Table 5.3. *Fitted parameters for several vesicular solutions and a micellar solution.*

Solution	β	K_{OH}^{Cl}	k_{ves} (s^{-1})	K_S (M^{-1})	$10^{-3} \cdot K_S \cdot k_{ves}$ ($M^{-1}s^{-1}$)
100 mol% **$C_{18}C_{18}$+**[a]	0.89	1.6	295	32	--[b]
5 mol% SAINT-44 [a]	0.89	1.6	290	41	--[b]
5 mol% SAINT-44 [c]	0.89	1.6	360	32	--[b]
100 mol% **$C_{18}C_{18}$G+** [a]	0.89	1.6	210	7.7	1.6
100 mol% **$C_{18}C_{18}$G+** [c]	0.89	1.6	70	25	1.8
100 mol% **$C_{18}C_{18}$G+** [d]	0.89	1.6	350	4.4	1.6

[a] k_{ves} and K_S allowed to vary. [b] Not relevant. [c] Only k_{ves} varied. [d] Only K_S varied.

5.4 Conclusion

The presence of ethylene glycol units in the Stern region affects the catalysis of the base-catalysed reaction of 5-nitrobenzisoxazole. Despite extensive parameter compensation, the analysis of the kinetic data suggests that the binding constant increases as a result of the presence of ethylene glycol units, irrespective of the hydrophobic part of the molecule.
The single-tailed surfactant **$C_{16}EO_{20}$** solubilises the vesicles formed from **$C_{18}C_{18}$+**. However, this process has only little effect on the observed rate constants. We contend that K_S increases whereas k_{ves} decreases (twice as small). In micellar solutions formed from **C_{18}+** (without ethylene glycol units in the Stern region) the bimolecular rate constant is even further lowered by a factor of around four. In these solutions K_S is increased similar as for **$C_{16}EO_{20}/C_{18}C_{18}$+**.
Incorporation of 5 and 10 mol% of **$C_{16}EO_{20}$** shows that permeation of the reactants is not a rate limiting step in the absence of this surfactant.
The presence of only 5 mol% of SAINT-44 already leads to an increase in the maximum observed rate constants by 20%. It remains unclear whether this effect originates from the presence of ethylene glycol units in the Stern region, or from the double bonds in the tails of SAINT-44.
The phospholipid analogue **$C_{18}C_{18}$G+** induces a low observed catalysis (factor about 200). However, dynamic light scattering shows that part of the amphiphiles is present in micelles and/or bilayer fragments.

5.5 Acknowledgements

Mr A. Wagenaar is thanked for the synthesis of **$C_{18}C_{18}$G+** and SAINT-44.

5.6 References

(1) Marsh, D.; Bartucci, R.; Sportelli, L. *Biochim.Biophys.Acta* **2003**, *1615*, 33-59.
(2) Metselaar, J. M.; Bruim, P.; De boer, L. W. T.; De Vringer, T.; Snel, C.; Oussoren, C.; Wauben, M. H. M.; Crommelin, D. J. A.; Storm, G.; Hennink, W. E. *Bioconjugate Chem.* **2003**, *14*, 1156-1164.
(3) Gabizon, A.; Shmeeda, H.; Barenholz, Y. *Clin.Pharmacokinet.* **2003**, *42*, 419-436.
(4) Johnsson, M.; Edwards, K. *Biophys.J.* **2001**, *80*, 313-323.
(5) Sottmann, T.; Strey, R.; Chen, S. H. *J.Chem.Phys.* **1997**, *106*, 6483-6491.
(6) Edwards, K.; Johnsson, M.; Karlsson, G.; Silvander, M. *Biophys.J.* **1997**, *73*, 258-266.
(7) Silvander, M.; Johnsson, M.; Edwards, K. *Chem.Phys.Lipids* **1998**, *97*, 15-26.
(8) Silvander, M.; Bergstrand, N.; Edwards, K. *Chem.Phys.Lipids* **2003**, *126*, 77-83.
(9) Heerklotz, H.; Binder, H.; Lantzsch, G.; Klose, G. *Biochim.Biophys.Acta* **1994**, *1196*, 114-122.
(10) Heerklotz, H.; Lantzsch, G.; Binder, H.; Klose, G.; Blume, A. *J.Phys.Chem.* **1996**, *100*, 6764-6774.
(11) Heerklotz, H.; Seelig, J. *Biochim.Biophys.Acta* **2000**, *1508*, 69-85.
(12) Barreleiro, P. C. A.; Olofsson, G.; Brown, W.; Edwards, K.; Bonassi, N. M.; Feitosa, E. *Langmuir* **2002**, *18*, 1024-1029.
(13) Heerklotz, H.; Seelig, J. *Biophys.J.* **2000**, *78*, 2435-2440.
(14) Leidy, C.; Kaasgaard, T.; Crowe, J. H.; Mouritsen, O. G.; Jorgensen, K. *Biophys.J.* **2002**, *83*, 2625-2633.
(15) le Maire, M.; Møller, J. V.; Champeil, P. *Biochemistry* **1987**, *26*, 4803-4810.
(16) Khan, M. N.; Ismail, E.; Yusoff, M. R. *J.Phys.Org.Chem.* **2001**, *14*, 669-676.
(17) Lajis, N. H.; Khan, M. N. *J.Phys.Org.Chem.* **1998**, *11*, 209-215.

(18) Davies, D. M.; Gillitt, N. D.; Paradis, P. M. *J.Chem.Soc., Perkin Trans.2* **1996**, 659-666.
(19) Davies, D. M.; Foggo, S. J. *J.Chem.Soc., Perkin Trans.2* **1998**, 247-251.
(20) Bunton, C. A.; Wright, S.; Holland, P. M.; Nome, F. *Langmuir* **1993**, *9*, 117-120.
(21) Fernández, G.; Rodríguez, A.; Graciani, M. D. M.; Muñoz, M.; Moyá, M. L. *Int.J.Chem.Kinet.* **2003**, *35*, 45-51.
(22) Zakharova, L.; Valeeva, F.; Zakharov, A.; Ibragimova, A.; Kudryavtseva, L.; Harlampidi, H. *J.Colloid Interface Sci.* **2003**, *263*, 597-605.
(23) Abuin, E. B.; Lissi, E. A. *J.Colloid Interface Sci.* **1991**, *143*, 97-102.
(24) Rispens, T.; Engberts, J. B. F. N. *J.Org.Chem.* **2003**, *68*, 8520-8528.
(25) Khan, M. N.; Arifin, Z.; Yusoff, M. R.; Ismail, E. *J.Colloid Interface Sci.* **1999**, *220*, 474-476.
(26) Rejman, J.; Wagenaar, A.; Engberts, J. B. F. N.; Hoekstra, D. *Biochim.Biophys.Acta* **2004**, *1660*, 41-52.
(27) Plaisance, M.; Ter-Minassian-Saraga, L. *J.Colloid Interface Sci.* **1976**, *56*, 33-41.
(28) Chaimovich, H.; Bonilha, J. B. S.; Politi, M. J.; Quina, F. H. *J.Phys.Chem.* **1979**, *83*, 1851-1854.
(29) Bartet, D.; Gamboa, C.; Sepúlveda, L. *J.Phys.Chem.* **1980**, *84*, 272-275.
(30) Quina, F. H.; Politi, M. J.; Cuccovia, I. M.; Baumgarten, E.; Martins-Franchetti, S. M.; Chaimovich, H. *J.Phys.Chem.* **1980**, *84*, 361-365.
(31) Romsted, L. S. In *Surfactants in Solution*; Mittal, K. L., Lindman, B., eds., Plenum Press: New York, **1984**; pp 1017-1065.
(32) Broxton, T. J.; Christie, J. R.; Sango, X. *J.Org.Chem.* **1987**, *52*, 4814-4817.
(33) Garcia-Rio, L.; Hervés, P.; Leis, J. R.; Mejuto, J. C.; Pérez-Juste, J. *J.Phys.Org.Chem.* **1998**, *11*, 584-588.
(34) Ruan, K.; Zhao, Z.; Ma, J. *Colloid Polym.Sci.* **2001**, *279*, 813-818.
(35) Al-Lohedan, H.; Bunton, C. A.; Romsted, L. S. *J.Phys.Chem.* **1981**, *85*, 2123-2129.
(36) Kawamuro, M. K.; Chaimovich, H.; Abuin, E. B.; Lissi, E. A.; Cuccovia, I. M. *J.Phys.Chem.* **1991**, *95*, 1458-1463.
(37) Hervés, P.; Leis, J. R.; Mejuto, J. C.; Pérez-Juste, J. *Langmuir* **1997**, *13*, 6633-6637.
(38) Ueoka, R.; Moss, R. A.; Swarup, S.; Matsumoto, Y.; Strauss, G.; Murakami, Y. *J.Am.Chem.Soc.* **1985**, *107*, 2185-2186.
(39) Ramesh, V.; Labes, M. M. *J.Am.Chem.Soc.* **1986**, *108*, 4643-4644.
(40) Pérez-Juste, J.; Hollfelder, F.; Kirby, A. J.; Engberts, J. B. F. N. *Org.Lett.* **2000**, *2*, 127-130.
(41) Lim, Y.; Fendler, J. H. *J.Am.Chem.Soc.* **1979**, *101*, 4023-4029.
(42) Fendler, J. H.; Hinze, W. L. *J.Am.Chem.Soc.* **1981**, *103*, 5439-5447.
(43) Tanford, C.; Nozaki, Y.; Reynolds, J. A.; Makino, S. *Biochemistry* **1974**, *13*, 2369-2376.
(44) Sepúlveda, L.; Lissi, E. A.; Quina, F. H. *Adv.Colloid Interface Sci.* **1986**, *25*, 1-57.
(45) Van Os, N. M.; Haak, J. R.; Rupert, L. A. M. *Physico-Chemical Properties of Selected Anionic, Cationic and Nonionic Surfactants*; Elsevier: Amsterdam, **1993**.
(46) Sasahara, K.; Uedaira, H. *Colloid Polym.Sci.* **1993**, *271*, 1035-1041.
(47) Van den Mooter, G.; Augustijns, P.; Kinget, R. *Int.J.Pharm* **1998**, *164*, 81-89.
(48) Graciani, M. D. M.; Rodriguez, A.; Muñoz, M.; Moyá, M. L. *Langmuir* **2003**, *19*, 8685-8691.

CHAPTER 6

EFFECTS OF HYDROPHOBICALLY-MODIFIED SUGARS ON THE VESICLE-CATALYSED KEMP ELIMINATION REACTION

*The rate-determining deprotonation of 5-nitrobenzisoxazole (Kemp elimination) by hydroxide ions is efficiently catalysed by vesicles formed from dimethyldi-n-octadecylammonium chloride (**$C_{18}C_{18}$+**). Gradual addition of n-dodecyl-β-glucoside (**C_{12}Glu**) and n-dodecyl-β-maltoside (**C_{12}Mal**) leads to an increase in the observed catalysis. A detailed kinetic analysis, taking into account substrate binding site polarities, counterion binding percentages and binding affinity of the kinetic probe, suggests that the catalytic changes depend strongly on the detailed structure of the additive. Whereas the **C_{12}Glu**-induced effect can be explained by an increase in the vesicular rate constant (k_{ves}), the effect of **C_{12}Mal** can only be explained by an increase in the binding constant of the kinetic probe (K_S). However, for these pyranoside-containing vesicles others factors, such as dehydration of the hydroxide ion, and micelle formation have to be considered.*

The kinetic analysis is discussed with respect to changes in the main phase transition temperature and membrane polarity.

The results obtained indicate that the presence of sugar-based lipids in biological membranes can strongly increase the observed rate of deprotonation reactions. The details of the mechanism of acceleration (increase in k_{ves}, and/or increase in K_S) are a complex interplay between the number and type of the sugar units in the head group.

6.1 Introduction

Almost all animal cell plasma membranes contain about 5-25% of glycolipids (GL).[1,2] Glycolipids are lipids that have an oligosaccharide head group rather than, for example, a phosphatidylcholine (PC) or phosphatidylethanolamine (PE) head group. They reside preferably in the outer leaflet of membranes,[3] and therefore it is believed that GLs play an important role in the interaction of cells with their environment.[4,5] Especially since there is a large potential of possible structures, there can be a large variety of functions. For example, GLs can act as receptor for recognition or as protection against harsh conditions (low pH, degradative enzymes). Another feature of GLs is to influence the interlipid spacing and therefore the lateral pressure profile of the membrane.[6] Since sugar units are rather bulky, their presence in membranes leads to an increased curvature.[7]

In model membranes and/or micelles, the presence of sugar moieties in the Stern region gives rise to several new properties, such as a relatively low effective dielectric constant,[8] hydroxide-ion adsorption onto the vesicular surface, [9-15] dehydration of the polar shell[16-18] and weak carbohydrate-carbohydrate interactions (under debate).[19-27] Some of these properties have been attributed to the extent to which the sugar groups fit into the water

structure.[28-30] However, most of these properties are only poorly understood, since subtle changes in the molecular structure can induce large changes in the properties. Currently, the field of carbohydrate-related amphiphilic systems is emerging.

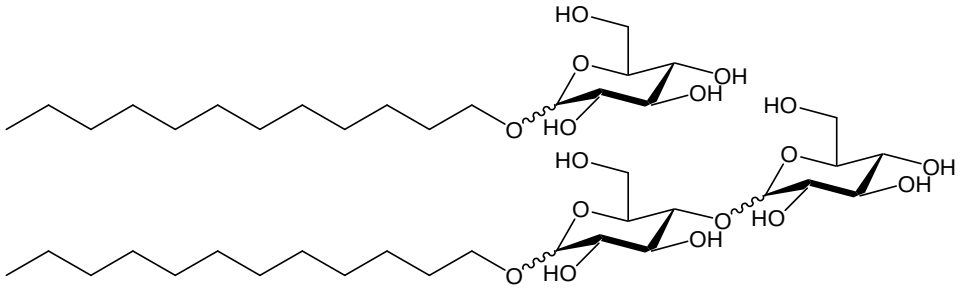

Scheme 6.1. *n-Dodecyl-β-glucoside (top) and n-dodecyl-β-maltoside (bottom).*

These intriguing properties of GLs made us decide to study the effects of two sugar-based surfactants (fourth class of additives) that bind to cationic vesicles formed from dimethyldi-*n*-octadecylammonium chloride (**$C_{18}C_{18}$+**) on the base-catalysed reaction of 5-nitrobenzisoxazole (Scheme 6.2).[31] In order to limit the number of possible interactions of the sugar groups with their environment the structurally simple *n*-dodecyl-*β*-glucoside (**C_{12}Glu**) and *n*-dodecyl-*β*-maltoside (**C_{12}Mal**; Scheme 6.1) were chosen. In order to ascertain anchoring of the sugars into the membranes *n*-dodecyl tails were chosen, since shorter tails lead to a decrease in the binding efficiency of these surfactants to vesicles[32] and longer alkyl tails increase the Krafft temperature, which makes sample handling/preparation and data analysis more difficult.[9,33] In addition, these compounds are commercially available in high purity.

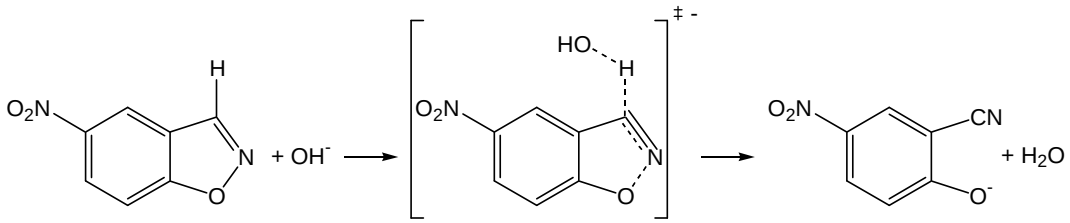

1

Scheme 6.2. *Kemp elimination reaction.*

The structures of the sugar-based surfactants are logical extensions of the *n*-alcohols studied in Chapter 4, making it easier to discriminate between the influence of the hydrophobic anchor and the sugar head group. In addition, it allows making distinction between the influence of the mono- and dihydric alcohols studied in Chapter 4 on the one hand, and the polyhydric alcohols studied in this chapter on the other hand.

The bimolecular base-catalysed deprotonation reaction of 5-nitrobenzisoxazole (**1**; Scheme 6.2) is sensitive to the local environment and the local hydroxide-ion concentration as has been discussed in Chapter 1 and 3.

6.2 Experimental

Materials and the vesicle preparation have been described in Chapter 2, kinetic experiments in Chapter 3.
DOPC (>99%; Avanti) was used as received. GS4 was synthesised according to the literature.[15]

6.3 Results and Discussion

6.3.1 Kinetic Analysis

The observed rate constants were analysed using a slightly modified version of the pseudophase model with ion exchange developed by Menger[34] and Romsted[35] and which we used in Chapter 4 and 5.

$$k_{obs} = \frac{k_w[OH^-]_{tot} + (k_{ves}K_S - k_w)m_{OH}[C_{18}C_{18}+]}{1+K_S[amph]_{tot}} \tag{6.1}$$

$$m_{OH}^2 + m_{OH}\left[\frac{[OH^-]_{tot} + K_{OH}^{Cl}[Cl^-]_{tot}}{(K_{OH}^{Cl}-1)[C_{18}C_{18}+]} + \beta\right] - \left[\frac{\beta[OH^-]_{tot}}{(K_{OH}^{Cl}-1)[C_{18}C_{18}+]}\right] = 0 \tag{6.2}$$

In these equations k_{obs}, k_w and k_{ves} are the observed, aqueous and vesicular rate constant, respectively. K_S is the binding constant of the kinetic probe to the bilayer (amphiphile and additives). K_{OH}^{Cl} is the exchange constant for binding of hydroxide and chloride ions to the bilayer and β is the total counterion binding to the bilayers. $[OH^-]_{tot}$ is the total hydroxide-ion concentration and m_{OH} is the ratio of concentrations of bound hydroxide ions and cationic amphiphiles.
The ion-exchange constant K_{OH}^{Cl} can be calculated under the assumptions mentioned in Chapter 3 via eq. (6.3):

$$\frac{1}{k_{obs}} = \frac{1 + K_S[C_{18}C_{18}+]_{tot}}{k_{ves}K_S[C_{18}C_{18}+]_{tot}\beta} + \frac{(1 + K_S[C_{18}C_{18}+]_{tot})K_{OH}^{Cl}}{k_{ves}K_S[C_{18}C_{18}+]_{tot}\beta[OH^-]_{tot}}[Cl^-]_{tot} \tag{6.3}$$

6.3.2 Kinetic Experiments and Fitted Parameters

6.3.2.1 Ion Exchange Constant

In order to study the relative binding efficiency of chloride and hydroxide ions, the observed rate constants were measured as a function of the chloride-ion concentration by externally adding chloride ions. Since chloride ions will expel hydroxide ions from the Stern region, the observed rate constants will decrease. Fitting the data using eq. (4.3) the ion exchange constant can be obtained. In Figure 6.1 the observed rate constants versus the total chloride concentration are shown. The calculated values for K_{OH}^{Cl} from the fits are given in Table 6.1. The fits are good and agree well with earlier observations (Chapter 3-5), and therefore we used a value of 1.6 for K_{OH}^{Cl}.

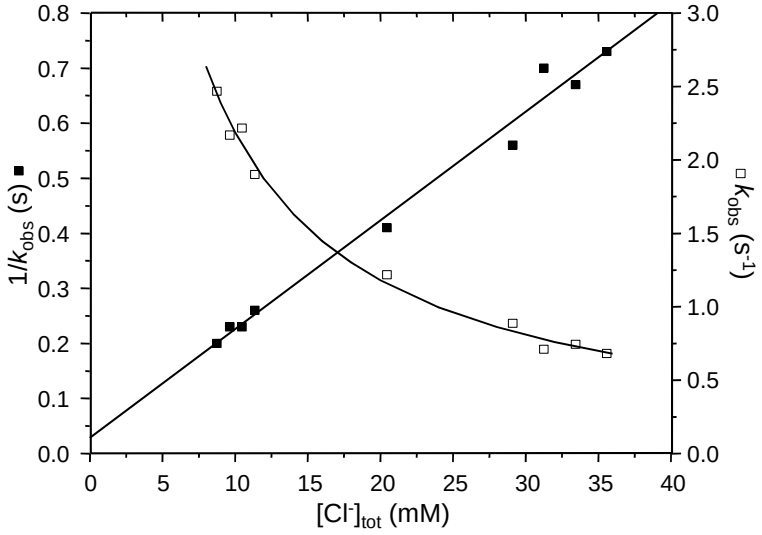

Figure 6.1. *Linear (■) and non-linear (□) plots used to calculate K_{OH}^{Cl} for 26 mol% of* ***C_{12}Glu****. Lines are best fits.*

Table 6.1. *Values of K_{OH}^{Cl} obtained from linear and non-linear fits.*

Solution	slope	intercept	K_{OH}^{Cl} [a]	slope	intercept	K_{OH}^{Cl} [b]
100% **$C_{18}C_{18}$+**	477 ± 19	0.58 ± 0.06	1.8 ± 0.2	480 ± 21	0.62 ± 0.17	1.7 ±0.5
26% **C_{12}Glu**	19.7 ± 0.9	0.0283 ± 0.0005	1.6 ± 0.1	19 ± 3	0.03 ± 0.02	1.3 ± 0.9

[a] From a linear fit. [b] From a non-linear fit.

6.3.3 Catalytic Effects upon the Addition of Various Linear Alcohols

6.3.3.1 Experimental Observations

Upon the addition of **C_{12}Glu** and **C_{12}Mal** to vesicles formed from **$C_{18}C_{18}$+** the observed rate constants increase with increasing *n*-alkyl pyranoside content up to 50 mol% (Figure 6.2). At 50 mol% of pyranoside the maximum observed rate constant is 7 and 4 times higher than in the absence of **C_{12}Glu** and **C_{12}Mal**, respectively.

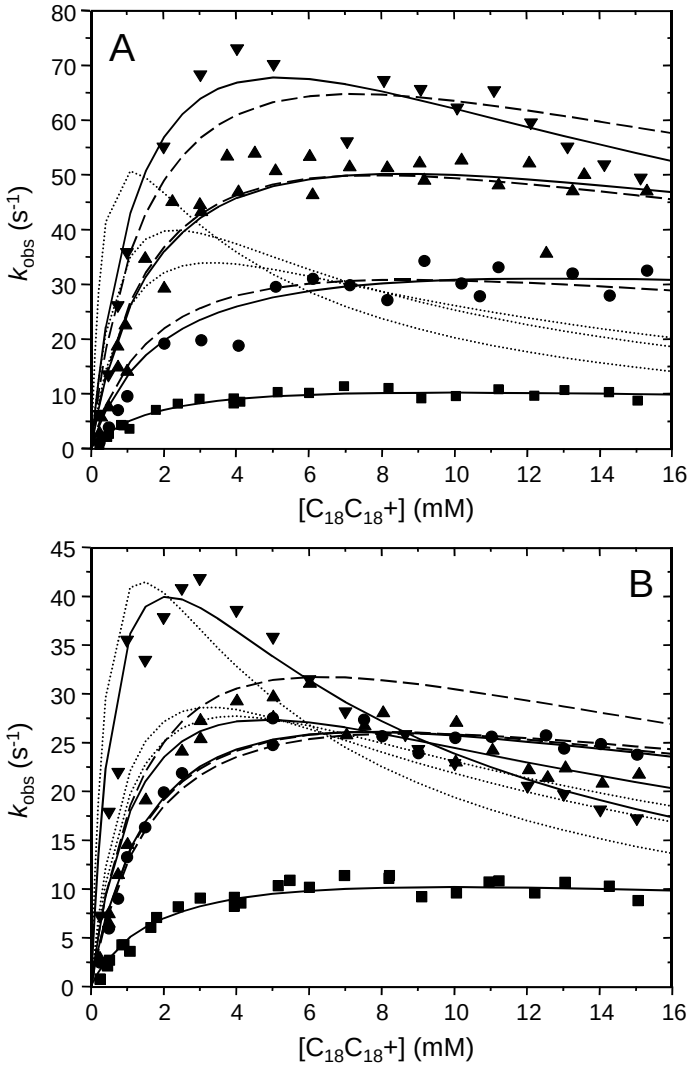

Figure 6.2. *Kinetic curves for* ***$C_{18}C_{18}$+*** *vesicles with* ***C_{12}Glu*** *(A),* ***C_{12}Mal*** *(B) where the additive is present in 0 mol % (■), 10 mol% (●), 25 mol% (▲), and 50 mol% (▼). Solid lines are fits allowing k_{ves} and K_S to vary, dotted lines are fits allowing K_S to vary, and dashed lines are fits allowing k_{ves} to vary.*

6.3.3.2 Fitting Procedures

As in Chapter 4 the experimental data was fitted via several different procedures in order to quantify the extent of parameter compensation. Taking into account that two of the four unknown parameters do not change, or only to a negligible extent considering the large change in observed rate constants, the ion exchange constant K_{OH}^{Cl} (taken as 1.6)[36] and the counterion binding (taken as 0.89) were not allowed to vary. In the first and second method only one of the two remaining parameters, K_S and k_{ves}, was allowed to vary. The other parameter was taken from the fit of the solution containing 100 mol% of **$C_{18}C_{18}$+** (k_{ves} = 295 s^{-1} and K_S = 32 M^{-1}). In the first method k_{ves} was allowed to vary and in the second method K_S was allowed to vary. As can be seen in Figure 6.2 the second method does not lead to any reasonable fit, and the first method only leads to reasonable fits for 10 and 25 mol% of

C_{12}Glu and 10 mol% of **C_{12}Mal**. Therefore, as was also observed in Chapter 4, the most reasonable fits were obtained by allowing both k_{ves} and K_S to vary.

From Figure 6.3 the different results for **C_{12}Mal** and **C_{12}Glu** are obvious. Whereas for **C_{12}Glu** the increase in the maximum observed rate constant mainly comes from an increase in k_{ves}, for **C_{12}Mal** this effect mainly originates from an increase in K_S. In fact above 10 mol% of **C_{12}Mal** k_{ves} *decreases* upon addition of more pyranoside. It should be noted that **C_{12}Mal**, just as the more often used **C_{10}Mal**, can be used as a membrane solubilising agent.[32] Therefore, as discussed in Chapter 2, at higher mole fractions the vesicles will be (partially) solubilised. However, dynamic light scattering experiments (at 0.5 mM **$C_{18}C_{18}$+**) show that there are still large aggregates present in the solution, although the decreased scattered intensity indicates that there is also significant (worm-like) micelle formation. The relative amount of amphiphile in vesicles and micelles depends on the total concentration of both amphiphile and single-tailed surfactant.

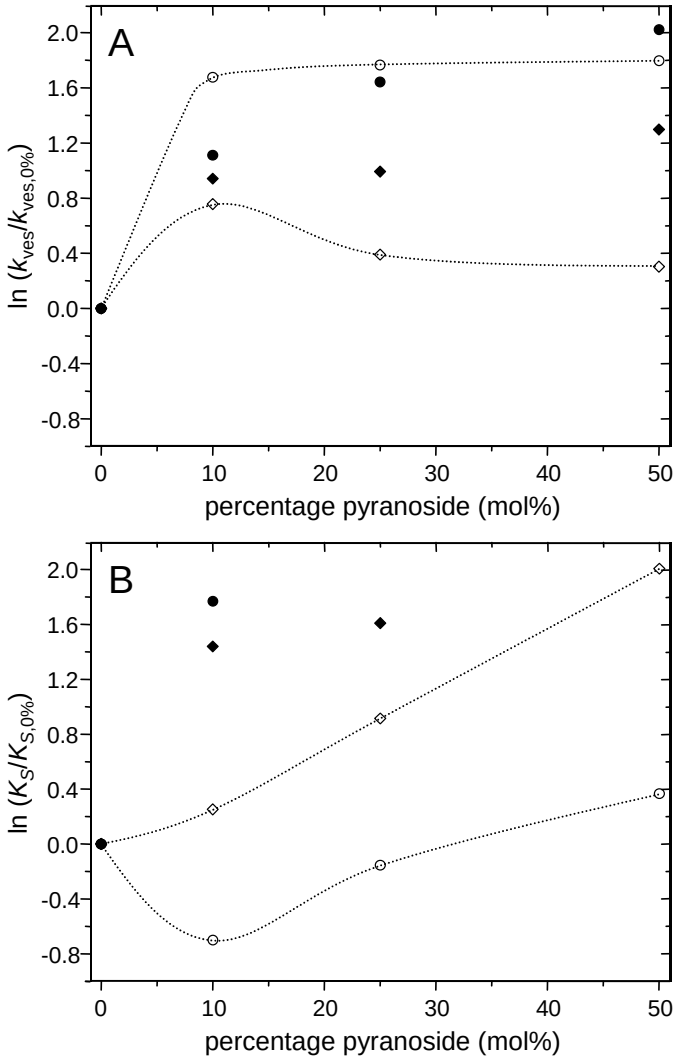

Figure 6.3. *Plot of ln ($k_{ves}/k_{ves,0\%}$) (A) and ln ($K_S/K_{S,0\%}$) (B) versus the mol% of the added pyranoside. Fits were obtained by allowing both k_{ves} and K_S to vary (open symbols), or by allowing only one parameter to vary (closed symbols).* ***C_{12}Glu*** *(○);* ***C_{12}Mal*** *(◇). Lines are only drawn to guide the eye.*

As we already discussed in Chapter 5, when both micelles and vesicles are present in solution the kinetic analysis becomes more complex. The current model (eqs. (6.1) and (6.2)) only takes into account two pseudophases; an aqueous one and a vesicular one. Addition of a micellar one would lead to more variables, making it impossible to obtain any meaningful number for the fitted parameters. Therefore we do not perform this analysis quantitatively, but only qualitatively. The Kemp elimination is slower in micelles than in vesicles (Chapter 5), since these aggregates contain more water in their Stern region. Upon increasing amounts of **C_{12}Mal** (worm-like) micelles are formed, and therefore the micellar rate constant will be more pronounced in the fitted value of k_{ves}. This effect can be seen in Figure 6.3A where k_{ves} decreases again after an initial increase. This decrease is not seen for **C_{12}Glu** which is not able to solubilise vesicles. Instead, k_{ves} increases with increasing **C_{12}Glu** content in the vesicles. The inability of **C_{12}Glu** to solubilise vesicles is nicely shown by Carion-Taravella *et al.*[37] who showed that vesicles were formed upon enzymatic hydrolysis of **C_{12}Mal** to **C_{12}Glu** starting from mixed micelles containing **C_{12}Mal** and DPPC.

As discussed in Chapter 2 the binding constant of single-tailed surfactants to membranes is inversely related to their CMC.[32,38] Despite that we were not able to solubilise **C_{12}Glu** in pure water, CMC values have been reported[9,32,39,40] leading to an estimated binding constant of around $2 \cdot 10^4$ M^{-1} (above 0.9 mM amphiphile more than 95% is bound).[32] Therefore we can safely assume that the amount of **C_{12}Glu** in the aqueous phase is negligible. The CMC of **C_{12}Mal** is slightly higher[8,9,32,41] and hence the binding constant is slightly smaller than that of **C_{12}Glu**. However, its binding constant ($5 \cdot 10^3$ M^{-1}) is smaller, only leading to full binding (>95%) to the membrane above 3.5 mM amphiphile.[32]

The large increase in K_S for the **C_{12}Mal**-containing solutions is striking, whereas for **C_{12}Glu** the increase in K_S amounts to only a factor of 2 after an initial decrease at low mole fraction. Apparently, despite the structural similarity between **C_{12}Glu** and **C_{12}Mal**, the effect of both additives on the fitted parameters is quite different (section 6.3.4). We speculate that this is the result of a complex interplay between a disturbance of the bilayer packing by these single-tailed surfactants (increase in water content in the polar-apolar interface) and a partial dehydration (water replacement) of the Stern region by sugars (decrease in water content at the polar-apolar interface). These properties of alkyl pyranosides are discussed in more detail in Section 6.3.4.

Binding of **1** to vesicles is a result of stabilisation of the initial state in the vesicular pseudophase relative to the aqueous pseudophase. An increase in K_S originates from a further stabilisation in the vesicular pseudophase. By contrast, an increase in the vesicular rate constant originates from a decrease in the Gibbs energy of activation. Apparently, addition of **C_{12}Glu** induces the latter effect.

6.3.3.3 Hydroxide-Ion Adsorption and Hydration

In the fitting procedures, specific binding of hydroxide ions to the sugar-based surfactants was not taken into account. Therefore we did control experiments to see whether such binding can actually be neglected, since certain nonionic sugar-derived surfactants are able to induce adsorption of hydroxide ions onto the vesicular surface. [9-15] However, the adsorption mechanism of this hydroxide binding has not yet been revealed, although the

structure of the first hydration shell of the polar-apolar interface might be important.[42] Pure DOPC does not adsorb these ions,[14,15] although there is evidence that tiny amounts of hydroxide ions are able to bind.[43] Despite this latter observation, in a first control experiment we compared the observed rate constants in a system with DOPC (Scheme 6.3) and DOPC with 25 mol% of **C_{12}Glu**. As can be seen in Figure 6.4A both types of vesicles show inhibition with respect to the rate constant in pure water (dashed line). As a reference we measured the rate constant for a nonionic sugar-based gemini surfactant (GS4; Scheme 6.3) synthesised in our laboratory,[14,15] for which it has been proven that hydroxide-ion binding takes place. As can been seen, this surfactant *catalyses* the Kemp deprotonation reaction. Therefore we can exclude that there is specific hydroxide binding by **C_{12}Glu**.

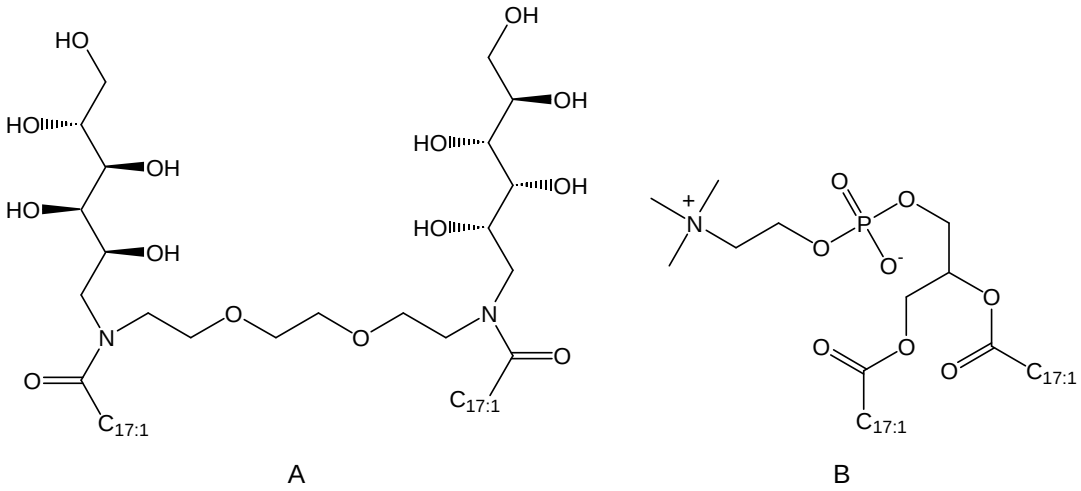

Scheme 6.3. *GS4 (A) and dioleylphosphatidylcholine (DOPC; B).*

Now it is necessary to consider the unexpected (*i.e.* anti-Hofmeister) preferential binding of hydroxide ions over chloride ions. The reasonable value we obtained for K_{OH}^{Cl} (Table 6.1) does not indicate such a process. However, considering that each sugar unit has five hydrogen bond donors (and six acceptors), we anticipate that these might increase the binding of hydroxide ions relative to chloride through (multiple) hydrogen bonds. In a second experiment (Figure 6.4B) we compared four different vesicular solutions. Solution A contained 100 mol% of **$C_{18}C_{18}$+**, and solution B 35 mol% of **$C_{10}C_{10}$-** (**$C_{18}C_{18}$+**:**$C_{10}C_{10}$-**:**C_{12}Glu** = 65:35:0). The maximum observed rate constants of these solutions differ by a factor of about ten, due to a reduced counterion binding (27%) to the excess **$C_{18}C_{18}$+** in solution B (Chapter 3). Then about 10 mol% of **C_{12}Glu** was added to solutions A and B, which gave solutions C (90:0:10) and D (61:33:7), respectively. The maximum observed rate constants increased by a factor of 3 and 5 going from solution A to C and B to D, respectively.

In an attempt to fit the data of solution C and D by only changing the counterion binding and the ion exchange constant K_{OH}^{Cl} (keeping K_S and k_{ves} constant) we only found a fit for solution D. It was not possible to fit the data of solution C. Not even when only hydroxide ions were considered as counterions, since there is only 2.25 mM hydroxide ions in solution. Above this concentration the two reagents are diluted within the vesicular pseudophase. In addition, in both cases the value of K_{OH}^{Cl} was just slightly above the mathematically and chemically acceptable lower limit of 1 (compare eq. (5.2)).

Therefore, we decided to fit the data again, but use the Langmuir isotherm and mass balance to calculate the vesicular hydroxide concentration (m_{OH}; eq.(5.1)) instead of using eq. (5.2).[44] The advantage is that instead of a relative binding constant for hydroxide and chloride ions, K_{OH}^{Cl}, and a fixed counterion binding β, the Langmuir isotherm uses separate binding constants for both ions, K_{OH} and K_{Cl}, respectively. The disadvantage is that the ion concentrations in the Stern region have to be calculated iteratively. For moderate salt concentrations and the presence of at least one counterion with a binding constant that is not too small, the concentration of vesicular-bound hydroxide ions in both models is comparable to that obtained from the ion exchange model,[45] except that the ion exchange model has a higher concentration of bound hydroxide ions at amphiphile concentrations below 2 mM.

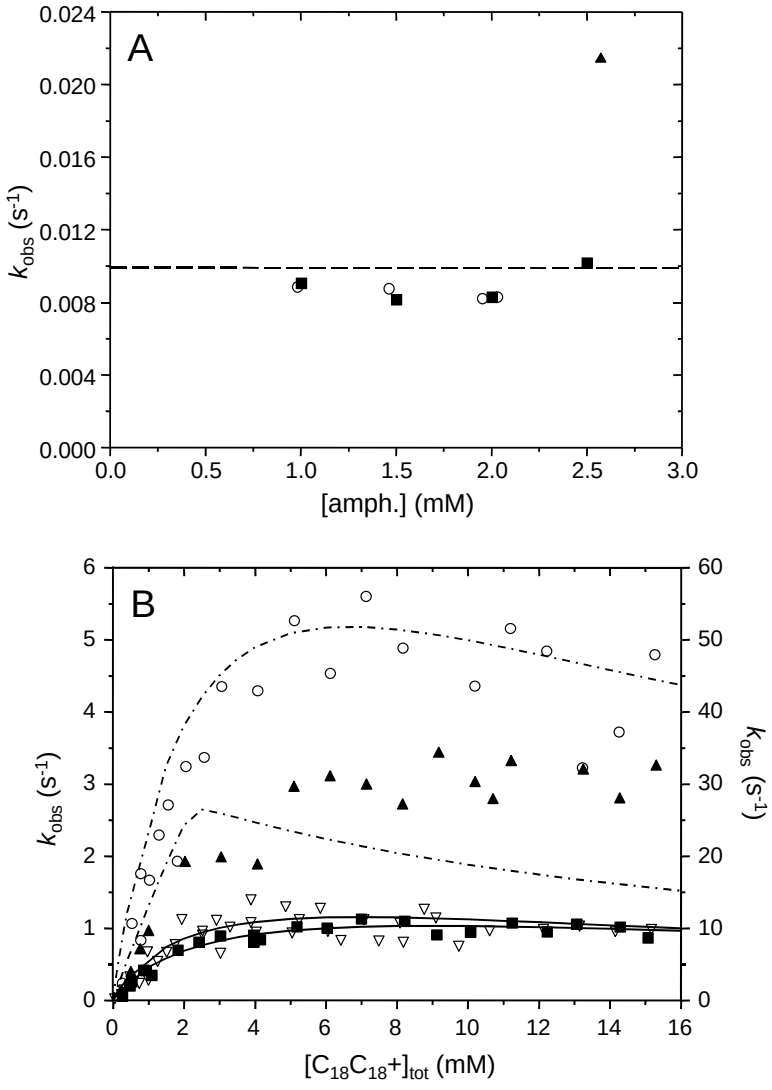

Figure 6.4. *A: Observed rate constant for DOPC (■), DOPC with 25 mol% of* ***C_{12}Glu*** *(○) and GS4[14,15] (▲). Dashed line represents the rate constant in water.* ***B:*** *Observed rate constant of vesicles with different degrees of counterion binding with and without* ***C_{12}Glu****. Left axis:* ***$C_{18}C_{18}$+:$C_{10}C_{10}$-:C_{12}Glu*** *65:35:0 (▽) and 61:33:7 (○). Right axis: 100:0:0 (■) and 90:0:10 (▲). Lines are best fits using the Langmuir isotherm of ion adsorption and a constant value for K_S and k_{ves}.*

For obvious reasons the data of solution C could still not be fitted, but it was possible to fit the data of solution D with a binding constant K_{OH} that was 7.5 times larger than that for the data of solution B.[46] These latter results indicate that preferential binding might play a role in systems containing alkyl pyranosides, but considering that the data of solution C could not be fitted, additional effects have to play a role as well, leading to further changes in k_{ves} and K_S. This latter observation is reasonable since the addition of linear alcohols (which are just alkyl pyranoside without the sugar part) induces changes in k_{ves} and K_S (Chapter 4).

6.3.3.4 Potential Deprotonation of Sugar Hydroxyl Groups

The possibility of deprotonation of sugar hydroxyl groups has to be considered, since it might affect the catalysis of the Kemp elimination reaction in vesicles formed from **$C_{18}C_{18}$+** in the presence of **C_{12}Glu** and **C_{12}Mal**. In this section a number of arguments about the probability of deprotonation will be given as well as expected effects on the catalysis will be discussed.

The pK_a of the hydroxyl groups of glucose and maltose is typically around 12-13,[47] which is 2 to 3 units lower than the average pK_a of monohydric *n*-alcohols.[48] The pH of the vesicular solutions under study is 11.4 ([OH^-] = 2.25 mM). This suggests that the hydroxyl groups of the sugar moiety of **C_{12}Glu** and/or **C_{12}Mal** incorporated in vesicles formed from **$C_{18}C_{18}$+** will not be significantly deprotonated under these circumstances.

However, in general, two effects have to be considered for deprotonation of acids (*e.g.* alcohols) bound to the vesicular surface.[49] The first effect arises from the positive surface charge of vesicles formed from **$C_{18}C_{18}$+**, leading to the attraction of anions, such as hydroxide ions. As a result, the ion concentration in the Stern region is in the order of a few molar.[50-53] Consequently, the surface pH might be in the order of 13-15, which is above the pK_a of glucose and maltose.

It should be noted that due to the choice of a constant total hydroxide-ion concentration and competition with chloride ions to bind to the cationic charges, in the kinetic experiments described in Section 6.3.3 the surface pH depends on the amphiphile concentration (eq. (5.2)). At low amphiphile concentration the surface pH will be highest. Hence, if deprotonation of hydroxyl groups occurs, the fraction of deprotonated hydroxyl groups will decrease if the pH becomes low enough (*i.e.* close to or below the pK_a of the sugar hydroxyl groups).

The second effect results from a change in medium properties. Upon going to the vesicular pseudophase, the local polarity decreases and the hydration of both hydroxide ions and sugars changes relative to the bulk aqueous pseudophase. In general, a decrease in polarity and/or hydration leads to an increase in pK_a value for water and other acids, due to destabilisation of the anion in apolar (aprotic) media.[48] For example, the pK_a of water, methanol and ethanol in water is around 15.5, whereas it increases to around 30 in DMSO.

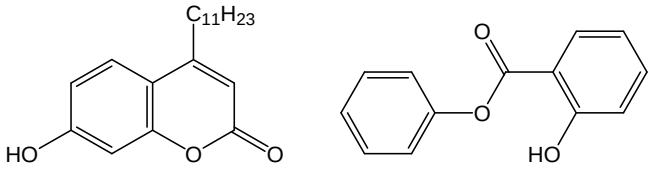

A B

Scheme 6.4. *Hydrophobically-modified hydroxycoumarin (A) and phenyl salicylate (B).*

The two effects have an opposing effect, and therefore upon binding of acids to positively charged membranes the pK_a value of these acids might increase, decrease or not change at all. Some examples of pK_a shifts of micellar-bound acids are known from the literature. Early work on indicators bound to cationic micelles showed that the pK_a values of acids are affected, but conclusions were hampered due to experimental limitations.[54] Later work has overcome these problems. For example, the bulk pH at which 50% of hydrophobically-modified hydroxycoumarin (Scheme 6.4) is deprotonated in the presence of CTAB micelles is lowered by about 1.5 units relative to water.[55] In the case of phenyl salicylate (Scheme 6.4) the bulk pH at which 50% is deprotonated is unaffected by the presence of CTAB micelles.[56] These examples include structures of which the anionic charge can be delocalised upon deprotonation leading to a less unfavourable situation relative to structures where charge delocalisation is not possible. Therefore, in the case of the sugar hydroxyl groups, where charge delocalisation is not possible, we anticipate that the approximate thousand-fold increase in hydroxide-ion concentration at the vesicular cationic surface (local pH around 13 to 15), cannot compensate for the increase in pK_a of the sugar hydroxyl groups as a result of the decrease in polarity. This means that we expect that the change in polarity leads to a pK_a of the sugar hydroxyl groups that is at least larger than 15.

As briefly discussed in sections 6.1 and 6.3.3.3, nonionic sugar-based amphiphiles are able to adsorb hydroxide ions.[9-15] This conclusion was made on the basis of observed negative ζ potentials. In fact, other nonionic hydrophobic surfaces, such as oil droplets,[42,57] gas bubbles[58-60] and oligo ethylene glycol surfactants[61-65] are also able to adsorb these ions. Although the details of the mechanism(s) of adsorption have not yet been revealed,[66] it has been ruled out that the negative ζ potentials are due to adsorption of other anions (Cl^-, HCO_3^-) or anionic (organic) impurities, or due to depletion of H^+.[14,15,42] Besides the argument of the increase in pK_a values (previous paragraph) also on the basis of the general appearance of the adsorption phenomenon (*i.e.* adsorption occurs to different types of nonionic hydrophobic surfaces), it seems unlikely that in the case of sugar-based surfactants, despite the relatively high surface pH, hydroxyl groups are deprotonated.

If it is assumed that deprotonated sugar-hydroxyl groups are present in the Stern region then two pathways for the Kemp elimination are possible: (i) a hydroxide-ion catalysed pathway, and (ii) a deprotonated-sugar catalysed pathway. Eq. (5.1) only accounts for the hydroxide-ion catalysed pathway. In addition, the fraction of deprotonated hydroxyl groups might vary with amphiphile concentration as a result of a decreasing surface pH. Consequently, the deprotonated-sugar catalysed pathway becomes less important at higher amphiphile concentrations. Assuming that the deprotonated-sugar catalysed reaction has a

higher rate constant than the hydroxide-ion catalysed reaction, an increase in observed rate constants at low amphiphile concentration is expected, decreasing relatively sharply at higher amphiphile concentration.[67] The use of eq. (5.1) in such a situation would lead to an increase in K_S. In fact, for both vesicular solutions containing **C_{12}Glu** and **C_{12}Mal** an increase in K_S is observed. The pK_a values of maltose and glucose do not vary much. However, the number of hydroxyl groups per sugar does, and therefore a larger effect is expected for vesicular solutions containing **C_{12}Mal**. Similarly, a larger effect is expected increasing the mole fraction of pyranoside. As can be seen in Figure 6.2 the expected trends are observed, indicating that deprotonation might occur in these solutions.
In conclusion, most arguments point in the direction that deprotonation of hydroxyl groups of sugars is unlikely. However, on the basis of the kinetic data it cannot be ruled out.

6.3.3.5 A Simple Stern Region Mimic

In an attempt to study the influence of high concentrations of sugar groups in the Stern region on the vesicular rate constant we measured the aqueous rate constant in solutions containing solely up to 500 mM of glucose. In these solutions the normalised polarity ($P^{w/d}$; Chapter 2) as sensed by the $E_T(30)$ dye decreases from 1 to 0.94.[68] Based on experiments in water-1,4-dioxane and water-acetonitrile mixtures (Chapter 3) this change in polarity should increase the observed rate constant by a factor of around 2. However, we observed a (non-linear) *decrease* in the observed rate constant by a factor of at most 5 at 500 mM of glucose (Figure 6.5). Considering the large increase (*ca.* 5 fold; Figure 6.3A) in vesicular rate constant in vesicles formed from **$C_{18}C_{18}$+** and **C_{12}Glu**, this water-glucose mixture is most likely only a poor representation of a Stern region. In fact, various mixtures of water, an organic solvent and a salt have been used as a Stern region mimics,[50,52,69,70] but it appears that several different mixtures can mimic the Stern region depending on the type of reaction. A complex mixture of glucose, a salt resembling the head group of **$C_{18}C_{18}$+** and an organic solvent such as *n*-propanol should, in principle, resemble the Stern region of a vesicle formed from **$C_{18}C_{18}$+** and **C_{12}Glu** more accurately. However, it will be difficult to determine reasonable concentrations of these additives and their relation to the properties of the Stern region. In addition, the conformation of the glucose moiety in **C_{12}Glu** is restricted in vesicular membranes due to the anchoring by the hydrophobic tail,[71,72] an effect that cannot be mimicked in these mixtures.
Hydrolysis reactions are also decelerated in aqueous solutions containing sugars.[73-75] However, they are inhibited to a lesser extent (only about 10% at 0.5 molal) than for the reaction of **1** with hydroxide ions. The natural logarithm of the relative rate of the alkaline hydrolysis of an iron(II)-complex deviates from linearity with respect to the molal concentration of sugar, similar to our observations.[76] However, it should be noted that the extent to which deceleration is observed and the magnitude of deviation from linearity are significantly smaller compared to what has been observed for the reaction of **1** with hydroxide ions in the presence of glucose. Unfortunately, a detailed explanation for the effects of sugars on these reactions is lacking at the moment.

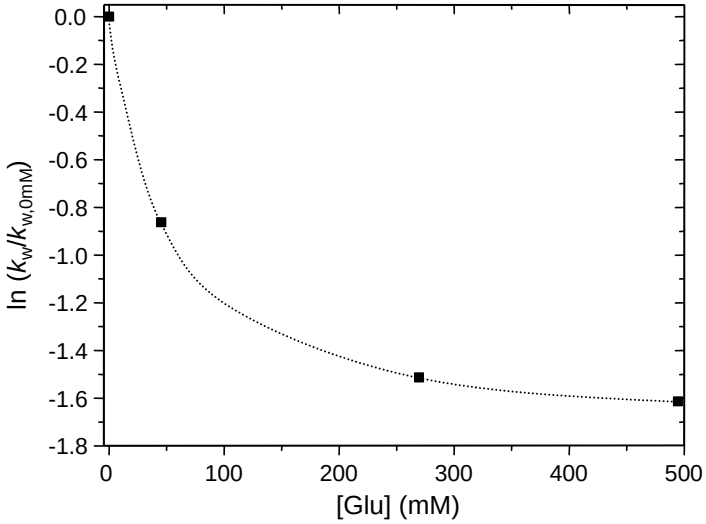

Figure 6.5. *Observed aqueous rate constants (■) as a function of the concentration of glucose in water. The line is only drawn to guide the eye.*

6.3.4 Kinetic Consequences of Changes in Membrane Properties

In Chapter 2 the bilayer properties with respect to the main phase transition temperature and the polarity as sensed by a variety of fluorescent and absorption dyes was measured. Strikingly, the changes in k_{ves} and K_S for vesicular solutions containing alkyl pyranosides are not apparent from the changes in measured normalised polarity, or by a transition of the tails from gel-like to liquid-crystalline. Since we expect that the vesicular rate constant scales with the normalised polarity as sensed in vesicles, similarly as in mixtures of water/1,4-dioxane and water/acetonitrile, the vesicular rate constant should not change too much.

Compared to the influence on k_{ves} and K_S in vesicles containing **C_{10}OH** (*n*-decanol), which has a similar mismatch in tail size with **$C_{18}C_{18}$+** as **C_{12}Mal** and **C_{12}Glu** do, the differences are remarkable. Since **C_{10}OH** has only a small effect, we can attribute the observed changes in k_{ves} and K_S fully to the presence of glucose and maltose in the Stern region. Interestingly, going from the addition of the monohydric alcohol **C_{18}OH** (*n*-octadecanol) to the dihydric alcohol **C_{18}GlyOH** (batyl alcohol) the vesicular rate constant is increased (by a factor of *ca.* 2), similar as going from **C_{10}OH** to **C_{12}Glu**. However, the increase for the latter change in bilayer composition is much larger (by a factor of *ca.* 5). In addition, the binding constant of the kinetic probe is decreased which is not in agreement with the observations in this chapter.

Nonionic micelles containing **C_{12}Mal** or **C_{12}Glu** have an interface that is "aqueous-like" in nature,[8] *i.e.* the effective dielectric constant is larger than that for nonionic micelles with an oligo-ethylene oxide head group. **C_{12}Glu** and **C_{12}Mal** retain their hydration cospheres, and, as a result, anions present in the same region are less hydrated similar to what has been observed for mixed micelles of CTAB and a nonionic cosurfactant (**C_{10}SO**, **C_{12}PO**; Scheme 4.4),[77,78] leading to an increase in k_{ves} (as discussed in Chapter 1).[79-81] Since the ion exchange constant does not change upon the addition of **C_{12}Glu** (Section 6.3.2.1), it can be

concluded that both hydroxide ions and chloride ions are dehydrated to a similar extent since otherwise the ion exchange constant would have changed as well. This observation is confirmed by the inability to fit the data of solution C (Section 6.3.3.3) by only allowing the ion exchange constant (or K_{OH}) to vary.

The observation of ion dehydration has also been noted for mixed micelles of SDS and *n*-dodecylmalono-bis-*N*-methylglucamide. Below a mole fraction SDS of 0.3, the head group region is completely dehydrated, since the sugar units have replaced all the water molecules in the interfacial region.[17] However, at this stage the counterion binding is still about 40%. The dyes used to measure the local polarity are (apparently) not sensitive towards these changes, and hence they report a constant polarity upon increasing amounts of **C_{12}Mal** and **C_{12}Glu**. If this process is also occurring for **C_{12}Glu**, and especially for **C_{12}Mal**, the polar-apolar interface is very poor in water content leading to a further lowering of the initial state, and hence a strong increase in K_S.

Considering the observations above and those made in Chapter 5 about micelle formation, we speculate that upon binding of a single-tailed surfactant (alkyl pyranoside) the bilayer packing is disturbed. This leads to an increase in water content in the Stern region. The magnitude of this effect is more pronounced if the sugar head group is larger. As a result, this leads to a lowering in k_{ves} and K_S. However, the sugar head groups will replace water from the Stern region at the same time, leading to dehydration of ions. As a result of the latter process, k_{ves} and K_S will increase. Due to different structures of the head groups of the alkyl pyranosides these two opposing effects will have different magnitudes for both k_{ves} and K_S in both mixed systems of **$C_{18}C_{18}$+** with **C_{12}Glu** and **C_{12}Mal**, respectively.

6.4 Conclusions

Cationic vesicles of **$C_{18}C_{18}$+** catalyse the Kemp elimination *ca.* 50 times relative to the second-order rate constant in water (Chapter 3). This effect is mainly attributed to a change in polarity going from water to the aqueous pseudophase, where partial dehydration of the hydroxide ion is the main contribution to the rate enhancement.

The observed catalysis is increased upon the addition of **C_{12}Mal** and **C_{12}Glu**. A detailed kinetic analysis reveals that addition of **C_{12}Glu** leads to an increase in k_{ves} by a factor of about 5. At low mole percentage, **C_{12}Mal** also shows an increase in k_{ves}, but due to the formation of (worm-like) micelles k_{ves} decreases at higher mole fractions. The binding constant of the kinetic probe to vesicles containing **C_{12}Mal** is almost ten fold larger at 50 mol%. After a decrease of K_S in **$C_{18}C_{18}$+** vesicles containing a small mole fraction of **C_{12}Glu** content (probably due to disturbance of the bilayer packing), a 2-fold increase is also observed at higher **C_{12}Glu** content.

The effects cannot be attributed to a change in the main phase transition temperatures for these mixtures or a significant change in polarity as sensed by ANS, Nile Red, pyrene and laurdan (Chapter 2). Based on this latter observation, literature evidence on polar shell dehydration[16-18] and our observation that neither specific nor preferential hydroxide binding can satisfactory explain our observations, we anticipate that water is replaced from the polar shell. This leads to a decreased hydration of the hydroxide ion, and hence to an increase in the reactivity of the vesicle-bound hydroxide ions and an accompanying increase

in k_{ves}. In addition, this is consistent with literature evidence that sugar-based surfactants dehydrate the interfacial region, without destroying its "aqueous-like" nature.
Finally, deprotonation of hydroxyl groups of the **C_{12}Glu** and **C_{12}Mal**, leading to a different reaction pathway not accounted for in the applied equations, has to be considered. On the basis of literature data it seems unlikely that the hydroxyl groups are deprotonated. However, the kinetic data indicate that it cannot be ruled out.

6.5 Acknowledgements

Mr A. Wagenaar is gratefully acknowledged for the gift of GS4. Markus Johnsson is acknowledged for fruitful discussions on the solution behaviour of sugar-based gemini surfactants.

6.6 References

(1) Tanford, C. *The Hydrophobic Effect: Formation of Micelles and Biological Membranes*; Wiley: New York, **1980**.
(2) Alberts, B.; Bray, D.; Lewis, J.; Raff, M.; Roberts, K.; Watson, J. D. In *Molecular Biology of the Cell*; Garland Publishing: New York, **1994**; pp 477-485.
(3) Hirai, M.; Iwase, H.; Hayakawa, T.; Koizumi, M.; Takahashi, H. *Biophys.J.* **2003**, *85*, 1600-1610.
(4) Saxena, K.; Zimmermann, P.; Schmidt, R. R.; Shipley, G. G. *Biophys.J.* **2000**, *78*, 306-312.
(5) Popova, A. V.; Hincha, D. K. *Biophys.J.* **2003**, *85*, 1682-1690.
(6) Bagatolli, L. A.; Maggio, B.; Aguilar, F.; Sotomayor, C. P.; Fidelio, G. D. *Biochim.Biophys.Acta* **1997**, *1325*, 80-90.
(7) Bagatolli, L. A.; Gratton, E.; Fidelio, G. D. *Biophys.J.* **1998**, *75*, 331-341.
(8) Drummond, C. J.; Warr, G. G.; Grieser, F.; Ninham, B.; Evans, D. F. *J.Phys.Chem.* **1985**, *89*, 2103-2109.
(9) Balzer, D. *Langmuir* **1993**, *9*, 3375-3384.
(10) Waltermo, A.; Claesson, P. M.; Simonsson, S.; Manev, E.; Johansson, I.; Bergeron, V. *Langmuir* **1996**, *12*, 5271-5278.
(11) Sierra, M. L.; Svensson, M. *Langmuir* **1999**, *15*, 2301-2306.
(12) Baba, T.; Zheng, L. Q.; Minamikawa, H.; Hato, M. *J.Colloid Interface Sci.* **2000**, *223*, 235-243.
(13) Zheng, L. Q.; Shui, L. L.; Shen, Q.; LI, G. Z.; Baba, T.; Minamikawa, H.; Hato, M. *Colloids Surf.A* **2002**, *207*, 215-221.
(14) Johnsson, M.; Wagenaar, A.; Engberts, J. B. F. N. *J.Am.Chem.Soc.* **2003**, *125*, 757-760.
(15) Johnsson, M.; Wagenaar, A.; Stuart, M. C. A.; Engberts, J. B. F. N. *Langmuir* **2003**, *19*, 4609-4618.
(16) Bales, B. L.; Howe, A. M.; Pitt, A. R.; Roe, J. A.; Griffiths, P. C. *J.Phys.Chem.B* **2000**, *104*, 264-270.
(17) Griffiths, P. C.; Pettersson, E.; Stilbs, P.; Cheung, A. Y. F.; Howe, A. M.; Pitt, A. R. *Langmuir* **2001**, *17*, 7178-7181.
(18) Bales, B. L.; Ranganathan, R.; Griffiths, P. C. *J.Phys.Chem.B* **2001**, *105*, 7465-7473.
(19) Klotz, I. M.; Franzen, J. S. *J.Am.Chem.Soc.* **1962**, *84*, 3461-3466.
(20) Venkatesan, P.; Cheng, Y.; Kahne, D. *J.Am.Chem.Soc.* **1994**, *116*, 6955-6956.
(21) Simons, K.; Ikonen, E. *Nature* **1997**, *387*, 569-572.
(22) Veiga, M. P.; Goñi, F. M.; Alonso, A.; Marsh, D. *Biochemistry* **2000**, *39*, 9876-9883.
(23) Pincet, F.; Le Bouar, T.; Zhang, Y. M.; Esnault, J.; Mallet, J. M.; Perez, E.; Sinaÿ, P. *Biophys.J.* **2001**, *80*, 1354-1358.
(24) Sugahara, M.; Uragami, M.; Tokutake, N.; Yan, X.; Regen, S. L. *Langmuir* **2002**, *18*, 981-983.
(25) Bazito, R. C.; El Seoud, O. A. *Langmuir* **2002**, *18*, 4362-4366.
(26) Schneider, M. F.; Zantl, R.; Gege, C.; Schmidt, R. R.; Rappolt, M.; Tanaka, M. *Biophys.J.* **2003**, *84*, 306-313.
(27) Santacroce, P. V.; Basu, A. *Angew.Chem.,Int.Ed.Engl.* **2003**, *42*, 95-98.

(28) Uedaira, H.; Uedaira, H. *J.Sol.Chem.* **1985**, *14*, 27-34.
(29) Franks, F. *Pure Appl.Chem.* **1987**, *59*, 1189-1202.
(30) Franks, F. In *Water; A Matrix of Life*; The Royal Society of Chemistry: Cambridge, UK, **2001**; pp 86-107.
(31) Casey, M. L.; Kemp, D. S.; Paul, K. G.; Cox, D. D. *J.Org.Chem.* **1973**, *38*, 2294-2301.
(32) Heerklotz, H.; Seelig, J. *Biochim.Biophys.Acta* **2000**, *1508*, 69-85.
(33) Boyd, B. J.; Drummond, C. J.; Krodkiewska, I.; Grieser, F. *Langmuir* **2000**, *16*, 7359-7367.
(34) Menger, F. M.; Portnoy, C. E. *J.Am.Chem.Soc.* **1967**, *89*, 4698-4703.
(35) Romsted, L. S. In *Micellization, Solubilization and Microemulsions*; Mittal, K. L., ed., Plenum Press: New York, **1977**; pp 509-530.
(36) Rodríguez, A.; Muñoz, M.; Graciani, M. D. M.; Moyá, M. L. *J.Colloid Interface Sci.* **2002**, *248*, 455-461.
(37) Carion-Taravella, B.; Lesieur, S.; Ollivon, M.; Chopineau, J. *J.Am.Chem.Soc.* **1998**, *120*, 10588-10595.
(38) Heerklotz, H.; Seelig, J. *Biophys.J.* **2000**, *78*, 2435-2440.
(39) Shinoda, K.; Yamaguchi, T.; Hori, R. *Bull.Chem.Soc.Jpn.* **1961**, *34*, 237-241.
(40) Anatrace Catalogue.
(41) Kragh-Hansen, U.; le Maire, M.; Møller, J. V. *Biophys.J.* **1998**, *75*, 2932-2946.
(42) Marinova, K. G.; Alargova, R. G.; Denkov, N. D.; Velev, O. D.; Petsev, D. N.; Ivanov, I. B.; Borwankar, R. P. *Langmuir* **1996**, *12*, 2045-2051.
(43) Pincet, F.; Cribier, S.; Perez, E. *Eur.Phys.J.B* **1999**, *11*, 127-130.
(44) Rodenas, E.; Vera, S. *J.Phys.Chem.* **1985**, *89*, 513-516.
(45) Graciani, M. D. M.; Rodríguez, A.; Muñoz, M.; Moyá, M. L. *Langmuir* **2002**, *18*, 3476-3481.
(46) For solutions A to D we used K_{OH} = 380, 70, $5 \cdot 10^5$, 525 M^{-1}, respectively. K_{Cl} was kept constant at 494 M^{-1}.
(47) Izatt, R. M.; Rytting, R. H.; Hansen, L. D.; Christen, J. J. *J.Am.Chem.Soc.* **1966**, *88*, 2641-2645.
(48) Olmstead, W. N.; Margolin, Z.; Bordwell, F. G. *J.Org.Chem.* **1980**, *45*, 3295-3299.
(49) Seelig, J. *Biochim.Biophys.Acta* **1997**, *1331*, 103-116.
(50) Buurma, N. J.; Herranz, A. M.; Engberts, J. B. F. N. *J.Chem.Soc., Perkin Trans.2* **1999**, *5*, 113-119.
(51) Rispens, T.; Engberts, J. B. F. N. *J.Org.Chem.* **2003**, *68*, 8520-8528.
(52) Tada, E. B.; Ouarti, N.; Silva, P. L.; Blagoeva, I. B.; El Seoud, O. A.; Ruasse, M. F. *Langmuir* **2003**, *19*, 10666-10672.
(53) Buurma, N. J.; Serena, P.; Blandamer, M. J.; Engberts, J. B. F. N. *J.Org.Chem.* **2004**, *69*, 3899-3906.
(54) Hiskey, C. F.; Downey, T. A. *J.Phys.Chem.* **1954**, *58*, 835-840.
(55) Fernández, M. S.; Fromherz, P. *J.Phys.Chem.* **1977**, *81*, 1755-1761.
(56) Khan, M. N.; Arifin, Z.; Yusoff, M. R.; Ismail, E. *J.Colloid Interface Sci.* **1999**, *220*, 474-476.
(57) Bergeron, V.; Waltermo, A.; Claesson, P. M. *Langmuir* **1996**, *12*, 1336-1342.
(58) McShea, J. A.; Callaghan, I. C. *Colloid Polym.Sci.* **1983**, *261*, 757-766.
(59) Usui, S.; Sasaki, H.; Matsukawa, H. *J.Colloid Interface Sci.* **1981**, *81*, 80-84.
(60) Graciaa, A.; Morel, G.; Saulner, P.; Lachaise, J.; Schechter, R. S. *J.Colloid Interface Sci.* **1995**, *172*, 131-136.
(61) Elworthy, P. H.; Rogers, J. A.; Florence, A. T. *J.Colloid Interface Sci.* **1971**, *35*, 23-33.
(62) Elworthy, P. H.; Rogers, J. A.; Florence, A. T. *J.Colloid Interface Sci.* **1971**, *35*, 34-40.
(63) Yoon, R. H.; Yordan, J. L. *J.Colloid Interface Sci.* **1986**, *113*, 430-438.
(64) Manev, E. D.; Pugh, R. J. *Langmuir* **1991**, *7*, 2253-2260.
(65) Tajima, K.; Koshinuma, M.; Nakamura, A. *Colloid Polym.Sci.* **1992**, *270*, 759-767.
(66) Recent MD simulations indicate the mechanism of adsorption is independent of the system. This means that any nonionic hydrophobic surface can adsorb hydroxide ions. Zangi, R.; Mark, E.A.; Engberts, J.B.F.N. *submitted for publication*
(67) Relative to the observed rate constants as measured in the presence of vesicles formed from solely $\mathbf{C_{18}C_{18}^+}$.
(68) Spange, S.; Keutel, D. *Liebigs Ann.Chem.* **1993**, 981-985.
(69) Soldi, V.; Keiper, J.; Romsted, L. S.; Cuccovia, I. M.; Chaimovich, H. *Langmuir* **2000**, *16*, 59-71.
(70) Rispens, T.; Engberts, J. B. F. N. *J.Org.Chem.* **2002**, *67*, 7369-7377.
(71) Sanders, C. R.; Prestegard, J. H. *J.Am.Chem.Soc.* **1991**, *113*, 1987-1996.
(72) Sanders, C. R.; Prestegard, J. H. *J.Am.Chem.Soc.* **1992**, *114*, 7096-7107.
(73) Blokzijl, W.; Engberts, J. B. F. N.; Blandamer, M. J. *J.Am.Chem.Soc.* **1990**, *112*, 1197-1201.
(74) Galema, S. A.; Blandamer, M. J.; Engberts, J. B. F. N. *J.Am.Chem.Soc.* **1990**, *112*, 9665-9666.
(75) Galema, S. A.; Blandamer, M. J.; Engberts, J. B. F. N. *J.Org.Chem.* **1992**, *57*, 1995-2001.

(76) Milde, S. P.; Blandamer, M. J.; Burgess, J.; Engberts, J. B. F. N.; Galema, S. A.; Hubbard, C. D. *J.Phys.Org.Chem.* **1999**, *12*, 227-232.
(77) Foroudian, H. J.; Bunton, C. A.; Holland, P. M.; Nome, F. *J.Chem.Soc., Perkin Trans.2* **1996**, 557-561.
(78) Blaskó, A.; Bunton, C. A.; Toledo, E. A.; Holland, P. M.; Nome, F. *J.Chem.Soc., Perkin Trans.2* **1995**, 2367-2373.
(79) Tanaka, K.; Mackay, G. I.; Payzant, J. D.; Bohme, D. K. *Can.J.Chem.* **1976**, *54*, 1643-1659.
(80) Henchman, M.; Paulson, J. F.; Hierl, P. M. *J.Am.Chem.Soc.* **1983**, *105*, 5509-5510.
(81) Dewar, M. J. S.; Storch, D. M. *Chem.Commun.* **1985**, 94-96.

CHAPTER 7

EPILOGUE

7.1 Introduction

This final chapter briefly discusses and evaluates the results obtained from the experimental work described in this thesis.[1,2] These findings will be compared to the goal set out at the end of Chapter 1. On the basis of this discussion some suggestions for future work will be given.

7.2 Aims and Achievements

In Chapter 1 the properties of vesicles and biological membranes are presented. In addition, the use of vesicles as mimics for biological membranes is discussed, since their general properties are remarkably similar. They both enclose an aqueous compartment with a bilayer of amphiphile molecules. Among the most important parameters of the membranes are the phase of the tails and the permeability towards water, ions, and organic molecules. The cellular membrane consists of three main components, namely (glyco)lipids, steroids and proteins. In all three components there is a large variety in structures, which originates from a broad spectrum of functions (proteins) or from different conditions under which the membrane needs to retain structural integrity (lipids, steroids). Due to its complex composition there is only little understanding of the interactions in biological membranes on a molecular scale. On the contrary, studies of vesicles formed from synthetic amphiphiles are usually much less complicated because the chemical structure of the amphiphiles as well as the membrane composition (*i.e.* usually only one or two components) are much less complex.

As a result of the above considerations, vesicular catalysis has mainly been studied using vesicles composed of structurally simple amphiphiles and the amphiphile is usually the only component. These notions lead to the main aim of the present thesis. We anticipate that by studying the effects of various additives on vesicular catalysis in cationic vesicles can lead to a better understanding of non-enzymatic catalysis taking place at the polar-apolar interface (Stern region) of biological membranes. The basic idea was that the use of four different classes of structurally simple additives would unravel some of the interactions that might be important in biological membranes. This would avoid the problem that in biological membranes phospholipids can undergo multiple interactions with their environment due to the large number of functional groups in these types of molecules. As a consequence, the use of structurally simple additives and amphiphiles would allow discussion of molecular interactions between additive and amphiphile. The additives are expected to change properties not only in the hydrophobic part of the membrane, but also in the Stern region. Properties that can be affected include the local polarity, counterion binding, head group hydration, local water concentration, and the phase of the tails.

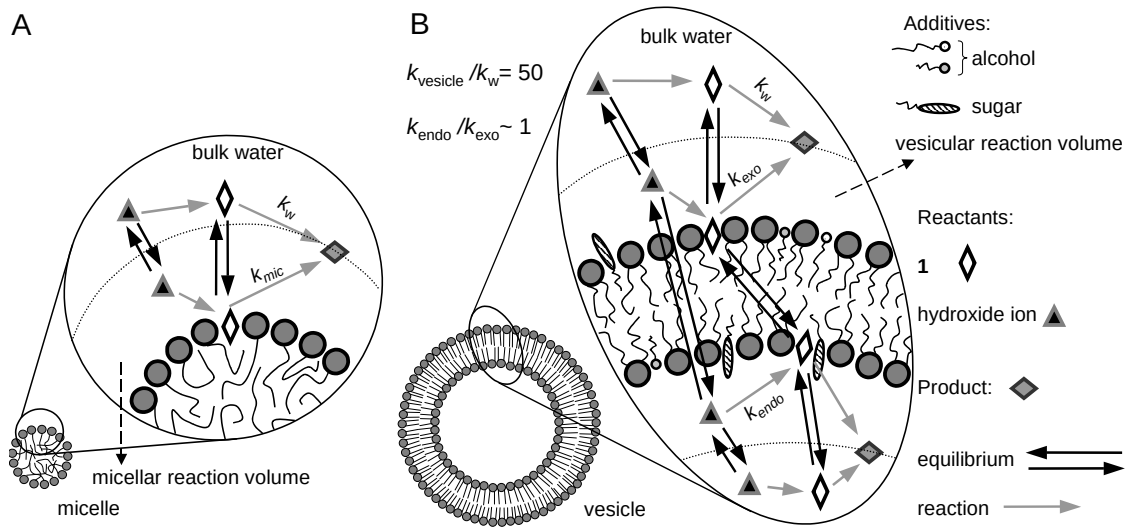

Scheme 7.1. *Schematic representation of micellar (A) and vesicular (B) catalysis. For details see text.*

Before discussing to what extent this goal has been achieved, it is important to consider a number of parameters that are important in vesicular catalysis. A brief comparison with micellar catalysis is made, since micellar catalysis has been widely studied in the literature for a long time.[3] In general, micelles and vesicles catalyse bimolecular reactions by bringing the two reactants together if they both bind to the micelle or vesicle. In this way, the two reactants are in close vicinity of each other, and hence their local concentration is high. In addition, due to a change in polarity between the aqueous and micellar or vesicular pseudophase, the micellar or vesicular rate constant might be different from the aqueous rate constant. In micellar catalysis only distribution of the reactants between the aqueous and the micellar pseudophase has to be considered (Scheme 7.1A). The observed rate constant is then a distribution-average of the micellar (k_{mic}) and aqueous (k_w) rate constant. Vesicular catalysis is considerably more complex (Scheme 7.1B), since also the distribution within the pseudophases has to be considered. This results from the fact that vesicles have an inner and outer leaflet, where the reaction proceeds with an endovesicular (k_{endo}) and exovesicular (k_{exo}) rate constant, respectively. In addition, the aqueous reaction that proceeds in the inner aqueous compartment might be different from the aqueous reaction in the bulk aqueous pseudophase. Little is known about the difference between the endo- and exovesicular rate constant, but they appear not to be so different.[4] In addition, permeation of reactants has to be considered as well, depending on the solution preparation method (vesicles plus reactants) and the endovesicular rate constant relative to the rate constant of permeation. The rate of permeation is affected by the phase of the tails. However, the phase of the tails also affects the rate constant.[5,6]

Based on the above-mentioned considerations, the deprotonation of 5-nitrobenzisoxazole (**1**; Kemp elimination; Scheme 7.2) was selected to be studied in the presence of vesicles formed from a cationic amphiphile and in the presence of various additives. The choice of this reaction was made on the basis of the different interactions that both reactants have with vesicles. Whereas binding of the hydroxide ion is purely electrostatic, binding of **1** is largely driven by hydrophobic interactions. In addition, the rate constant is sensitive towards the local polarity. Permeation of both reactants through the bilayer is fast on the time scale of the reaction, which simplifies the kinetic analysis.

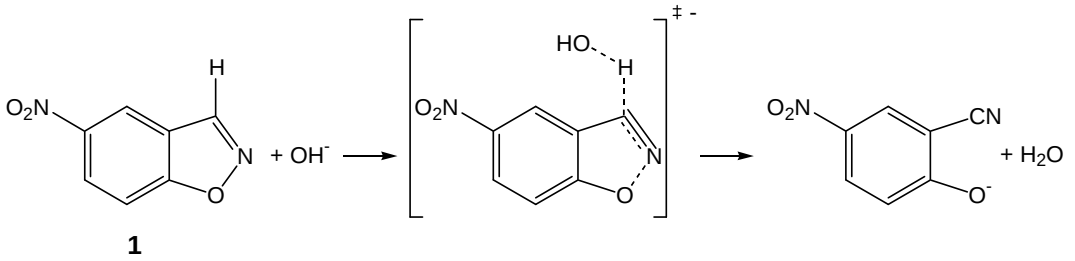

1

Scheme 7.2. *Kemp elimination reaction.*

In the presence of cationic vesicles the *observed vesicular catalysis* ($k_{obs,max}/k_{obs,w}$) of the base-catalysed reaction of **1** amounts to a factor of *ca.* 1000. The data was analysed using a modification of the pseudophase model with ion exchange as derived by Romsted.[7] Parameters that can be obtained using this model are the vesicular rate constant (k_{ves}), the binding constant of **1** to the vesicles (K_S), the counterion binding (β) and the ion-exchange competition constant. This latter constant describes the competition of hydroxide and chloride ions to bind to the vesicular surface (K_{OH}^{Cl}). Application of this model to the catalysis in the presence of cationic vesicles formed from dimethyldi-*n*-octadecylammonium chloride (**2**; Scheme 7.3) shows that the *catalytic rate acceleration* as calculated from the bimolecular rate constants (k_{ves}/k_w) is *ca.* 50.

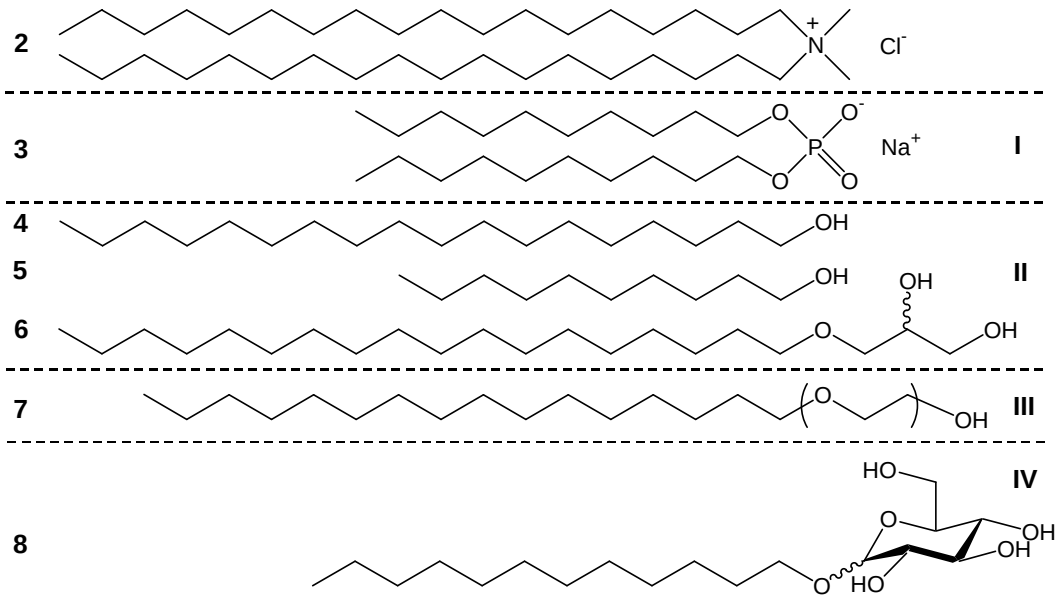

Scheme 7.3. *Cationic amphiphile employed in the experiments (**2**) and some examples of the four classes (**I**-**IV**) of additives. Class **I** are anionic double-tailed amphiphiles, class **II** alcohols, class **III** ethylene glycol surfactants and class **IV** n-alkyl pyranosides. Dimethyldi-n-octadecylammonium chloride (**2**); sodium di-n-decylphosphate (**3**); n-octadecanol (**4**); n-decanol (**5**) batyl alcohol (**6**), eicosa-ethylene glycol mono n-hexadecyl ether (**7**) and n-dodecyl-β-glucoside (**8**).*

A detailed error analysis in Chapter 3 reveals (1) that varying all four, or even only three, parameters at the same time leads to meaningless numbers[8] and (2) that all parameters can compensate each other to a large extent, leading to large errors in the obtained values. This latter observation can be exemplified by considering that for a certain amphiphile concentration an increase in the observed rate constant can be accounted for by either increasing the vesicular rate constant, increasing the binding constant, increasing the counterion binding, or by decreasing the ion exchange constant. Especially, as is clear from the mathematical equations, K_S and k_{ves} are well able to compensate each other when K_S is smaller than 30 M^{-1}. Therefore, fitting the experimental data requires knowledge of at least one or two of the parameters in order to obtain reasonable fitted parameters. Attempts were made to measure each of these parameters independently. Despite some experimental limitations, the ion exchange constant could be estimated by measuring the observed rate constant as a function of externally added sodium chloride. The composition of the vesicles did not have an influence on the value of this parameter and therefore this parameter was kept constant throughout the kinetic analysis. Unfortunately, attempts to elucidate the influence of the additives on the other three parameters failed. These attempts included the use of isothermal titration microcalorimetry to measure the binding constant of counterions and UV/vis spectroscopy to measure the binding constant of the kinetic probe to the vesicles.[9] Therefore, the experimental kinetic data was fitted allowing at most two of the remaining three parameters to vary, and using, if possible, educated guesses (from the literature) for the other parameter(s).

In Chapter 3, the addition of small amounts (< 50 mol%) of the first class of additives, anionic double-tailed amphiphiles (Scheme 7.3), is described. As anticipated, upon increasing amounts of additives the catalysis of the Kemp elimination is decreased. Above 50 mol% the reaction is inhibited. The anionic amphiphiles are sodium di-*n*-decylphosphate and sodium *n*-decyl-*n*-octadecylphosphate.

By using five different dyes, that have proven to report the polarity at the surface area of aggregates, pyrene, Nile Red, 1,8-ANS, Laurdan and the E_T(30) dye, changes in the membrane polarity were examined. All dyes indicated that the polarity of the bilayer is comparable to the polarity of methanol, and no significant change in the polarity was observed upon increasing amounts of anionic amphiphile. A change in the local polarity of the membrane would affect both the vesicular rate constant and the binding constant of the kinetic probe. Upon going from the initial state of the two reactants to the activated complex the localised charge of the hydroxide ion is being delocalised in the activated complex. Due to the charge delocalisation a change in polarity leads to a change in Gibbs energy to different extents for the initial state and the transition state. The vesicular rate constant is a function of the difference in Gibbs energy between the initial state and the activated complex. Hence a change in polarity affects the vesicular rate constant. The binding constant of the kinetic probe depends on the difference in Gibbs energy of the kinetic probe (and not the hydroxide ion) between the initial state in the membrane and the aqueous phase. Since the Gibbs energy in the aqueous pseudophase does not depend on the membrane polarity, any change in the membrane polarity will lead to a change in the binding constant. In the fitting procedure of the kinetic data the vesicular rate constant and the binding constant were assumed to remain constant, since no change in membrane polarity was sensed. Therefore, the decrease in catalysis must be explained by a decrease in counterion binding. This can be explained as the result of two effects. The first effect is a

replacement of the hydrophilic counterions (including reactive hydroxide ions) from the Stern region, since the anionic amphiphiles themselves serve as excellent counterions, binding with high efficiency. The second effect comes from a dilution of the remaining cationic charges[10] leading to a lower surface charge density, and hence an even further lowered counterion binding. A closer look at the charge density as a function of the bilayer composition reveals that the overall surface charge density remains constant up to 35 mol% of anionic amphiphile. In Chapter 2 the zeta (ζ) potential of these mixed vesicles is discussed and the magnitude and sign of the potential is in accord with the previous discussion.

In the previous discussion two observations, described in Chapter 2, that complicate the kinetic analysis were not taken into account. Cryo-EM pictures reveal that the shape of the vesicles changes as a function of bilayer composition. Whereas in the absence of anionic amphiphile lens-shaped vesicles are formed, spherical vesicles are observed at 40 mol% of anionic amphiphile. As a result, the packing of the amphiphile might be different, which can lead to changes in the vesicular rate constant and the binding constant. However, the observation of a constant polarity indicates that either the dyes are not sensitive towards these changes, or that the change in shape has no effect on the polarity. The second observation concerns the number of peaks in the DSC scans between 5 and 50 mol% of anionic amphiphile. The presence of more than one peak can either indicate the presence of more than one type of transition, or the existence of domains of different composition. In the former case, the first peak is usually small in enthalpy and can be assigned to a transition to the rippled phase. However, since in our experiments the first peak is usually large we anticipate that domain formation occurs, with domains rich in cationic amphiphile and other domains mainly consisting of 1:1 cationic and anionic amphiphiles. This conclusion was derived on the basis of the temperature of the transitions. The presence of domains leads to a significant complication of the pseudophase model and cannot be accounted for if these domains are large. Under those circumstances in the neutral domains inhibition would occur, whereas in the cationic domains there would be catalysis similar as that for cationic vesicles. In such a situation the distribution of hydroxide ions throughout the Stern region would be inhomogeneous. However, if the neutral domains are small, the distribution of hydroxide ions is expected to be homogenous, although it can be argued that due to the lack of electrostatic attraction the hydroxide ions are not close enough to the vesicular surface in the domains to react with membrane-bound **1**.

In Chapter 4 the effects of the second class of additives, which comprises four long linear alcohols containing 10 to 18 carbon atoms, is discussed. The alcohols are *n*-octadecanol (**4**), *n*-decanol (**5**), batyl alcohol (**6**) and oleyl alcohol. These alcohols were chosen on the basis of their match and mismatch in size with the *n*-octadecyl tails of the amphiphile, the number of hydroxyl groups and the double bond in the tail, respectively. In the plots of the observed rate constant versus the amphiphile concentration the maximum observed rate constant decreases by at most a factor of *ca.* 2. This relatively small change complicates a detailed discussion of the origin of these effects.

Similarly as for the addition of anionic amphiphiles, addition of the alcohols should lead to a decrease in counterion binding. However, since alcohols are nonionic, they cannot act as counterions and hence they can only “dilute” the charges of the cationic amphiphile. Therefore, their effect on the counterion binding is expected to be significantly smaller. The DSC scans show several peaks indicating a variety of domains (transitions), but no

information has been obtained on the nature on these domains. On the basis of the polarity experiments no change in vesicular rate constant and binding constant is expected. However, only allowing the counterion binding to change could not satisfactorily fit the data. In addition, it led to significantly different results for the alcohols, which seems a bit unexpected considering the similar head group area for the different alcohols. Strikingly, addition of oleyl alcohol even leads to an *increase* of the observed rate constant, which cannot be explained by changing the counterion binding. Therefore, the counterion binding is assumed to be smaller assuming that four alcohol molecules take up the space of one cationic-anionic amphiphile pair. Then the vesicular rate constant and binding constant were allowed to vary in order to fit the experimental data. Although there are no indications that the membrane polarity changes, we anticipate that the changes in membrane polarity are too small to be detected using the fluorescent dyes, but large enough to be detected kinetically. In general, the effects on the vesicular rate constant and the binding constant are less than a factor of *ca.* 4, whereby the binding constant decreases and the vesicular rate constant increases. The effects on the catalysis are least pronounced in the case of *n*-decanol, and most pronounced in the case of batyl alcohol.

Chapter 5 describes the influence of the addition of the third class of additives, ethylene glycol surfactants. This class contains two surfactants, namely eicosa-ethylene glycol mono *n*-hexadecyl ether (**7**) and a PEG-ylated SAINT-2 amphiphile. This latter amphiphile has been used as steric stabiliser in transfection experiments. Their structure consists of a pyridinium ion with two oleyl tails in the position *para* to the nitrogen and a PEG-5000 unit attached to the nitrogen. The influence of these surfactants on the catalysis of the Kemp elimination reaction is surprisingly small. Above 35 mol% of **7** care has to be taken since single-tailed surfactants can solubilise vesicles into mixed micelles. In fact, such behaviour is observed. Hence, the kinetic model is complicated similar as for domain formation. Despite that the DSC scans and light scattering experiments, described in Chapter 2, indicate that a vesicular solution containing 35 mol% of **7** contains mainly mixed micelles, the observed rate constants are still about 60% of the values in the absence of **7**. This agrees with experiments where the observed rate constants measured in the presence of vesicles formed from **2** were compared with micelles formed from *n*-octadecyltrimethylammonium chloride. In these experiments the maximum observed rate constant in the presence of micelles is approximately half the value measured in the presence of vesicles.

In Chapter 6 it is reported that the maximum observed rate constant increases up to a factor of 7 upon the addition of 50 mol% of *n*-alkyl pyranosides, the fourth class of additives. Like the third class, this series contains two compounds, *n*-dodecyl-*β*-glucoside (**8**) and *n*-dodecyl-*β*-maltoside. The head group of the latter compound consists of two glucose units. Due to its high Krafft temperature, **8** is barely soluble in water, but *n*-dodecyl-*β*-maltoside can be easily solubilised. As a result, the single-tailed surfactant *n*-dodecyl-*β*-maltoside is able to solubilise vesicles into micelles, as is described in Chapter 2. When present above 25 mol% in vesicles (or micelles) formed from **2**, addition of sodium hydroxide leads to immediate precipitation. The material can be redissolved upon shaking. At 25 mol%, in the absence of sodium hydroxide, the vesicles aggregate loosely. Dynamic light scattering experiments indicate the presence of vesicles, but micelle formation cannot be excluded. In fact, the observed rate constants are considerably higher in solutions

containing **8**, which is unable to solubilise vesicles. This agrees with the observation made in Chapter 5 that vesicles have a higher efficiency than micelles to catalyse the reaction. Analysis of the kinetic data reveals that for both pyranosides the binding constant increases, but to different extents. The vesicular rate constant also increases, but it decreases again for *n*-dodecyl-*β*-maltoside when micelle formation becomes significant.

The origin of the increased catalysis is difficult to determine. Based on the membrane polarity experiments no significant change is expected, although the use of Nile Red seems to indicate that the polarity decreases slightly upon increasing amounts of incorporated pyranosides. The change in polarity is comparable to a change in $E_T(30)$ value from 56 to 54.[11] A decrease in polarity leads to an increase in the vesicular rate constant and binding constant. The decrease could be a result of water being replaced from the Stern region by the sugar moieties as has been reported in the literature.[12] A decrease in the water concentration in the Stern region would also lead to a decrease in the hydration of the hydroxide ion, explaining the increase in the vesicular rate constant. In addition, **1** would be dehydrated as well. The effect of dehydration of **1** on the vesicular rate constant is not so large as for dehydration of the hydroxide ion, but it does stabilise **1** leading to an increase in the binding constant. The importance of the hydration of the reactants was already shown in Chapter 3 where a large increase in rate constant was observed in mixtures of water and an organic solvent. A similar change in polarity in these solvent mixtures, compared to the change in polarity as sensed by Nile Red, leads to an increase of the rate constant by a factor of two. However, a five-fold increase in vesicular rate constant is observed upon the addition of pyranosides. This probably reflects the inability of water/organic solvent mixtures to correctly mimic the Stern region rather than that kinetic medium effects have been overlooked.

Experiments to study specific or preferential binding of hydroxide ions to pyranoside-containing vesicles show that these processes do not occur, since the ion-exchange constant is not affected, and no catalysis is observed in phospholipid vesicles containing 25 mol% of **8**. This indicates that if dehydration of the hydroxide ion were the origin of the increase in vesicular rate constant, the chloride ion is also dehydrated to a similar extent, since otherwise the ion exchange constant would have decreased.

Deprotonation of the sugar hydroxyl groups can account for the changes in observed rate constants as well. However, on the basis of literature data it appears unlikely.

Throughout the kinetic analysis we assumed the counterion binding to be constant, since we have no accurate knowledge of (the extent of the change in) the counterion binding. However, in the literature[12] it has been suggested that the counterion binding decreases upon pyranoside addition,[13] but even at very low water concentrations it is still about 30%. If changes in the counterion binding had been taken into account the fitted vesicular rate constants would even be higher, which is consistent with dehydration (and decrease in polarity).

In summary, the experiments, which are described in this thesis, reveal that even in relatively simple bilayer mimics of biological membranes, interactions can be highly complex. This is especially true for sugar-containing surfactants.

7.3 Some Comments on Aspects of Vesicular Catalysis

Few studies have dealt with vesicular catalysis involving additives that were incorporated into the vesicular membrane.[6,14-16] As discussed in Section 7.2, the two most important differences between micellar and vesicular catalysis are (1) the possibility that the tails can be in two phases and (2) the presence of a bilayer leading to an inner and outer leaflet. As will be discussed, additives affect these properties, and hence they affect rate constants as well.

Different observed rate constants between the inner and outer leaflet can be obtained, due to a potential non-random substrate distribution between the leaflets. For example, Ellman's reagent, which is dianionic, is expected to permeate only slowly or not at all through membranes formed from cationic amphiphiles, and hence depending on the method of vesicle preparation, the distribution of the reactants can be random or non-random.[17] Attention has been focussed on this leaflet discrimination in vesicular catalysis including catalysis by cholesterol-containing vesicles,[14,15] since cholesterol decreases the permeability of membranes. Unfortunately, similar experiments in the absence of cholesterol have been subject of misinterpretation[18] and poor reproducibility,[19,20] which largely clouds the influence of the cholesterol. Therefore, the details of the redistribution of charged organic substrates over the leaflets remains unclear. As a result, there is only one report that claims to have measured the endo- and exovesicular rate constant independently.[4] In addition, most experiments have not been performed as a function of the amphiphile concentration, which leads to the inability to calculate the vesicular rate constant. Therefore, rough trends rather than, more valuable, detailed information was obtained.

On the contrary, the reaction of **1** with hydroxide ions has been studied as a function of the amphiphile concentration in the presence and absence of cholesterol.[16] The distribution of the nonionic **1** was expected to be random irrespective of the method of solution preparation, age of the solution, and the presence of cholesterol. The rate of permeation of hydroxide ions through the bilayer was assumed to be faster than the vesicular rate constant. At 25 ^{o}C in vesicles formed from dimethyldi-*n*-octadecylammonium chloride or bromide the presence of up to 14 mol% of cholesterol leads to an increase in the vesicular rate constant. Above 14 mol% of cholesterol the observed rate constants decrease again as a result of a decreased counterion binding due to a lowering of the surface charge density. The initial increase was explained in terms of a change in the phase of the tails from gel-like to liquid-crystalline. This explanation is supported by the observation that (vesicular or observed) rate constants are not affected upon addition of 12 mol% of cholesterol to vesicles formed from di-*n*-dodecyldimethylammonium bromide, which are already in the liquid-crystalline phase.

The importance of the phase of the tails on the vesicular rate constant was also observed in earlier studies of vesicular catalysis.[5,6] An attempt was made to unravel the underlying thermodynamic activation parameters ($\Delta^{\ddagger}H^{o}$ and $\Delta^{\ddagger}S^{o}$), but instead of measuring the *vesicular* rate constant as a function of the temperature, *observed* rate constants were measured. This does not take into account that other parameters, such as the counterion binding, the binding constant of the substrate(s) and the aqueous rate constant, are also affected by a change in temperature. It should be noted that the enthalpy and entropy of

activation are usually difficult to interpret, since they depend on many parameters, such as restructuring of water (hydration and/or dehydration) and a local reorganisation of the aggregate. However, it might still reveal some valuable information if experiments are performed in a series of related vesicular systems.

7.4 Suggestions for Future Work

The work presented in this thesis leaves plenty of room for future work. In fact, more questions have been raised than have been solved. Especially the origin of the rate acceleration in the presence of *n*-alkyl pyranosides is intriguing. However, parameter compensation in the mathematical model leads to problems in interpreting the experimental data. Therefore, it would be wise to solve those problems first. This can be achieved by studying a system where independent determination of at least some of the parameters is possible. Using isothermal titration microcalorimetry, the binding constant of chloride and bromide ions to mixed vesicles of POPC and **2** could be measured. However, measuring the binding constant of hydroxide ions failed as a result from small heat effects that, in addition, depended on the age of the vesicular solution.[21] Therefore, choosing a probe reaction that involves reaction with bromide or chloride ions solves two problems at once. Firstly, one can measure the binding constant of these ions and hence, the concentration of bound counterions can be calculated. Secondly, the number of unknown parameters decreases as the ion exchange constant and the counterion binding can be replaced using the binding constant of bromide ions. As a result, the model used to analyse the experimental data in this thesis simplifies since it only contains three parameters of which two remain unknown. The use of an additional reaction between a substrate that does not bind to vesicles and bromide ions could be used to confirm the concentration of bromide ions in the aqueous pseudophase.
In addition, it would be particularly helpful if a kinetic probe would be chosen, such that its binding constant is larger than 30 M^{-1}, since then compensation of the binding constant and the vesicular rate constant is much less important. Choosing a probe reaction that has been well-studied in the literature, already gives some clues of binding constants and the vesicular rate constant. The S_N2 reaction of **9** and **10** with bromide ions meets all of these criteria (Scheme 7.4).[22-25]

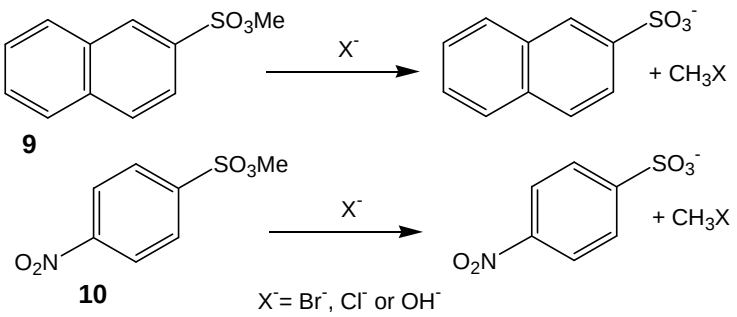

Scheme 7.4. *S_N2 reaction of methyl naphthalene-2-sulfonate (**9**) and methyl 4-nitrobenzenesulfonate (**10**) with a nucleophile.*

The binding constants of **9** and **10** to CTAB micelles are around 1500 and 75 M^{-1}, respectively. This difference in binding ability can be used to determine whether differences upon changing the system under study involve an effect of a change in vesicular rate constant or binding constant, since upon increasing the amphiphile concentration the amount of bound **9** will remain about constant, whereas the mole fraction of bound **10** will increase. A fully bound probe allows an easier determination of the vesicular rate constant, since the reaction in the aqueous phase can be neglected. Similarly as for the reaction of **1** with hydroxide ions, this reaction is sensitive towards changes in polarity and dehydration of the reactants.[23,24]

In order to study the dehydration of ions by sugar moieties, a series of compounds with increasing number of hydroxyl groups could be studied. For example, *n*-dodecanol, 3-*n*-dodecyloxy-propane-1,2-diol, *n*-dodecyl-*β*-glucoside (**8**) and *n*-dodecyl-*β*-maltoside. To avoid problems with (slow additive concentration-dependent) permeation of bromide ions through the membrane, it might be wise to add 10 mol% of $\mathbf{C_{16}EO_{20}}$ (**7**), so that under all circumstances permeation of all reactants is fast. In addition, problems with aggregation of the mixed vesicles under basic condition can be avoided.[26] This is important when this vesicular system is extended to the reaction of **1** at a later stage in the future.

Other factors that are worth to investigate are the size-dependence of the vesicular rate constant and binding constant of substrate and counterion, especially if various reactions are considered. In addition, studying the rate constants as a function of the temperature for a number of reactions in a number of comparable systems (described above) might reveal some additional valuable information.

7.5 References

(1) Parts of Chapter 2 and 3 have been published: *The Kemp Elimination in Membrane Mimetic Reaction Media. Probing Catalytic Properties of Catanionic Vesicles Formed from Double-Tailed Amphiphiles*. Klijn, J.E.; Engberts, J.B.F.N. *J.Am.Chem.Soc.* **2003**, *125*, 1825-1833.

(2) Parts of Chapter 2, 3, 4 and 5 have been published: *The Kemp Elimination in Membrane Mimetic Reaction Media. Probing Catalytic Properties of Cationic Vesicles Formed from a Double-Tailed Amphiphile and Linear Long-Tailed Alcohols or Alkyl Pyranosides*. Klijn, J.E.; Engberts, J.B.F.N. *Org.Biomol.Chem.* **2004**, *2*, 1789-1799.

(3) *Surfactant Science Series* Volume 100; Texter, J., ed.; Marcel Dekker: New York, **2001**.

(4) Cuccovia, I. M.; Kawamuro, M. K.; Krutman, M. A. K.; Chaimovich, H. *J.Am.Chem.Soc.* **1989**, *111*, 365-366.

(5) Kunitake, T.; Sakamoto, T. *Chem.Lett.* **1979**, 1059-1062.

(6) Kunitake, T.; Okahata, Y.; Ando, R.; Shinkai, S.; Hirakawa, S. *J.Am.Chem.Soc.* **1980**, *102*, 7877-7881.

(7) Romsted, L. S. In *Micellization, Solubilization and Microemulsions*; Mittal, K. L., ed., Plenum Press: New York, **1977**; pp 509-530.

(8) This is exemplified by a counterion binding larger than unity, or an ion exchange constant close to unity.

(9) These experiments have not been described in this thesis.

(10) The combination of an anionic and cationic amphiphile can be considered as a neutral pair, since both charges are compensated. The lifetime of such a pair is not important, since each anionic amphiphile can always form a pair with a cationic amphiphile in its vicinity, leading to the constant presence of a catanionic amphiphile pair.

(11) The normalised polarity decreases from 0.73 to 0.66 (Chapter 2).

(12) Griffiths, P. C.; Pettersson, E.; Stilbs, P.; Cheung, A. Y. F.; Howe, A. M.; Pitt, A. R. *Langmuir* **2001**, *17*, 7178-7181.

(13) The study concerns mixed micelles of sodium *n*-dodecylsulfate and a nonionic disaccharide.

(14) Moss, R. A.; Hui, Y. *Tetrahedron Lett.* **1983**, *24*, 3961-3964.

(15) Huffman, R. W.; McBride, P.; Brown, D. M. *J.Org.Chem.* **1994**, *59*, 1633-1637.
(16) Pérez-Juste, J.; Hollfelder, F.; Kirby, A. J.; Engberts, J. B. F. N. *Org.Lett.* **2000**, *2*, 127-130.
(17) A random distribution of Ellman's reagent over the leaflet is achieved by cosonication of amphiphile and substrate, whereas a non-random distribution is obtained by addition of substrate after sonication of the solution containing amphiphile (substrate bound to the outer leaflet), or filtration of a cosonicated solution over a column (substrate bound to inner leaflet).
(18) Moss, R. A.; Swarup, S.; Hendrickson, T. F.; Hui, Y. Z. *Tetrahedron Lett.* **1984**, *25*, 4079-4082.
(19) Moss, R. A.; Swarup, S.; Zhang, H. M. *J.Am.Chem.Soc.* **1988**, *110*, 2914-2919.
(20) Huffman, R. W.; Brown, D. M. *J.Org.Chem.* **1991**, *56*, 6477-6479.
(21) These experiments were performed at the University of Basel (Switzerland) under the guidance of Prof. dr. J. Seelig and dr. H. Heerklotz during a 2-month stay. Preliminary results indicate that reproducible and reasonable binding constants can be obtained.
(22) Bertoncini, C. R. A.; Nome, F.; Cerichelli, G.; Bunton, C. A. *J.Phys.Chem.* **1990**, *94*, 5875-5878.
(23) Blaskó, A.; Bunton, C. A.; Toledo, E. A.; Holland, P. M.; Nome, F. *J.Chem.Soc., Perkin Trans.2* **1995**, 2367-2373.
(24) Foroudian, H. J.; Bunton, C. A.; Holland, P. M.; Nome, F. *J.Chem.Soc., Perkin Trans.2* **1996**, 557-561.
(25) Muñoz, M.; Graciani, M. D. M.; Rodríguez, A.; Moyá, M. L. *J.Colloid Interface Sci.* **2003**, *266*, 208-214.
(26) Vesicles composed of **2** and POPC aggregate under basic conditions (pH 11; unpublished results).

Summary

Vesicular catalysis can be an important tool in understanding non-enzymatic catalysis in biological membranes. So far, most studies involving vesicular catalysis have focused on differences compared to micellar catalysis. As discussed in Chapter 1, these differences mainly result from the enclosement of an aqueous compartment by a hydrophobic bilayer of amphiphiles in vesicles (Scheme 1A), whereas micelles can be regarded as oil-like droplets (Scheme 1B). As a consequence, the inner and outer leaflet of the bilayer might be differentiated kinetically if permeation of reactants is relatively slow. In addition, the tails of the double-tailed amphiphiles can be in a more rigidly ordered (gel-like) phase or a more fluidly, disordered (liquid-crystalline) phase, whereas in micelles the tails are always in a fluid-like phase (Scheme 2). Due to differences in packing efficiency, micelles have a more "open" structure leading to a higher water concentration at the polar-apolar interface.

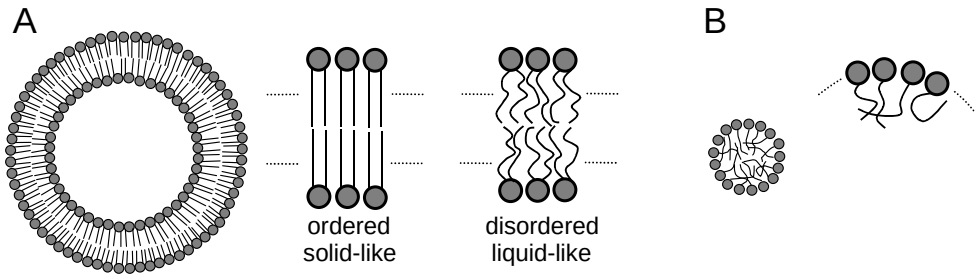

Scheme 1. *Schematic representation of a vesicle formed from double-tailed surfactants with tails in either the ordered or disordered phase (A) and a micelle formed from single-tailed surfactants (B).*

As is evident from the extensive literature reports on catalysis by micelles formed in the presence of (large) hydrophobic additives, this topic has been well studied for a wide variety of reactions and systems. Only few of such studies are known when it comes to vesicular catalysis.

It should be noted that biological membranes are complex mixtures of a large variety of compounds. In addition, these compounds have a number of functional groups. Therefore, they can undergo several interactions with their environment leading to a complex interplay of interactions.

Considering that vesicular catalysis has mainly been performed in single-component systems and that biological membranes are complex mixtures of a variety of compounds there is a void in the understanding of catalysis at the interface of biological membranes. The influence of the addition of four different classes of additives on the vesicular catalysis of a model reaction has been explored in this thesis. The amphiphile chosen is dimethyldi-*n*-octadecylammonium chloride (**$C_{18}C_{18}$+**). The four classes of additives are anionic double-tailed amphiphiles, long linear *n*-alcohols, ethylene-glycol surfactants and *n*-dodecyl-*β*-pyranosides. As a suitable model reaction the hydroxide-ion catalysed deprotonation reaction of 5-nitrobenzisoxazole (**1**; Scheme 2) was chosen. Not only is the rate constant sensitive to the local hydroxide-ion concentration at the vesicular binding sites, but also to the local polarity and the extent of dehydration of the reactants upon binding to the vesicular binding sites. In particular, dehydration of hydroxide ions can lead to large rate accelerations.

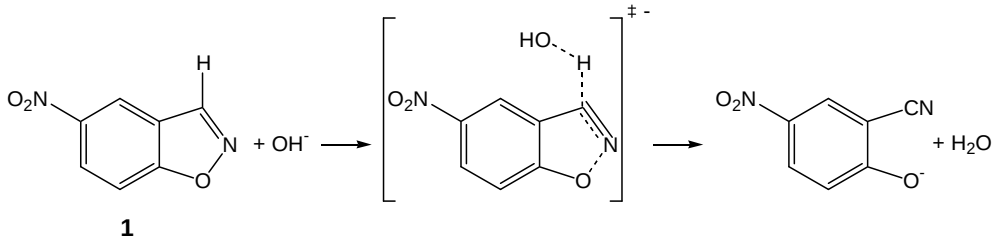

1

Scheme 2. *Kemp elimination reaction of 5-nitrobenzisoxazole by hydroxide ions.*

Before addressing catalytic effects modified by the addition of the four classes of additives, the overall properties of the vesicles formed in the presence of the additives are discussed in Chapter 2. The main phase transition temperatures (T_m), the temperature at which the tails go from the gel-like to the liquid-crystalline phase, is lowered in the presence of all additives at a low mole fraction (<10 mol%). At higher mole fractions, the T_m decreases further for the additives that are, in principle, single-tailed surfactants: *n*-dodecyl-*β*-glucoside (**C_{12}Glu**), *n*-dodecyl-*β*-maltoside (**C_{12}Mal**), and eicosa-ethylene glycol mono *n*-hexadecyl ether (**$C_{16}EO_{20}$**). For the saturated alcohols the T_m increases again, and the extent of the increase follows the trend *n*-decanol (**C_{10}OH**) < batyl alcohol (**C_{18}GOH**) < *n*-octadecanol (**C_{18}OH**). The mole fraction, at which the increase in T_m starts, follows the reverse order. Upon increasing the amounts of oleyl alcohol (**$C_{18:1}$OH**) the transition becomes progressively less cooperative. In the case of the anionic amphiphiles, sodium di-*n*-decylphosphate (**$C_{10}C_{10}$-**) and sodium *n*-decyl-*n*-octadecylphosphate (**$C_{10}C_{18}$-**), (neutral) microdomains are formed between 5 mol% and 35 mol%. However, the vesicular catalysis was in all cases studied at 15°C, which is above the T_m of vesicles formed in the presence of the additives.

Upon addition of **C_{12}Mal** and **$C_{16}EO_{20}$** vesicles are partially solubilised into mixed micelles. As is determined by both dynamic light scattering and turbidity experiments, the extent of solubilisation depends on both the mole fraction of single-tailed surfactant and the concentration of **$C_{18}C_{18}$+**.

Five different dyes, pyrene, the E_T(30)-dye, laurdan, Nile Red and 1,8-ANS, were used to address changes in the polarity of the vesicular surface. These dyes have been employed in the literature to report the polarity in solvents and solvent mixtures. They were selected on the basis of the different sensitivity towards interactions with their environment. For example, Nile Red and the E_T(30)-dye are particularly sensitive towards hydrogen-bond donation, whereas pyrene is not. Despite these differences in sensitivity no significant change in membrane polarity is observed upon addition of the additives.

In Chapter 3 it is shown that in 1,4-dioxane-water and acetonitrile-water mixtures the natural logarithm of the rate constant for the Kemp elimination increases linearly with the polarity as reported by Nile Red. The increase in rate constant mainly originates from dehydration of the hydroxide ion, leading to destabilisation of the initial state relative to the activated complex.

In a typical experiment solely in the presence of cationic vesicles, there is initially a sharp increase of the observed rate constant (k_{obs}) to a maximum value upon increasing the amphiphile concentration. Then k_{obs} slowly decreases. The *observed catalysis*, expressed as the ratio of the maximum observed rate constant and the observed aqueous rate constant ($k_{obs,max}/k_{w,obs}$), amounts to a factor of *ca.* 1000. This type of behaviour is characteristic for

vesicular catalysis of bimolecular reactions and can be described by the pseudophase model with ion exchange derived in the late 1970s. This model assumes two pseudophases, an aqueous one and a vesicular one. Two effects contribute to the observed catalysis. The first effect comes from a decreased effective reaction volume, since both reactants are efficiently bound to the vesicular pseudophase. Hence, the local concentration of reactants is much higher than in the bulk solution. The second effect originates from an increase in rate constant going from the aqueous pseudophase to the vesicular pseudophase mainly as a result of partial dehydration of the reactants, similar as for the water-organic solvent mixtures. Taking these effects into account the *catalytic rate acceleration*, defined as the ratio of the bimolecular vesicular and aqueous rate constants (k_{ves}/k_w), amounts to a factor of *ca.* 50.

The parameters that can be obtained by fitting the observed rate constant as a function of the amphiphile concentration by the pseudophase model are (i) the vesicular rate constant (k_{ves}), (ii) the binding constant of **1** (K_S), (iii) the counterion binding (β) and (iv) the ion exchange constant (K_{OH}^{Cl}). A detailed error analysis revealed that the parameters can compensate each other to a large extent. However, the ion exchange constant can be estimated independently and it was found that this parameter does not vary upon addition of the anionic amphiphiles. Allowing the other three parameters to vary simultaneously leads to erroneous results, such as a counterion binding that is larger than unity. Therefore, at most only two parameters were allowed to vary. As is apparent from the kinetic equation, compensation of k_{ves} and K_S is particularly large when the binding constant is small.

Based on the observation that the polarity does not change upon addition of the anionic amphiphiles **$C_{10}C_{10}$-** and **$C_{10}C_{18}$-** to vesicles formed from **$C_{18}C_{18}$+**, it is anticipated that the decrease in observed rate constant upon increasing amounts of **$C_{10}C_{10}$-** or **$C_{10}C_{18}$-** is due to a reduced counterion binding. Not only acts the anionic head group as a counterion, but also the formed neutral pairs dilute the remaining cationic head groups in the vesicle leading to a lower positive surface charge density. Hence, unfavourable head group-head group interactions are reduced and less counterion binding is required to reduce these interactions. Calculation of the charge per amphiphile (which is a measure of the surface charge density) from the counterion binding percentages reveals that the overall charge per amphiphile does not vary significantly upon the addition of **$C_{10}C_{10}$-** or **$C_{10}C_{18}$-** in concentrations up to 35 mol%.

In Chapter 4 it is reported that addition of 50 mol% of **C_{10}OH** to vesicles formed from **$C_{18}C_{18}$+** only leads to a decrease of 10% in the maximum observed rate constants, whereas addition of 50 mol% of **C_{18}GOH** and **C_{18}OH** leads to decreases by 40% and 60%, respectively. On the contrary, addition of 35 mol% of **$C_{18:1}$OH** leads to an *increase* by 75% in the maximum observed rate constant. At higher mole fractions the observed rate constant decreases again. It is discussed that solely a decrease in counterion binding cannot account for the change in observed rate constants, since (i) each alcohol would then have their own specific ability to reduce the counterion binding and (ii) addition of **$C_{18:1}$OH** would lead to an *increase* in counterion binding above unity. From the literature data on charged micelles containing neutral additives, it is found that the counterion binding decreases rather irrespective of the structure of the additive. Therefore, the experimental data was fitted using a decrease in counterion binding irrespective of the structure of the

alcohol based on the results obtained for **$C_{10}C_{10}$-**. It is assumed that four alcohol molecules require the same area as one (neutral) pair of **$C_{10}C_{10}$-** and **$C_{18}C_{18}$+**. Then, the rest of the increase or decrease in observed rate constants was attributed to a change in k_{ves} and/or K_S, since the ion-exchange constant does not depend on the structure or mole fraction of the additive. A detailed interpretation of the results is hampered by the small effects (typically smaller than a factor of four), but overall it appears to involve a subtle interplay.

Chapter 5 describes the influence of the presence of (oligo) ethylene glycol units in the Stern region of cationic vesicles. Addition of small amounts of **$C_{16}EO_{20}$** (≤ 10 mol%) to vesicles formed from **$C_{18}C_{18}$+** does not lead to any change in the observed rate constants. At 35 mol% of **$C_{16}EO_{20}$** the maximum observed rate constant has decreased by about 30% as a result of micelle formation. This difference in catalytic efficiency going from vesicles to micelles is confirmed by literature experiments using the single-tailed surfactant *n*-octadecyltrimethylammonium chloride (**C_{18}+**).

Chapter 6 reports the 7- and 4.5-fold increase in the maximum observed rate constants upon addition of 50 mol% of **C_{12}Glu** and **C_{12}Mal**, respectively, to vesicles formed from **$C_{18}C_{18}$+**. The origin of this large effect comes from a more extensive dehydration of the reactants, due to replacement of water molecules from the Stern region by the sugar moieties. It is discussed that specific or preferential binding of hydroxide ions cannot be the origin of the observed increase of the rate constant. Deprotonation of the hydroxyl groups by the vesicle-bound hydroxide ions of the pyranosides might account for the observed catalytic effects as well, although it appears to be unlikely. Analysis of the experimental data reveals that the increase in the maximum observed rate constant mainly originates from an increase in k_{ves} for **C_{12}Glu**, whereas it comes mainly from an increase in K_S for **C_{12}Mal**. Due to micelle formation upon the addition of **C_{12}Mal**, k_{ves} decreases after an initial increase.

Chapter 7 puts the results of the previous chapters into perspective. At the end of the chapter some possibilities for future research are given.

SAMENVATTING

KATALYSE ONDER MEMBRAANMIMETISCHE REACTIEOMSTANDIGHEDEN

Voordat het onderzoek, dat in dit proefschrift is beschreven, wordt samengevat, zal eerst een korte introductie worden gegeven over het wel of niet mengen van verschillende vloeistoffen (en de oplosbaarheid van vaste stoffen). Daarna wordt de link gelegd met membranen alvorens katalyse[1] in dergelijke systemen, het promotieonderzoek, wordt samengevat.

Benzine, zonnebloemolie en olijfolie zijn in alle verhoudingen mengbaar. Water en olijfolie mengen daarentegen slecht en vormen daarom twee lagen. Zout lost niet op in zonnebloemolie, maar juist weer wel in water. Dit komt omdat moleculen grofweg in twee categorieën kunnen worden verdeeld: polaire moleculen en apolaire moleculen. Zo zijn water en zout polair en zijn benzine, olijfolie en zonnebloemolie apolair. Over het algemeen mengen polaire moleculen alleen met andere polaire moleculen en apolaire moleculen alleen met apolaire moleculen.

De oorsprong hiervan is gelegen in de verdeling van elektronen binnen een molecuul. Ieder atoom bestaat uit een positief geladen kern met daaromheen negatief geladen elektronen, zodat het geheel precies elektronisch neutraal is. Een kern die bijvoorbeeld een lading van +7 heeft, heeft daaromheen 7 elektronen met een lading van –1. In een molecuul zijn atomen met elkaar verbonden door middel van bindingen. Een binding tussen twee atomen bestaat uit koppels van twee elektronen, waarbij ieder atoom, dat de binding aangaat, een elektron beschikbaar stelt. Er zijn ook dubbele bindingen, of zelfs nog bindingen van een hogere orde mogelijk. In die gevallen levert ieder atoom twee, of dus nog meer elektronen.

Omdat ieder type atoom andere eigenschappen heeft, kan het ene atoom harder aan de bindingselektronen trekken dan het andere atoom. Als gevolg hiervan wordt het atoom dat het hardst trekt in zekere mate negatief geladen, en de ander in gelijke mate positief geladen.

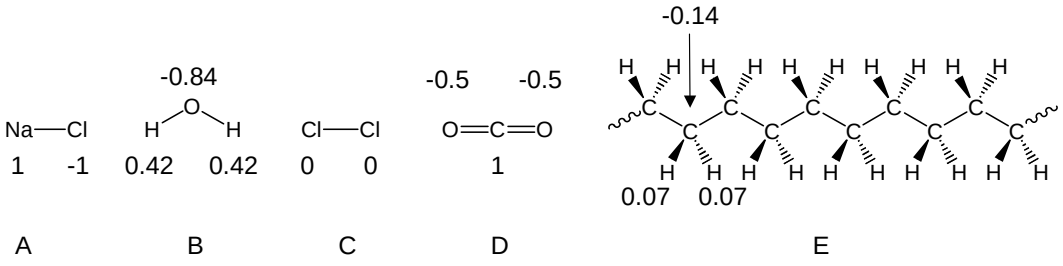

Schema 1. *Keukenzout (A; NaCl), chloorgas (B, Cl_2) water (C; H_2O), koolstof-dioxide (D; CO_2;) en een apolaire vetketen (E). De getallen zijn de ladingen per a-toom (zie tekst).*

Een voorbeeld hiervan is keukenzout (schema 1A). Dit molecuul bestaat uit een chlooratoom en een natriumatoom. Omdat het chlooratoom zo sterk aan de bindingselektronen trekt, is dit elektron volledig op het chlooratoom terug te vinden. Als gevolg hiervan is het chlooratoom negatief geladen met een lading van –1. Het getal –1 in schema 1 betekent dan ook dat het volledige elektron op dit atoom is te vinden. Het natriumatoom mist hierdoor een elektron en het heeft dan ook een lading van +1, omdat het molecuul als geheel wel elektronisch neutraal moet blijven. In water, dat bestaat uit twee waterstofatomen en een zuurstofatoom (B in schema 1), trekt het zuurstofatomen minder sterk de bindingselektro-

nen aan dan het chlooratoom in keukenzout. Hierdoor krijgt het zuurstofatoom een lading van -0.84. De waterstofatomen krijgen dus een lading van +0.42 (+0.84 gedeeld door 2). Het kan echter ook voorkomen dat in een molecuul atomen even hard trekken aan de bindingselektronen, waardoor de lading van elk der atomen nul blijft. Een voorbeeld hiervan is het uit twee chlooratomen bestaande chloorgas (C in schema 1).
Om te bepalen of een molecuul polair is of niet, dient te worden gekeken naar twee punten. Het eerste punt behelst de locatie van de gemiddelde ladingen. Dat betekent dat zowel de locatie van het gemiddelde van de positief geladen atomen als de locaties van het gemiddelde van de negatief geladen atomen bepaald moeten worden. Het tweede punt gaat over de grootte van zowel de som van de positief geladen atomen in het molecuul als de som van de negatief geladen atomen in het molecuul. Is de afstand tussen de locatie van de gemiddelde ladingen groot en zijn de sommen groot, dan is er sprake van een polair molecuul. Zoals eerder genoemd zijn water en keukenzout hiervan voorbeelden. Is de afstand klein (of nul), dan heffen de ladingen elkaar op en wordt gesproken van een apolair molecuul. Koolstofdioxide is hier een goed voorbeeld van (schema 1D). Ondanks dat de atomen in dit molecuul een behoorlijke lading hebben, is het molecuul toch apolair doordat de sommen van de ladingen samenvallen. In het geval van oliën en vetten (benzine, olijfolie, enz.) moet vooral rekening worden gehouden met de grootte van de sommen. Deze moleculen zijn opgebouwd uit lange ketens van koolstofatomen met aan ieder koolstofatoom twee waterstofatomen. Zoals is te zien in schema 1E, trekken de koolstofatomen niet zo hard aan de elektronen en stoten de waterstofatomen ze niet zo hard af. Hierdoor zijn ook dit soort verbindingen apolair.
Al met al is er door de verschillende ladingsverdelingen eigenlijk geen strikte scheiding, maar eerder een geleidelijk oplopende schaal van heel apolaire moleculen tot heel polaire moleculen. Dit verklaart waarom sommige verbindingen beter dan andere verbindingen oplossen in water. Of in olie.

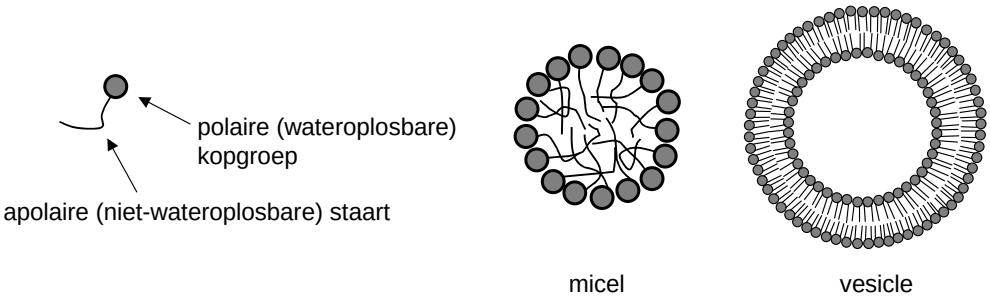

Schema 2. *Surfactant (links) en mogelijk gevormde structuren (aggregaten). Een vesicle heeft over het algemeen een diameter die 5 tot 500 keer zo groot is als die van een micel.*

Een bijzondere categorie moleculen wordt gevormd door de “amfifielen” (Grieks voor “geliefd aan beide zijden”) die ook wel “surfactanten” (surface active agents) genoemd worden. Dit zijn moleculen die zowel een polair (wateroplosbaar) als een apolair (niet-wateroplosbaar) gedeelte bevatten (schema 2). Deze moleculen kunnen bijvoorbeeld bestaan uit een kleine geladen kopgroep met daaraan verbonden één of meer olieachtige staarten. De kopgroep is vaak vergelijkbaar met een zout zoals keukenzout. Wanneer deze verbindingen in contact komen met water vormen ze clusters van moleculen. Hierbij hebben de staarten de neiging

om bij elkaar te blijven en wel zodanig dat ze zo min mogelijk in contact komen met water, terwijl de kopgroep juist zoveel mogelijk in contact met water wil zijn. Afhankelijk van de precieze structuur van de verbinding kunnen onder andere micellen en vesicles worden gevormd. Micellen zijn een soort kleine oliedruppeltjes met aan de buitenkant de polaire kopgroepen. Door deze vorm zijn deze "druppeltjes" als geheel in water oplosbaar, omdat ze alleen van binnen apolair zijn. Over het algemeen worden micellen gevormd wanneer er één staart aan de kopgroep zit. Vesicles worden gevormd wanneer er aan de kopgroep twee staarten zitten. Vesicles zijn blaasjes met binnenin ook water, die over het algemeen veel groter (5 tot 500 keer in diameter) zijn dan micellen.

Celmembranen spelen een belangrijke rol in het bij elkaar houden van de inhoud van een cel. Daarnaast bevatten celmembranen speciale enzymen die controleren welke verbindingen de cel binnenkomen en uitgaan. Celmembranen vormen een soortgelijke structuur als vesicles. Daarom worden vesicles vaak gebruikt als modelsysteem voor celmembranen. Een belangrijk verschil is dat vesicles vaak gemaakt worden van slechts één type amfifiel, terwijl celmembranen uit een mengsel van vaak tientallen verschillende amfifielen bestaan. Ook bevinden zich in celmembranen nog honderden andere verbindingen, zoals bijvoorbeeld cholesterol.

In cellen vinden veel reacties plaats, waarvan de snelheid veelal door enzymen (eiwitmoleculen die als katalysator werken) wordt vergroot. Vaak heeft ieder type reactie zijn eigen enzym. Ook op het oppervlak van celmembranen worden reacties versneld door de aanwezigheid van membraangebonden enzymen. Daarnaast worden er ook reacties versneld, doordat de reactanten aan het membraan(oppervlak) binden, of omdat de omstandigheden aan het oppervlak gunstiger zijn dan in het binnenste van de cel. Dit laatste kan bijvoorbeeld komen doordat het celmembraan apolairder is dan water. Studies van de katalyse door vesicles is een belangrijke methode om soortgelijke processen in celmembranen te begrijpen.

Tot nu toe hebben de meeste studies van modelsystemen zich beperkt tot micelkatalyse of tot verschillen tussen micel- en vesiclekatalyse. Er zijn echter slechts weinig van dergelijke studies verricht met betrekking tot vesiclekatalyse. In hoofdstuk 1 wordt besproken dat de verschillen in eigenschappen vooral het gevolg zijn van de structuur van het surfactantaggregaat (bilaag die een water compartiment omsluit of een olieachtig druppeltje). Als gevolg hiervan kan de snelheid van de reactie aan de binnenkant van het membraan anders zijn dan aan de buitenkant als de reactanten maar langzaam door het membraan heen kunnen gaan. Daarnaast is de pakking van amfifielen in vesicles anders dan in die in micellen. Dit leidt er toe dat micellen een meer open structuur hebben, waardoor er op het oppervlak van micellen een hogere concentratie van watermoleculen is.

Alhoewel biologische membranen complexe mengsels van verbindingen zijn, is vesiclekatalyse vooral in één-componentsystemen bestudeerd. Het onderzoek, beschreven in dit proefschrift, maakt gebruik van vesicles die uit twee of drie verbindingen bestaan. De samenstelling kan systematisch worden gevarieerd en zo kan informatie worden verkregen over de mate waarin additionele verbindingen in een membraan de katalytische eigenschappen van het membraan beïnvloeden.

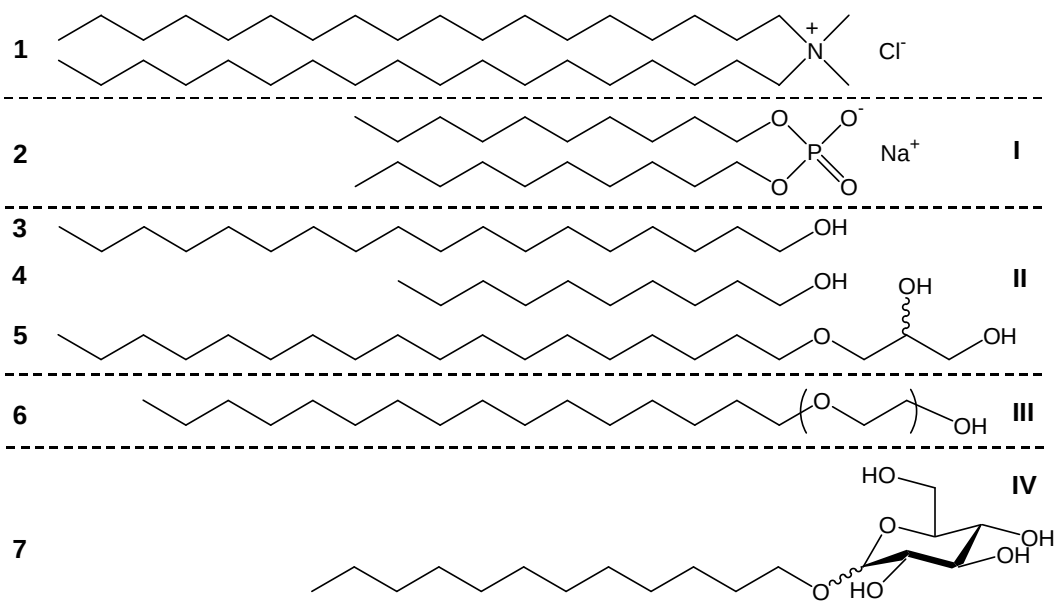

Schema 3. *Kationisch amfifiel gebruikt in de experimenten (**1**) en enkele voor-beelden uit de vier klassen verbindingen die als additief gebruikt zijn (**I**-**IV**). Klasse **I** zijn anionische dubbelstaartige amfifielen, klasse **II** alcoholen, klasse **III** ethyleenglycol surfactanten and klasse **IV** n-alkyl pyranosiden. Dimethyldi-n-octadecylammonium-chloride (**1**); sodium di-n-decylfosfaat (**2**); n-octadecanol (**3**); n-decanol (**4**) batyl alcohol (**5**), eicosa-ethyleenglycol mono n-hexadecyl ether (**6**) and n-dodecyl-β-glucoside (**7**).*

Het gekozen amfifiel is dimethyldi-*n*-octadecylammoniumchloride (**$C_{18}C_{18}$+**; **1** in schema 3). De vier klassen verbindingen, die aan de vesicles worden toegevoegd (additieven), zijn anionische dubbelstaartige amfifielen (I in schema 3), lange lineaire *n*-alcoholen (II), ethyleenglycol surfactanten (III) en *n*-dodecyl-*β*-pyranosiden (IV).

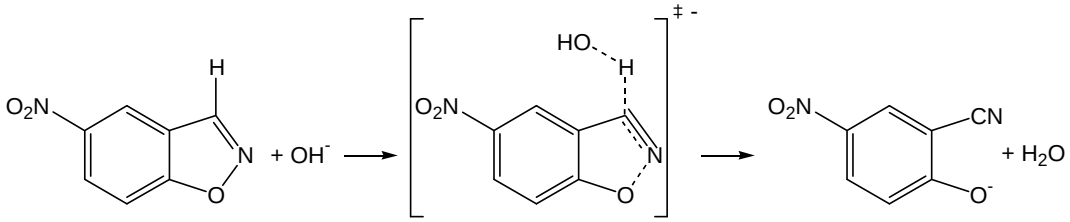

8

Schema 4. *Kemp eliminatie reactie of 5-nitrobenzisoxazool door hydroxide ionen.*

Als geschikte modelreactie is de hydroxide-iongekatalyseerde deprotoneringsreactie van 5-nitrobenzisoxazool (**8**; schema 4) gekozen. Het polaire hydroxide-ion bindt aan het vesicle-oppervlak vanwege de positief geladen kopgroep van de amfifielen, terwijl **1** vooral aan het membraanoppervlak bindt omdat het redelijk apolair is. Daarnaast is de snelheidsconstante (een maat voor de snelheid van een reactie) ook gevoelig voor de lokale polariteit en de mate waarin de reactanten zijn gehydrateerd (door watermoleculen omringt). Vooral dehydratatie van het hydroxide ion kan leiden tot grote versnellingen.

Voordat de katalytische effecten als gevolg van de toevoeging van de vier klassen additieven worden bepaald, wordt in hoofdstuk 2 eerst besproken wat de invloed van deze additieven is op andere eigenschappen van de vesicles.

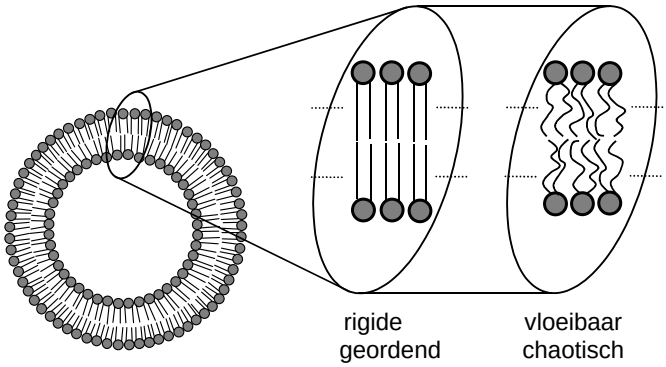

Schema 5. *Schematische weergave van twee van de toestanden waarin de amfifielen zich kunnen bevinden.*

De apolaire staarten van een amfifiel kunnen overgaan van een rigide en sterk-geordende toestand naar een meer vloeibare en meer chaotische toestand (schema 5). Dit wordt een fase-overgang genoemd. De temperatuur waarbij deze overgang plaatsvindt wordt de fase-overgangstemperatuur genoemd. De exacte fase-overgangstemperatuur hangt af van de moleculaire structuur van het amfifiel en eventueel andere aanwezige componenten in het membraan.

De fase-overgangstemperatuur (T_m) van de vesicles, zoals beschreven in dit proefschrift, wordt verlaagd in aanwezigheid van alle additieven in een molfractie kleiner dan 10%. Bij hogere molfracties van de additieven wordt de T_m verder verlaagd voor de additieven die in principe enkel-staartige surfactanten zijn: *n*-dodecyl-*β*-glucoside (**C_{12}Glu**), *n*-dodecyl-*β*-maltoside (**C_{12}Mal**), en eicosa-ethyleenglycol mono *n*-hexadecyl ether (**$C_{16}EO_{20}$**). Voor de verzadigde alcoholen neemt de T_m weer toe en de mate waarin deze toeneemt volgt de trend *n*-decanol (**C_{10}OH**), batyl alcohol (**C_{18}GOH**) and *n*-octadecanol (**C_{18}OH**). Bij een toename van de hoeveelheid oleyl alcohol (**$C_{18:1}$OH**) wordt de overgang minder coöperatief. In het geval van de anionische amfifielen, natrium di-*n*-decylfosfaat (**$C_{10}C_{10}$-**) en natrium *n*-decyl-*n*-octadecylfosfaat (**$C_{10}C_{18}$-**), worden (neutrale) microdomeinen gevormd tussen de 5 en 35 mol%. De katalyse wordt gevolgd bij een temperatuur van 15°C en deze temperatuur is ruim beneden de fase-overgangstemperatuur van alle vesicles met additieven.

Het toevoegen van **C_{12}Mal** en **$C_{16}EO_{20}$** leidt er toe dat de vesicles gedeeltelijk worden afgeroken tot gemengde micellen. Dit gedrag is bestudeerd met dynamische lichtverstrooiing en turbiditeit. De mate waarin micellen worden gevormd hangt zowel af van de molfractie enkelstaartig surfactant als de concentratie **$C_{18}C_{18}$+**.

Vijf verschillende kleurstoffen (pyreen, de E_T(30)- kleurstof, laurdan, Nijl Rood en 1,8-ANS) werden gebruikt om veranderingen in de polariteit van het vesiculaire oppervlak te meten. In de literatuur zijn deze kleurstoffen gebruikt om de polariteit van oplosmiddelen en oplosmiddelmengsels te meten. Ze zijn geselecteerd op basis van hun verschillende gevoeligheid met betrekking tot interacties met hun omgeving. Zo zijn bijvoorbeeld Nijl Rood en de E_T(30)-kleurstof bijzonder gevoelig voor waterstofbrugdonatie, terwijl pyreen dat absoluut niet is. Ondanks deze verschillen in gevoeligheid zijn er geen significante verschillen in

membraanpolariteit gemeten voor de vesicles met de verschillende (hoeveelheden) additieven.
In hoofdstuk 3 wordt aangetoond dat in 1,4-dioxaan-water en acetonitril-water mengsels het natuurlijk logaritme van de snelheidsconstante lineair toeneemt met polariteit zoals gemeten met Nijl Rood. De toename van de snelheidsconstante is vooral het gevolg van dehydratatie van het hydroxide-ion. Dit leidt tot destabilisatie van de grondtoestand ten opzichte van het geactiveerde complex.
In aanwezigheid van kationische vesicles is er een grote toename in de waargenomen snelheidsconstante (k_{obs}) bij een toenemende amfifielconcentratie tot een maximum waarde. Daarna neemt de waargenomen snelheidsconstante langzaam af. De *waargenomen katalyse*, uitgedrukt als de verhouding van de maximaal waargenomen snelheidsconstante en de waargenomen snelheidsconstante in water ($k_{obs,max}/k_{w,obs}$), bedraagt ongeveer een factor 1000. Dit soort gedrag is typisch voor vesiculaire katalyse van bimoleculaire reacties en kan worden beschreven met behulp van het pseudofasemodel met ionenuitwisseling, afgeleid aan het eind van de jaren 70. Het model gaat uit van twee pseudofasen, een waterige pseudofase en een vesiculaire pseudofase. Op basis van het model kan worden geconcludeerd dat twee oorzaken bijdragen aan de waargenomen katalyse. De eerste oorzaak ligt in het feit dat het reactievolume afneemt, omdat beide reactanten aan de vesicles binden. Als gevolg daarvan is de lokale concentratie veel hoger dan in de bulkoplossing. De tweede oorzaak is een toename van de snelheidsconstante gaande van de waterige pseudofase naar de vesiculaire pseudofase. Dit is het gevolg van een gedeeltelijke dehydratatie van de reactanten, vergelijkbaar met de water-organische oplosmiddelmeng-sels. Als met deze twee oorzaken rekening wordt gehouden kan de katalytische versnelling worden berekend. Deze is gedefinieerd als de verhouding van de bimoleculaire vesiculaire en de waterige snelheidsconstante (k_{ves}/k_w). De katalytische versnelling bedraagt ongeveer een factor 50.
De parameters, die met behulp van het pseudofasemodel bepaald kunnen worden uit de fits van de waargenomen snelheidsconstante als een functie van de amfifielconcentratie, zijn (i) de vesiculaire snelheidsconstante (k_{ves}), (ii) de bindingsconstante van **1** (K_S), (iii) de tegenionbinding (β) en (iv) de ionuitwisselingsconstante (K_{OH}^{Cl}). Een gedetailleerde foutenanalyse toont aan dat de parameters elkaar in grote mate kunnen compenseren. De ionuitwisselingsconstante kan onafhankelijk worden geschat en het blijkt dat deze niet varieert met een toenemende molfractie anionisch amfifiel. Foutieve en nietszeggende waarden voor de andere drie parameters werden gevonden indien deze drie parameters tegelijkertijd werd toegestaan om te variëren. Zo volgt uit de fit dan vaak dat de tegenionbinding groter dan één wordt, wat onrealistisch is. Als gevolg van deze compensatie werden maximaal twee parameters tegelijk gevarieerd. Zoals blijkt uit de kinetische vergelijkingen, kunnen k_{ves} en K_S elkaar vooral goed compenseren als de bindingsconstante klein is.
Op basis van de constatering dat de polariteit niet erg fluctueert als gevolg van de aanwezigheid van anionische amfifielen **$C_{10}C_{10}$-** en **$C_{10}C_{18}$-** in de bilaag, wordt verwacht dat de afname van de waargenomen snelheidsconstanten vooral het gevolg is van een afnemende tegenionbinding bij een toenemende molfractie anionisch amfifiel. Niet alleen kan de anionische kopgroep dienen als tegenion, maar de gevormde neutrale amfifielparen verdunnen ook nog eens de overblijvende kationische kopgroepen waardoor de oppervlakteladingdichtheid afneemt. Ongunstige kopgroep-kopgroepinteracties zijn verminderd en een lagere tegenionbinding is vereist om deze interacties te verminderen. Berekening van de lading per amfifiel met behulp van de tegenionbindingpercentages, die een maat is voor de oppervlak-

teladingsdichtheid, toont aan dat de netto lading per amfifiel niet erg varieert als gevolg van de toevoeging van **$C_{10}C_{10}$-** en **$C_{10}C_{18}$-** tot molfracties van 35 mol%.
In hoofdstuk 4 wordt aangetoond dat toevoeging van 50 mol% **C_{10}OH** aan vesicles gevormd door **$C_{18}C_{18}$+** slechts leidt tot een afname van 10% in de maximum waargenomen snelheidsconstante, terwijl de aanwezigheid van 50 mol% **C_{18}GOH** en **C_{18}OH** in de bilaag leidt tot een afname van respectievelijk 40% en 60%. Toevoeging van 35 mol% **$C_{18:1}$OH** daarentegen leidt tot een *toename* van 75% in de maximum waargenomen snelheidsconstante. Boven de 35 mol% neemt deze weer af. Een verandering in alleen tegenionbinding kan deze resultaten niet verklaren, omdat (i) ieder alcohol dan zijn eigen specifieke effect zou moeten hebben om de tegenionbinding te verlagen en (ii) incubatie van **$C_{18:1}$OH** in de bilaag zou leiden tot een tegenionbinding groter dan één. Uit literatuurstudies blijkt dat niet-ionische additieven de tegenionbinding verlagen onafhankelijk van de moleculaire structuur van deze additieven. Daarom zijn de experimentele data gefit, met een afnemende tegenionbinding zoals deze gemeten voor **$C_{10}C_{10}$-**. Er is aangenomen dat vier alcoholmoleculen hetzelfde oppervlak innemen als één (neutraal) paar van **$C_{18}C_{18}$+** en **$C_{10}C_{10}$-**. Het overgebleven deel van de waargenomen verandering in de snelheidsconstanten kan dan worden toegeschreven aan veranderingen in de vesiculaire snelheidsconstante en bindingsconstante, aangezien de ionuitwisselingsconstante niet afhankelijk is van de structuur van het additief. Een gedetailleerde interpretatie is moeilijk, omdat de gevonden effecten over het algemeen kleiner zijn dan een factor vier. Het lijkt erop dat de waargenomen effecten het gevolg zijn van een ingewikkeld samenspel van verscheidene factoren.
Hoofdstuk 5 beschrijft de invloed van de aanwezigheid van (oligo) ethyleenglycol groepen in de Sternlaag van kationische vesicles. Toevoeging van kleine hoeveelheden **$C_{16}EO_{20}$** (≤ 10 mol%) aan vesicles van **$C_{18}C_{18}$+** leidt niet tot enige verandering in de waargenomen snelheidsconstanten. In oplossingen met 35 mol% **$C_{16}EO_{20}$** is de maximum waargenomen snelheidsconstante afgenomen met 30% als gevolg van micelvorming. Experimenten uit de literatuur met het enkelstaartige surfactant *n*-octadecyltrimethylammoniumchloride (**C_{18}+**) bevestigen het verschil in katalytische efficiëntie tussen vesicles en micellen.
Hoofdstuk 6 rapporteert de respectievelijk 7- en 4,5-voudige toename in waargenomen snelheidsconstante na toevoeging van 50 mol% **C_{12}Glu** en **C_{12}Mal** aan vesicles gevormd van **$C_{18}C_{18}$+**. De oorzaak van dit effect is toegenomen dehydratatie van de reactanten als gevolg van de verdrijving van water uit de Sternlaag door de suikergroepen. Het kan niet helemaal worden uitgesloten dat katalyse door gedeprotoneerde hydroxylgroepen van de suikers hier ook debet aan zijn. Specifieke of voorkeursbinding van hydroxide-ionen kan de gevonden resultaten in ieder geval niet verklaren. Analyse van de experimentele data toont aan dat de toename in de maximum waargenomen snelheidsconstanten wordt veroorzaakt door een toename in k_{ves} voor **C_{12}Glu**, terwijl voor **C_{12}Mal** een toename in K_S vooral de reden is. Overigens kunnen de waargenomen effecten eventueel ook verklaard worden door deprotonering van de suikerhydroxylgroepen. In het geval van **C_{12}Mal** zorgt micelvorming ervoor dat de initiële toename in k_{ves} later weer afneemt.
Hoofdstuk 7 plaatst de gevonden resultaten van de voorgaande hoofdstukken in perspectief. Aan het eind van het hoofdstuk worden enkele mogelijkheden voor toekomstig onderzoek gegeven.

Voetnoot

(1) Onder katalyse wordt verstaan dat reacties versneld worden zonder dat de katalysator die de versnelling veroorzaakt in de reactie wordt verbruikt.